R 216

Technical Report

BLAST LOADING OF SMALL BURIED ARCHES

3 April 1963

U. S. NAVAL CIVIL ENGINEERING LABORATORY

Port Hueneme, California

BLAST LOADING OF SMALL BURIED ARCHES

Y-F008-10-108, Y-F008-10-402

Type C Final Report

by

J. R. Allgood, C. R. White, R. F. Swalley, H. L. Gill

ABSTRACT

The objective of the work represented by this report was to gain information which will serve as a guide in developing design methods for underground structures. In pursuit of this goal, preliminary tests have been conducted on small buried arches to determine the influence of the dominant parameters. Information has been obtained on the response to long-, medium-, and short-duration blast loads including the deflection, thrust, and moment patterns. One static test also was performed. Curves showing the form of arching under static and blast loading are given. In addition, buckling and the variation of interface pressure are discussed briefly.

The response of the buried arches consisted primarily of a body motion upon which was superimposed the first inextensional symmetrical mode of vibration. As the entire structure moved downward, the sides moved outward slightly and then inward. It was evident that the passive pressures which developed on the sides played the dominant role in providing resistance.

It has been found that in static tests some of the surface load is carried by arching through the soil. In the dynamic tests the inertial forces of the soil above the arch were found to be important. The inertial load overcame the soil shear resistance so that a load approximately equal to the surface load acted on the structure.

A model analysis of the system and subsequent comparison of the deflections from the small-structure tests and the Operation Plumbbob Structure 3.3 tests indicate that modeling of deflections is possible.

CONTENTS

INTRODUCTION

Subject and Purpose of Report

This report presents a review of the soil-structure interaction problem and gives data from preliminary tests on small buried arches. The work was accomplished under Task Y-F008-10-108, Studies of Soil-Structure Interaction, and Task Y-F008-10-402, Fundamental Behavior of Soils Under Time-Dependent Loads, both sponsored by the Defense Atomic Support Agency through the Bureau of Yards and Docks. The objectives of the tests and studies were directed toward satisfying research requirements of these agencies.

The specific system under study was the semicircular shallow-buried arch which constitutes the Navy's standard personnel shelter.[1] It was desired to learn something of the response to static and blast loads, including information on pressure distribution around the arch, the influence of arching and passive pressure in providing resistance, and the nature of the body motions of the arch. The ultimate goal of the buried-arch studies is to provide and substantiate theoretical methods which will enable the economical design of underground structures and the prediction of their behavior.

Analysis of the Problem

The arch, when employed as a shelter, is buried with sufficient depth of earth over the crown to reduce the radiation level from a nuclear blast to a tolerable level within the shelter. The arch is loaded by the soil and by the stress wave in the soil induced by the blast wave as it travels over the surface. It is assumed that the shelter is in the intermediate overpressure region (of the order of 100 psi) so that direct ground shock can be neglected.

A portion of the load is carried by arching through the soil; the remainder reaches the structure. As the structure commences to deflect under load, it reacts against the soil. Thus, resistance is provided by the soil. Also, the footings deflect into the soil, which relieves the load in the arch to a degree. The nature of this interaction and the influence of the various parameters involved are not well understood, but the parameters considered to be of prime importance are:

1. The stiffness, EI, of the arch.

2. The width of the footings.

3. The ratio of the depth of cover to the arch radius.

4. The properties of the foundation and backfill material, including density, angle of internal friction, and the load settlement relationship.

5. Load characteristics, especially rise time, peak load, and load duration.

Eventually each of these parameters should be studied, but first it is necessary to develop the means for such investigations.

Since the number of tests in a study of the problem is large, it is necessary to resort to small-structure or model tests. Model tests, however, involve difficulties because of uncertainty about the modeling laws for soils. For this reason the most promising approach appeared to be the testing of small structures, (as indicated in Figure 1), developing theories which agree with the results, and finally extrapolating these theories to larger structures. Simultaneously, it would be highly desirable to study the dominant parameters independently and to utilize the principle of synthesis to predict the behavior of soil-structure systems.

Investigation of soil-structure interaction by experiments involves numerous difficulties. Most of these are due directly to the nature of soil. The nonlinear stress-strain properties and the difficulty in measuring soil pressure are the major problems. Among others are the need for relatively large volumes of material and the effects of confining boundaries. These difficulties must not deter pursuit of answers to the problem, but they do limit the probability of success of any investigation.

Philosophy, Approach, and Scope

At the outset of a study it is necessary to establish a basic philosophy upon which to base an approach. The experience of the authors has been that in structural dynamics the ultimate-load approach based on fundamental mode response has proved the most fruitful. In treating reinforced concrete beams, for example, a multiple-mode solution for the elastic-plastic behavior leads to mathematical complexities which yield little useful information not obtainable from a simple fundamental-mode solution. It is expected that the same will hold for buried arches.

At least until basic phenomena are more clearly understood, there seems little to be gained from elaborate theoretical developments or parallel experiments which consider various types of shock waves transmitted through the soil, impinging upon the arch surface, refracting and reflecting, as higher modes are excited in the arch. Rather, initial theoretical and experimental efforts should be directed at gaining an understanding of the dominant parameters and aspects of behavior.

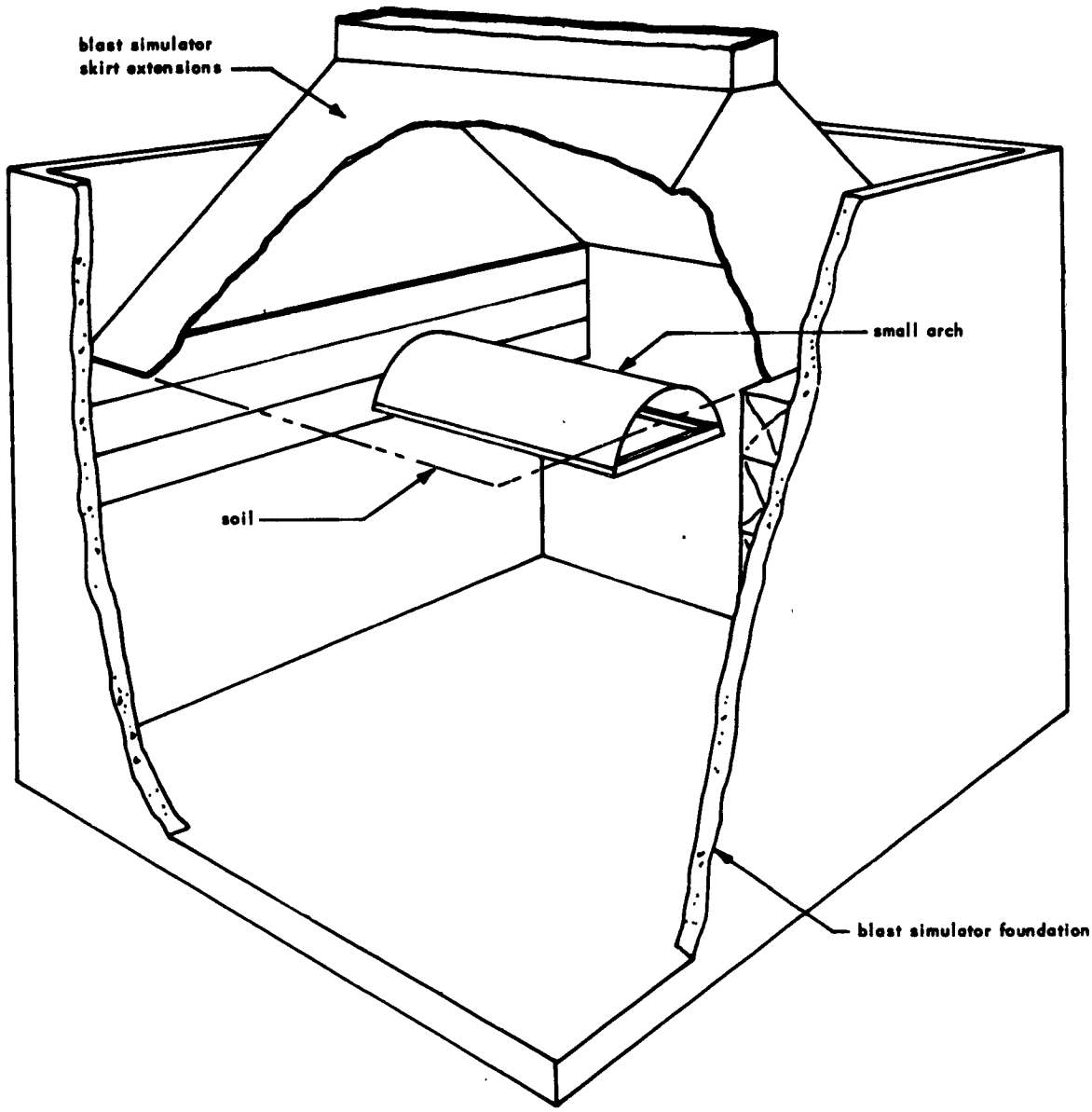

Figure 1. Perspective of blast simulator pit showing 40-ton soil mass and buried arch.

Next, the question might be considered whether it would be better to perform experiments designed to provide information on specific parameters known to be important or whether to attempt to gain information of a more general nature first. Again the philosophy of directing initial work towards gaining an understanding of general behavior was considered to offer the most promise of results which would be immediately useful. Based on this philosophy, an approach was pursued as follows:

1. A relatively crude replica of a section of a buried arch was made to give some idea of the deflection patterns which might be expected. This was intended primarily as an aid to proper location of instrumentation.

2. A two-dimensional model was constructed, instrumented, and tested in the blast simulator.[18] These tests proved to be inadequate for reasons to be discussed later; thus,

3. A series of three-dimensional small-structure tests were performed.

Prior to beginning the experimental work, the pertinent literature was reviewed. Also, a theoretical development was undertaken which, it is hoped, eventually may be modified to agree with the test results and be used for the generation of design charts. Only the results of the experimental work and preliminary analytical approximations are reported here.

For brevity, the scope of this report is restricted to the treatment of a simple two-hinged arch buried in dry sand. This is an admittedly idealized system, but it has the advantage of simplifying soil control and repeated testing. The idealized system also permits simplifications in the parallel theoretical development over what would be necessary with cohesive soils.

In the sections which follow, essential background information is summarized, then the experimental work performed to date is described, and the results are presented and discussed. This is followed by a list of tentative findings.

BASIC ASPECTS

Topics of Concern

In this section the main factors involved in the study of soil-structure interaction are briefly reviewed to enhance understanding of the test results presented in the following pages. The topics of concern are: the properties of dry sand, shock propagation in soil, soil-structure interaction, foundations, and model analysis. These topics are reviewed only to the extent that the information is useful in discussing and interpreting the test results.

The properties of dry sand and strip footing behavior are reviewed in Appendix A. Analysis of modeling of the system is given in Appendix B. The prime aspects of shock propagation in soil and of soil-structure interaction are reviewed in the following paragraphs.

Shock Propagation in Soil

The system under consideration is the shallow-buried semicircular arch subjected to a nuclear blast. As the shock wave moves out from ground zero, stress waves are induced in the soil field. These waves travel through the soil and interact with the buried arch.

Unfortunately, stress waves measured in field tests do not appear to conform to idealized theoretical cases of wave propagation in fluids or solids.[6] This is undoubtedly because soil is not a fluid nor a solid but a nonhomogeneous "semisolid" with highly dissipative characteristics. Further, as indicated in Appendix A, the stress-strain characteristics, and consequently the stress wave characteristics, of even such an idealized soil as dry sand are quite variable.

Ideally, the stress waves which would be expected in the soil are elastic dilatation and distortion waves and plastic-type compaction waves.[4,5] Plastic waves may also be of the dilatation or shear type. Apparently Rayleigh waves also are induced in a soil field, but the picture obtainable from available pressure records does not permit the separation of any of these waves with certainty.

Stress waves induced in soil by air blast are, strictly speaking, not shock waves although they are often called shock waves. The connotation usually ascribed to the term shock wave is that the wave front becomes steeper and steeper as it propagates through the material. In soil, the front generally gains a successively longer rise time. For this reason, the term soil stress wave will be used here.

Prime characteristics of a soil stress wave are attenuation of amplitude and increase in rise time as the wave travels to greater depths.[6] Attenuation at shallow depths is small and may be neglected for the system under study, but the rise time becomes significant even at shallow depths.[7,27] The peak stress and the duration of the wave near the surface should be essentially the same as the peak overpressure and duration of the surface shock wave.

As the stress wave strikes the surface of the arch, a reflection might be expected at the interface. That is, the stiffness of the structure relative to the stiffness of the soil might be expected to affect the pressure transmitted to the structure. To date, however, there is no conclusive indication of major stress reflection at the soil-structure interface of underground structures. Ultimately, a more detailed study of this problem must be made to determine just what happens at the interface.

Soil-Structure Interaction

As the stress wave travels down through the soil and envelops the arch, a complex interaction occurs: the soil and structure respond as a unified system. This process involves deflection of the footings with the foundation soil, distribution of a portion of the load through the soil mass surrounding the structure by arching, and development of soil pressures in the passive sense* where the arch deflections are into the soil.

Footing deflection and its consequences have been observed in full-scale field tests[6] and an approximate analysis has been developed for predicting its magnitude.[8] Yet, there is still a great deal to be learned about this action and the parameters which govern it. In all probability, the amount of footing deflection which occurs will influence the amount of arching through the soil, the pressure distribution around the extrados, and thus the radial and tangential response of the arch proper.

It has been hypothesized that arching through the soil considerably reduces the load which gets to the structure.[3] Arching is developed by virtue of the shear strength of the soil.[9] As such, for sand, it is expected to be primarily a function of the angle of internal friction of the soil, and the ratio of the depth of cover over the crown to the radius of the arch. Arching studies have been made in "trap-door" experiments.[10] Also, a recent study gives experimental results on arching across small-size structures subjected to static loading.[11]

The soil pressures which confine the arch are considered far more important than soil arching in providing resistance by relieving the load. As the crown is loaded, the haunches of an arch would be expected to move outward into the soil, developing large pressures which result in a near radial pressure distribution around the arch. Confining or passive-sense pressures in well-compacted sand are developed with exceedingly small deflections, as is readily seen from tests of deadman anchors.[12] Further, passive-sense pressures much greater than the active pressure are readily developed. As has been shown, the soil surrounding an underground arch contributes the major portion of the resistance to lateral deformation.[13] The tests reported here provide limited information on these passive-sense pressures.

There have been several attempts at developing a satisfactory theory for predicting the behavior of buried structures. Certain of these are rather sophisticated,[14, 19, 28] while others have attempted more gross predictions.[15, 16, 29] One

---

* By passive-sense pressure is meant pressures between the at-rest value and the passive value. In contradistinction, the passive pressure is the value at failure, as explained in Appendix A.

of the more promising approaches is based on the selection of planes within the soil (where the shear stress equals the ultimate shear resistance) and the writing of equations of motion of the mass of soil bounded by these planes, the structure, and the ground surface.[17] By this means, an equation is developed for a pseudo-period and a plot is given which shows the effect of load duration on the peak overpressure required to produce failure of a structure. From these curves it is evident, for example, that for structures of 100-man personnel shelter proportions (1000 square feet), the peak pressure to produce failure is essentially the same for all loads with a duration greater than about 300 milliseconds. For shorter load durations, the load to produce failure goes up rapidly. Thus, the method permits the attainment of at least an approximate idea of the influence of the various load and soil parameters.

EXPERIMENTAL WORK

Considerations in Experimental Design

The experimental program described was based on the fundamental objective of gaining an understanding of the general behavior of buried structures subjected to blast loads. Specifically, it was desired to define the time variation of deflection, moment, thrust, and pressure; and the character of arching, footing deflection, and passive pressure. Secondary objectives were to obtain information on the soil pressure and movements in the free field which influence the arch behavior.

To accomplish these objectives it was deemed desirable to test a model of Operation Plumbbob Structure 3.3b[6] since results of field tests of this structure could be used for comparative purposes. It was doubtful, however, that contemporary knowledge would permit true modeling of buried structures with any degree of certainty. The alternative was to scale the Plumbbob Structure 3.3b as well as possible but to consider the resulting system as a small structure test and not as a model test. With this approach it was hoped that once the underground modeling problem is solved, the data might be useful from a modeling point of view.

Prior to initiating a test program, the simple configuration described in Appendix C was devised to get pictures of the probable deformation patterns to aid in location of instrumentation. Normally, this type of preliminary investigation is not reported, but serendipitious qualitative results from these tests warrant their inclusion. Further, they give rather interesting deformation patterns.

Once the probable deformation patterns had been defined, a series of two-dimensional tests were designed in an effort to accomplish the task objectives. These tests, as described in Appendix D, were only partly successful because of the

deleterious effects of boundary friction. The two-dimensional tests were performed in the skirt extensions of the blast simulator, which formed a boxlike chamber 6 feet deep by 9 feet long by 8 1nches wide. The results of supplementary tests to determine arching and friction from the boundaries of the chamber are also described in Appendix D. Studies aimed at reducing boundary friction and arching have been made;[11] however, the methods which have proved successful are uneconomical for relatively large models. Two-dimensional experiments have the advantage of permitting visual and photographic monitoring of behavior, which is difficult to achieve in three-dimensional tests. The two-dimensional tests were eventually abandoned, however, in favor of three-dimensional tests because of the boundary difficulties.

Three-Dimensional Tests

The configuration of the setup for the three-dimensional tests, Figure 2, consisted of a small structure buried in a soil field of dry sand. The sand was contained by the pit of the blast simulator, which is 9 feet by 10 feet in plan and 13 feet deep. The structure used was a 30-inch-diameter semicircular arch with a length of 5 feet and a thickness of 0.0478 inch. The arch was fabricated from galvanized sheet steel and the endwalls, floor, and footings were made of Douglas fir. Piano hinges were brazed to the sheet metal and screwed to the foundation to simulate pinned-end conditions. The footings were tied at mid-span with a strap-steel bracket located to prevent rotation or lateral motion of the footings. Fundamental physical properties of the arch are given in Table I.

Table I. Fundamental Physical Properties of Arch

Type	= two-hinged semicircular
Material	= steel
Modulus of elasticity, E	= 30×10^6 psi
Radius, r	= 15 in.
Length	= 57.6 in.
Thickness	= 0.0478 in.
Weight (including ends and instrumentation)	= 68 lb
Depth of crown below surface	= 6 in.
Side footing width	= 1.20 in.
Side footing height	= 1.80 in.
End footing width	= 1.75 in.
End footing height	= 3.75 in.
Natural period (1st inextensional mode)	= 29 msec
Moment of inertia, I	= 9.1×10^{-6} in.^{4}
Radius of gyration of section	= 1.38×10^{-2} in.

Figure 2. Small structure in test pit.

The sand was placed in the pit in vertical lifts of 2 feet and vibrated as described in Appendix A. When the depth of sand was at the elevation of the footings, the arch was placed in the pit as shown in Figure 2. Care was taken to seat the footings, then the remainder of the soil (backfill) was placed and vibrated. The contour of the arch was maintained during backfilling by an internal bracing system located at mid-length and rigged so that it could be collapsed by pulling a cable after the backfill was in place. Properties of the sand as placed are given in Table A-I in Appendix A.

A polyethelene sheet 8 mils thick was placed over the surface of the sand and sealed around the edges to prevent gas pressure from entering the soil. Subsequently, static or dynamic gas pressure was applied to uniformly load the soil surface. The gas was confined by skirt extensions which passed downward from the bottom of the blast simulator to the sides of the pit. These are shown in Figure 3, which illustrates the transverse section of the test arrangement. Figure 4 illustrates the longitudinal section. Stiffened steel plates were placed over the ends of the skirt extensions. Blast loads generated in the simulator traveled downward through the skirts and expanded into the volume enclosed by the extensions.

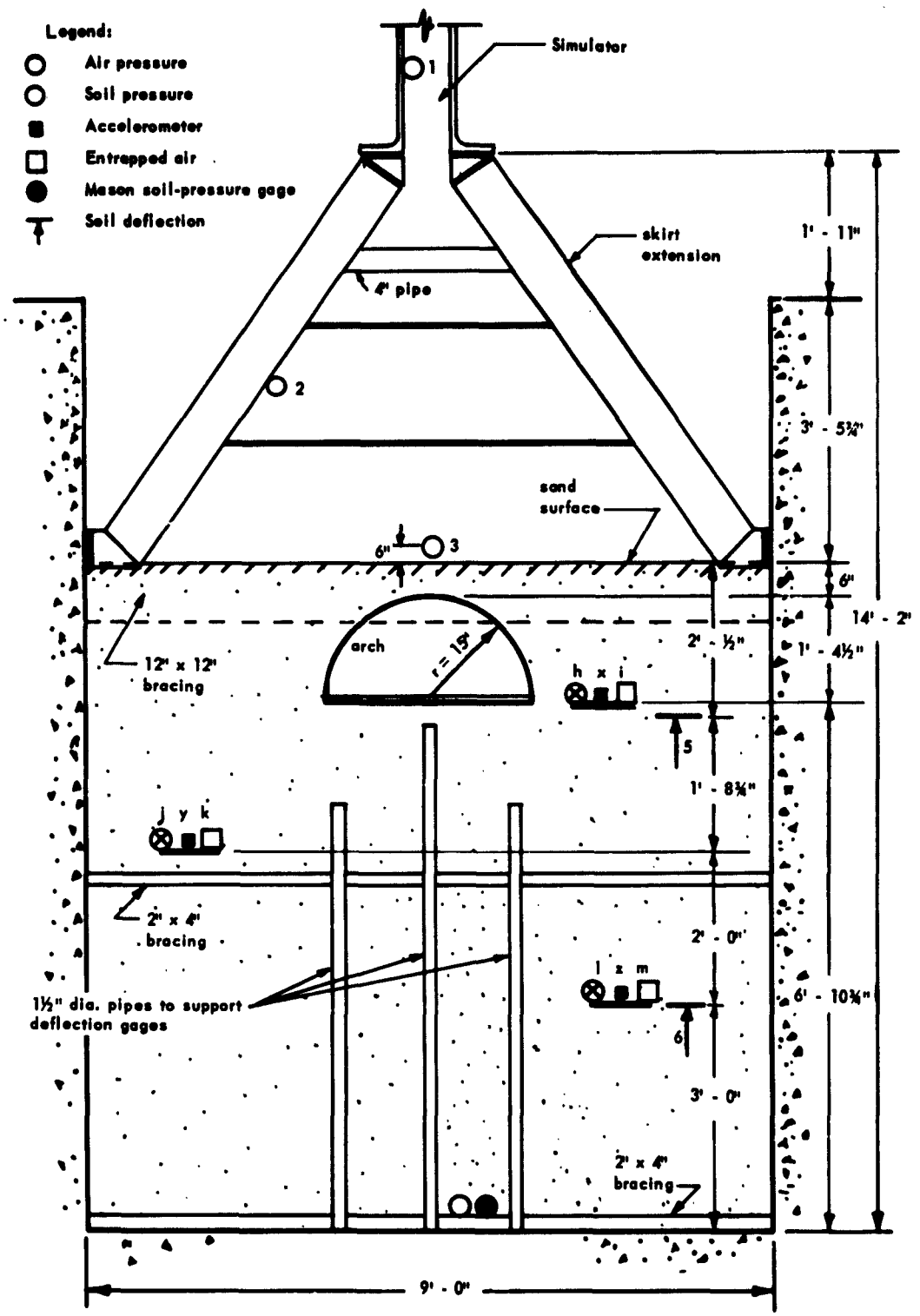

Figure 3. Transverse section of test setup.

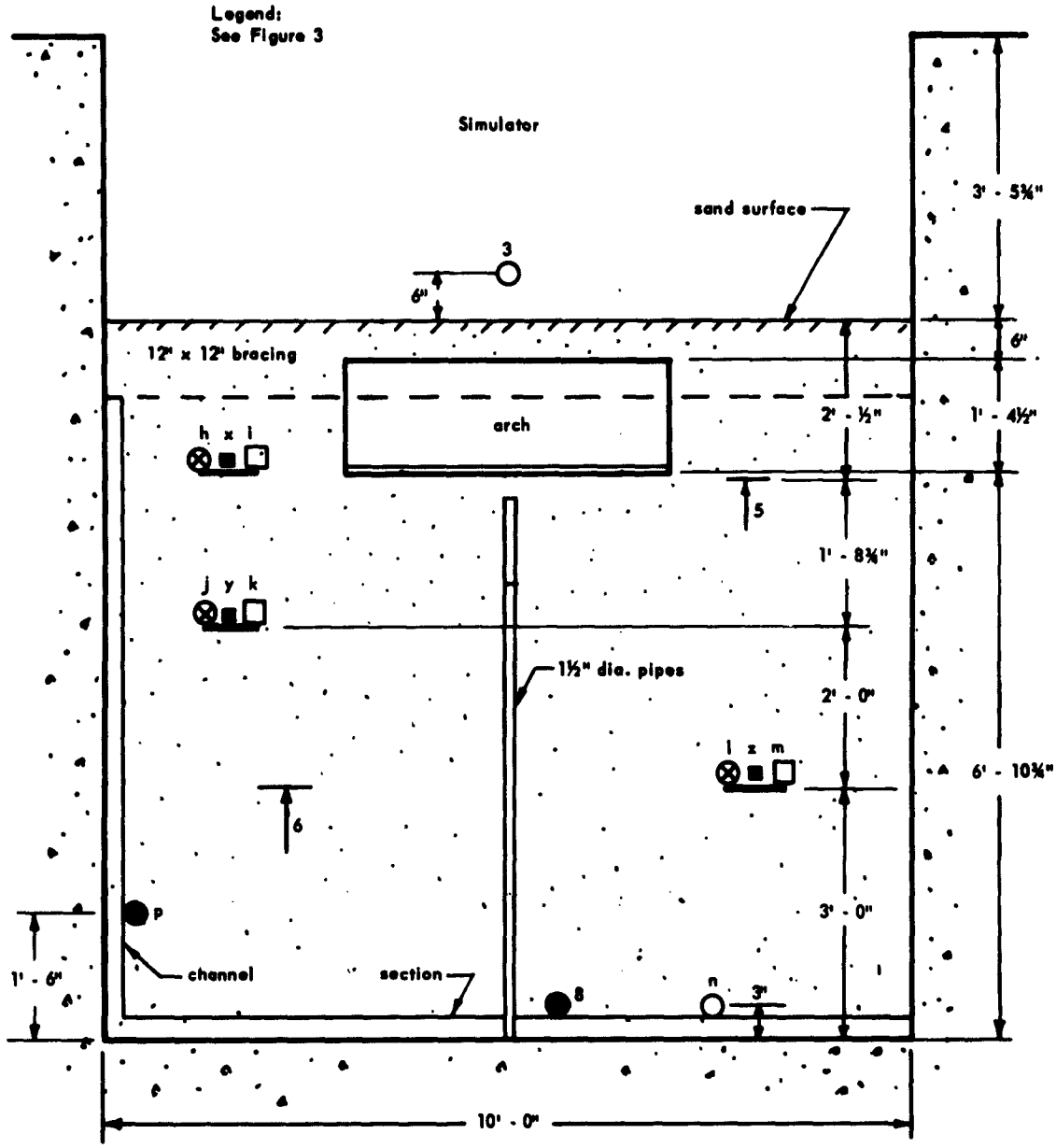

Figure 4. Longitudinal section of test setup.

It was not possible to completely seal the joints of the skirt extensions with the simulator and end plates. Thus, to obtain static loads, a plastic bag was made to fit the contour of the confining chamber. For static loading, air was pumped into the plastic bag. Obviously, it was necessary to have all instrumentation in place prior to backfilling and installation of the confining system.

Two series of three-dimensional tests were run. The test setup for both was the same, except (1) the density of the soil in the Series I tests was greater than in the Series II tests, and (2) the instrumentation was modified slightly for the second series of tests based on information gained in the earlier series.

Instrumentation

Recording Equipment. Instrumentation was provided to measure pressures, strains, deflections, and accelerations. All measurements were recorded using Consolidated Electrodynamics Corporation (CEC) System D equipment with two CEC 5-119 oscillographs. Slightly different instrument layouts were used in the Series I and the Series II tests, as shown in Figures 5 through 10.

Gas Pressure. Gas pressures generated within the blast simulator were measured with Statham Model PA-208TC cells. These cells were located as shown in Figures 3 and 4, and were precalibrated with a Wallace and Tiernan Model FA-145 static-pressure gage prior to installation in the simulator. Gage 3 measured side-on pressure.

Strains. Strains in the arch were measured with SR-4 bonded strain gages Type A-5-1 which had a gage factor of 1.98. These gages were located on the intrados and extrados of the arch at the locations shown in Figures 7 and 10. The gages can be seen in Figure 11, which is a view of the underside of the arch. The strains were used to determine the thrust and moment in the arch.

Deflections. Deflections of the structure were measured with Bourns linear-motion potentiometers, Model 108. These gages were located as shown in Figures 6 and 9. Potentiometers numbered 1, 2, and 3 had a range of 6 inches and measured vertical motions of the footings and the crown relative to the floor of the pit. Potentiometers 4 and 5, capable of 1.31 inches of travel, detected motion of the haunches at the 25-degree points relative to the respective opposite footings. The potentiometers were calibrated versus linear scale.

Soil Pressures. An effort was made to obtain data on the entrapped air pressure and the intergranular pressure in the free field. To do this, 100-psi CEC Type 4-312 fluid-pressure pickups with a maximum error of 0.009 percent of full range per degree Fahrenheit were mounted in a plate, one in contact with the sand

and one covered by a fine wire screen, at the locations indicated in Figures 3 and 4. The intent was to measure entrapped air pressure with the covered gage and entrapped air plus intergranular pressure with the gage in contact with the sand. It was recognized that the probability of getting reliable soil-pressure readings with these gages was poor, but unfortunately there is no reliable means of measuring soil pressure known at the present time. In spite of the recognized difficulties, an attempt to measure soil pressures was considered worthwhile. The gages employed were calibrated with static air pressure and statically in sand in a test bin. An unsuccessful attempt also was made to calibrate the gages dynamically in a triaxial soil test.

Interface Pressures. CEC Type 4-312A pickups also were used to detect the interface pressures. These transducers, located as shown in Figures 5 and 8, were mounted in holes cut through the arch in such a way that their faces were flush with the extrados. They were covered with a thin plastic film prior to placement of the backfill.

Boundary Pressures. Boundary pressures were detected with a specially built gage which has been successfully used in static tests to measure soil pressure against laterally loaded piles. These gages are described in detail elsewhere.[20] In essence, they consist of an oil-filled bellows-type housing 11/16-inch thick with a rigid face 3-27/32 inches in diameter. A CEC Type 4-312A pickup is mounted in the back of the gage to detect changes in fluid pressure. These gages are not suited to the measurement of dynamic stress waves because of their long natural period. The housings were mounted in 12-inch-wide steel channels so that the face plates were flush with the outside surface of the channel web. The channels were then placed around the boundary of the test pit at the locations indicated in Figures 3 and 4.

Accelerations. Accelerometers were placed at positions on the arch and in the free field as indicated in Figures 9 and 4. Statham Type A5A accelerometers with a range of 100 g's were mounted on the underside of the 6-inch by 6-inch by 12-gage steel plates placed in the free field. Small accelerometers, Statham Model A52, with a 100-g range were attached to the arch. The accelerometers were intended to provide information on accelerations, velocities, and deflections. Both types of accelerometers were accurate to within ±1 g and had a 0.02 g per g limit of response to transverse acceleration.

Measurement Errors. The expected maximum errors for the various measurements are summarized in Table II. The values given for the pressure pickups are valid only when measuring gas pressure. As the last column in Table II indicates, the maximum expected error is of the order of ±6 percent. In some traces the error may exceed this due to intermittent electrical noise on certain of the records. Every effort was made to minimize errors in performing the tests and reducing the data.

Table II. Maximum Error Ranges

Gage Type	Transducer Error		System "D" Error			Reading Error[d] (%)	Error Due to Paper Expansion (%)	Max. Error Possible (%)	Max. Error After Calibration Correction[e] (%)
	Nonlinearity[a] (%)	Hysteresis (full range) (%)	Amplifiers (%)	Power Supply[b] (%)	Galvanometer[c] (%)				
Strain gages	0	±0.23[f]	±2	±1	±1	±1	±1	±6.23	±5.23
Accelerometers	±1[g]		±2	±1	±1	±1	±1	±7.00	±6.00
Pressure pickups	±0.75	±0.75	±2	±1	±1	±1	±1	±7.50	±6.50
Displacement pickups	±0.50	±0	±2	±1	±1	±1	±1	±6.50	±5.50

a/ The error due to nonlinearity applies for the full range; if a partial range is used for the test this error can be reduced by calibrating over that partial range.

b/ Power supply errors are based on power fluctuation between 105 and 125 volts.

c/ The error listed for the galvanometer is a linearity error, over full-scale deflection (±2 inches). With damping at optimum (64% of critical) the maximum overshoot for the galvanometer at the leading edge of a square wave is 7%.

d/ The reading error is based on a trace amplitude of 1 inch. The absolute error expected in reading the trace is 0.01 inch. For small trace amplitudes the percentage error will increase.

e/ The error that, with reasonable assurance, can be eliminated is power-supply nonlinearity due to fluctuation in input voltage. Amplifier nonlinearity can also be reduced by calibration.

f/ This hysteresis error is for a range of ±1500 microinches per inch.

g/ Represents the combined transducer nonlinearity and hysteresis error.

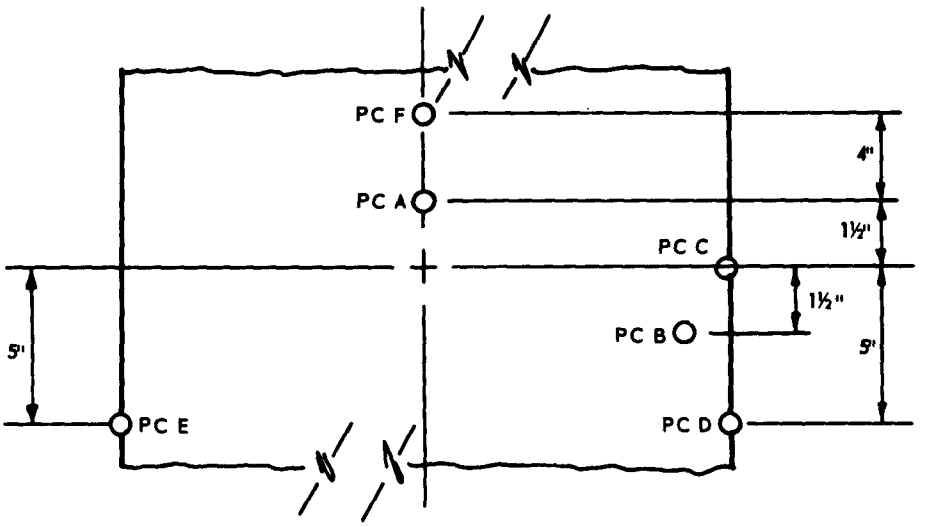

Plan View

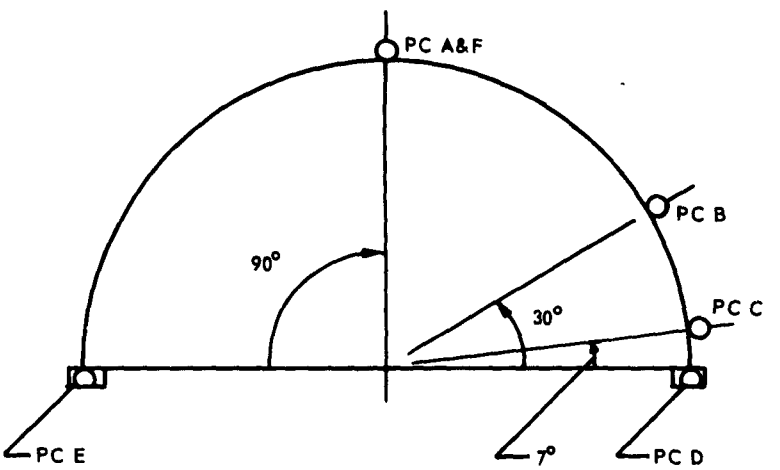

End View

Figure 5. Pressure cell locations — Series I.

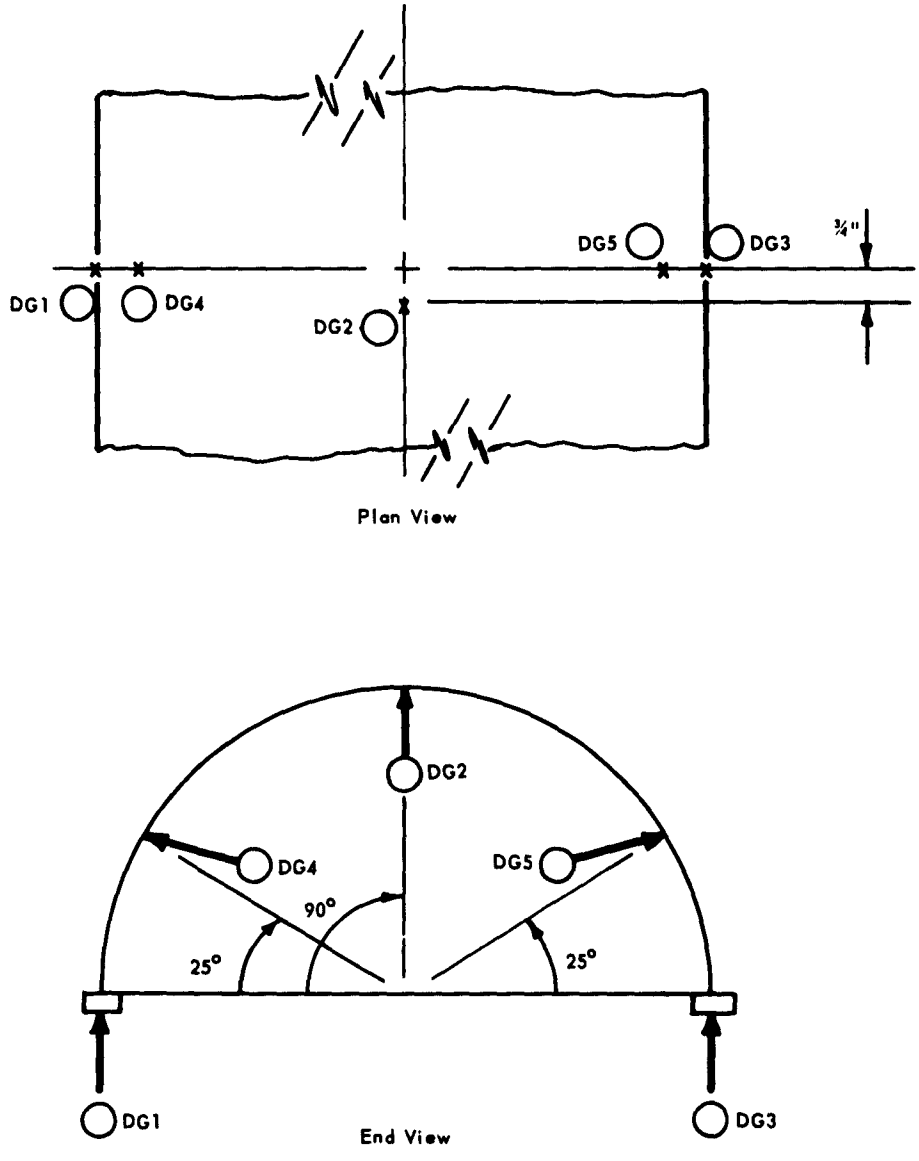

Figure 6. Deflection gage locations — Series I.

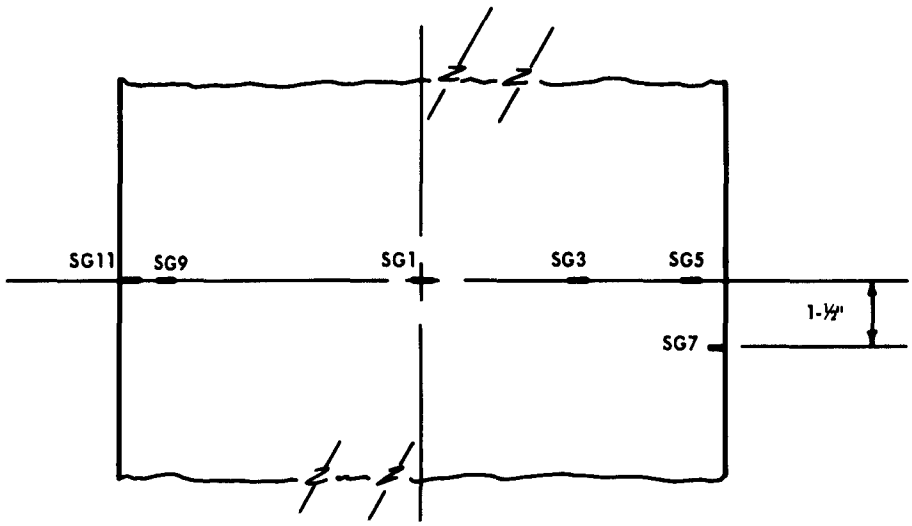

Plan View

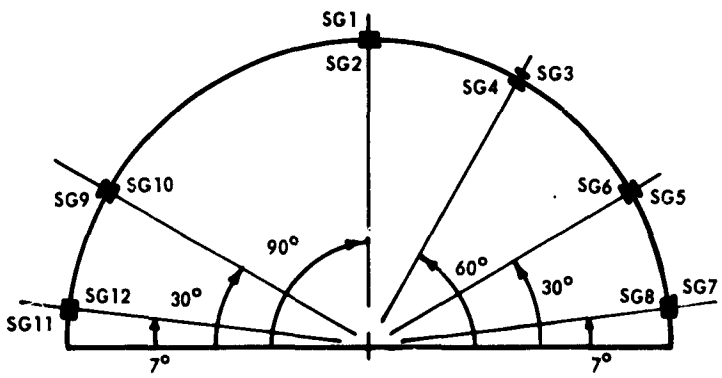

End View

Figure 7. Strain gage locations — Series I.

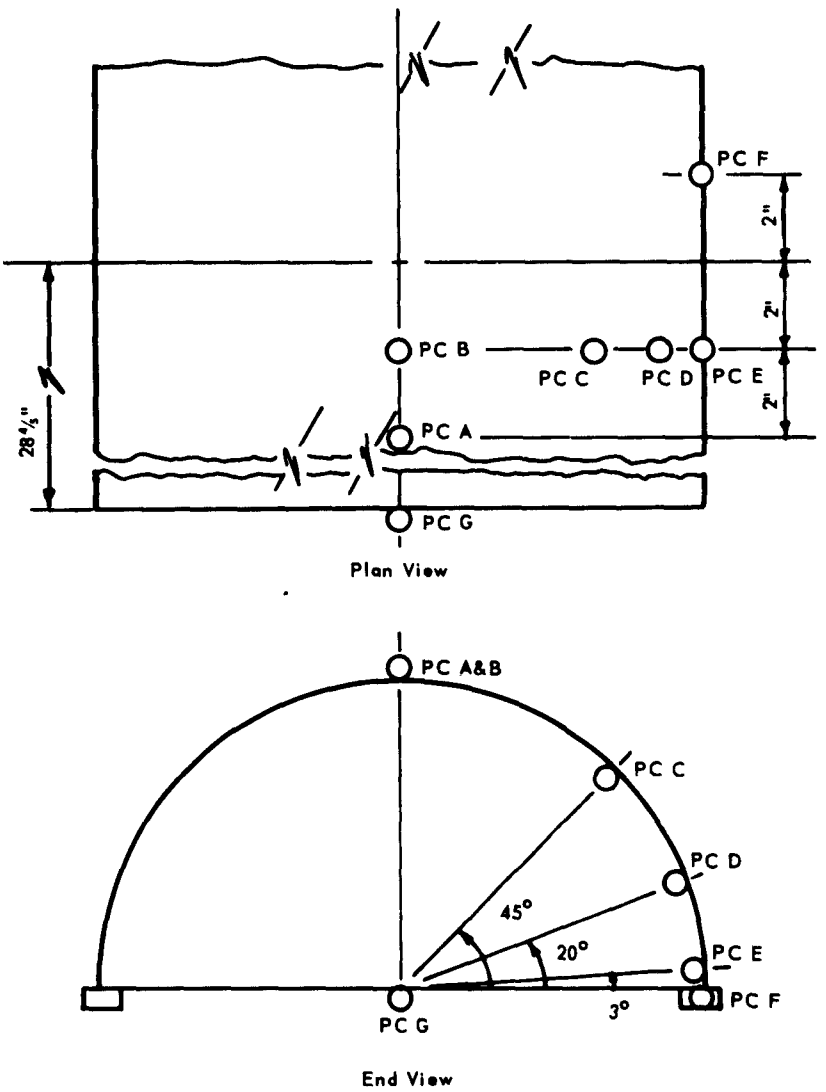

Figure 8. Pressure cell locations — Series II.

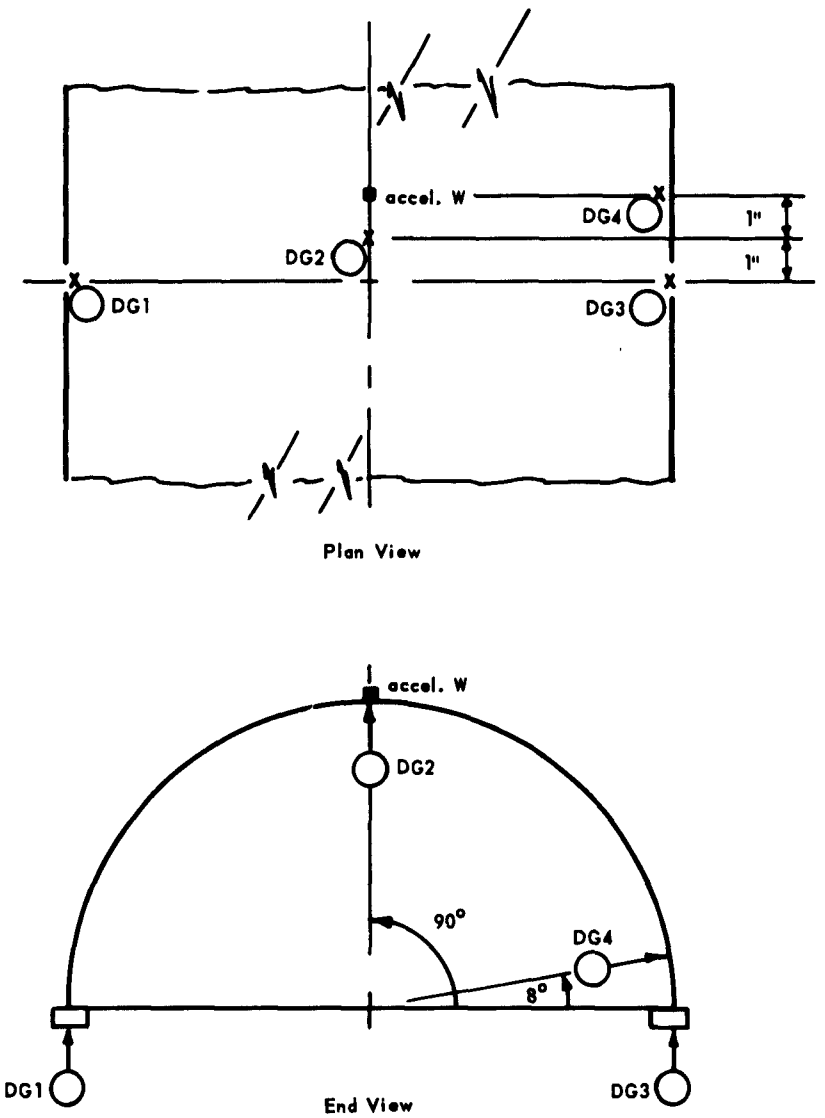

Figure 9. Deflection gage and accelerometer locations — Series II.

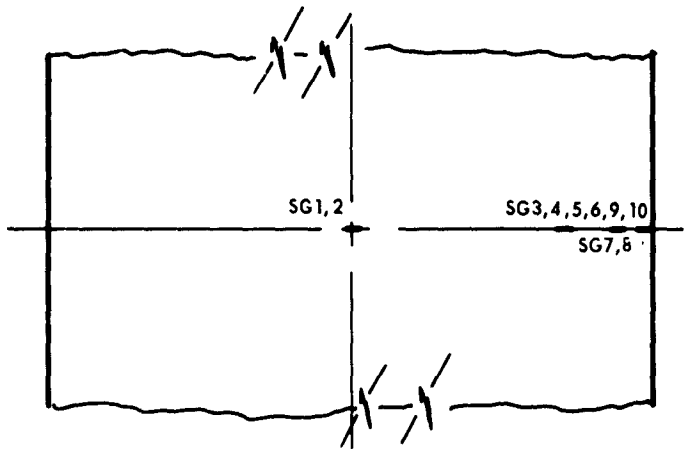

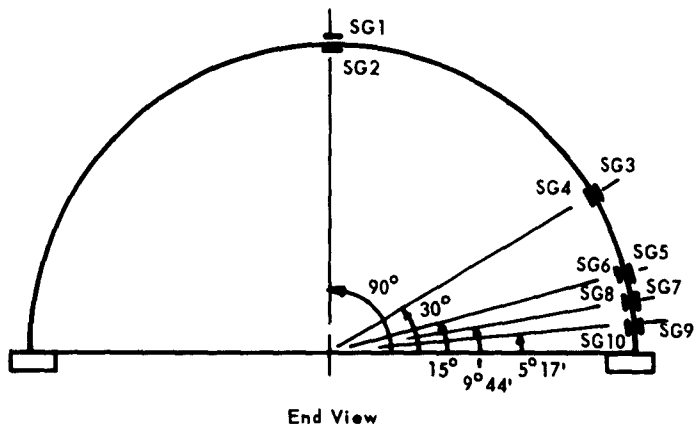

Figure 10. Strain gage locations — Series II.

Figure 11. Underside of instrumented arch.

Test Program and Procedure

The test schedules and main objectives for the Series I and Series II three-dimensional (3D) tests are given in Tables III and IV.

Vibration Tests. The arch was vibrated prior to backfilling to obtain its unconfined natural frequency in the first inextensional symmetrical and antisymmetrical modes, Table V. These were the only modes which could be excited independently by the simple expedient of pushing on the arch and suddenly releasing it to vibrate. After the arch had been covered with sand, the first inextensional symmetrical mode was excited by detonating a small charge of high explosive one foot above the surface.

Dead-Load Tests. Gage readings were taken with the arch in the unloaded condition and again when the backfilling was completed to obtain the strains, deflections, and pressures due to the soil cover. Instead of the System "D" equipment used in the dynamic tests, Baldwin Type "M" strain indicators were used for the dead-load tests. All transducers had been previously calibrated for use with these indicators.

Table III. Test Schedule — Series I

Test[a/]	Load (psi)	Duration	Main Objective
Vibration	—	—	Determine natural periods of modes of vibration
No load	dead load	static	Determine dead-load readings
3D-6A	5	long	Determine response of arch to long-duration loads; investigate importance of soil inertial forces
3D-6B	6	long	
3D-6C	7	long	
3D-7A	10	long	
3D-7B	10	long	
3D-7C	10	long	
3D-6D	6	short	Determine response to short-duration loads
3D-7D	10	short	
3D-6E	6	medium	Determine response to intermediate-duration loads
3D-7E	10	medium	
3D-6F	7	long	Determine extent of pore pressure with plastic sheet removed
3D-8	24	long	Determine response at high overpressure

a/ Tests were performed in sequence listed.

Table IV. Test Schedule — Series II

Test[g]	Load (psi)	Duration	Main Objectives
Vibration	—	—	Determine natural periods of modes of vibration
No load	dead load	static	Determine dead-load readings
3D-11A	6.5	short	Determine response of arch to short-duration loads; investigate importance of soil inertial forces
3D-11B	7	short	
3D-12A	7	long	Same as above except for long-duration loads
3D-12B	7	long	
3D-13A	12	long	Evaluate arch response at higher load levels
3D-13B	17	long	
3D-13C	25	long	
3D-14A	7	short	Determine the pore pressures
3D-15A	to 4	static	Compare static and dynamic behavior

[g] Tests were performed in sequence listed.

Table V. Deflection Modes of an Arch

I. Extensional Mode

Sometimes called compression or "breathing" mode

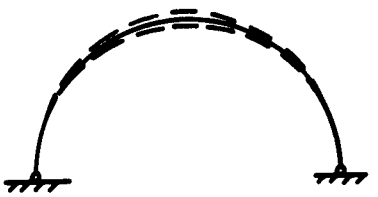

II. Inextensional Modes

A. Symmetrical

1. 1st symmetrical (bending-compression)

2. 2nd symmetrical (bending-compression)

B. Antisymmetrical

1. 1st antisymmetrical (lateral bending mode, flexural mode, deflection mode)

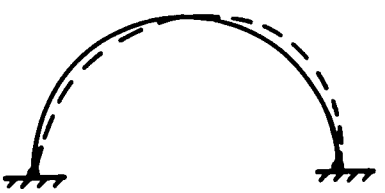

2. 2nd antisymmetrical

Blast-Load Tests. Short-, medium-, and long-duration loads were applied to the soil-structure system as indicated in Tables III and IV. The terms short and long duration mean that the loadings are short or long with respect to the natural period of the system. The distinction, as usually employed with beams, is whether the effective duration of the load is greater than or less than 6 times the lowest natural period. Until more is known about the behavior of buried arches no such numerical distinction is considered justified. At present it is deemed more satisfactory to classify a loading as of long, medium, or short duration on the basis of the nature of the response which it produces in the soil-structure system. This has been done in the tabulations of data which follow.

It is to be noted especially that the system was not altered for a given series of tests as the load was increased. That is, the sand was not recompacted or otherwise disturbed in any way. The only exception was that the soil may have been disturbed in installing the plastic bag for the last test of Series II.

Static Tests. The static test was not completed because a leak developed in the thin (8-mil) plastic bag at a pressure of 4 psi. Complete static tests, therefore, must await a future test series.

RESULTS AND DISCUSSION

Introduction

The behavior of the small arches appeared much the same as that of the full-size corrugated-metal arches tested in Operation Plumbbob.[6] However, since the data from the full-scale tests is limited it is only possible to make comparisons of peak deflections. Results of the Series I and II tests also were consistent, although there were anomalies that will be cited in another context.

Considerable data was collected in these tests, but the body of data on underground structure behavior remains exceedingly small. Consequently, conclusions and inferences drawn from the test data may need modification as better control, better means of measurement, and more data are accumulated. The data obtained should be especially useful for comparison purposes in theoretical analyses and model studies. Likewise, it is expected that these theoretical studies, when available, will markedly influence the direction of future testing.

Measurements obtained were, in general, quite good except for soil-pressure traces. Some soil-pressure measurements are reported but their validity is questionable since, as has been remarked, no satisfactory means for sensing soil pressures is

available. Despite the lack of adequate soil-pressure measurements, considerable information about arch behavior is derivable from the strain, deflection, and acceleration measurements which were taken.

Natural Period

In the discussion of natural period and response, repeated reference will be made to the deflection modes of an arch. In these discussions, the formal definitions of Table V will be used. Descriptive names for the various mode shapes shown in the accompanying sketches and often used in the literature are listed in parentheses.

A convenient form for the relation expressing the frequency of the natural modes of vibration of a 180-degree arch is

$$\omega_n = \frac{2\pi}{T_n} = \frac{C_n}{r^2}\sqrt{\frac{EI}{\gamma}} \qquad (1)$$

where C_n equals a constant corresponding to the various mode shapes as follows:

C_1 (extensional mode) = 13.7

C_2 (first inextensional symmetrical mode) = 8.1

C_3 (first inextensional antisymmetrical mode) = 2.2

and T_n = natural period of vibration corresponding to the nth mode

r = radius of arch

EI = stiffness of arch

γ = mass density of arch

These constants may be determined by means of the Rayleigh-Ritz method. General expressions for them in terms of angle of opening, radius, and radius of gyration of the section are available in the literature and have been collected in a single source.[19]

Using the appropriate constants, the computed values for the natural period of the uncovered arch and the corresponding experimentally determined values are:

	Computed (msec/cycle)	Experimental (msec/cycle)
T_1 (extensional mode)	35.8	—
T_2 (first inextensional symmetrical mode)	60.5	62.5
T_3 (first inextensional antisymmetrical mode)	223	187

The preceding experimental values were determined with no endwalls in the arch. When the endwalls were installed, attempts at determining the first symmetrical mode resulted in an oscillation with a period of 11 milliseconds. Similar attempts at determining the first antisymmetrical mode also resulted in a period of 11 milliseconds. The measured period was probably that of the second inextensional symmetrical mode. From these measurements, one would conclude that the endwalls have a very marked effect on which modes of response are excited.

The natural period will also be markedly affected by the earth cover and any subsequent surface loading. The earth cover has two opposite effects: (1) the added mass tends to increase the period of the various modes, and (2) the stiffness of the soil acting with the structure tends to decrease these same periods. Additional surcharge loading such as from a blast is expected to produce a similar stiffening and reduction in period, as has been predicted in theoretical studies.[13]

Vibration tests on the covered arch resulted in a period of 29 milliseconds. This was the first inextensional symmetrical mode. Comparing the 29-millisecond period of the covered arch with the corresponding 62.5-millisecond period of the uncovered arch confirms the theoretical prediction that the stiffening effect of the soil is more influential on the period than the added mass.

Dead-Load Tests

Strains induced in the structure during backfilling were so small that they are of little value; many of them were within the error band of strain readings. They do serve to show that the moments and thrusts from the dead load will be small if a proper backfilling procedure is followed.

Special dead-load tests were performed on the sand-covered model arch in a large metal box for the express purpose of defining the deflection pattern produced by the backfill. Dial deflection gages were located as shown in Figure 12 and were read through an opening in the end of the box. The backfill was placed in the same manner as for the tests in the simulator. The resulting deflection pattern is shown in Figure 13. The deflection pattern shows clearly that thin metal arches with hinged springlines and tied footings are no longer circular when backfilled. This fact greatly influences the moments in the arch, as will be obvious from subsequently presented test data. The observation also aids in explaining the buckling behavior of metal arches as discussed in the following section.

Static Test

The data from static test 3D-15A are given in Tables VI and VII and in the plots of Figures 14 through 17. As previously mentioned, it was possible to obtain static loads of only 4 psi because of failure of the plastic bag used to contain the pressure. The uniform pressure applied to the soil surface through the bag induced pressures on the arch as indicated in Figure 14. At 3 psi the pressure at the crown was more than twice the value in the vicinity of the springline. The curve at 4 psi is not given because the oscillogram with the pressure traces was accidentally destroyed during developing.

Table VI. Arch Deflections[a] Due to Static Loading — 3D-15A

Load (psi)	Deflection 1, South Footing (in.)	Deflection 2, Crown (in.)	Deflection 3, North Footing (in.)	Deflection 4, $\theta = 8^{\circ}$ (in.)
1	0.0059	0.0097	0.0062	0.0020
2	0.0117	0.0322	0.0124	0.0054
3	0.0235	0.0548	0.0248	0.0060
4	0.0294	0.0773	0.0310	0.0080

[a] Downward body deflections and inward arch deflections are taken as positive.

Table VII. Moments and Thrusts Due to Static Loading — 3D-15A

Over-pressure (psi)	$\theta = 5^{\circ}17'$		$\theta = 9^{\circ}44'$		$\theta = 15^{\circ}00'$		$\theta = 30^{\circ}00'$		$\theta = 90^{\circ}00'$	
	Moment (in.-lb)	Thrust (lb)	Moment (in.-lb)	Thrust (lb)	Moment (in.-lb)	Thrust (lb)	Moment (in.-lb)	Thrust (lb)	Moment (in.-lb)	Thrust (lb)
1	+0.364	-0.14	+0.954	-3.58	+0.0504	-4.90	+0.0901	-8.48	+0.0041	-11.70
2	+0.931	-8.39	+0.219	-13.50	+0.0668	-16.85	+0.186	-21.90	-0.204	-2.47
3	+1.46	-25.95	+0.293	-25.50	+0.0552	-29.50	+0.270	-36.70	-0.292	-6.81
4	+1.97	-36.60	+0.332	-37.40	+0.0435	-42.20	+0.372	-49.40	-0.370	-9.67

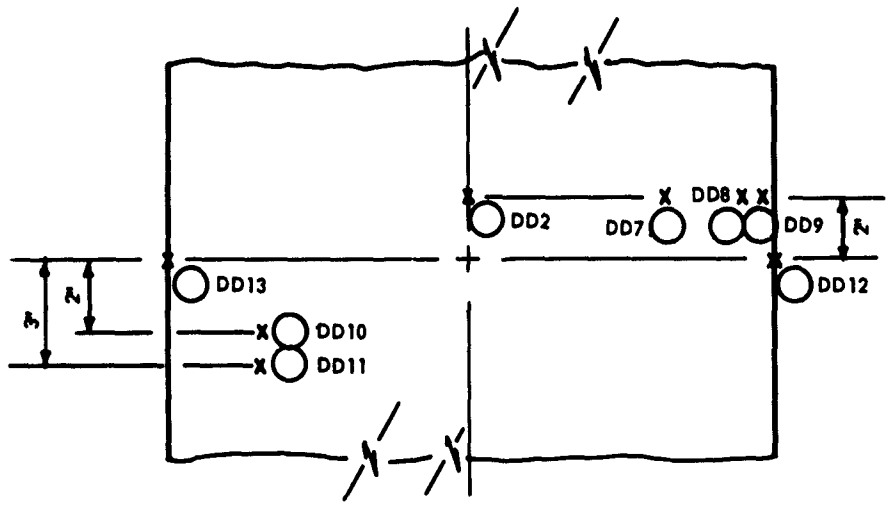

Plan View

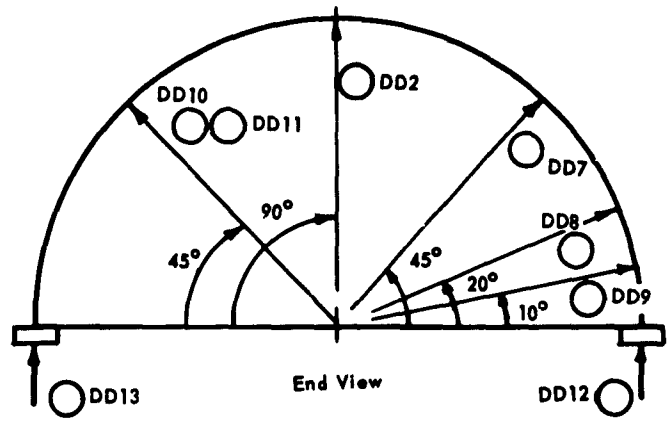

End View

Note: All deflections are absolute with the exception of deflection 11, which is with respect to the metal box. Strain gages were positioned the same as in the Series II tests. In addition, strain gages 11 and 12 were placed at the 12.3° point on the right-hand side of the arch.

Figure 12. Ames deflection dial locations — Dead-load test.

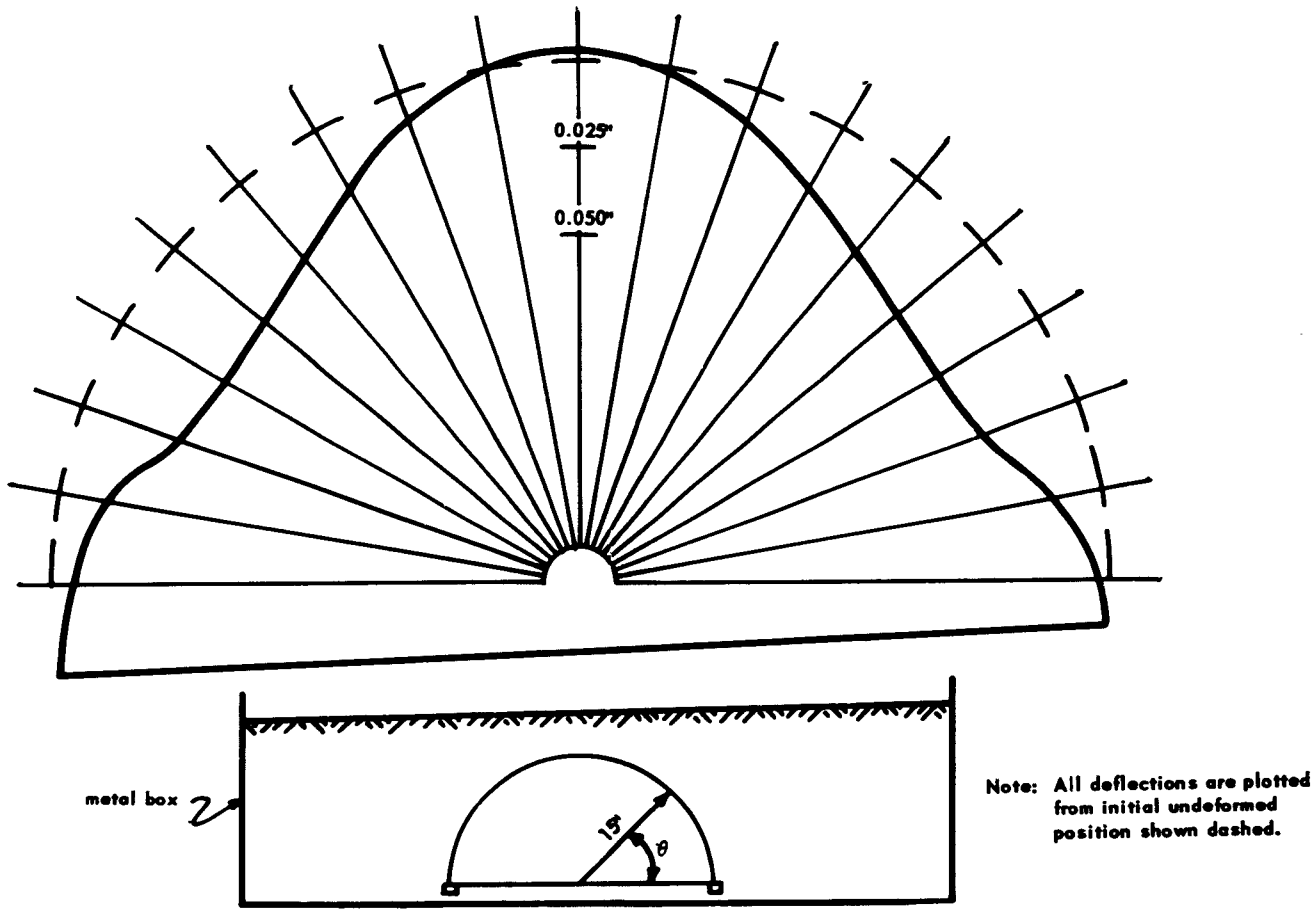

Figure 13. Arch deflection due to dead load.

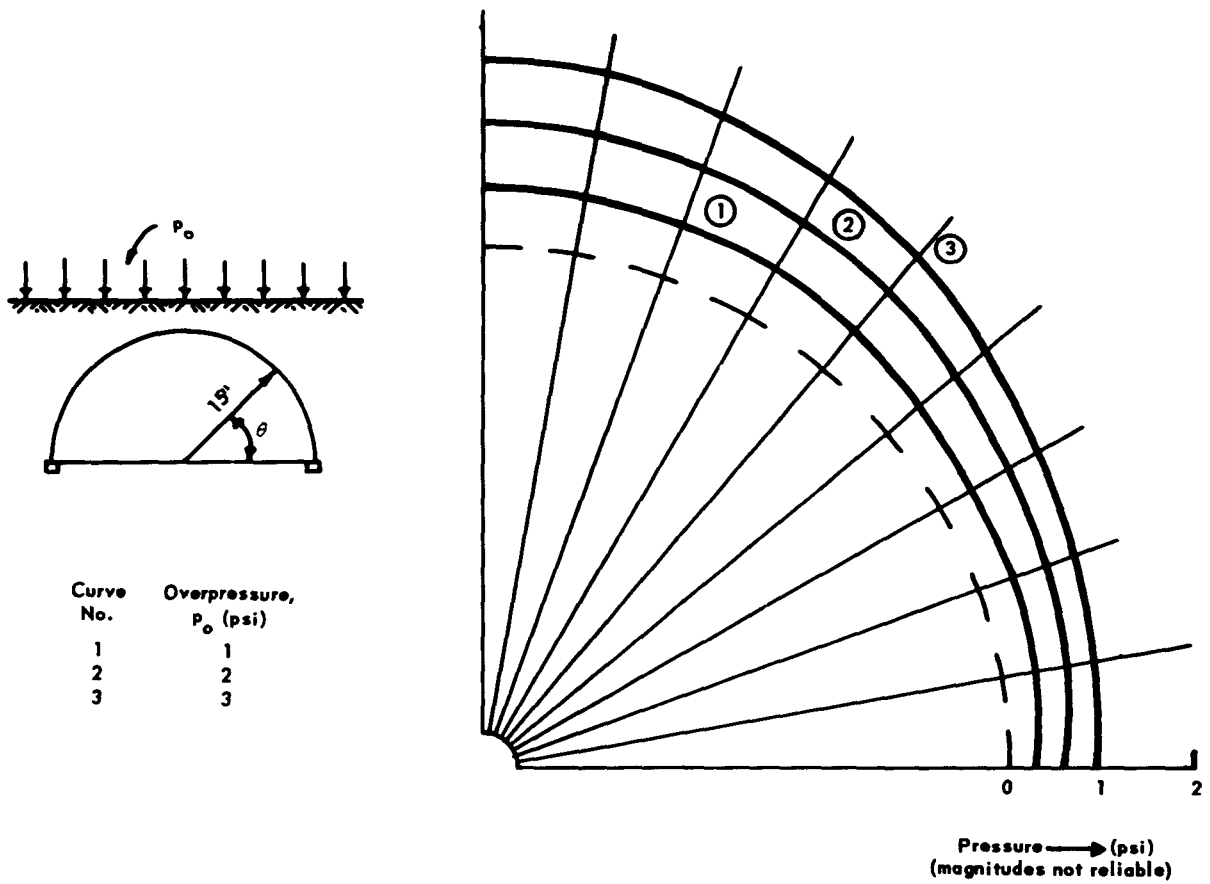

Figure 14. Interface pressure distribution for static loading — 3D-15A.

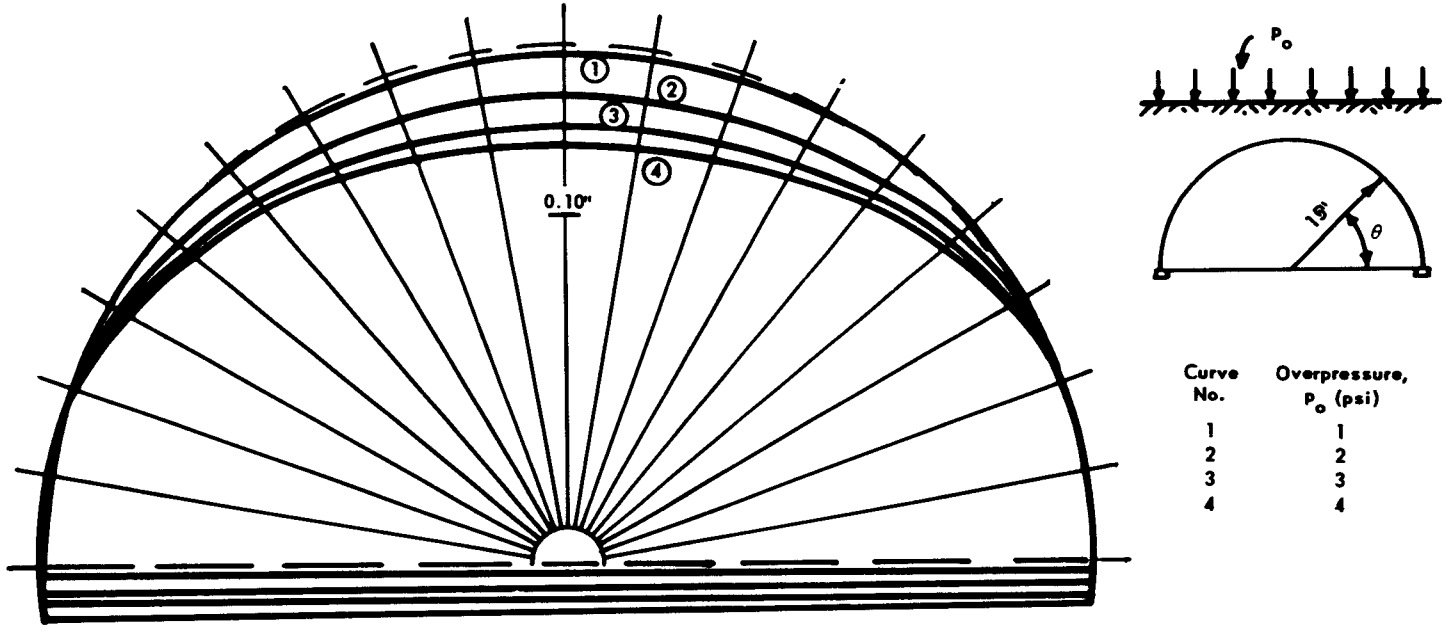

Figure 15. Arch deflections due to static loading — 3D-15A.

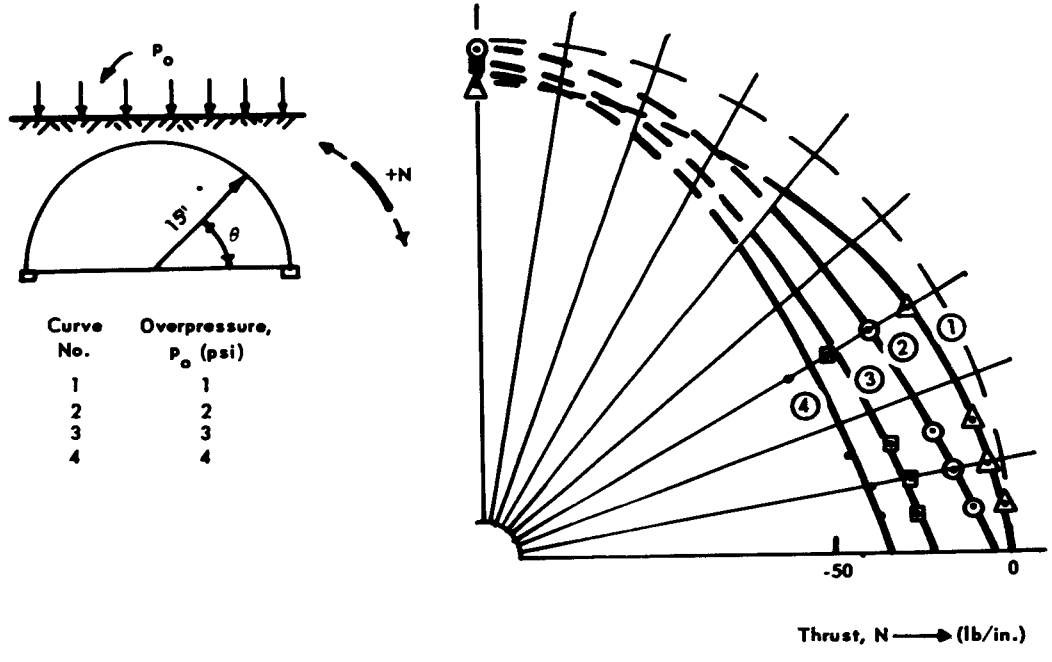

Figure 16. Thrust due to static loading — 3D-15A.

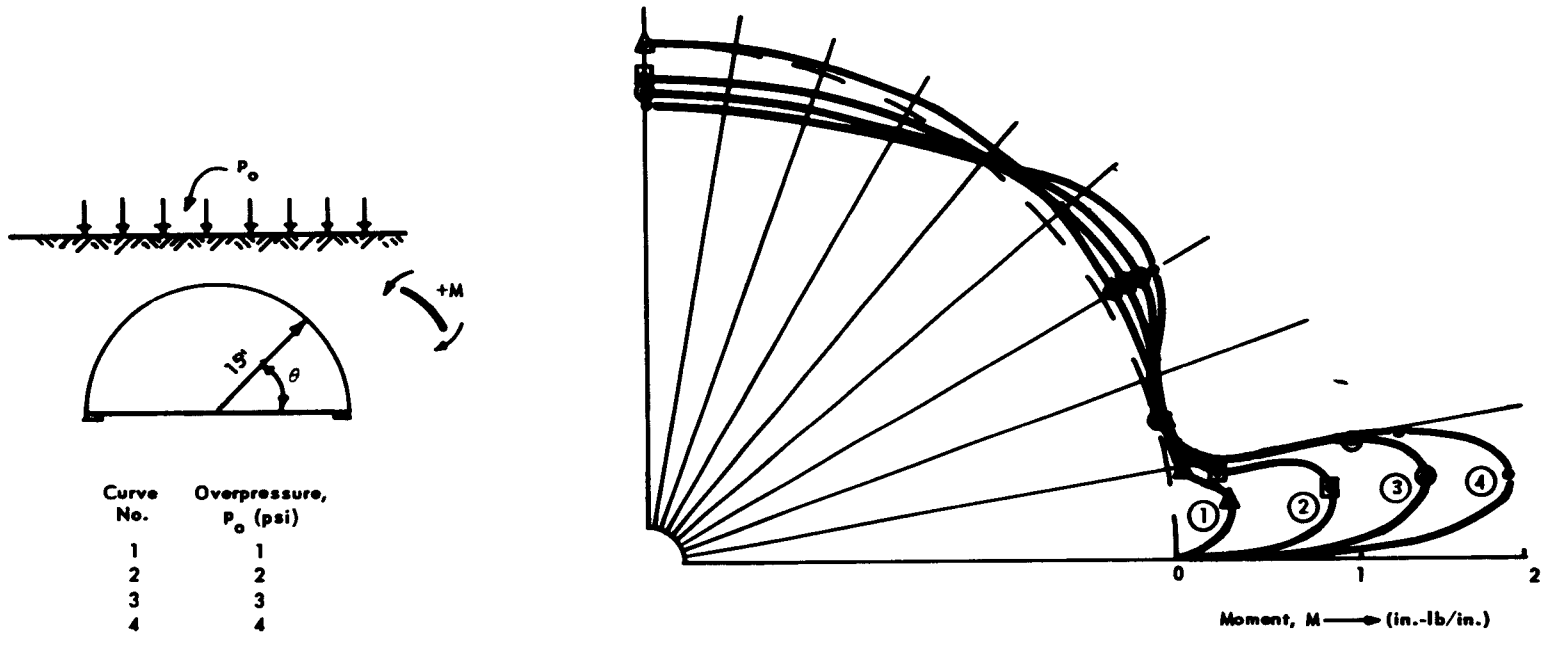

Figure 17. Moment due to static loading — 3D-15A.

As the pressure was applied to the surface, the arch moved downward as shown by the deflection patterns, Figure 15. The left footing, as viewed in Figure 15, moved downward slightly more than the right footing. With that exception, the deflections were symmetrical with respect to a vertical axis through the crown of the arch.

The moments induced by the static loading are shown in Figure 17. These moments, which are also listed in Table VI, do not include the dead-load moment. The moment distribution shown is different from the expected distribution, but careful checks on the instrumentation and data reduction, plus a similar distribution in two separate series of dynamic tests lends credence to the results. Subsequent theoretical study indicates that the moment distribution in thin arches is very sensitive to the initial deformation due to backfilling. Evidently positive or negative moments are possible in the vicinity of the springline. The moment distribution could have been influenced to some extent by friction in the piano hinges used to obtain a pinned base, but this influence was probably small. (Hinges were brazed to the sheet metal of the arch which provided added stiffness 1/2 inch up from the springline. It is expected that some moment-restraint was provided by the hinges although this is not indicated on any of the moment diagrams.)

The noted shape of the moment curve is also attributable to the deformations which occur in a flexible arch with footings which are restrained against lateral motion. Certainly the significance of the occurrence of the maximum moment at 5 degrees from the springline is exceedingly important in design. The moment there was 5 times larger than any other moment in the arch and, since it is so highly localized, designing and fabricating this section for high moment would be a relatively simple and inexpensive operation.

Observing that the moment increases from a small value at the springline to a maximum at 5 degrees, returns to a small value at the 10-degree point, and remains small to the 20-degree point provides a clue to a reasonable method of predicting the buckling load of the arch. The clue is further evinced by the buckling in the model described in Appendix C, the deflection curve of Figure 13 from the dead-load tests, and the distribution of active- and passive-sense pressures, Figure 18. To expatiate: a uniformly loaded "equivalent arch" is assumed with an included angle of 20 degrees; this corresponds to buckling in the fourth inextensional symmetrical mode. The static buckling load is found from[21]

$$p_{cr} = \frac{EI}{(1 - \nu^2) r^3} \left(\frac{\pi^2}{\alpha^2} - 1 \right) \qquad (2)$$

where p_{cr} = critical buckling load

ν = Poisson's ratio

α = one-half of the included angle between the springlines

For the arch tested, p_{cr} = 27.9 psi. Assuming as discussed later in the report, that 35 percent of the surface load would be carried by arching, the static surface pressure to produce buckling is estimated as

$$p_{s_{cr}} = \frac{27.9}{1.00 - 0.35} = 43 \text{ psi} \qquad (3)$$

The distribution of thrust induced by the static load is shown in Figure 16. The accuracy of the thrust data is poor at low loads because thrust is determined from the numerical difference of relatively small strains. As a consequence, the thrust curves of Figure 16 are of questionable accuracy at the lower loads and in the vicinity of the crown. The accuracy of the data is discussed further in the section on deficiencies of the work. Eventually it is intended to compute the thrusts and moments based upon measured interface loading for comparison with the experimental values.

The thrust distribution in Figure 16 is different from what was expected, but the peak thrusts at the various pressure levels are close to the values determined by assuming a radial loading of magnitude equal to the average interface overpressure. The values of thrust at the 5°17' point, Table VII, were used to compute the arching through the soil as described later in the report.

Dynamic Tests

General. Because of the large quantity of data accumulated, only the records for tests 3D-6B (a long-duration loading) and 3D-6D (a short-duration loading) of Series I were reduced completely. Pertinent pressures and deflections were reduced, however, for other tests of this series. The data is presented in Tables VIII and IX. All of the records for the Series II tests were reduced and the data are summarized in Tables X, XI, and XII. Traces of pertinent portions of typical oscillograms are included as Figures E-1 through E-5 in Appendix E. With few exceptions the boundary and free-field pressure results were not intelligible for the dynamic tests and, consequently, the results of these records are not tabulated.

In reducing the data, zero time was taken as the time at which the pressure wave impinged upon the soil surface.

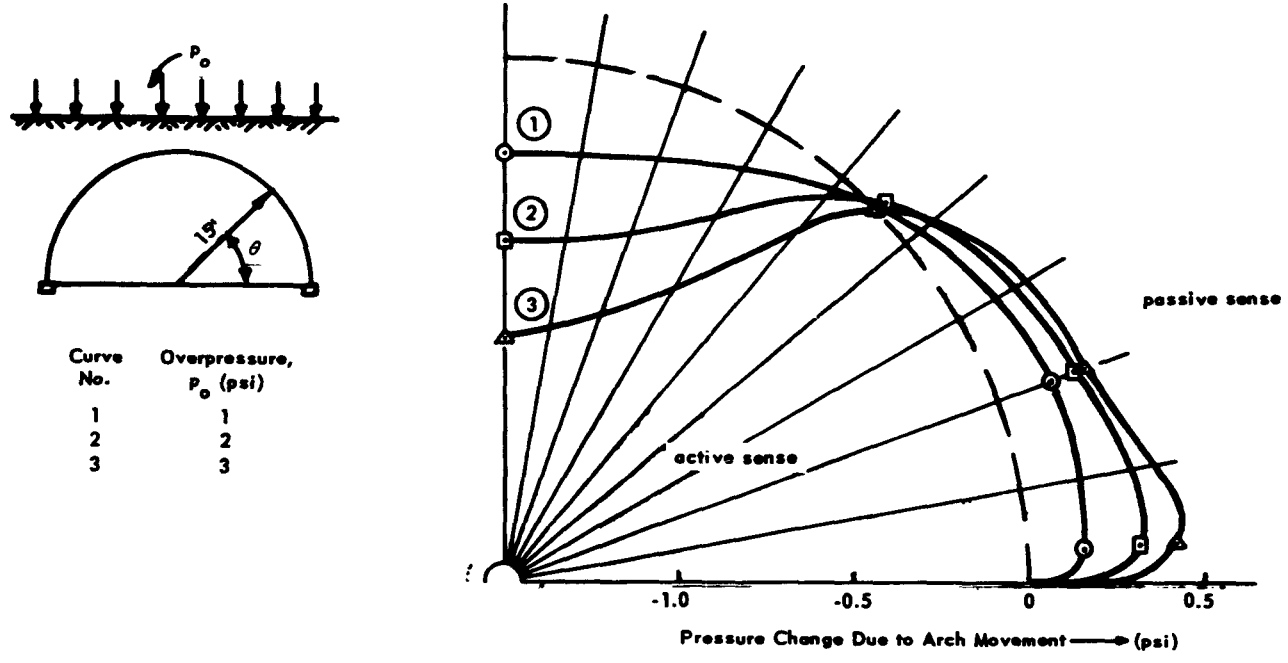

Figure 18. Distribution of active- and passive-sense pressures due to static loading — 3D-15A.

Table VIII. Dynamic Test Results — Series I

Test No.	Peak Surface Overpressure (psi)	Peak Crown Pressure (psi)	Times				Ratio, Peak Crown Pressure to Peak Overpressure	Surface Overpressure at t_b (psi)	Ratio, Overpressure at t_b to Peak Overpressure	Remarks
			Effective Decay (msec)	Rise (msec)	Maximum Response at Crown (msec)	Peak at Crown, t_b [a] (msec)				
6A	7.5	5.3	76	4	15	13	0.707	6.1	0.813	1st loading of system
6B	7.5	5.7	108	6	15	7	0.706	7.2	0.961	
6C	7.9	6.2	98	4	15	9	0.785	7.3	0.923	
6D	6.0	5.8	28	4	11	8	0.967	4.4	0.733	1st short-duration load
6E	6.5	9.0	47	6	13	9	1.385	5.6	0.862	Medium-duration load
6F	7.5	8.9	66	6	13	10	1.188	7.1	0.948	
7A	10.9	8.1	520	6	12	11	0.743	10.8	0.990	
7B	10.1	8.1	770	4	13	12	0.802	10.1	1.000	
7C	11.0	7.9	220	5	13	13	0.718	10.7	0.973	
7D	10.0	6.8	33	6	13	14	0.670	8.1	0.810	Short-duration load
7E	10.3	12.0	43	7	12	15	1.065	10.3	1.000 (?) [b]	Medium-duration load
8	24.0	20.3				—	0.846			

[a] t_b = time at which pressure reaches a maximum on the crown of the arch.

[b] (?) = results questionable.

Table IX. Deflections From Series I Dynamic Tests

Test No.	Peak Defl. South Footing, Deflection 1 (in.)	Peak Defl. North Footing, Deflection 3 (in.)	Peak Crown Deflection, Deflection 2 (in.)	Residual So. Footing Defl. (in.)	Cumulative (in.)	Residual No. Footing Defl. (in.)	Cumulative (in.)	Residual Crown Defl. (in.)	Cumulative (in.)
6A	0.137	0.126	0.172	0.098	0.098	0.094	0.094	0.127	0.127
6B	0.075	0.079	0.121	0.056	0.154	0.057	0.151	0.046	0.173
6C	0.060	0.076	0.110	0.042	0.196	0.044	0.195	0.044	0.217
6D	0.040	0.048	0.085	0.000	0.381	0.000	0.394	-0.019	0.377
6E	0.047	0.065	0.116	0.012	0.428	0.023	0.461	0.022	0.440
6F	0.054	0.052	0.114	0.018	0.493	0.016	0.526	0.019	0.501
7A	0.103	0.136	0.138	0.071	0.267	0.084	0.279	0.078	0.295
7B	0.099	0.102	0.143	0.064	0.331	0.058	0.337	0.047	0.344
7C	0.085	0.095	0.156	0.050	0.381	0.057	0.394	0.052	0.396
7D	0.078	0.091	0.140	0.035	0.416	0.044	0.438	0.041	0.418
7E	0.076	0.104	0.157	0.047	0.475	0.044	0.510	0.042	0.482
8	0.233	0.278	0.383	-0.134	0.359	0.065	0.591	0.000	0.501

Table X. Dynamic Test Results — Series II

Test No.	Peak Surface Overpressure (psi)	Peak Crown Pressure (psi)	Times				Ratio, Peak Crown Pressure to Peak Overpressure	Surface Overpressure at t_b (psi)	Ratio, Overpressure at t_b to Peak Overpressure	Remarks
			Effective Decay (msec)	Rise (msec)	Maximum Response at Crown (msec)	Peak at Crown t_b [a] (msec)				
11A	6.42	5.36	24	1	19	6	0.835	5.25	0.818	1st test short duration
11B	5.61	2.89	28	1	20	8	0.516	5.49	0.979	short duration
12A	5.43	2.37	160	1	20	6	0.437	4.03	0.742	1st test long duration
12B	7.06	2.62	129	2	20	7	0.371	5.16	0.731	long duration
13A	12.20	3.87	174	2	20	6	0.317	9.52	0.780	long duration
13B	14.80	4.18	110	2	20	5	0.282	11.60	0.784	long duration
13C	22.50	7.54	154	2	20	6	0.335	16.30	0.725	long duration
14A	8.18	3.95	21	2	20	6	0.483	6.96	0.851	short duration

[a] t_b = time at which pressure reaches a maximum on the crown of the arch.

Table XI. Deflections From Series II Dynamic Tests

Test No.	Peak Defl. South Footing, Deflection 1 (in.)	Peak Defl. North Footing, Deflection 3 (in.)	Peak Crown Deflection, Deflection 2 (in.)	Residual So. Footing Defl. (in.)	Cumulative (in.)	Residual No. Footing Defl. (in.)	Cumulative (in.)	Residual Crown Defl. (in.)	Cumulative (in.)
11A	0.126	0.135	0.226	0.114	0.114	0.116	0.116	0.1344	0.1344
11B	0.0905	0.0995	0.203	0.0701	0.1841	0.0684	0.1844	0.0708	0.2052
12A	0.0624	0.0795	0.15o	0.0475	0.2316	0.0531	0.2375	0.0795	0.2847
12B	0.0584	0.0708	0.1296	0.0438	0.2754	0.0431	0.2806	0.0454	0.3301
13A	0.1075	0.141	0.266	0.0814	0.3568	0.110	0.3906	0.138	0.4681
13B	0.137	0.211	0.358	0.1105	0.4673	0.176	0.5666	0.183	0.6511
13C	0.200	0.350	0.643	0.162	0.6293	0.304	0.8706	0.322	0.9731
14A	0.0524	0.088	0.167	0.0408	0.6701	0.0565	0.9271	0.0257	0.9988

Table XII. Peak Strains in Arch — Series II

Test No.	Peak Over-pressure p_o (psi)	Strains (μ in./in.)									
		SG 1	SG 2	SG 3	SG 4	SG 5	SG 6	SG 7	SG 8	SG 9	SG 10
11A	6.42	-66.4	+58.6	-39.4	-56.1	-56.1	-184.5	+73.0	-142.0	+203.0	-231.0
11B	5.60	-125.0	+115.5	-59.7	-69.4	-38.1	-179.5	-90.6	-132.4	+216.4	-267.0
12A	5.43	-111.0	+59.6	-43.3	-65.0	-34.5	-110.4	-56.7	-83.7	+129.0	-281.0
12B	7.06	-114.5	+43.0	-53.3	-84.6	-57.7	-115.5	-85.0	-74.1	+126.0	-291.0
13A	12.20	-150.4	+98.6	-76.7	-169.0	-123.0	-81.4	-167.6	-95.6	+185.6	-412.0
13B	14.80	-179.8	+128.0	-93.8	-210.0	-137.4	-136.4	-97.8	-83.4	+335.0	-501.0
13C	22.50	-350.0	+252.0	-96.7	-277.0	-210.5	-178.5	-134.0	-199.0	+533.0	-759.0
14A	8.18	-111.5	+86.0	-34.2	-150.8	-93.0	-50.1	-15.7	-138.5	+282.0	-420.5

Surface Pressure. Pressure-time curves for long- and short-duration loads are shown in Figures 19 and 20. The surface pressures were oscillatory during the first 10 milliseconds for long-duration loading but approximated the ideal blast pressure versus time curve thereafter. The irregularities in the initial portion of the traces were undoubtedly caused by reflections from the walls of the chamber which confined the pressure.

In determining the peak overpressure, a smooth curve was drawn through the mean of the perturbations as shown by the dashed line in Figure 19. The intersection of the mean line with the initial rise of the trace was taken as the peak pressure. This procedure is justified since the period of the perturbations was short in comparison with the lowest natural period of the arch; implying, of course, that the arch will not sense the perturbations but only their mean value. Overpressures 1 and 2, (Figure 8), gave the same results as overpressure 3 except for expected differences in the time of initial movement and rise time. These differences were directly attributable to the respective locations of the gages, and to unlike perturbations during the first 5 to 10 milliseconds. Because of the marked similarity, only the data from overpressure 3 is given for the Series II tests. For the Series I tests the pressure-time data is taken from gage 2 because records for gage 3 were not obtained due to faulty wiring.

Control of the peak surface pressure was not as good as is generally attainable in the simulator. This is evident on comparison of the programmed pressures in the test schedule, Tables III and IV, and the measured peak pressures from Tables VIII and X. Actual peak pressures were on the order of 0.5 to 1 psi higher than programmed. The difficulty in maintaining control was due to the large volume of the chamber and the consequent greater influence of ambient temperature, and to the small pressures used. (Normally the simulator is operated in the range of 35 to 185 psi rather than the 5 to 25 psi generated in these tests.) Fortunately, it was not critical to the results of the tests that the precise programmed pressures be obtained.

The rise time and the effective decay time of the surface pressure, given in Tables VIII and X, were reasonably consistent for loadings of a given magnitude and type. The rise time was 4 to 6 milliseconds for the Series I tests and 1 to 2 milliseconds for the Series II tests. The difference in indicated rise time is because overpressure gage 2 was used in the Series I tests. Actually, the rise time at the surface above the arch was probably 1 to 2 milliseconds for the Series I tests also.

The effective decay time is determined from the intersection of the base line of the best straight-line fit of the pressure-time curve between the initial peak and the time of maximum displacement at the crown of the arch. Obviously, the effective decay time is sensitive to small variations in the initial shape of the pressure-time trace and, therefore, varies through quite a wide range.

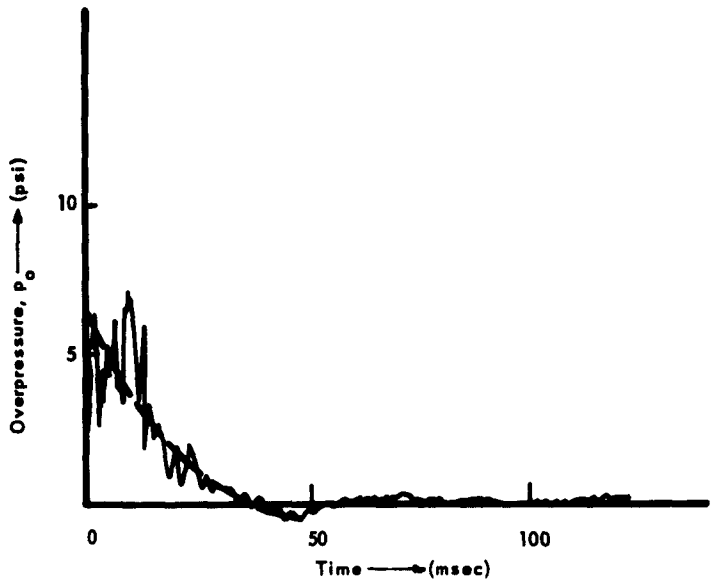

Figure 19. Overpressure-time curve for short-duration loading — 3D-11B.

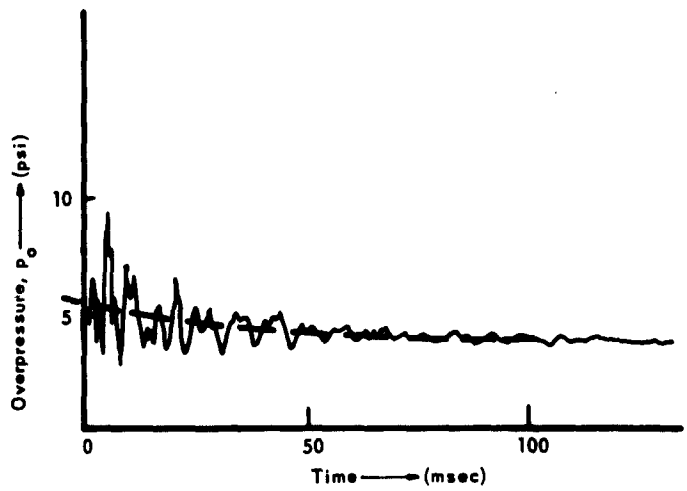

Figure 20. Overpressure-time curve for long-duration loading — 3D-12A.

Soil-Field Pressure. As the air pressure wave impinged on the surface, a stress wave was induced in the soil which was found to travel at an average velocity of 1300 feet per second. Two sets of gages were used to find the velocity, both of which provided the same results. In one case, overpressure 3 and accelerometer z were used; in the other, soil pressure cell h and soil pressure cell l were employed. The procedure, of course, was to divide the distance between a pair of gages by the time for the pressure wave to travel from one to the other.

At a velocity of 1300 feet per second, the stress wave requires approximately 11 milliseconds to travel from the bottom of the footings to the bottom of the pit and back. There is no distinct indication on pressure cell f or other gages of the appearance of the reflected wave. Thus, reflections from the pit boundaries do not appear to be a problem in conducting small-structure tests in the simulator. What happens in the way of dispersion, reflection, and decay of the wave is not known at present; however, this problem is being studied under another Laboratory task.

Traces from the pressure gages in the plates in the soil field were completely unintelligible and gave no information about the stress wave except time of arrival. Typical traces are included in the oscillogram of Figure E-1, Appendix E, in the event that their shape may eventually reveal something of significance.

Interface Pressure. Measurement of soil pressure has long plagued research workers as one of the most difficult of all instrumentation problems. The difficulties involved have been discussed by many investigators (e.g., Reference 22), and soil-pressure cells for static loads have been developed to meet special needs. To date, no universally satisfactory soil-structure or free-field soil-pressure gage has been made available, particularly for dynamic loading.

Still, in performing the small-structure studies, measurements of interface pressure were needed. It was decided, therefore, to attempt to get some information using fluid-pressure gages which possessed certain of the features desired of a soil-pressure gage; namely, the CEC 4-312 cell. The writers had no illusions about getting soil-pressure measurements of the correct magnitude from these gages, but it was hoped that the gages would at least indicate relative magnitudes of soil pressures at the various gage locations. It was recognized that arching of the soil might be slightly different across each gage due to load and soil placement. Nevertheless, it was hoped that some indication of pressure distribution around the arch could be obtained.

The results of the pressure measurements were disappointing in that there was obviously a different amount of arching across each gage face and the amount of arching across a given gage face varied from one test setup to the next. The interface

gages did serve to show the arrival of the soil-stress wave at a given location, and within a given test series (for a given test setup) the magnitude of the pressure readings were proportionately consistent. This is evident from observing the ratios of peak crown pressure to peak overpressure for various groups of tests. For example, tests 6A, 6B, and 6C, which were all long-duration loadings at about the same pressure, gave an average ratio of 0.733 with a variation from 0.706 to 0.785. Similar consistency was observable for other corresponding groups, with a few conspicuous anomalies such as test 6F.

Corresponding results from Series II gave ratios of peak crown pressure to peak surface overpressure of about one-half that of the Series I tests. Evidently, the pressure which is sensed by these gages is a function of the manner in which the sand is placed initially over the face of the gage. From a fundamental point of view, gages which operate on the diaphragm principle probably cannot be expected to give true soil pressures, since arching will always develop across the face of the gage.

Even though the indicated relative magnitude of the interface pressure readings cannot be guaranteed to be the same from one gage to the next, it is interesting to examine the distributions measured. The interface pressure distribution for test 3D-6B is shown in Figure 21 at times of 3, 5, 7, and 33 milliseconds and has a peak magnitude at the crown of 5.7 psi. Corresponding distributions of pressure were obtained from other loadings. A similar space-time variation of pressure also was obtained from Operation Plumbbob Structure 3.1n,[23] which was a reinforced concrete arch buried with 5 feet of cover over the crown.

Pressure distributions for other of the Series I tests and for the Series II tests are not given because of doubt as to the validity of the pressure measurements. In general, however, the curves showed consistency of form for corresponding load groups. An abrupt change in the distribution occurred between tests 13B and 13C; that is, between a load of 14.8-psi and 22.5-psi surface pressure. The reasons for this disturbance are not yet known.

Indications are that the peak load on the crown is greater for short-duration loads than for long-duration loads. This may be seen by comparing the ratios of the pressure on the crown to the pressure at the surface from tests 11B and 12A or from 6D and 6E with 6A, 6B, and 6C in Tables VIII and X. Pressures from tests 7B and 7D do not confirm these results; however, as will be shown, the moments do.

The shape of the pressure-time traces at various locations around the arch may be observed from the oscillograms, Figures E-1 and E-2 in Appendix E. The relative shapes from one gage to another should be indicative of the interaction influences at these locations. However, experience with soil-pressure gages tested at the U. S. Army Ballistics Research Laboratory has shown that the shape of the unloading curve is a function of the stiffness of the pressure-measuring gage, therefore not too much faith can be placed even in these indications.

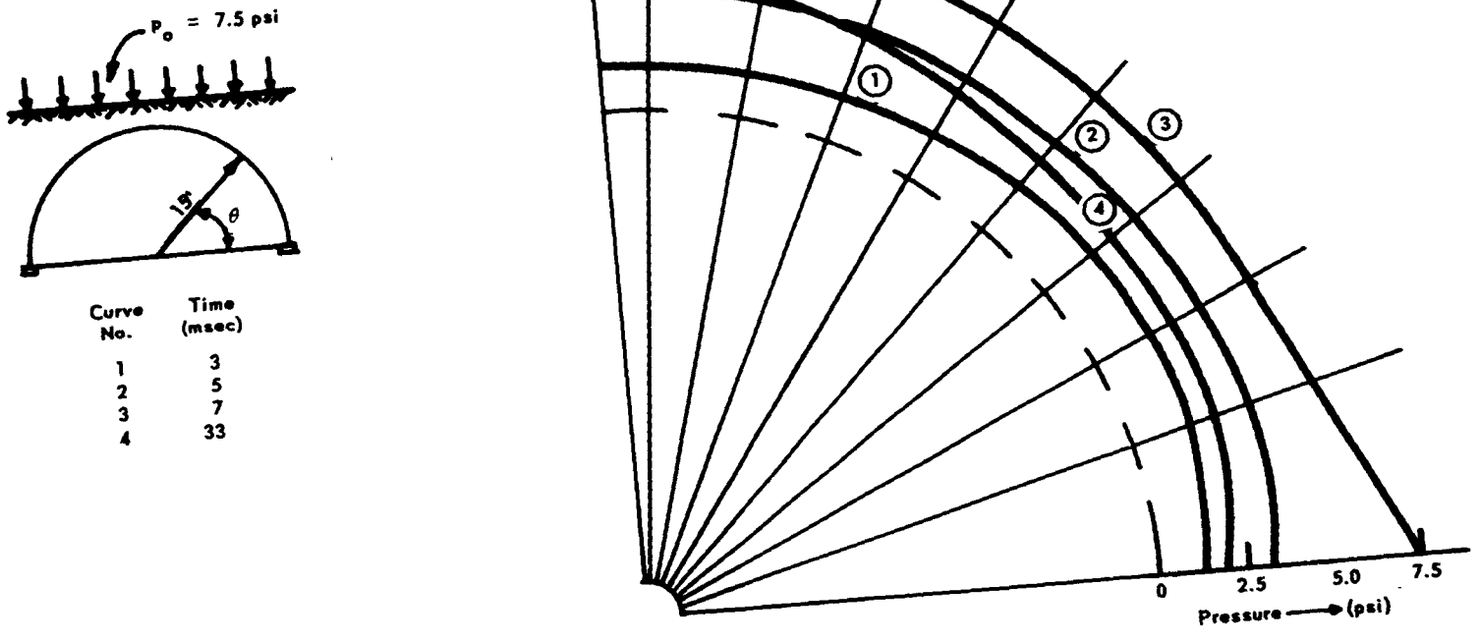

Figure 21. Interface pressure distribution for long-duration loading — 3D-6B.

Though the magnitudes of the pressure readings are not reliable, the stiffness of the Type 4-113 gages is sufficient that the times should be correct. If so, why did it takes 6 milliseconds for the pressure on the crown to reach a maximum when the rise time of the pressure on the surface was only 1 to 2 milliseconds? Theoretically, the rise time should have been much less. Is the rise time a function of the stiffness of the gage or is the rise time actually 6 milliseconds? These questions cannot be answered as yet, and thus are dedicated to future studies.

Deflections. The behavior of the arch is most conveniently described by the deflection curves. Deflection patterns at various times for tests 3D-6B and 3D-6D are presented in Figures 22 and 23. Deflection patterns for the Series II tests are shown in Figures 24 through 26. The time variations of deflections at various points on the arch may be seen in the composite plot of Figure 27. Finally, peak loads versus peak deflections of the footing and crown from the Series I and Series II tests are plotted in Figures 28 and 29.

These deflection curves reveal that the fundamental action is a downward body motion of the entire structure into the soil upon which is superimposed the extensional and inextensional symmetrical mode deflections of the arch. From the deflection curves of test 3D-12B, Figure 27, whereon the free-field soil deflection at the elevation of the footing is plotted, it is seen that the crown commences to move downward, followed shortly by the footings. About 2 milliseconds later the stress wave in the soil reaches the elevation of the footings. As the crown moves downward, the 8-degree points on the sides move outward slightly and then move inward after the peak deflection of the crown has been reached. A similar action occurs at the 25-degree points, as is readily observed from the oscillogram traces of deflections 4 and 5 in Figures E-1 and E-2, Appendix E. A portion of the inward deflection is probably due to axial compression which results in radial deflections of the order of 0.0015 inch for a hydrostatic pressure of 10 psi. Tests at higher loadings did not produce precisely the same results. For example, in contrast to test 3D-12B, the deflection at the 8-degree point for test 3D-13A was initially outward to a magnitude 5 times that for 3D-12B, after which the deflection reduced rapidly to a small outward value. The sides did not move inward as for 3D-12B.

Peak deflection, as evidenced by the curves of Figures 28 and 29, is very much a function of soil density. The absolute peak crown deflections at the higher loads were much greater for the Series II tests than for the Series I tests. Curiously, the footings of the Series I tests acted as though they were bearing on an elastic solid, while those of the Series II tests behaved as though they were supported on visco-inelastic material. The difference probably was due to the difference in the density of the sand in the two series of tests and illustrates the relatively large difference in behavior which can result from relatively small differences in soil properties.

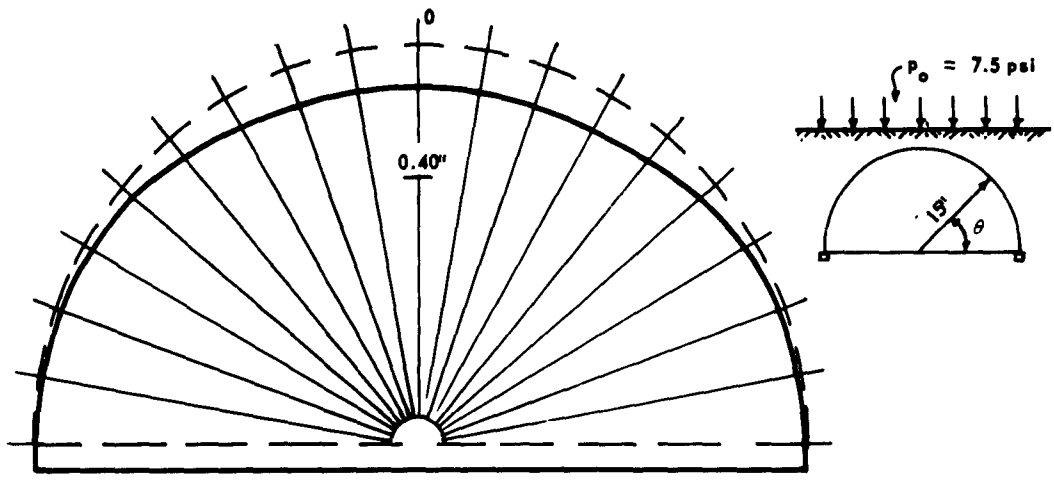

Figure 22. Peak arch deflections due to long-duration loading — 3D-6B.

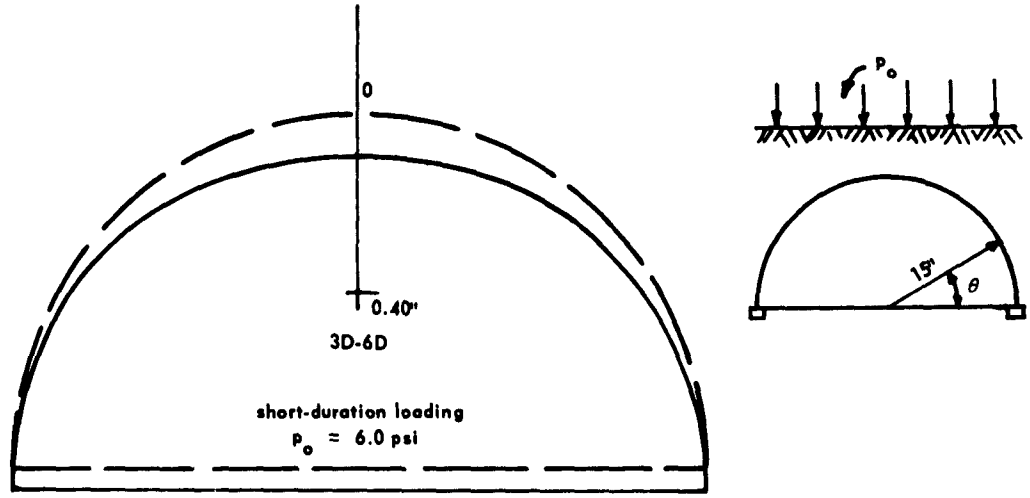

Figure 23. Peak arch deflections due to dynamic loading — 3D-6D.

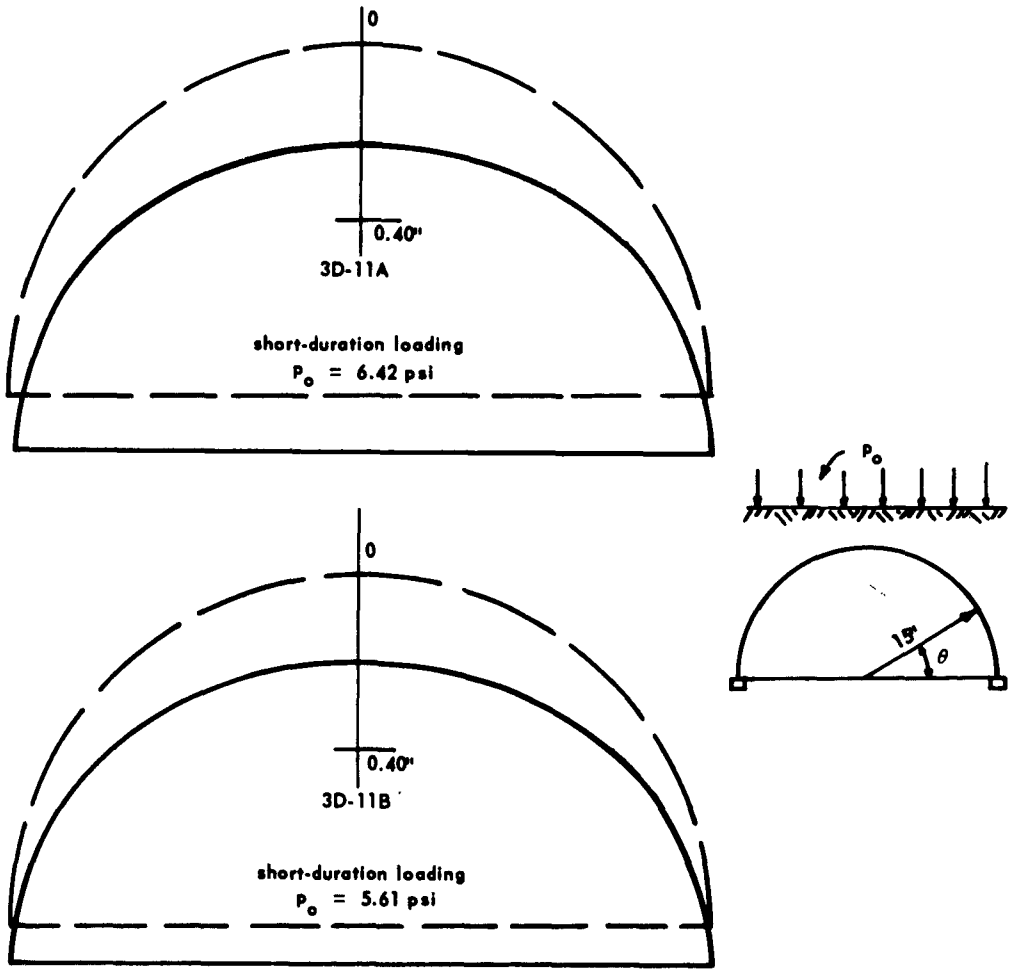

Figure 24. Peak arch deflections due to dynamic loading — 3D-11A, 3D-11B.

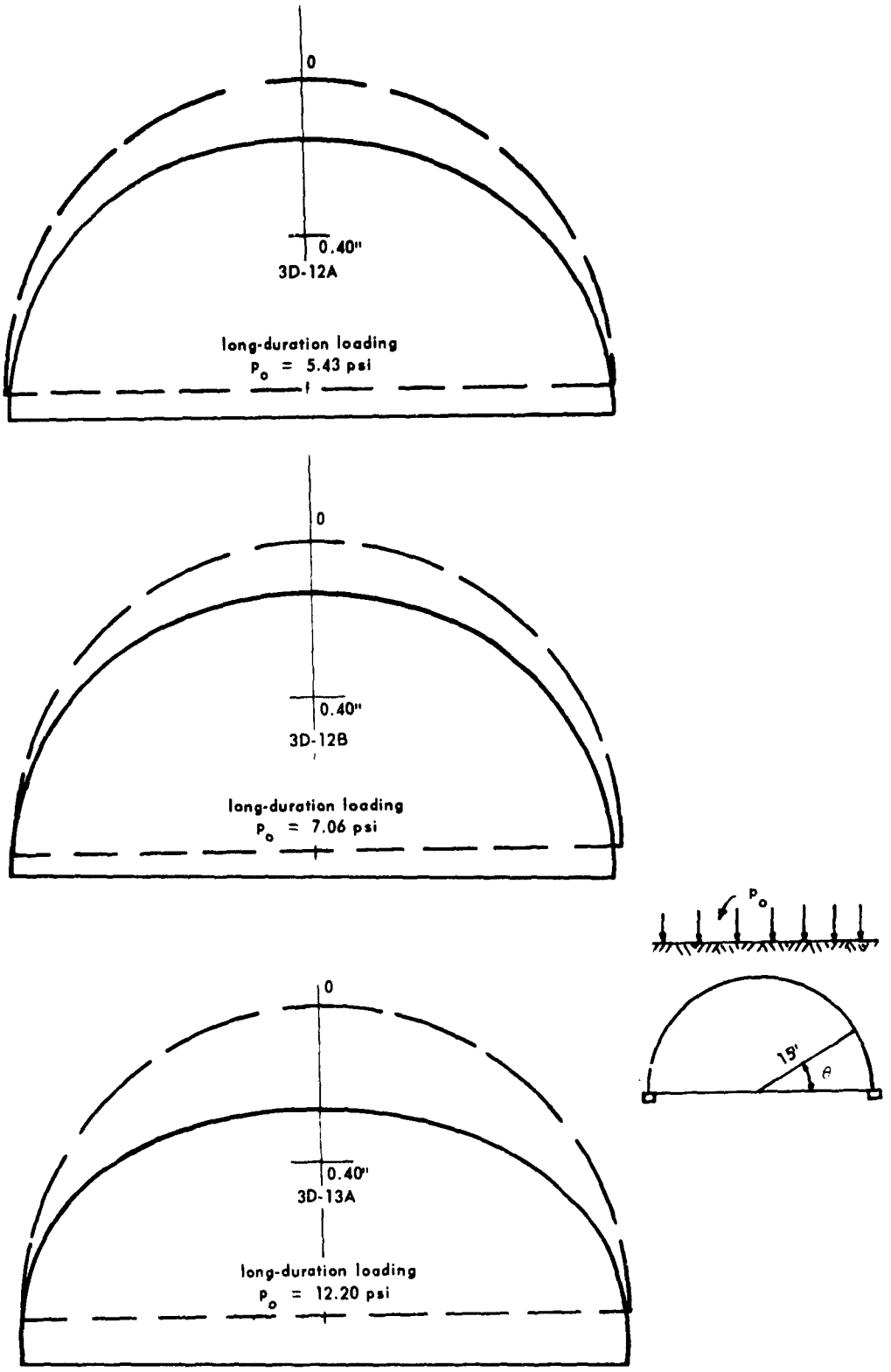

Figure 25. Peak arch deflections due to dynamic loading — 3D-12A, 3D-12B, 3D-13A.

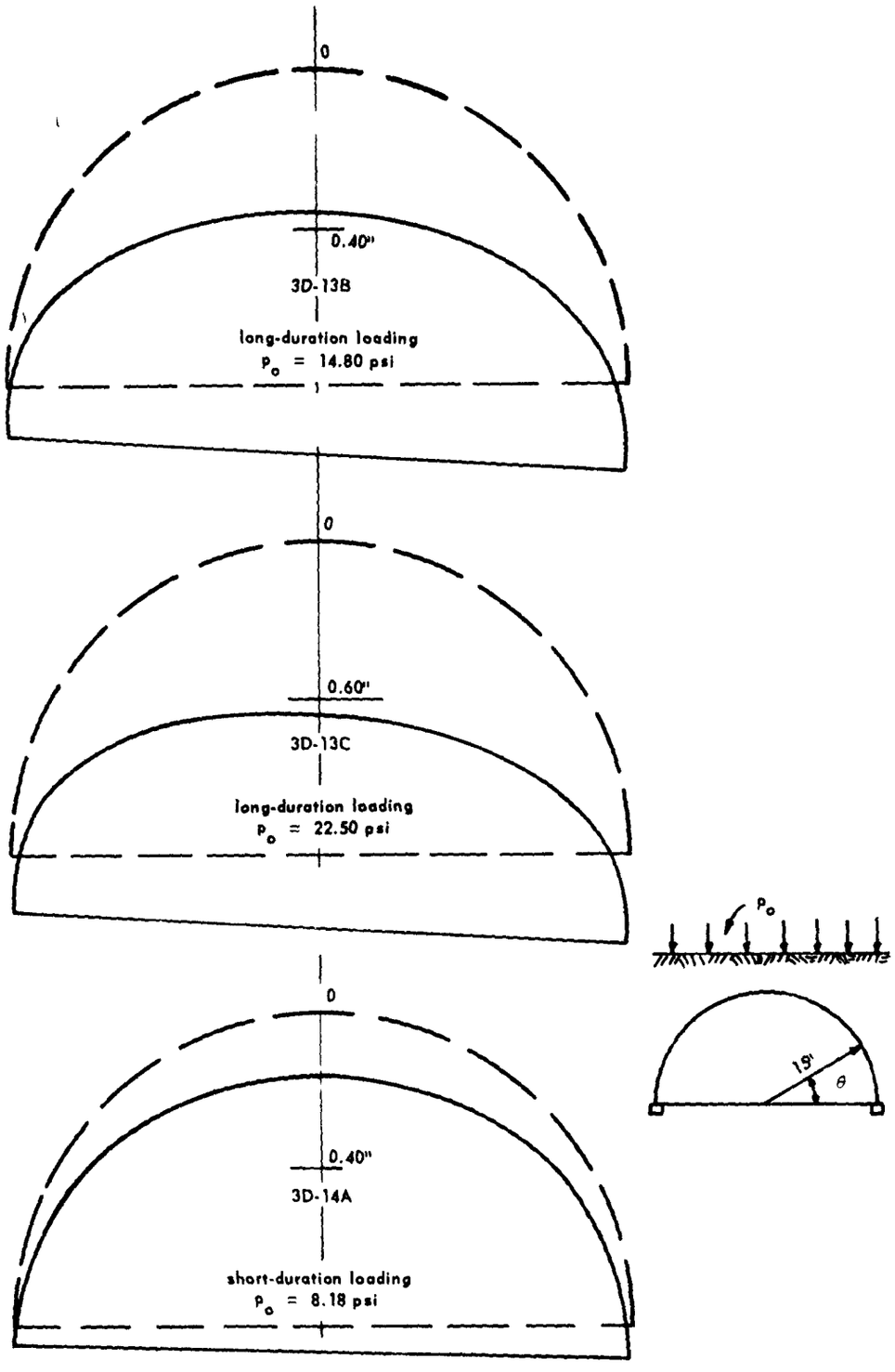

Figure 26. Peak arch deflections due to dynamic loading — 3D-13B, 3D-13C, 3D-14A.

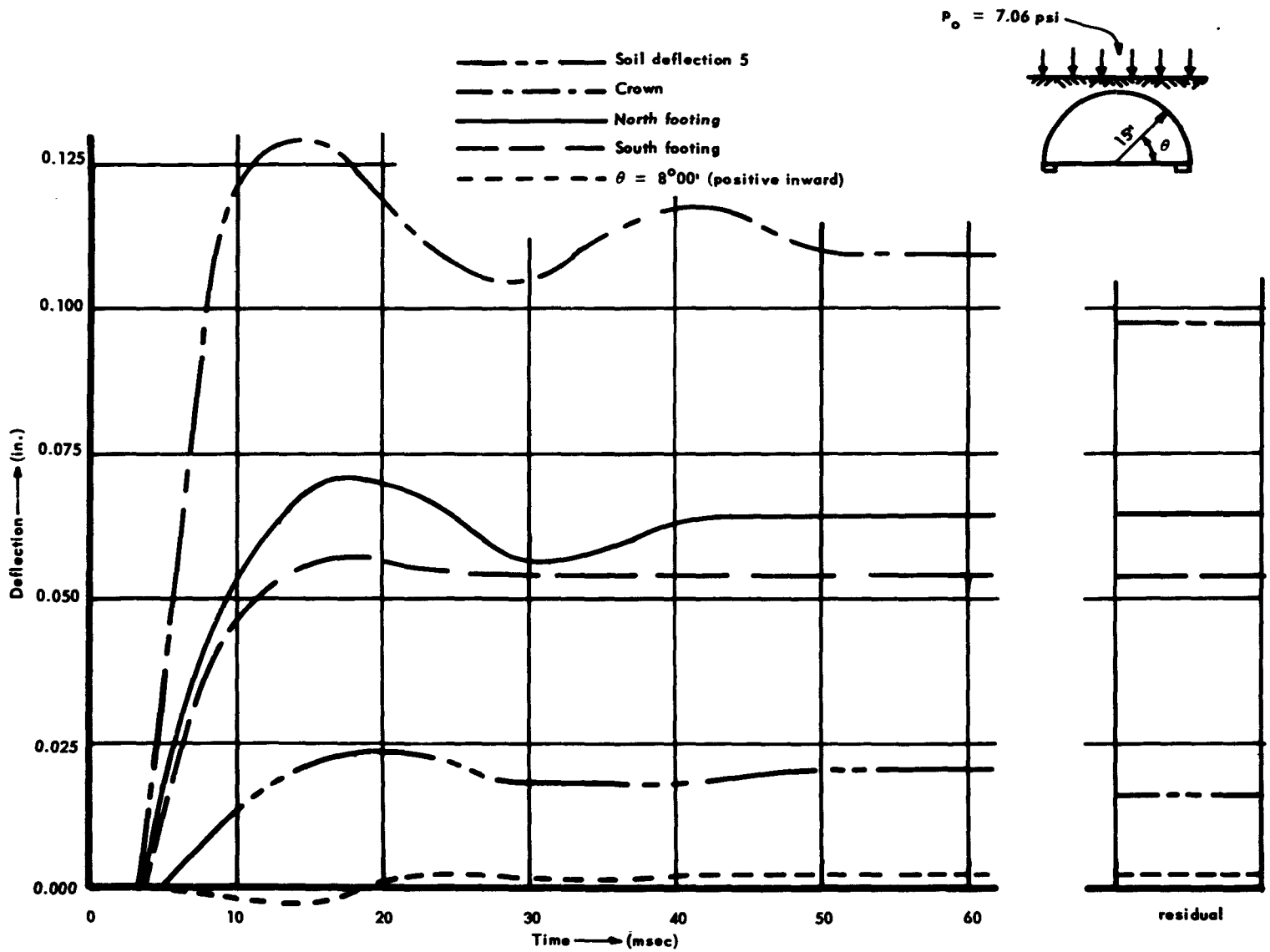

Figure 27. Arch and soil deflections vs time — 3D-12B.

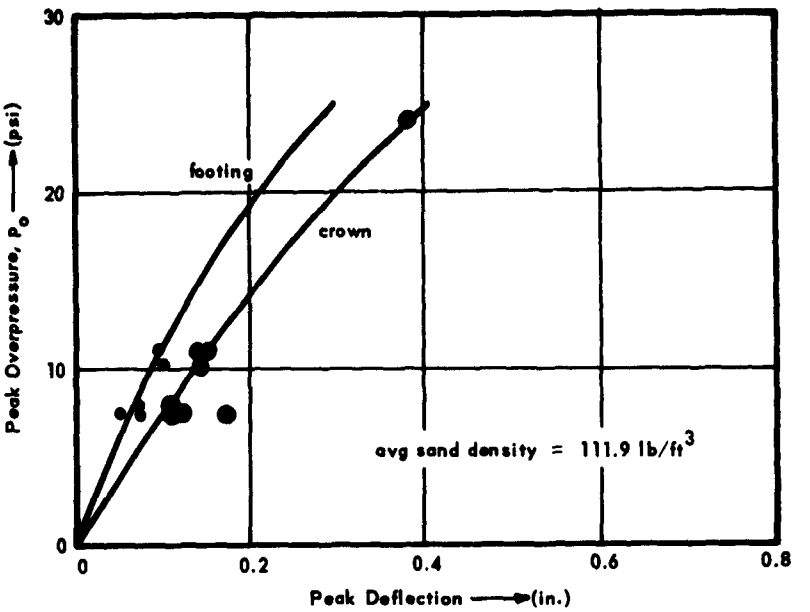

Figure 28. Peak deflections for long-duration loading — Series I.

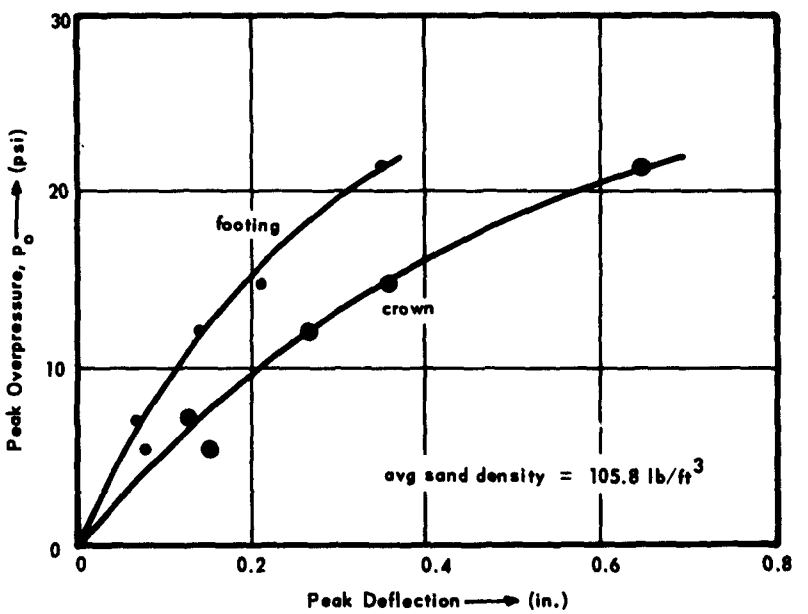

Figure 29. Peak deflections for long-duration loading — Series II.

Two further points of interest in regard to deflections experienced in the tests are: (1) that the deflection from the first loading was considerably greater than in subsequent tests, and (2) that with each successive loading at a given level, the peak deflection was less than at the preceding loading. The first point is illustrated by tests 3D-6A and 3D-6B and tests 3D-11A and 3D-11B. Both sets were loaded at about 6 psi, yet, in each case, the deflection from the first loading was 60 to 75 percent greater than the corresponding deflection from the second loading. The second point is illustrated by tests 3D-7A, 3D-7B, and 3D-7C, and tests 3D-11B and 3D-12A. For these groups, the peak deflection decreased on the order of 10 to 25 percent per additional loading for the load range of 6 to 11 psi.

In an inelastic material irreversible strains such as those encountered in the long-duration tests are expected. From Figure 30, the peak footing deflections are compared with the deflection of plates 5 and 6 in the free field. It is seen that the peak deflection of the footing and plates varied approximately linearly with load, and that the peak footing deflections are 2-1/2 times the peak deflection of plate 5, which was in the free field at the same elevation as the footings. A plot of the relative displacement between the footing and the soil free field for the Series II tests and the static test is shown in Figure 31.

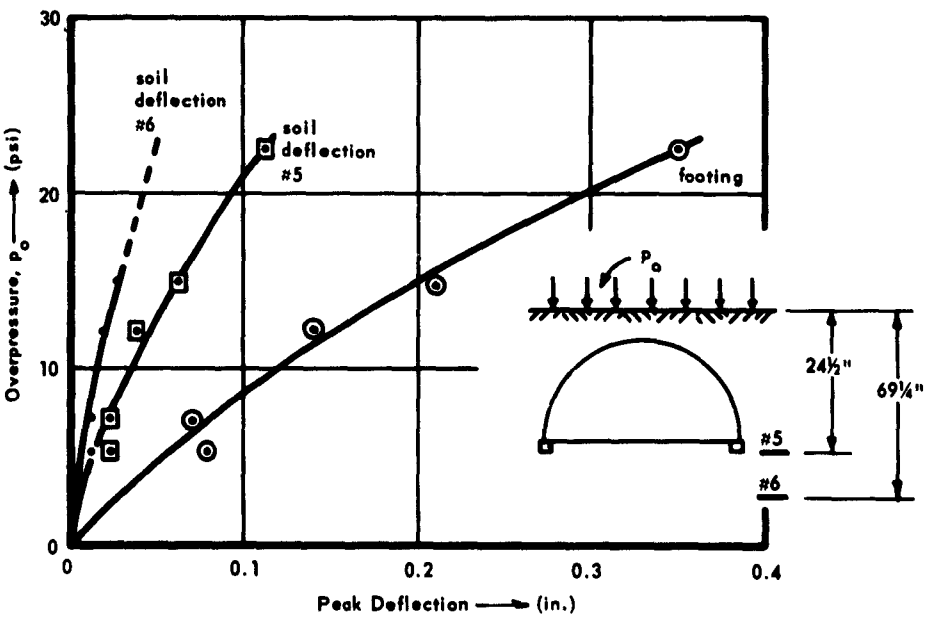

Figure 30. Peak deflections for long-duration loading — Series III.

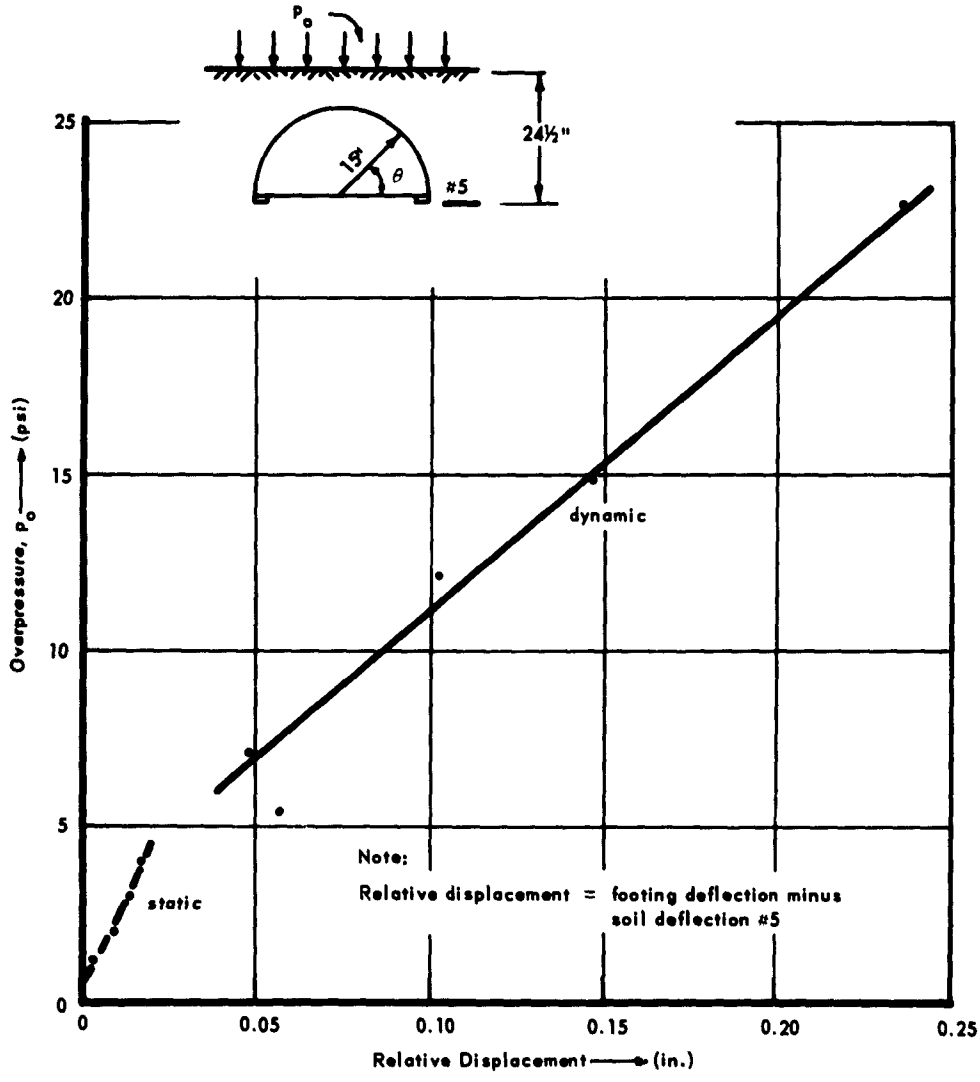

Figure 31. Relative footing displacement vs overpressure for static and long-duration dynamic loading — Series II.

Some elastic recovery does occur, as is seen from the plot of Figure 32. At the elevation of the footings, the elastic recovery of the soil in the free field was about 30 percent at the higher loads, but was less than 15 percent for the footings themselves.

The maximum deflection of the surface of the sand was not measured but was computed, by relating the deflections from deflection gages 5 and 6 back to the surface, with the following formula:[14]

$$d_{se} = d_{ye} + 2.4\left(\frac{P_o}{100}\right)\left(\frac{1000}{C_s}\right)^2 \frac{y}{100} \qquad (4)$$

where d_{se} = deflection at surface, inches

d_{ye} = deflection at some point below the surface, inches

p_o = overpressure, psi

C_s = seismic velocity, fps

y = depth below surface, inches

The results of the calculations are shown in Figures 33 and 34.

Among items yet to be studied are the influences of footing size and shape, load magnitude, and depth of burial on the behavior of dynamically loaded footings.

Moments and Thrusts. Moments, M, and thrusts, N, in the arch were computed from the relations

$$M = \frac{SE}{2}(\epsilon_a - \epsilon_b) \qquad (5)$$

$$N = \frac{AE}{2}(\epsilon_a + \epsilon_b) \qquad (6)$$

where ϵ_a = unit strain on the extrados at $\theta = \theta_a$

ϵ_b = unit strain on the intrados at $\theta = \theta_a$

A = area of longitudinal section of arch

S = section modulus of longitudinal section of arch

The accuracy of the thrust and moment depends upon the accuracy with which the strains are determinable and on the relative signs of the strains on the extrados and intrados at a given location on the arch. The magnitude of the peak strains for the Series II tests are given in Table XII, from which it is readily observed that the majority of the strains were less than 200 microinches per inch. Strains are determinable within 5 to 10 microinches per inch, a maximum error of about 5 percent.

Values of moment are determined by the algebraic subtraction of strains of opposite sign and, therefore, will have an accuracy comparable to that of the strain measurements. Thrusts, however, are determined by the algebraic addition of strains of opposite sign (a numerical subtraction) and, therefore, would be expected to contain a large error when the strains are of nearly the same magnitude. To summarize, the accuracy of the moments is generally good while the accuracy of the thrusts is often poor. This should be kept in mind when studying the tables and curves presented.

Moment and thrust distributions in the dynamic tests were not appreciably different from those in the static tests. Distributions at various times are shown in Figures 35 and 36 for test 3D-12B. Moment and thrust distributions at or near the time of maximum moment are given in Figures 37 through 50 for other Series II tests. The shape of the distributions is essentially the same for all of the tests. There was a wider variation in the distribution of thrusts than of moments for the reasons mentioned previously. For practical purposes, the thrust distribution was uniform, although there appears to be a tendency for greater thrusts below the haunch than near the crown.

A plot of the peak moments versus surface overpressure, Figure 51, shows that the maximum moment varies roughly linearly with overpressure for the range of loading encompassed by the tests. Maximum moments for short-duration loads tend to be greater than for long-duration loads. The reason for this is probably that the soil under the footings does not deform plastically under short-duration loads as it does for long-duration loads, and consequently a greater portion of the load is transmitted to the effectively stiffer structure, inducing larger moments.

The variation of moment with time at various locations around the arch is displayed in Figure 52. In the vicinity of the haunch the moments are small; they reach their peak value in a few milliseconds and retain it until the load reduces appreciably. The moment at the crown behaves similarly except that its magnitude is larger than those near the haunch. At the 5°17' point, by contrast, the moment peaks at almost twice its quasi-static value in about 8 milliseconds then gradually decreases to a quasi-static value which subsequently decreases gradually as the load diminishes. The residual moment distribution about 3 seconds after removal of the load is shown in Figure 52.

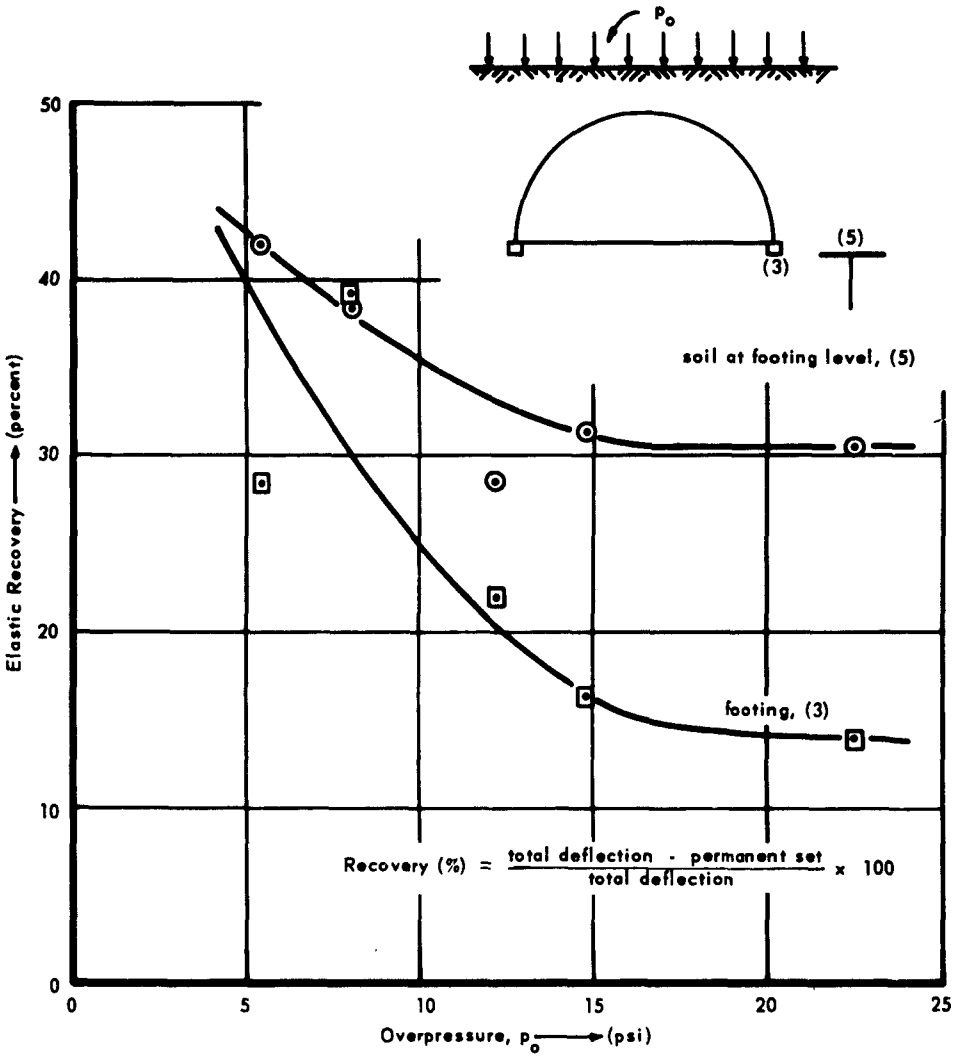

Figure 32. Percent elastic recovery for long-duration loading — Series II.

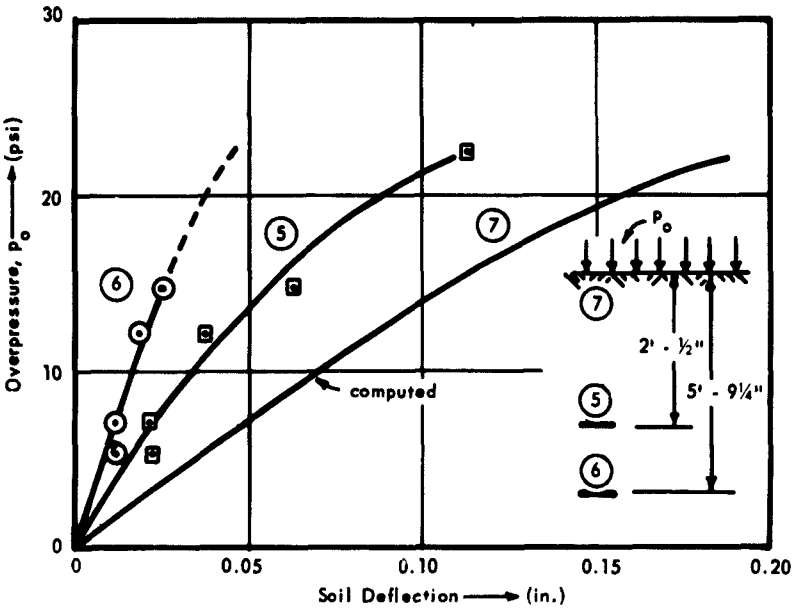

Figure 33. Computed deflection of sand surface for long-duration loading — Series II.

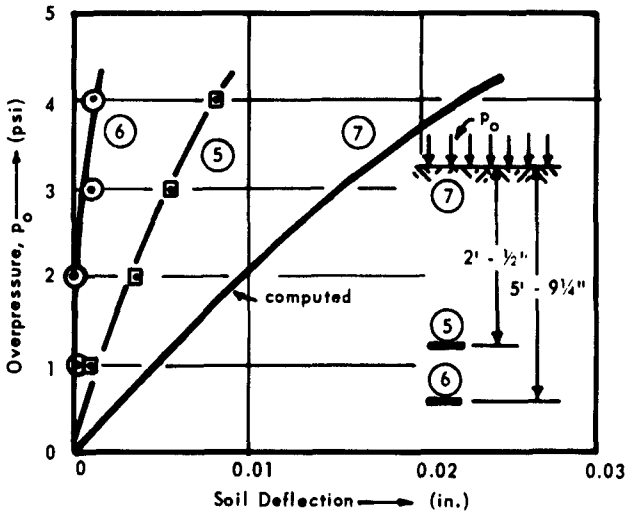

Figure 34. Computed deflection of sand surface for static loading — 3D-15A.

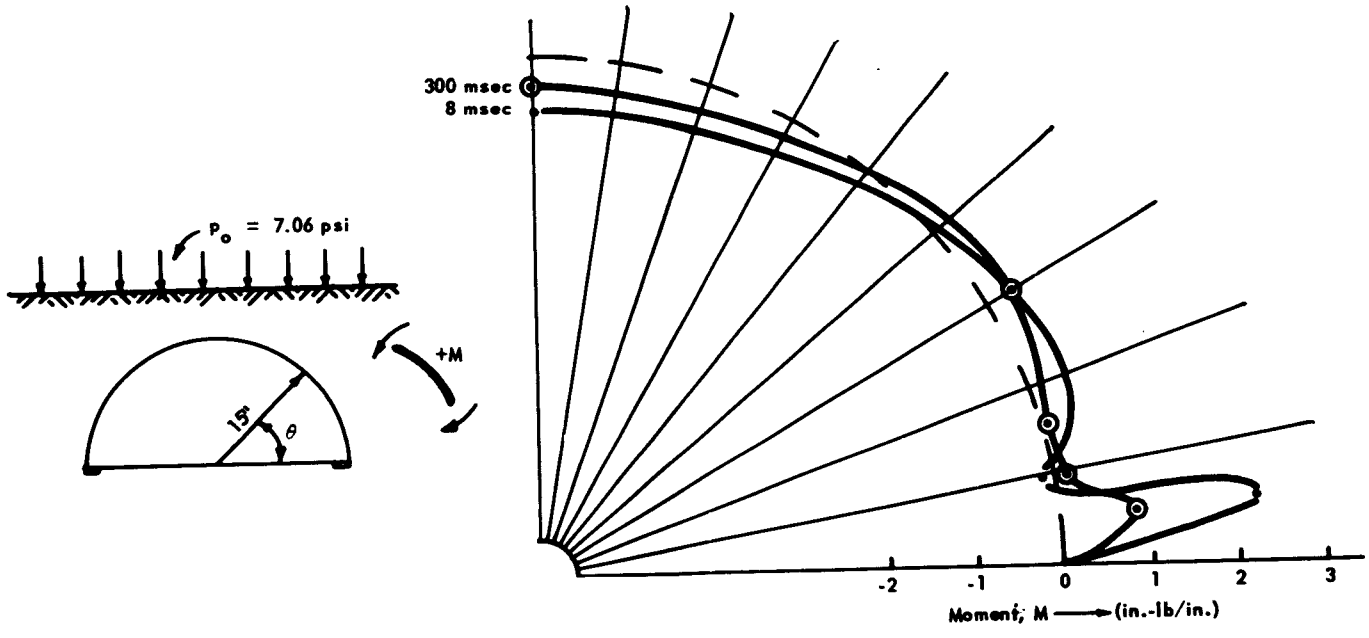

Figure 35. Moment diagram — 3D-12B.

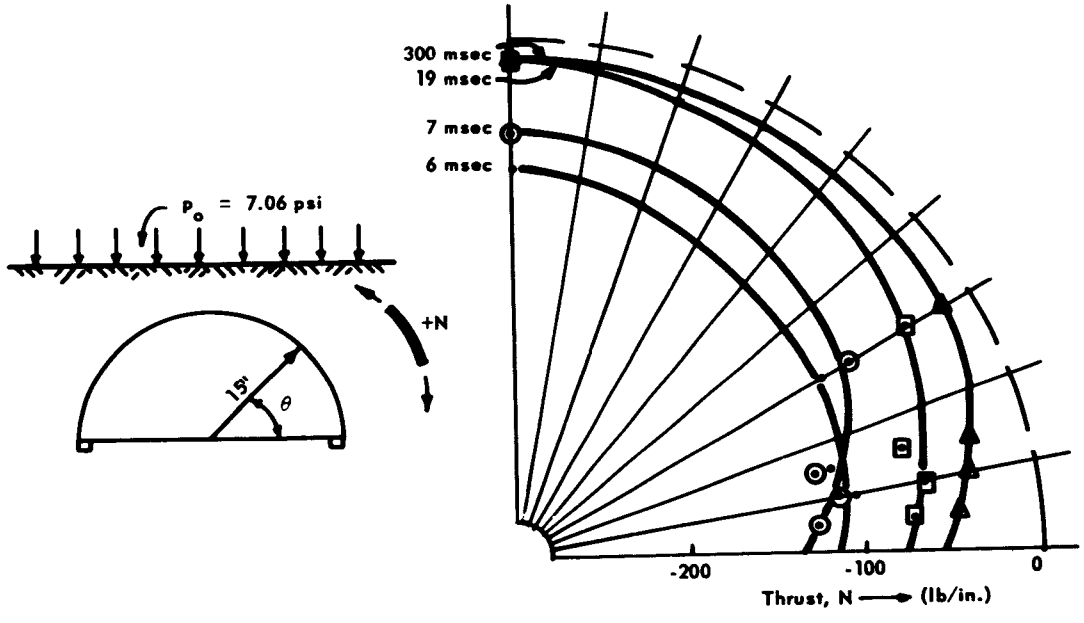

Figure 36. Thrust diagram — 3D-12B.

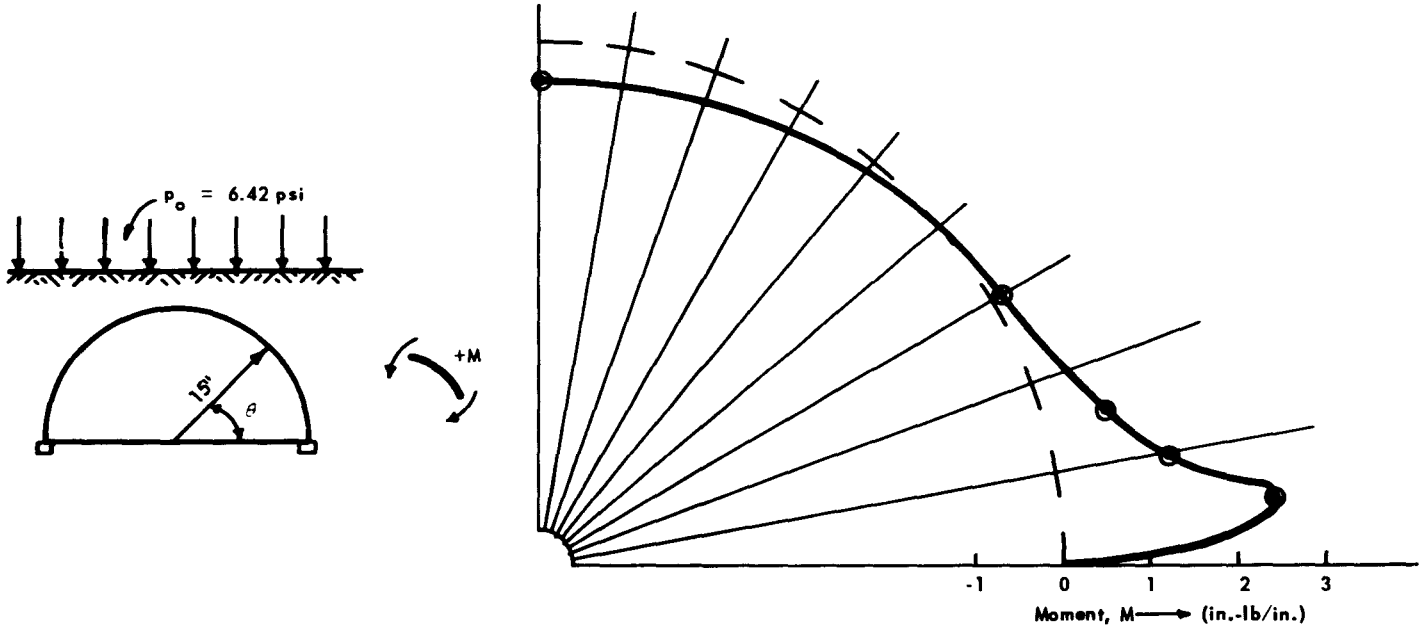

Figure 37. Moment diagram — 3D-11A.

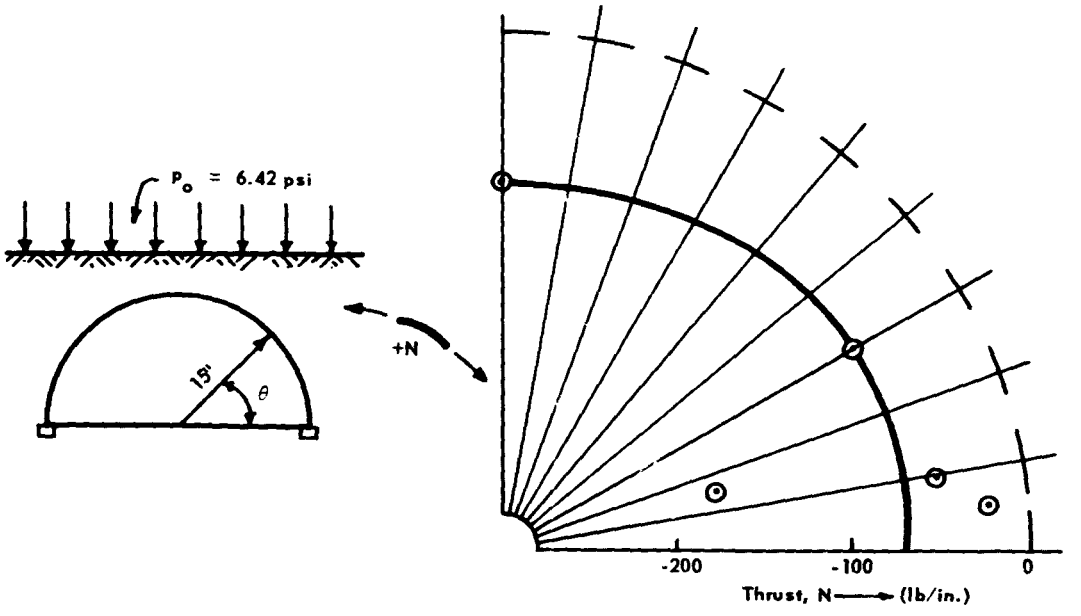

Figure 38. Thrust diagram — 3D-11A.

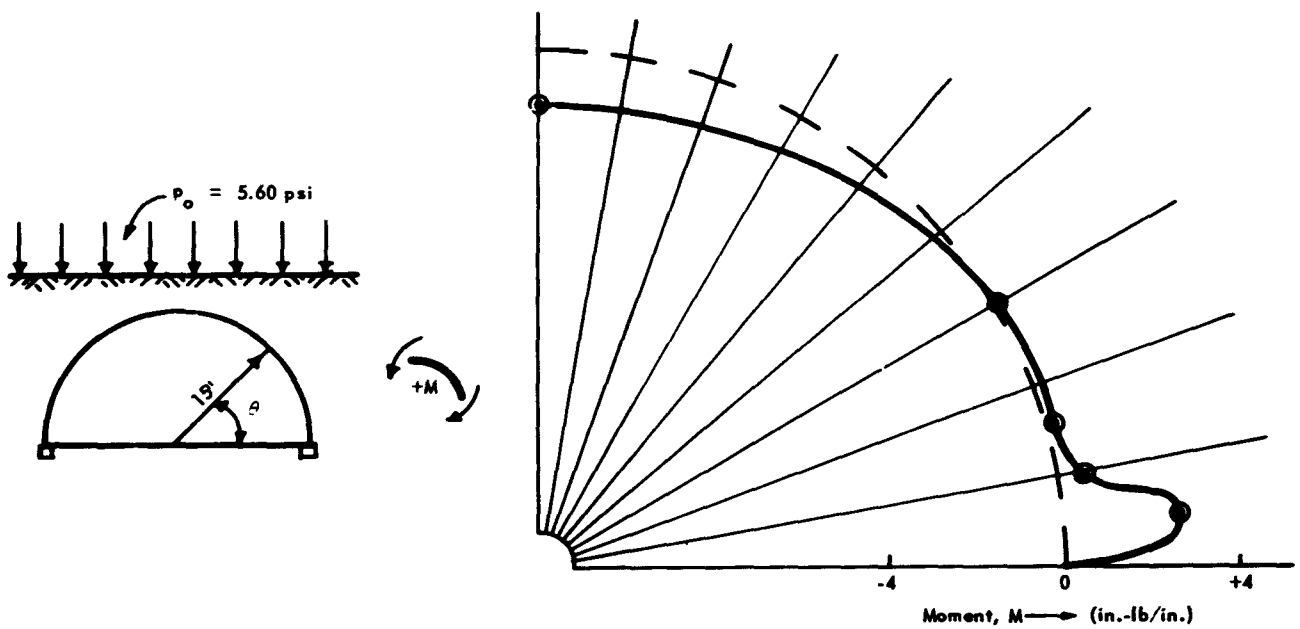

Figure 39. Moment diagram — 3D-11B.

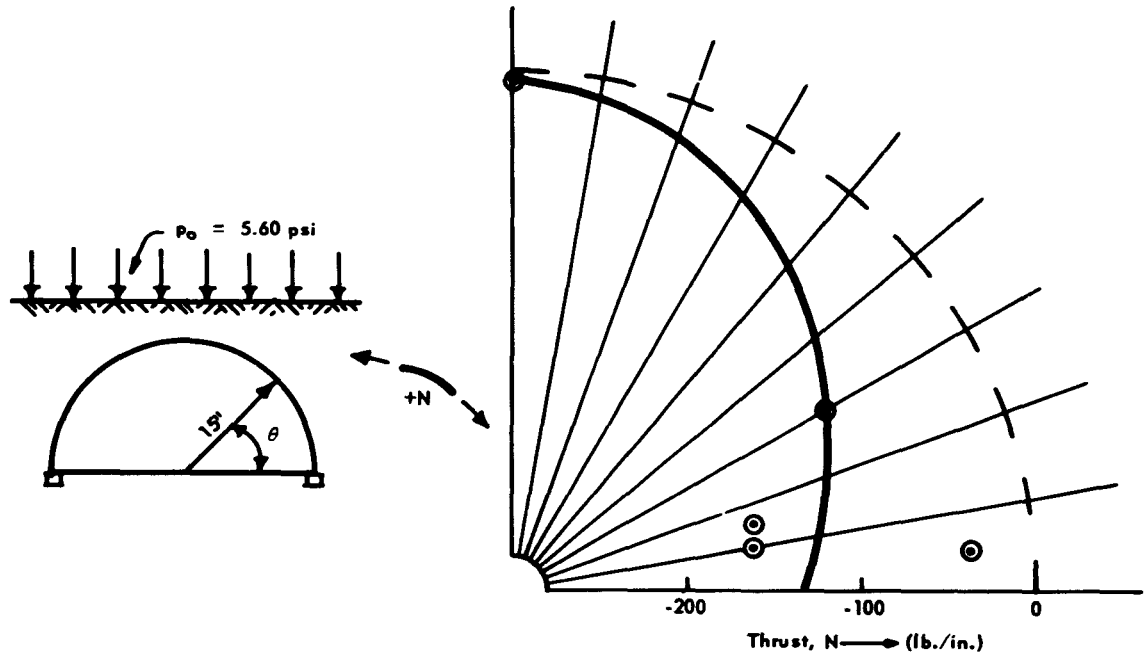

Figure 40. Thrust diagram — 3D-11B.

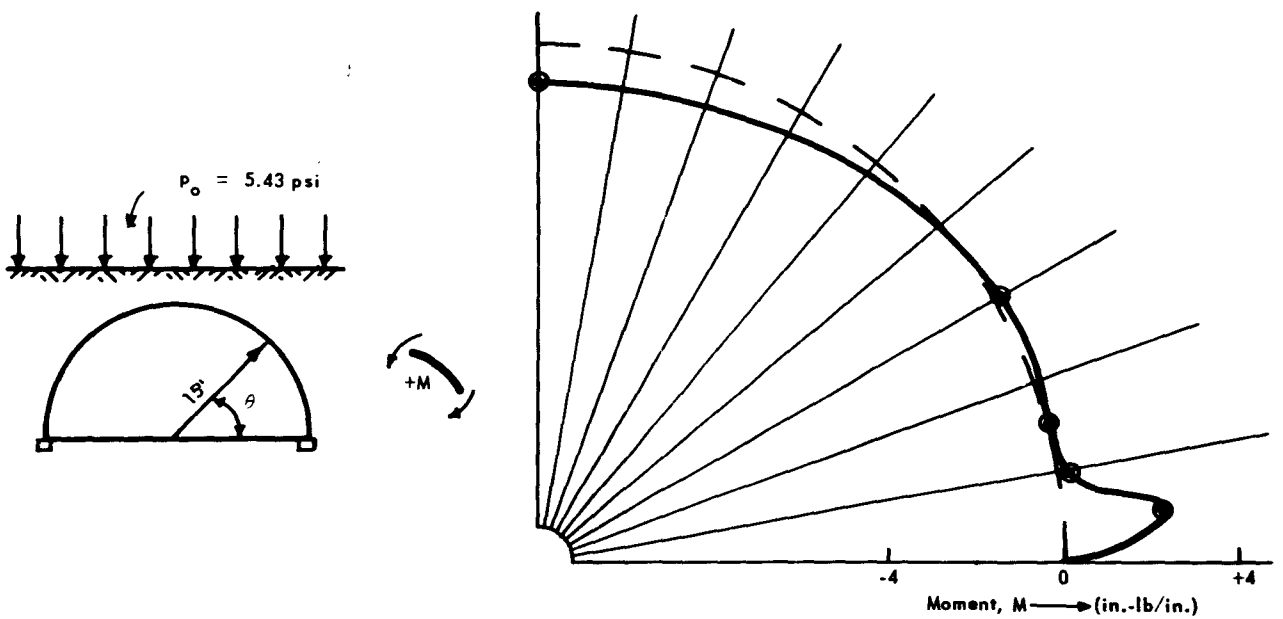

Figure 41. Moment diagram — 3D-12A.

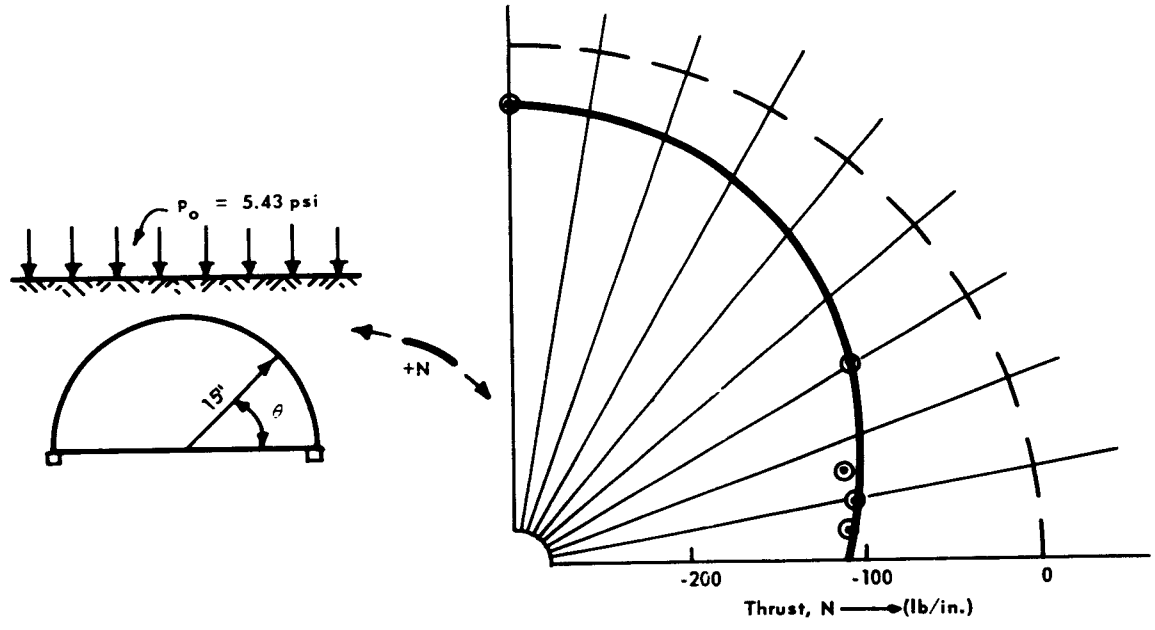

Figure 42. Thrust diagram — 3D-12A.

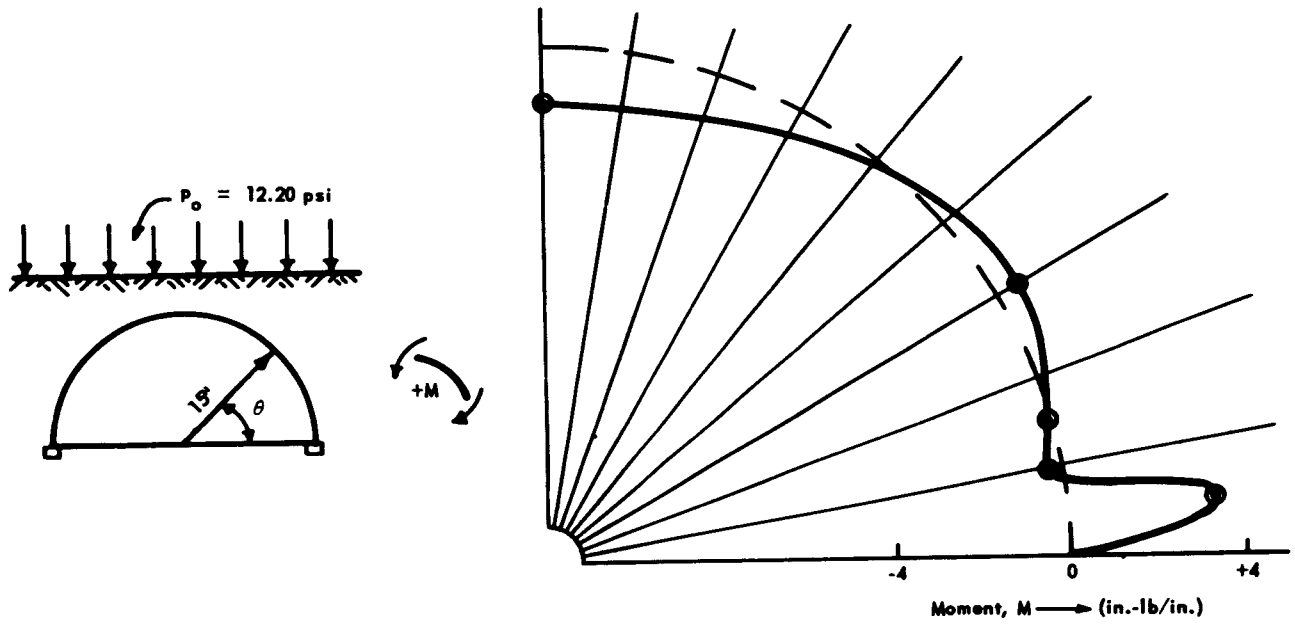

Figure 43. Moment diagram — 3D-13A.

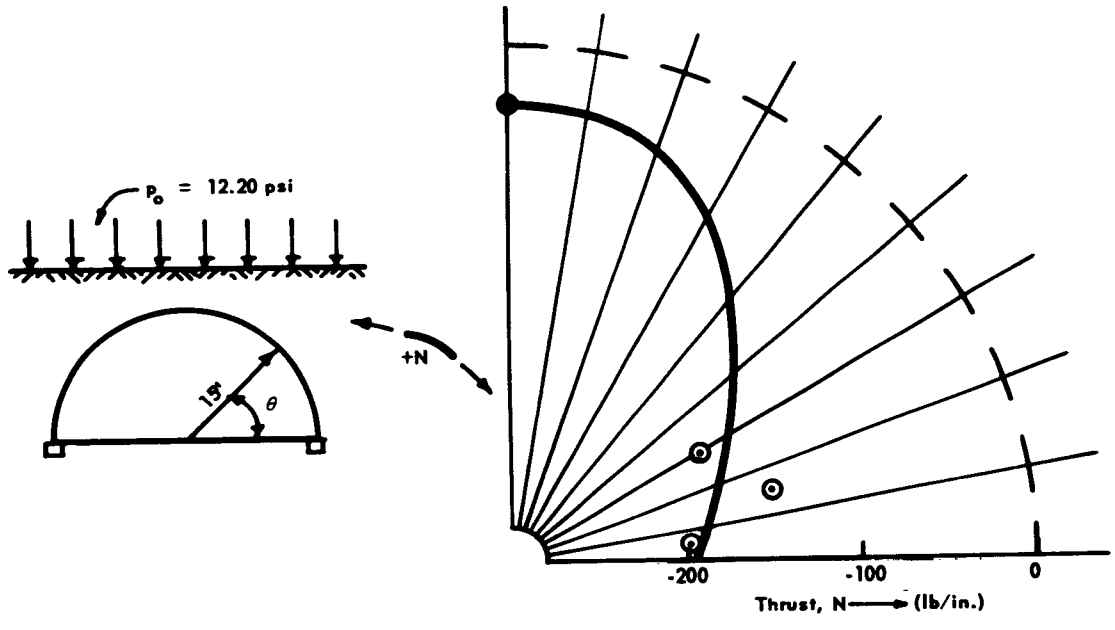

Figure 44. Thrust diagram — 3D-13A.

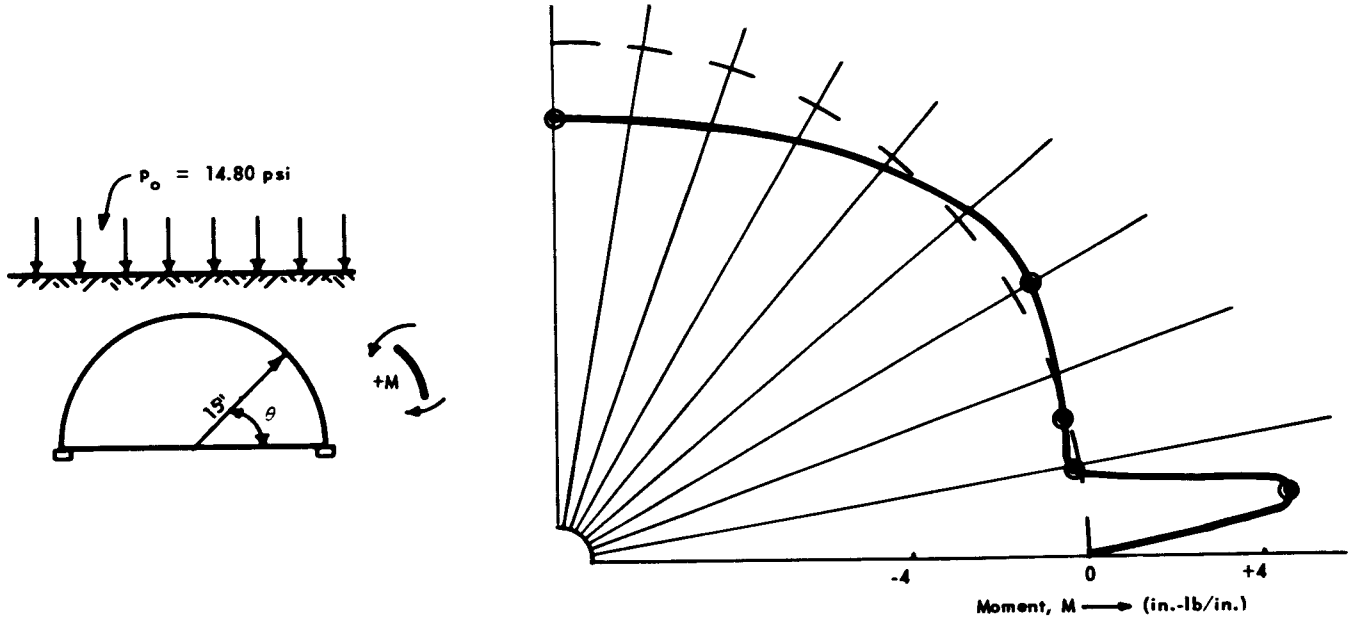

Figure 45. Moment diagram — 3D-13B.

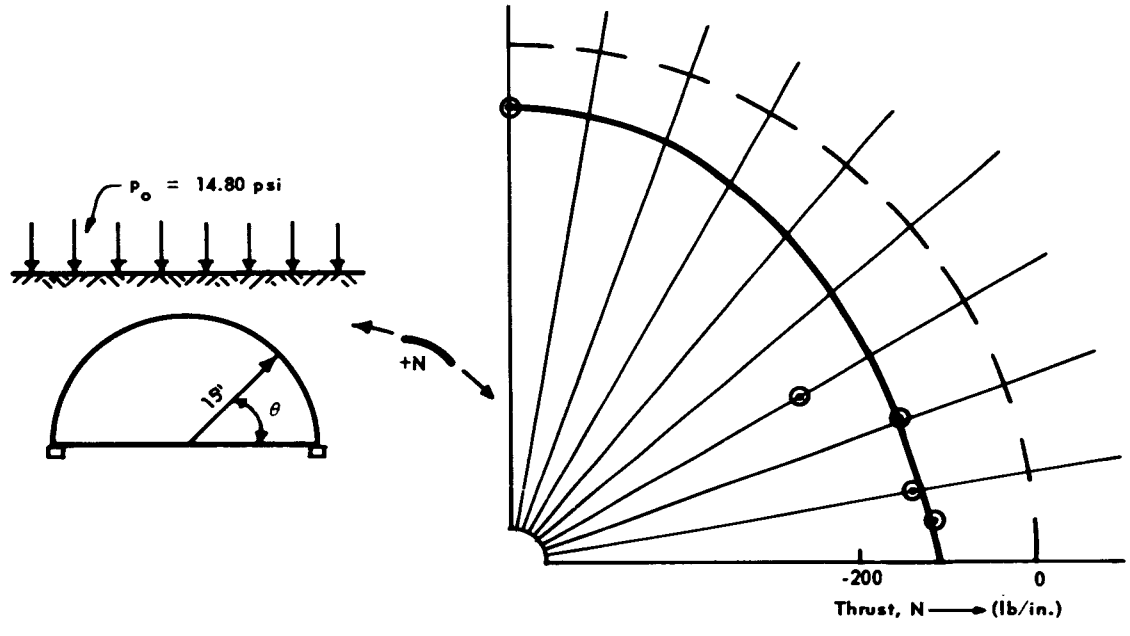

Figure 46. Thrust diagram — 3D-13B.

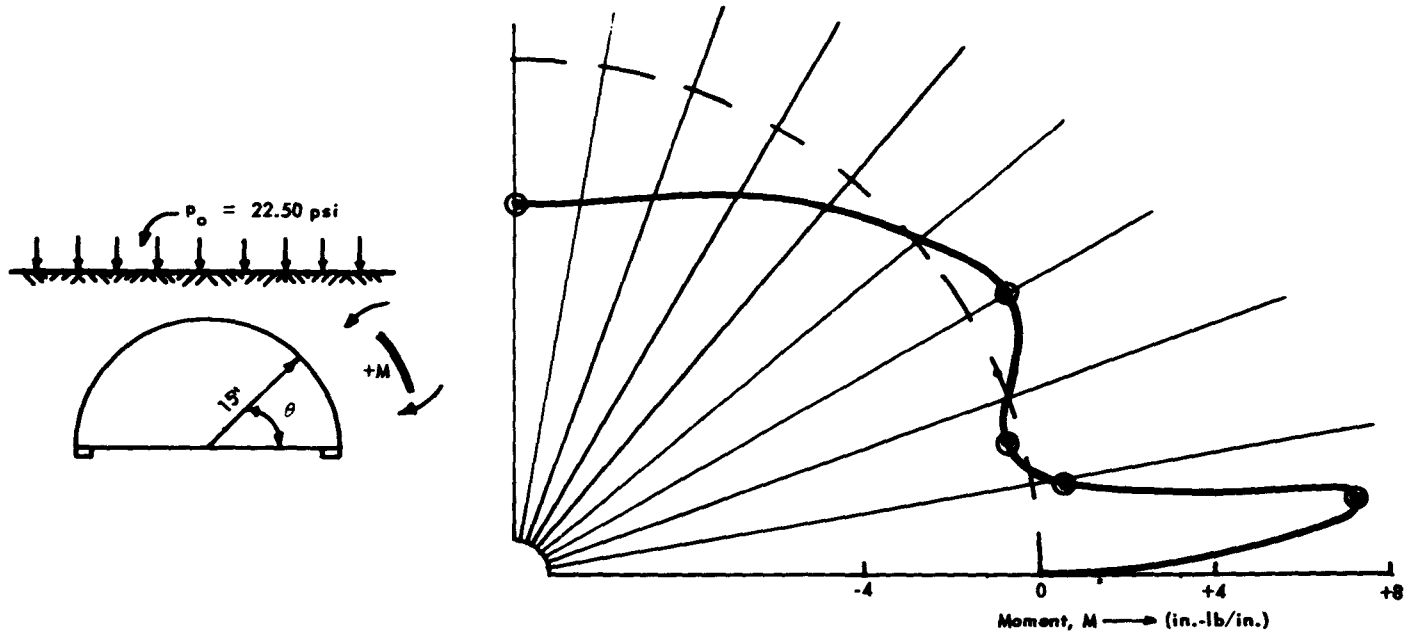

Figure 47. Moment diagram — 3D-13C.

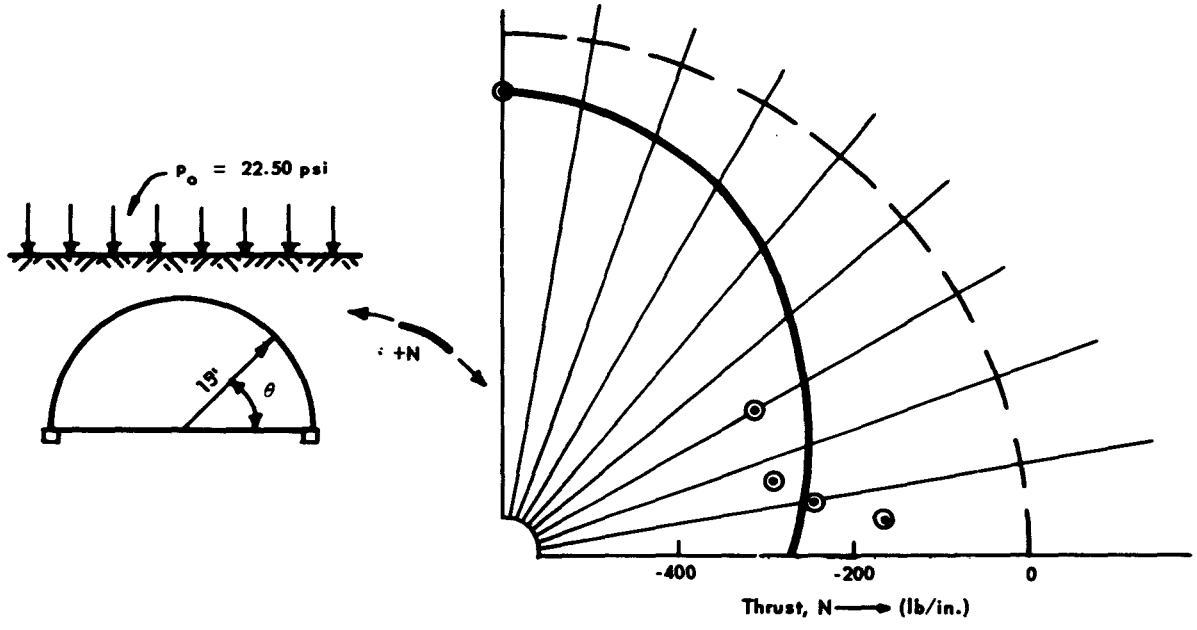

Figure 48. Thrust diagram — 3D-13C.

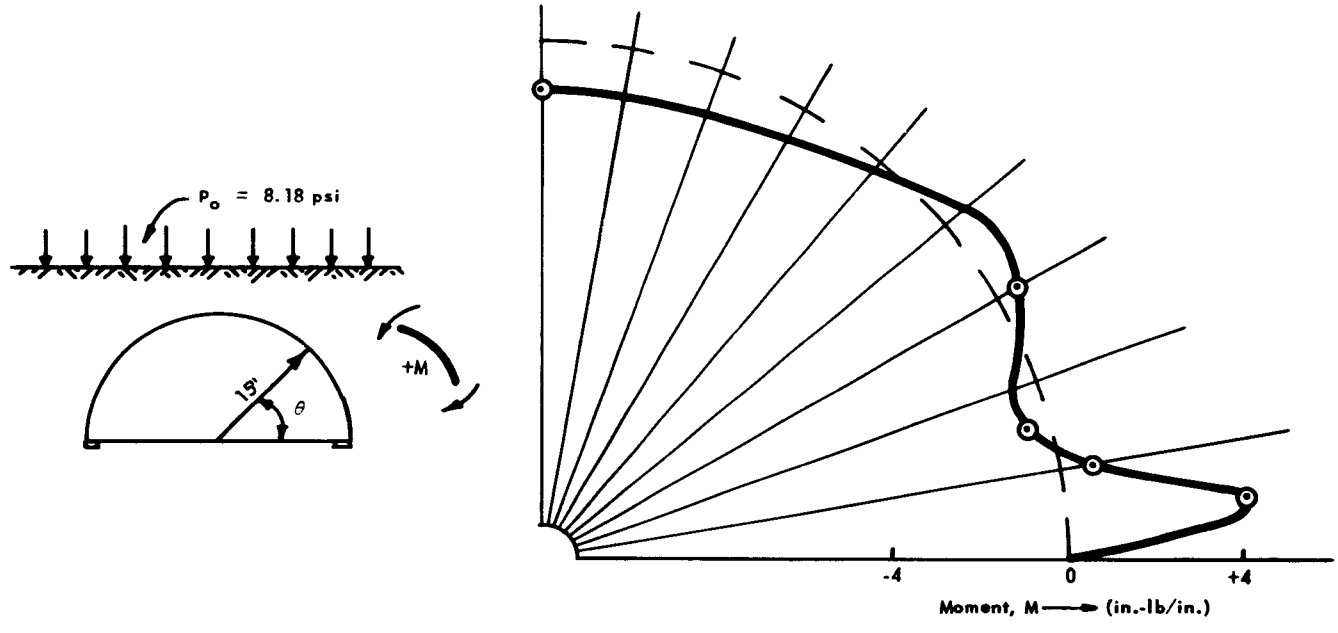

Figure 49. Moment diagram — 3D-14A.

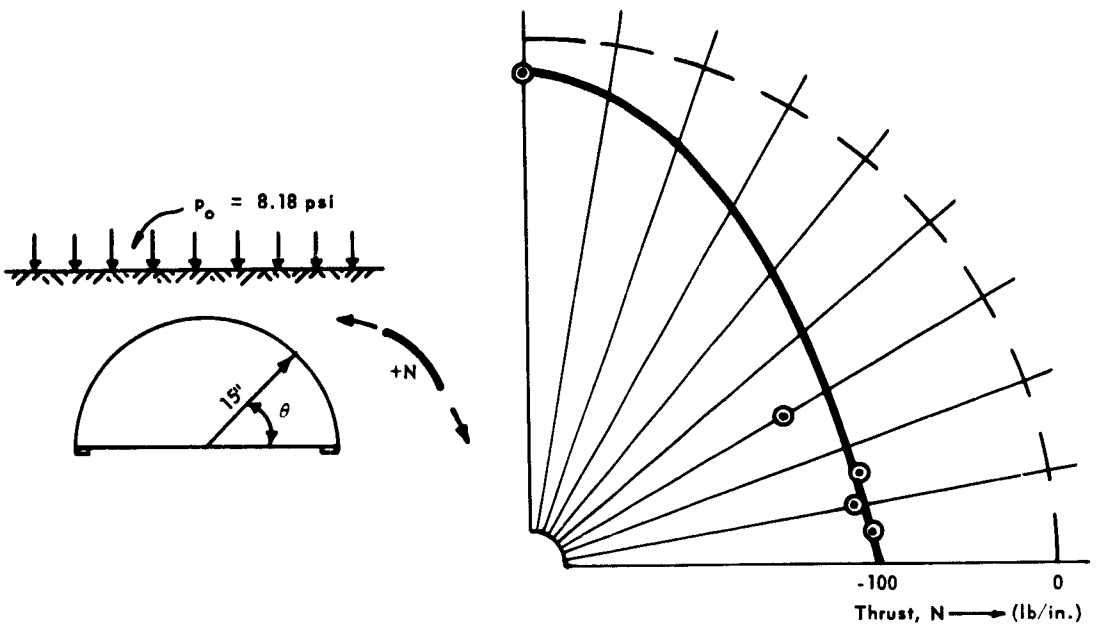

Figure 50. Thrust diagram — 3D-14A.

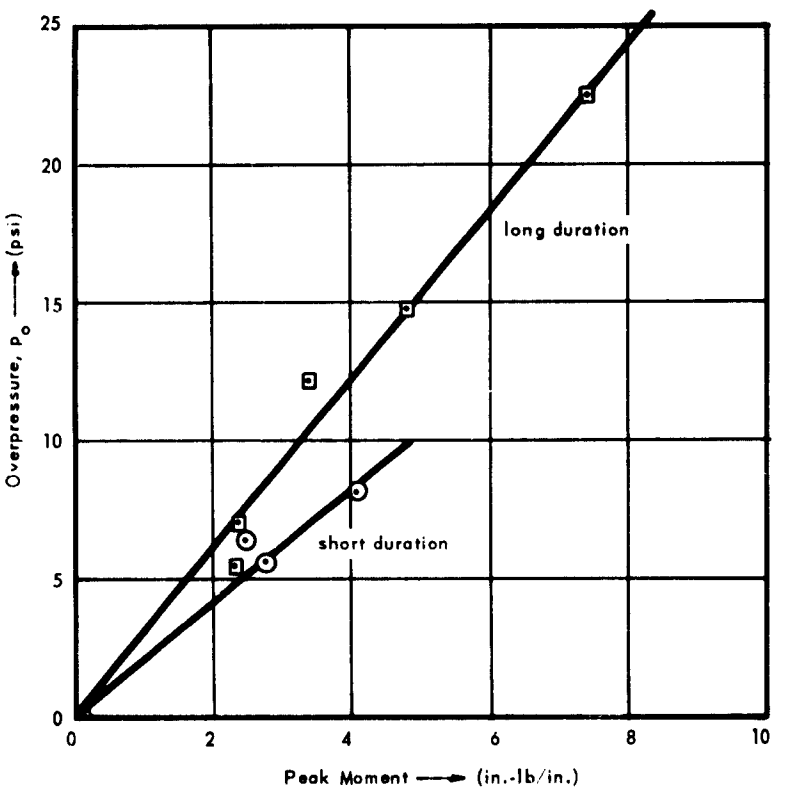

Figure 51. Peak moment vs surface overpressure — Series II.

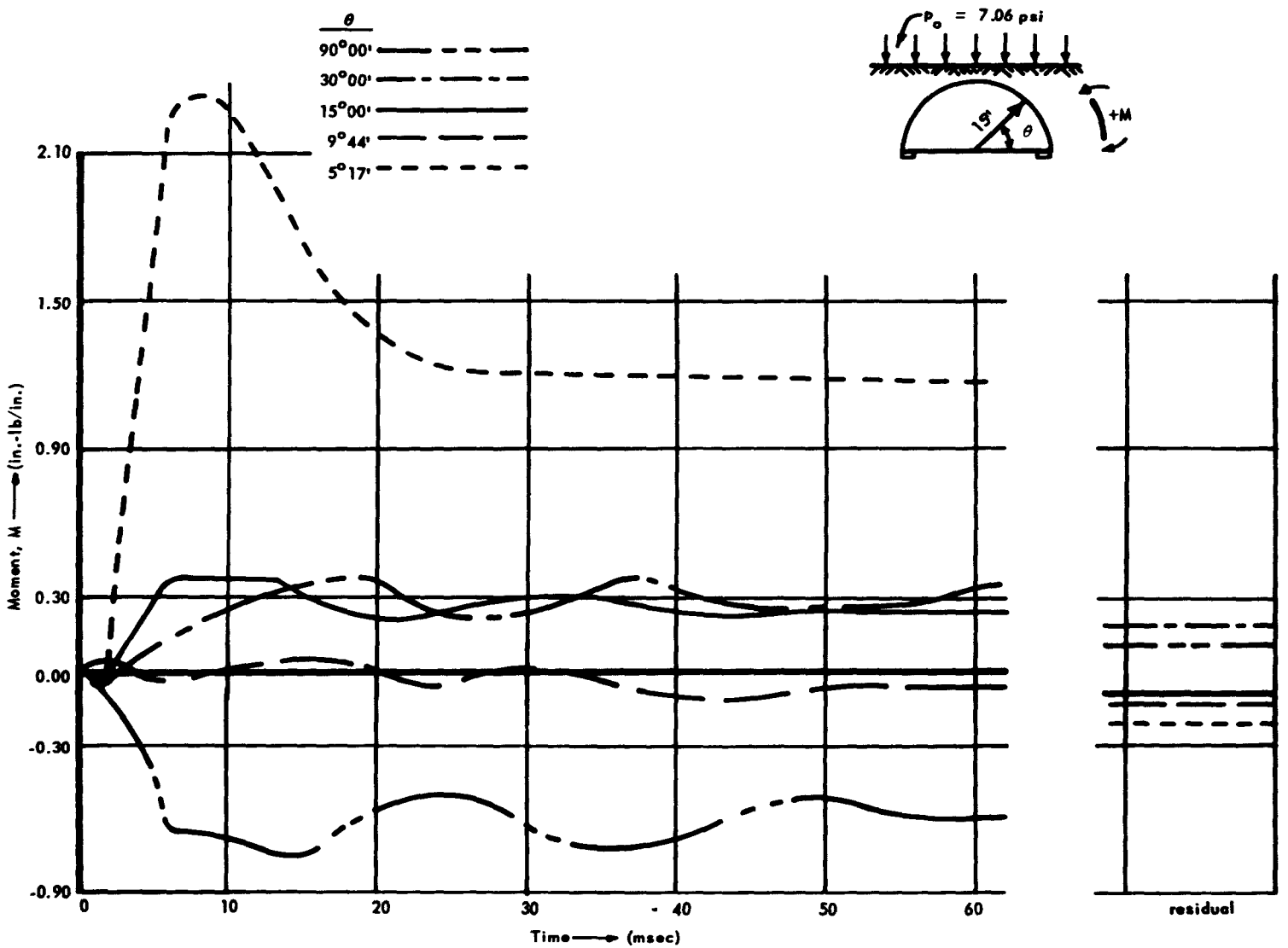

Figure 52. Moment vs time — 3D-12B.

Corresponding typical thrust-time curves are shown in Figure 53. The maximum value occurred at the gage station closest to the springing and, as did the moment, peaked in about 7 to 8 milliseconds. As with the moments, the peak thrusts were about twice their quasi-static values, which indicates that dynamic loading amplifies thrusts and moments to about twice the values they would have under a static load of the same magnitude. In addition to this very useful information, a knowledge of moments and thrusts is exceedingly helpful in understanding the behavior of the structure and in studying the phenomenon of soil-arching.

Arching. The term arching is used here to mean that portion of the surface load which is not transmitted through the structure. If the arch and the soil immediately above it are removed from the soil field, as shown in Figure 54, the arching is seen to be 2F. That is, from a vertical equilibrium for the static case, arching is the difference between the total load on the surface and the sum of the reactions, R.

A first approximation for arching over flexible structures subjected to static loading can be obtained by writing an equation for the vertical equilibrium of a free body consisting of an arch and the soil immediately above it as shown in Figure 54. From a vertical equilibrium of the footing, the thrust, N, at the springline approximately equals the reaction, R, thus:

$$R = pr - \mu H_s \tag{7}$$

where p = surface overpressure

μ = coefficient of friction

H_s = normal force on vertical section of soil through the footings

or with $\mu = \tan\varphi$ and $H_s = K_o p (r + d_o)$:

$$\frac{R}{pr} = 1 - K_o \left(1 + \frac{d_o}{r}\right) \tan\varphi \tag{8}$$

where K_o = coefficient of earth pressure at rest

d_o = depth of soil cover over crown of arch

φ = angle of friction of soil

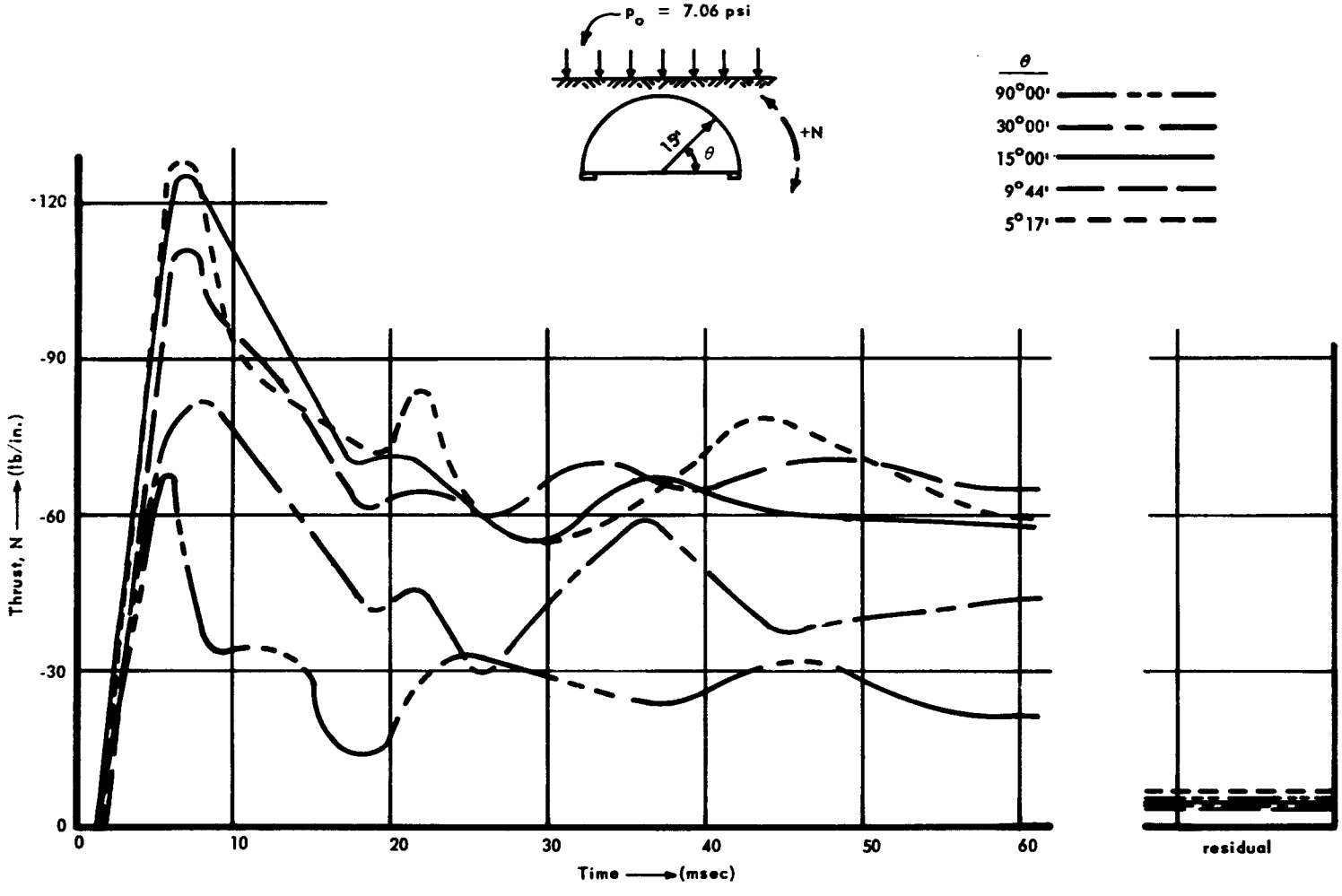

Figure 53. Thrust vs time — 3D-12B.

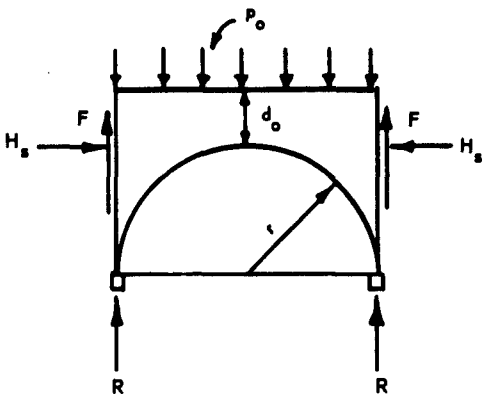

Figure 54. Free body showing arching forces.

The last term in Equation 8 is the portion of the load carried by arching.

$$P_{arch} = prK_o\left(1 + \frac{d_o}{r}\right)\tan\varphi \qquad (9)$$

In the above relations, the coefficient of earth pressure at rest is used since a pure shear along a vertical plane is assumed. The coefficient of earth pressure at rest is given by the relation

$$K_o \cong 1 - \sin\varphi \qquad (10)$$

A plot of Equation 9 is given in Figure 55. It indicates that 100 percent arching is not achieved until the depth of cover equals about 2-1/2 times the radius of the arch. For shallow-buried structures with d_o/r ratios between zero and one, the amount of static load carried by arching is predicted to be from 25 to 60 percent.

Taking the thrust at the springline equal to the reaction, R, the arching can be computed from the experimental results. A plot of arching versus overpressure is given in Figure 56, where the arching is expressed as a percentage of the total surface load. A dashed line is drawn through the leftmost data point because the expected accuracy of this point is poor. (Arching is determined by use of thrusts for which the potential error is large at low loads.) The results shown in Figure 56 indicate that at low surface pressures most of the load is transmitted through the soil around the arch, but that as the surface load increases, the proportion of load carried by arching decreases. It finally reaches a limiting value of about 38 percent and, according to Equation 9, thereafter remains constant. Equation 9, of course, does not agree with Figure 56 for loads less than 3 psi where the shear stress is not developed over the distance $d_o + r$.

The previous loadings on the arch probably would not appreciably affect the results except for the very low pressure region; here the effects of the hysteresis developed on prior unloading would be overcome.

Further tests will be needed to extend the arching curves to higher loads, to study the effect of depth of cover, and to investigate the influence of soil density on the amount of load carried through the soil. Because of the intriguing alteration in arching which occurs under dynamic loading, however, such investigations may have limited practical value for blast design.

For dynamic loading, arching varies dramatically with time as indicated in Figure 57. Data for this figure were determined by assuming that the effective acceleration of the mass of soil directly above the arch is two-thirds of the acceleration at the crown. This assumption is based on the reasoning that there is less resistance to displacement of the soil over the crown than to the soil directly over the footings. The inertia force, equal to the effective acceleration times the mass of soil above the arch, was included in the vertical equilibrium of Equation 8 to compute the arching. During approximately the first 6 milliseconds, the inertia force acts to oppose the applied load; thereafter, it acts as an additional load on the structure.

The corresponding arching curve to Figure 57 for test 3D-12B had the same general shape but gave a negative arching in the vicinity of 20 milliseconds. This implies that there was more load on the arch than on the surface directly above the arch; logically, this would only be expected for a very stiff structure.

The fundamental message from the arching study is that for dynamic loading essentially the entire surface load acts on the structure for at least a short period of time, while for static loading the load which acts on the structure is reduced 25 percent or more by arching. In blast loading, the inertia load produced by the soil offsets the resistance from arching.

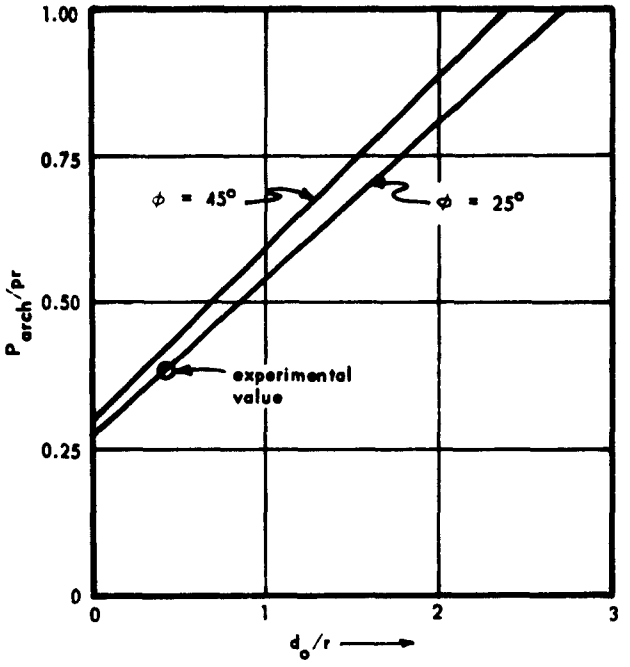

Figure 55. Arching as a function of depth of cover.

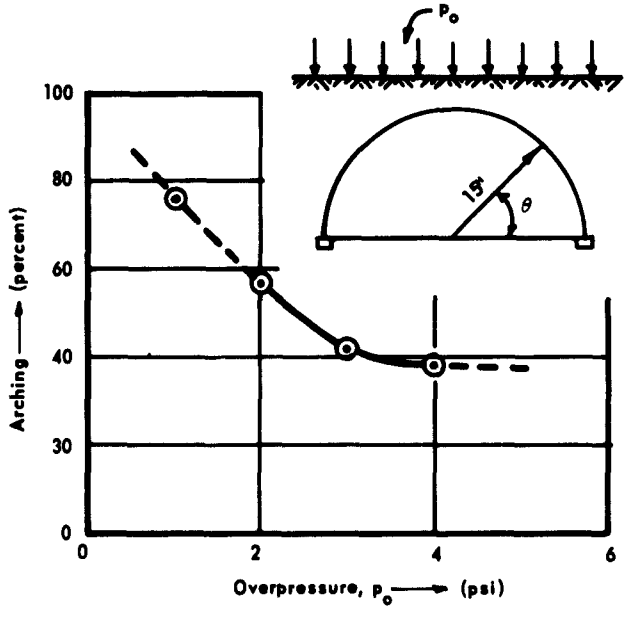

Figure 56. Arching vs overpressure for static loading — 3D-15A.

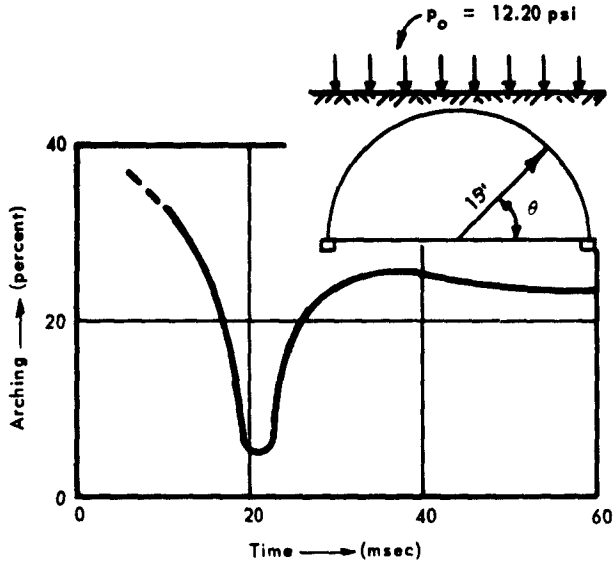

Figure 57. Arching vs time for long-duration loading — 3D-13A.

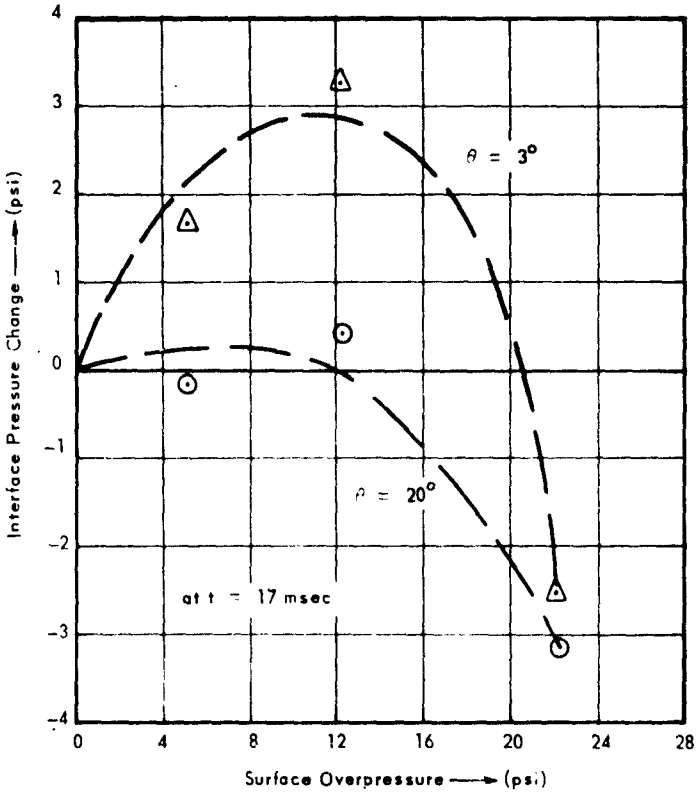

Figure 58. Change in pressure at interface due to arch movement — Series II.

Interface Pressure Change. From a study of the data some idea has been obtained about the change in pressure at different points of the soil-structure interface produced by movement of the structure. A plot of this change versus surface overpressure is shown in Figure 58 at the time the deflection at the sides (8-degree points) of the arch was a maximum; that is, at about 17 milliseconds. By change in pressure is meant the change in pressure from that which would exist at that point in the soil free field if the arch did not move. The plot of Figure 58 shows, in effect, that as the overpressure increases, increasing relief of interface pressure occurs at the 20-degree point due to movement of the arch. At 22.5 psi approximately a 50-percent decrease in pressure results by virtue of the body motion of the arch into the soil. At the 3-degree point, outward movement produces an increase in pressure of about 27 percent over what would occur at a corresponding point in the undisturbed soil at 12 psi, but at 22.5 psi there is a reduction of about 11 percent.

The data for Figure 58 were determined by calculating the pressure at a given point based upon the assumptions that the attenuation of pressure with depth is negligible and that the coefficient of lateral earth pressure is constant for all depths and pressures. Based upon these assumptions, the vertical component of pressure at a point equals the surface overpressure and the horizontal component is the coefficient of lateral earth pressure times the vertical component. With the vertical and horizontal components known, the pressure normal to the surface of the arch is readily calculated. Subtracting the measured incident pressure determined in the experiments from the calculated normal pressure gives the change in pressure attributable to the presence of the arch. Dependence of the measured pressure upon the soil placement made it necessary to do a little manipulation of figures to get the incident pressure. The procedure used was to apply a correction factor to the measured pressure to account for the arching of soil across the gages. The correction factor was arrived at by determining the unit radial pressure needed to produce the measured thrust at a point in time in the pseudo-static state. The correction factor was taken as the ratio of the unit pressure so determined to the actual measured pressure at that time. The ratio was found to be quite consistent at 1.75 for the Series II tests. The quantitative accuracy of Figure 58 is dependent upon the validity of the assumptions used in the described procedure.

Figure 59 shows a plot of the change in interface pressure with time at a point three degrees from the springline. Strangely enough, the change in interface pressure does not correspond to the deflection of the arch until a time of about 15 milliseconds. The reason for this behavior is not understood; however, the peak at 6 milliseconds might be due to refraction of the stress wave at the interface. Confirmation of this possibility awaits development of satisfactory soil-pressure gages.

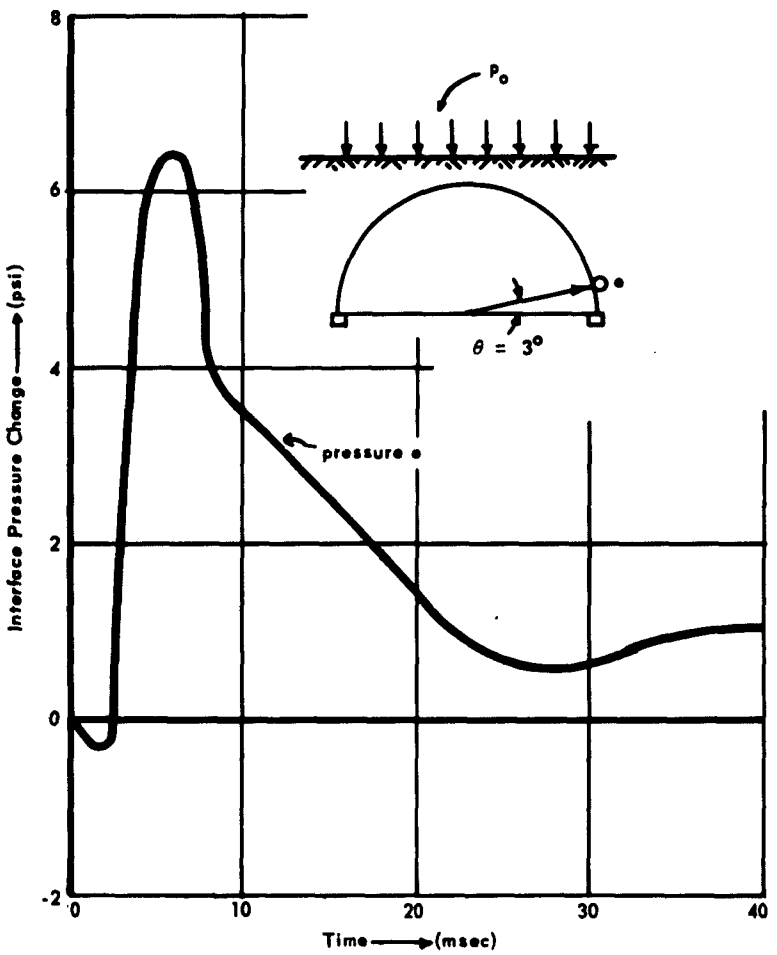

Figure 59. Change in pressure at interface due to arch movement — 3D-13A.

From the test data is it possible to estimate the regions around the arch in which pressures are developed in the active sense and the passive sense. To do this it is necessary to assume that the pressure attenuation with depth is negligible. With this assumption, the vertical and horizontal components of pressure at any point around the arch are p and $K_o p$ respectively. The computed sum of the projections of these components on the normal to the surface of the arch represents the pressure which would exist if the arch had the same compliance as the soil mass. The difference between the computed normal force at any point and the actual pressure measured at that point represents the loss or gain in pressure at the interface due to movement of the arch.

The results of calculations following the outlined procedure are presented in the plots in Figure 18. In the calculations, the value of K_o used was determined as the ratio of the readings of pressure cell p and pressure cell n. Figure 18 shows clearly that passive-sense pressures are developed in the region from 0 to 20 degrees on the arch and that active-sense pressures are developed elsewhere in the vicinity of the extrados.

Comparison of Laboratory and Field Tests

A comparison can be made between the behavior of the Operation Plumbbob 3.3 structures (25-foot span corrugated metal arches) and the small structures tested in the simulator if it is assumed that linear relationships exist among the parameters and that the deflection of the floor slab in the 3.3 structures was negligible compared to the deflection of the footings. The latter assumption is corroborated by all available evidence. Only the magnitude of deflections can be compared, however, since no other data was obtained in the field tests.

Other differences between the small arches and the prototype are considered to be negligible. Among the main features peculiar to the prototype are the slack between the bolted multiplate, the endwall strengtheners, and the fixity conditions. These factors might effect the response of the arch shell, but it is difficult to conceive of them affecting the body motions. Thus, in a comparison where the gross motions are of interest, the differences in the properties of the soil are of dominant concern.

Comparison of the small-structure deflections with those of the field arches is complicated by the different soils involved.

The Project 3.3 structures of Operation Plumbbob were tested in the Frenchman Flat area of the Nevada Test Site (NTS). Frenchman Flat is a dry lake bed of clayey silt. The natural soil at the site was considered unsatisfactory as backfill for the Project 3.3 experiments. Therefore a gravelly, silty sand was imported from borrow pits. This material was used to surround and cover the structures of Project 3.3. Indigenous soil was employed as the foundation material.

Soils investigations and soil field control for Project 3.3 and certain other projects of Operation Plumbbob were performed by the Waterways Experiment Station (WES), Corps of Engineers, U. S. Army. WES conducted classification and physical tests on the natural soil at the site and on the imported backfill soil. Results of these tests are reported in Reference 30. Certain of the values for the backfill material are listed below:

1. Average compacted dry density, 113.9 pcf

2. Average moisture content of compacted backfill, 8.6%

3. Modulus of deformation of consolidation specimen, 28,000 psi (average dry density, 117.2 pcf; average moisture content, 9.8%; applied stress, 50 psi)

4. Modulus of compression of triaxial test specimen, 10,000 psi (dry density, 113.7 pcf; moisture content, 10.2%)

The natural soil at the test site was classified by WES as sandy, clayey silt (CL-ML) to a depth of 2.5 feet, and as clayey silt (CL-ML) below 2.5 feet. Footings of the Project 3.3 structures were placed upon this undisturbed natural soil. The soil had the following properties:

1. Natural dry density, 90.0 to 93.2 pcf

2. Natural moisture content, 11.2% to 10.8%

3. Modulus of deformation of undisturbed sample, 6500 psi (at both 50-psi and 100-psi applied loads)

4. Subgrade modulus from 12-inch-square plate-bearing tests at a density of 79 pcf, 1850 $lb/in.^3$ (Information provided by WES.)

The suggested comparison can be effected by scaling up the deflections of the small structure tested in the simulator where this structure is considered as a model of the Structure 3.3b prototype. To do this it is necessary to employ the scaling relations of Appendix B and to assume linear relationships among the parameters involved. The model analysis requires that if the same materials are employed in the model and the prototype, the load must scale as unity, the time must scale as the length scale, and the stiffness of the arch must scale as the fourth power of the length scale. Obviously, the small arches are not true models of the Plumbbob 3.3 structures, but deflections can be compared if corrections are made for differences in the loading and the soil moduli. Comparative deflections made on this basis are given in Table XIII.

Table XIII. Comparative Deflections

Location	Deflections (in.)		
	Structure 3.3b (60 psi)	Structure 3.3a (100 psi)	Scaled-up 3D-6A
Footing	1.5	—	1.05
Crown	—	2.4	2.70[a/]
	4.1	—	1.38
Footing residual	1.4	—	0.768
Crown residual	1.3	—	1.02

a/ Based on test 3D-7A.

Plumbbob Structure 3.3b was a standard 25-foot by 48-foot Armco ammunition magazine of 8-gage multiplate. It was subjected to a surface overpressure of 60 psi and had an average backfill dry density of 112 pounds per cubic foot. Structure 3.3a was similar to 3.3b, but was stiffened with I-beam arch ribs on 4-foot centers. The stiffened arch was subjected to a surface overpressure of 100 psi and had an average backfill dry density of 113 pounds per cubic foot.

Footing deflections for test 3D-6A in Table IX are the averages of deflections of both footings. These are multiplied by the length scale and corrected to the proper load in Table XIII. A sample calculation for the scaled-up footing deflection is as follows:

$$y_f = \frac{0.126 + 0.137}{2} \times \frac{60}{7.5} \times \frac{77}{76 \times 10} \times 10 = 1.05 \text{ inches} \qquad (11)$$

The terms in the preceding equation are in order of occurrence: the average deflection of the small-structure footings, the ratio of the peak overpressures in the prototype and the model, the correction for the effective duration of the load, and the length scale. It is noteworthy that the secant modulus of compression at 50 psi was identical for the Frenchman Flat soil and the soil used in the Series I test.

In the paragraphs which follow the small buried arches will be referred to as models for convenience although they obviously are not true models.

The scaled-up deflections of the model were very close to the deflections of the prototype, which indicates that modeling of buried structures is possible, at least for predicting magnitudes of deflections. More reliance could be placed in the results if the foundation material in the prototype had properties more akin to those in the small arches.

Recapitulation

The sequence of events constituting the essence of behavior of the small arches was:

1. The surface overpressure reached a peak value in about 1 millisecond and gradually decayed thereafter.

2. The peak pressure on the crown of the arch was reached in about 6 milliseconds.

3. The peak pressure at the 20-degree and 3-degree points was reached in about 7 milliseconds.

4. Peak thrust and moment were reached in about 8 milliseconds.

5. Maximum deflection was reached in about 17 milliseconds.

6. Arching was a minimum at about 20 milliseconds.

The relatively long time required for the pressure to reach a peak on the arch must be attributable to the tendency of the arch to move away from the soil as it is loaded by it. This fortuitous interaction prevents a sudden build-up of pressure on

the surface and resultant generation of shock waves in the material of which the arch is fabricated. As has been shown for more elementary members,[24] increasing the rise time of the load beyond about one-fifth of the natural period materially reduces the maximum dynamic deflection. In the case of the buried arch, the slower rise time of pressure on the arch delays the time of occurrence of peak thrust and moment to a time at which the stress wave in the soil has had time to envelop the entire structure and thus provide increased confining loads on the sides of the structure. This confinement induces a nearly radial loading on the arch, which the arch is ideally suited to resist by virtue of its geometry. The peak moment is maintained over a long period of time, but the thrust rapidly decays to a value of about one-half its peak. The implication of this is that yielding produced by thrust is tolerable because the relatively short duration of the yielding results in little distress to the structure. The relatively long time during which the moment remains at its maximum could produce intolerable deformation of the structure were it not for the fact that deformations of the structure simultaneously mobilize passive resistance in the enveloping soil. Whatever weakness the structure demonstrates, the soil immediately compensates for; it is difficult to conceive of a system more mutually complementary.

Consequences of Observations

What information can be extracted from the test results which will aid in the design and construction of buried structures? First, and perhaps most important, the observed behavior will permit the establishment of sounder assumptions upon which response theories can be based and will provide data with which to compare the results of theories. Beyond this, possible practical consequences are:

1. The nature of the moment curves leads to the tentative conclusion that it is only necessary to achieve near optimum compaction up to about the 15-degree point on the sides of the arch. This may eventually justify revision of presently employed backfill specifications and result in decreased cost of backfilling.

2. The tests provide a basis of judgment regarding what magnitude of relative deflections may occur between the footings and floor slab of a shelter, and indicate the importance of soil density on this parameter.

3. Knowing the shape of the moment curve permits an approximation of the buckling load and, thus partially removes one of the biggest unknowns in buried shelter design. This knowledge, together with the observed time variation of moment and thrust, will permit approaching the ideal of a buried shelter of balanced design; that is, one which fails simultaneously due to punching, buckling, moment, and thrust, depending upon the criteria chosen for each.

There are two consequences of the observations which are of indirect importance. First, the tests have shown that for dry-sand backfill, and accounting for the slightly different initial soil conditions, repeated load tests can be employed on a particular soil-structure system to gain information on behavior without the necessity of reworking the soil between each test. Secondly, there are strong indications that the modeling outlined in Appendix B will be adequate for predicting the behavior and capacity of prototype structures.

The tests indicate that prediction of the magnitude of deflections through modeling is possible, at least under certain restricted conditions such as dry-sand backfill. This will enable detailed studies of the influence of the important variables in various protective systems, and finally permit the development of suitable analytical methods for designing economical underground protective systems.

Deficiencies of Work

Perhaps the most serious limitation of the tests reported is the limited magnitude of peak pressure which could be obtained. It would have been desirable to load the small structures to at least 100 psi to be within the range of dominant current interest. The capacity of the blast simulator is such, however, that the peak pressures which can be applied over the large area of the soil surface in the pit are of the order of 25 psi. Slightly higher static test pressures can be safely achieved.

Performing a series of static tests is considered of first-order importance because of the limited static data obtained in the Series I and II tests. It is regarded as extremely important to have static tests as controls for the dynamic tests. Actually, the static tests will not provide controls in the usual sense because little is known about soil-structure interaction under static conditions.

In addition to static-test data, information is lacking on the influence of the boundaries of the simulator test pit. Solution of this problem is largely dependent on development of suitable methods of measuring soil pressure. Soil-pressure measurement remains the biggest single obstacle to gaining knowledge of the behavior of buried structures. Concentrated efforts are being made by various groups to overcome this measurement problem and it is hoped that a solution will be forthcoming in the near future.

Progress in the measurement area can also be achieved through careful planning of the recording scheme. In dynamic tests it is not sufficient to provide a table of peak values because the parameters vary in time and the entire time variation is usually necessary to understand the behavior. The traces on the oscillograms in the Series I and II tests were crowded together and, because of the large

number of traces recorded, overlapped each other to the extent that the oscillograms could not be reproduced directly and included in the report; in several cases they would not have been intelligible to anyone not intimately familiar with the experiment. For this reason typical records for certain of the more informative tests were traced and are included. Certain of the detail and some of the accuracy is lost in such reproduction, and it is a poor substitute for the actual records. The knowledge and experience gained from the Series I and II tests will permit considerable improvement in future tests.

Problem Areas Remaining

The major problem areas remaining are embodied in questions to be answered as follows:

1. What is the influence of footing width on the behavior of buried arches?

2. Is it advantageous to design the structure so that the footings can move inward?

3. What is the influence of varying the stiffness of the arch? How will a five-hinged arch perform? What is the thinnest structure which can now be employed without incurring buckling failure?

4. What is the influence of varying the ratio of the depth of cover to span?

5. Can mechanical shielding between the structure and the soil be successfully employed to decrease the effects of loads transmitted by the soil?

6. Can modeling be employed to predict other than displacements in dry sand?

7. How does response to a traveling wave compare with the response of the structures tested in the blast simulator?

Answers to the last two questions require field testing. If the effect of a traveling wave on response is small, it should be possible to answer the remainder of the questions by tests in the blast simulator.

FINDINGS

1. The computed and experimental values of natural period agreed well for the uncovered arch without endwalls.

2. Insertion of endwalls altered the response and made it difficult to excite the first symmetrical and first antisymmetrical modes.

3. Earth cover apparently reduced the fundamental period; the stiffening effect of the soil seemed to be more influential on the period than the added mass.

4. Moments and thrusts due to backfill were very small.

5. The moment had the same form in the static and dynamic tests: the moment was a maximum at 5 degrees from the springline.

6. The shape of the moment curve permitted estimating the buckling load.

7. The moment at the 5-degree point was 5 times the moment at the crown.

8. Moment and thrust had peak values approximately twice their values in the quasi-static state.

9. The distribution of thrust was approximately uniform.

10. Passive-sense pressures were developed in the region from 0 to 20 degrees on the arch, and active-sense pressures were developed elsewhere at the interface.

11. Efforts at measuring soil pressure were largely unsuccessful, although some useful information was derived from the interface measurements. The reading of each gage was dependent upon the manner in which the soil was initially placed over the face of the gage. With repeated loading the same percentage of the surface load was indicated.

12. Pressure rise time on the arch was much longer than theoretical predictions.

13. The peak load on the crown was greater for the short-duration loads than for the long-duration loads.

14. The velocity of the soil stress wave was 1300 feet per second.

15. The deflection-time behavior differed for long- and short-duration loadings.

16. For long-duration loads the fundamental action was a downward body motion of the entire structure into the soil.

17. The nature of the deflection behavior was somewhat dependent upon the magnitude of the applied load.

18. Response of the buried arch was found to be very much dependent upon the soil stiffness as indicated by the soil density. A small reduction in density in the Series II tests resulted in a large percentage increase in peak deflection.

19. Peak deflections from the first loading in a series were much greater than for subsequent loadings at the same overpressure. With each successive loading at a given level, the peak deflection was less than in the preceding loading but not by a large amount.

20. In the long-duration tests, recovery from the maximum displacement was small. In the free field, at the elevation of the footings, elastic recovery was 30 percent, but for the footings the corresponding recovery was only 15 percent.

21. In most cases, the sides (8-degree points) moved outward slightly and then moved inward after the peak deflection of the crown had been reached.

22. The percent of load carried by arching in the static tests was found to be dependent upon the magnitude of the applied load; at low surface loads the proportion of the load carried by arching is large but the proportion decreases rapidly as the load is increased.

23. In the dynamic tests, arching varied with time.

24. The inertial forces of the backfill soil could not be neglected in studying the response of the buried structure to blast loads. Therefore, dynamic tests cannot be replaced by static tests.

25. Apparently, results of scale-model experiments can permit reasonably accurate predictions of prototype deflections.

Due to the limited number of tests performed and the idealized conditions of the tests, none of the findings are offered as firm conclusions. The tests results are exceedingly encouraging, however, and it is expected that tests scheduled for the near future will provide confirmation of most, if not all, of the above findings.

ACKNOWLEDGMENTS

Appreciation is extended to those colleagues who made helpful suggestions during the development of the experimental program and the review of the report. Special thanks are due Mr. J. L. Anderson who helped in the reduction and analysis of the data, Mr. H. Tomita who performed the free-field deflection measurements, and Dr. M. T. Davisson of the University of Illinois for valuable suggestions on the soils aspects of the work.

Dr. Glenn Murphy of Iowa State University reviewed the report under a personal services contract with NCEL.

REFERENCES

1. Department of the Navy, Bureau of Yards and Docks. P-81, Personnel Shelters and Protective Construction. Washington, D. C., 25 November 1958.

2. Air Force Special Weapons Center. TN-61-14, Design and Analysis of Foundations for Protective Structures, by K. E. McKee. Kirtland Air Force Base, New Mexico. Report prepared by Armour Research Foundation, Chicago, Illinois, May 1961.

3. Air Force Special Weapons Center. TDR-62-2, A Study of the Use of Models to Simulate Dynamically Loaded Underground Structures, by G. Murphy and D. F. Young. Kirtland Air Force Base, New Mexico, January 1962.

4. Mario G. Salvadori and Richard Skalak. "Stress Waves in Dissipative Media," New York Academy of Sciences, Ser. II, Vol. 21, No. 5 (March 1959), pp. 427-437.

5. S. Timoshenko and J. N. Goodier. Theory of Elasticity, Second Edition. The Maple Press Company, York, Pennsylvania, February 1951, p. 438.

6. Operation Plumbbob, Project 3.3. WT 1422, Evaluation of Buried Corrugated-Steel Arch Structures and Associated Components, by G. H. Albright, et al. February 28, 1961.

7. W. A. Walls. The Influence of Blast and Earth Pressure Loadings on the Dynamic Response of Flexible Underground Two-Hinged Arches. Ph. D. thesis, University of Illinois, 1960.

8. U. S. Naval Civil Engineering Laboratory. TR-191, Design for a Cast-In-Place Concrete Shelter, by J. R. Allgood, R. M. Webb, and R. F. Swalley. Port Hueneme, California, 13 December 1962.

9. G. S. Spangler. Soil Engineering. International Textbook Company, Scranton, Pennsylvania, 1951, pp. 409-447.

10. Karl Terzahi and Ralph B. Peck. Soil Mechanics in Engineering Practice. John Wiley & Sons, New York, 1948, p. 199.

11. Armed Forces Special Weapons Center. TR-61-32, Static Experiments for the Study of the Interaction of Buried Structures With Ground Shock Waves, by A. H. Wiederman. Armour Research Foundation, Kirtland Air Force Base, New Mexico, April 1961.

12. U. S. Naval Civil Engineering Laboratory. TR-199, Deadman Anchorages in Sand, by J. E. Smith. Port Hueneme, California, 12 July 1962.

13. Air Force Special Weapons Center. Numerical Studies of the Dynamic Response of Shallow-Buried Arches Subjected to Blast Loading, by Caryll R. Whipple. Kirtland Air Force Base, New Mexico. A draft of a report prepared by the University of Illinois under Contract AF29(601)-25901. August 1961.

14. A. Ang and N. M. Newmark. "Computation of Underground Structural Response," Progress Report No. 3, Technical Supplement, DASA Contract No. DA-49-146-XZ-104. University of Illinois, 1 March 1962.

15. U. S. Army Engineer Waterways Experiment Station. Analysis and Design of Flexible Underground Structures, Vol. II (1 May 1960), by N. M. Newmark, J. W. Brisco, and J. L. Merritt. Vicksburg, Mississippi. A report prepared by the University of Illinois under Contract DA-22-079-eng—225. CONFIDENTIAL.

16. University of Illinois. Structural Research Series No. 149, "Design of Underground Structures to Resist Nuclear Blast," by J. L. Merritt and N. M. Newmark. Urbana, Illinois, April 1958.

17. E. T. Selig, K. E. McKee, and E. Vey. "Underground Structures Subject to Air Overpressure," Journal of the Engineering Mechanics Division, Proceedings of the ASCE, August 1960.

18. W. A. Shaw and J. R. Allgood. "An Atomic Blast Simulator," Proceedings of the SESA, Vol. XVII, No. I, 1959.

19. A. Ang and N. M. Newmark. "Computation of Underground Structural Response," Progress Report No. 6, Technical Supplement, DASA Contract No. DA-49-146-XZ-104. University of Illinois, 4 September 1962.

20. H. G. Mason. "Field Tests on Laterally Loaded Piles in Sand and Clay," ASTM Special Technical Publication No. 206, 1957.

21. S. Timoshenko. Theory of Elastic Stability, First Edition. The Maple Press Company, York, Pennslyvania, May 1936, p. 7.

22. D. H. Trollope and I. K. Lee. "The Performance of a Laboratory Earth Pressure Cell," Australian Journal of Applied Science, Vol. 8, No. 2 (June 1957), pp. 84-87.

23. Operation Plumbbob, Project 3.1. WT 1420, Blast Loading and Response of Underground Concrete-Arch Protective Structures, by W. J. Flathau, R. A. Breckenridge, and C. K. Wiehle. June 5, 1959. CONFIDENTIAL.

24. J. M. Frankland. "Effects of Impact on Simple Elastic Structures," SESA, Vol. 4, No. 2, May 1947.

25. T. S. Landale. Investigations into the Dynamic Bearing Properties of Cohesionless Soils. Thesis, Massachusetts Institute of Technology, Cambridge, September 1954.

26. Massachusetts Institute of Technology. AFSWP-118, Behavior of Soils Under Dynamic Loading 3, by R. V. Whitman. Cambridge, August 1954.

27. Air Force Special Weapons Center. TR-59-70, Design of Protective Structures to Resist the Effects of Nuclear Weapons, by N. M. Newmark and J. G. Hammer. Kirtland Air Force Base, New Mexico, December 1959. CONFIDENTIAL.

28. Air Force Special Weapons Center. TN-61-6, A Theoretical Study of Structure-Medium Interaction, by A. M. Soldate and J. F. Hook. Kirtland Air Force Base, New Mexico, November 1960.

29. Air Force Special Weapons Center. TR-62-6, Preliminary Design Methods for Underground Protective Structures, by N. M. Newmark and W. J. Hall. Kirtland Air Force Base, New Mexico, June 1962. SECRET

30. Operation Plumbbob, Project 3.8. WT 1427, Soil Survey and Backfill Control in Frenchman Flat, by T. B. Goode, et al. 23 October 1959.

31. B. K. Hough. Basic Soils Engineering. The Roland Press, New York, 1957, p. 284.

32. Douglas Bond. "The Influence of Foundation Size on Settlement," Geotechnique, Vol. 9 (1961), pp. 121-143.

33. K. Terzaghi. "Evaluation of Coefficients of Subgrade Reaction," Geotechnique, Vol. 5 (1955), pp. 297-326.

34. L. A. Palmer and J. B. Thompson. "The Earth Pressure and Deflection Along the Embedded Lengths of Piles Subjected to Lateral Thrust," Proceedings, Second International Conference on Soil Mechanics and Foundation Engineering, Vol. V, Art. VII-b-3 (1948), pp. 156-161.

35. A. B. Chilton. The Deflection of Piles Under Lateral Thrust — An Analytical Solution. Unpublished report. (1954).

LIST OF SYMBOLS

A = area of arch section

a = exponent parameter in stress–strain approximation for dry sand

B = diameter of circular footing

b = width of footing

C_n = constant depending upon mode of vibration; n = 1, 2, 3 . . .

C_s = seismic velocity of soil

d_o = depth of cover over crown of arch

d_{se} = deflection at surface of soil

d_{ye} = deflection at some distance y below the surface

E = modulus of elasticity of arch material

E_i = initial tangent modulus

e = bulk modulus

f_b = ultimate unit strength (stress)

$H_s = K_o p(r + d_o)$ = normal force on a vertical section of soil through the footing

I = moment of inertia of longitudinal section

K_o = at-rest coefficient

k = modulus of subgrade reaction; coefficient of permeability; stiffness of arch (EI)

L = length of buried arch

M = moment

N = axial thrust

N_e = Newtonian constant

P_{arch} = portion of surface load directly above arch carried by the soil

p = unit pressure at interface

p_b = interface pressure at crown

p_{cr} = critical radial unit-buckling load of a buried arch

p_h = horizontal unit pressure in a soil field

p_o = peak surface overpressure

$p_{s_{cr}}$ = estimated surface pressure to produce buckling

p_v = vertical unit pressure in a soil field

R = footing reaction

r = arch radius

S = section modulus of arch

T_n = natural frequency corresponding to mode shapes n = 1, 2, 3 . . .

t = any time

t_b = time at which pressure reaches a maximum on crown of arch

v = stress-wave velocity

y = depth below surface of soil

y_f = deflection of footing

γ = density of sand; mass density of arch or arch-soil system

γ_d = dry unit weight of sand

δ = displacement at time t

ϵ = unit strain

ϵ_a = unit strain on extrados at $\theta = \theta_a$

ϵ_b = unit strain on intrados at $\theta = \theta_a$; unit strain at ultimate stress

η = linear scale factor

λ = any length in model

μ = $\tan \varphi$

ρ_a = mass density of arch material

ρ_s = mass density of sand

σ = unit stress

σ_f = unit stress at incipient shear failure of soil

$\sigma_1 - \sigma_3$ = deviator stress in standard triaxial soil shear test

τ = effective duration of blast load

φ = angle between base line and radius through a given point on the arch; angle of internal friction

ω_n = natural (circular) frequency

Appendix A

PROPERTIES OF SOIL AND FOUNDATION

Investigation of any soil-structure interaction problem is rendered difficult by the heterogeneous nature of soil, which makes the behavior of soil difficult to define with precision. The purpose of this appendix is to discuss the behavior of sand and the properties that influence this behavior. Included in this appendix is a description of the method of placement of sand for the soil-structure interaction experiments described in the main body of the report. Also included are a discussion of the behavior of sand under static loads and a review of the limited data available concerning the behavior of sand under dynamic loads.

For the three-dimensional soil-structure interaction experiments, sand was placed in 2-foot layers up to the elevation of the footings of the test structure. Each layer was compacted thoroughly and uniformly by the operation of a Lazan oscillator on the surface of the layer. For this application, the oscillator was mounted on an 18-inch by 18-inch by 2-inch wooden slab, which was moved about the surface of the sand in a regular pattern so as to afford complete coverage of the surface area of the pit. The oscillator was operated at a frequency near the natural frequency of the sand mass. After the structure was set into place on the compacted sand, the remaining sand was placed around and above the structure. All sand above the elevation of the footings was compacted by uniform insertion in a regular pattern of a concrete spud vibrator. Density of the sand at each 2-foot layer was determined by the conventional sand replacement method. Density and other important physical properties of the sand are shown in Table A-I. Grain size distribution is shown in Figure A-1. This sand was excavated from the bed of the Santa Clara River, California, and was crushed and kiln-dried before use.

It would be easier to duplicate density conditions from test to test, and from place to place in a given test, if the sand used had a narrower range of grain sizes. However, by careful control of placement, local variation of properties in the soil mass was minimized. Low cost of the sand used and its ready availability in large quantities offset the slight advantage of a "one-size" sand.

One of the most important properties of sand is the density, γ. Figure A-2 shows that density has an appreciable effect upon the ultimate strength of the sand. This plot, along with Figure A-3, also shows that the initial tangent modulus, E_i, increases with an increase in density.[10] Since lateral pressure increases with depth and density increases slightly with lateral pressure, it follows that E_i should increase with depth. An increase in surface load also will produce a small increase in the density of the sand, so it can be stated that E_i increases slightly with an increase in load.

Table A-1. Fundamental Physical Properties of Soil[a/]

Properties	Series I	Series II
Type of soil	Sand	Sand
Average unit weight above footing elevation (before test), lb/ft^3	—	106.1
Average unit weight below footing (before test), lb/ft^3	111.9	105.8
Angle of internal friction at approximately 111 lb/ft^3	43°	43°
Cohesion	0	0
Moisture content	0	0
Specific gravity	2.62	2.62
Seismic velocity, ft/sec	—	1,300
Secant modulus of compression[b/] at 50 psi and 111.9 lb/ft^3, psi	10,100	—
Secant modulus of compression[b/] at 50 psi and 105.8 lb/ft^3, psi	—	6,500

a/ Subgrade modulus, 15-in. circular plate at 0.1-in. settlement, lb/in.^{3}

b/ Consolidometer test

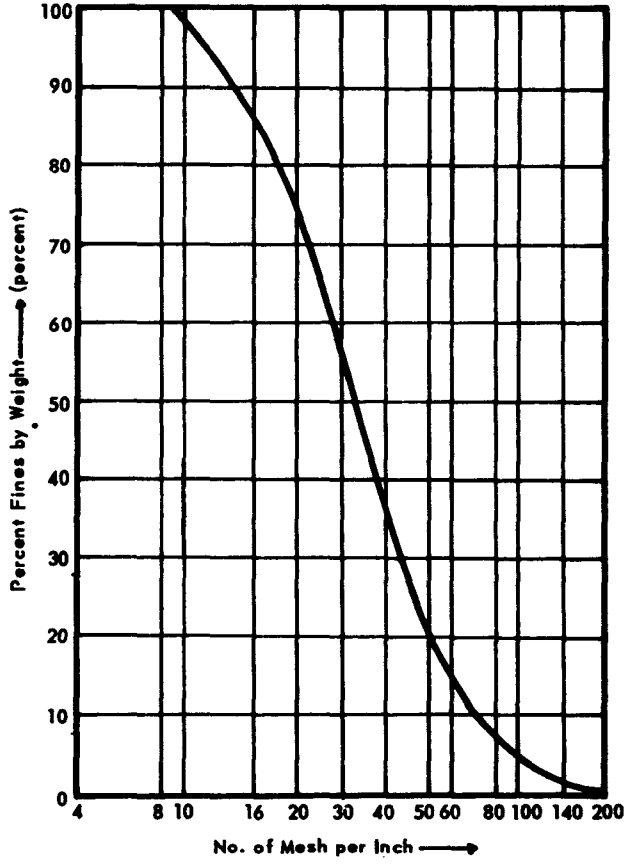

Figure A-1. Grain-size distribution of NCEL test sand.

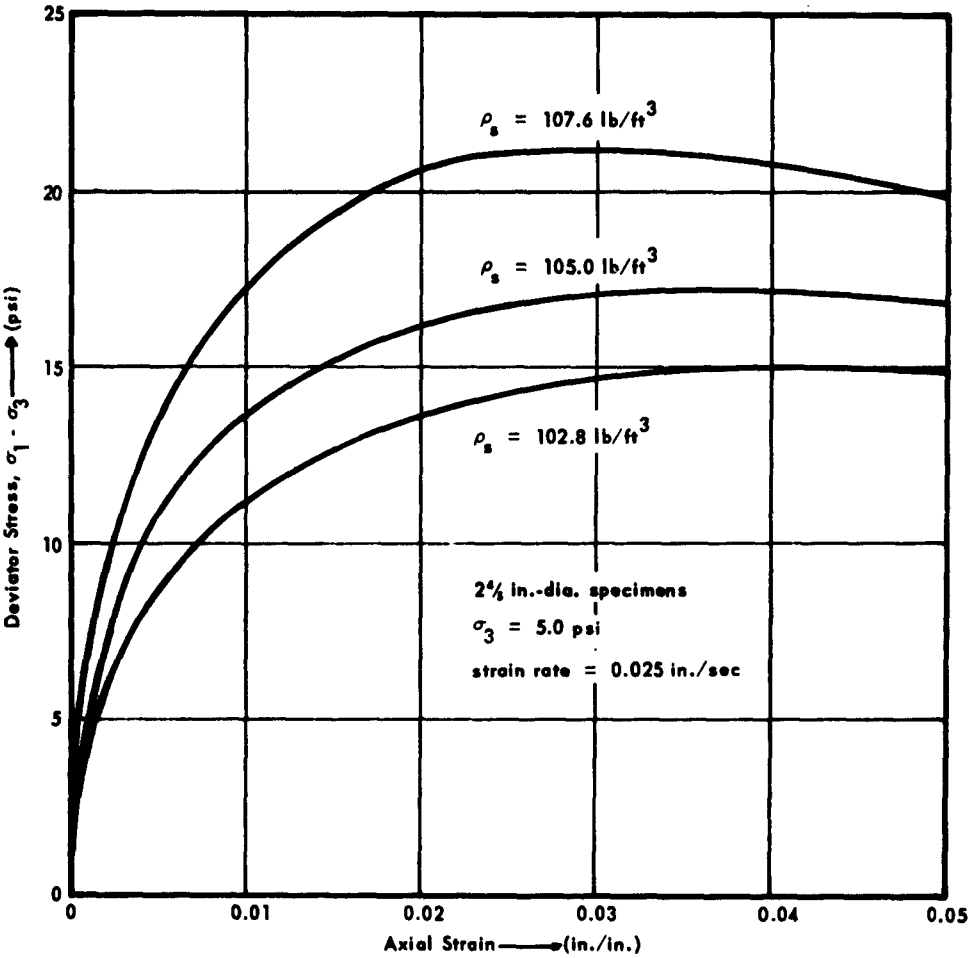

Figure A-2. Stress-strain curves for dry NCEL test sand.

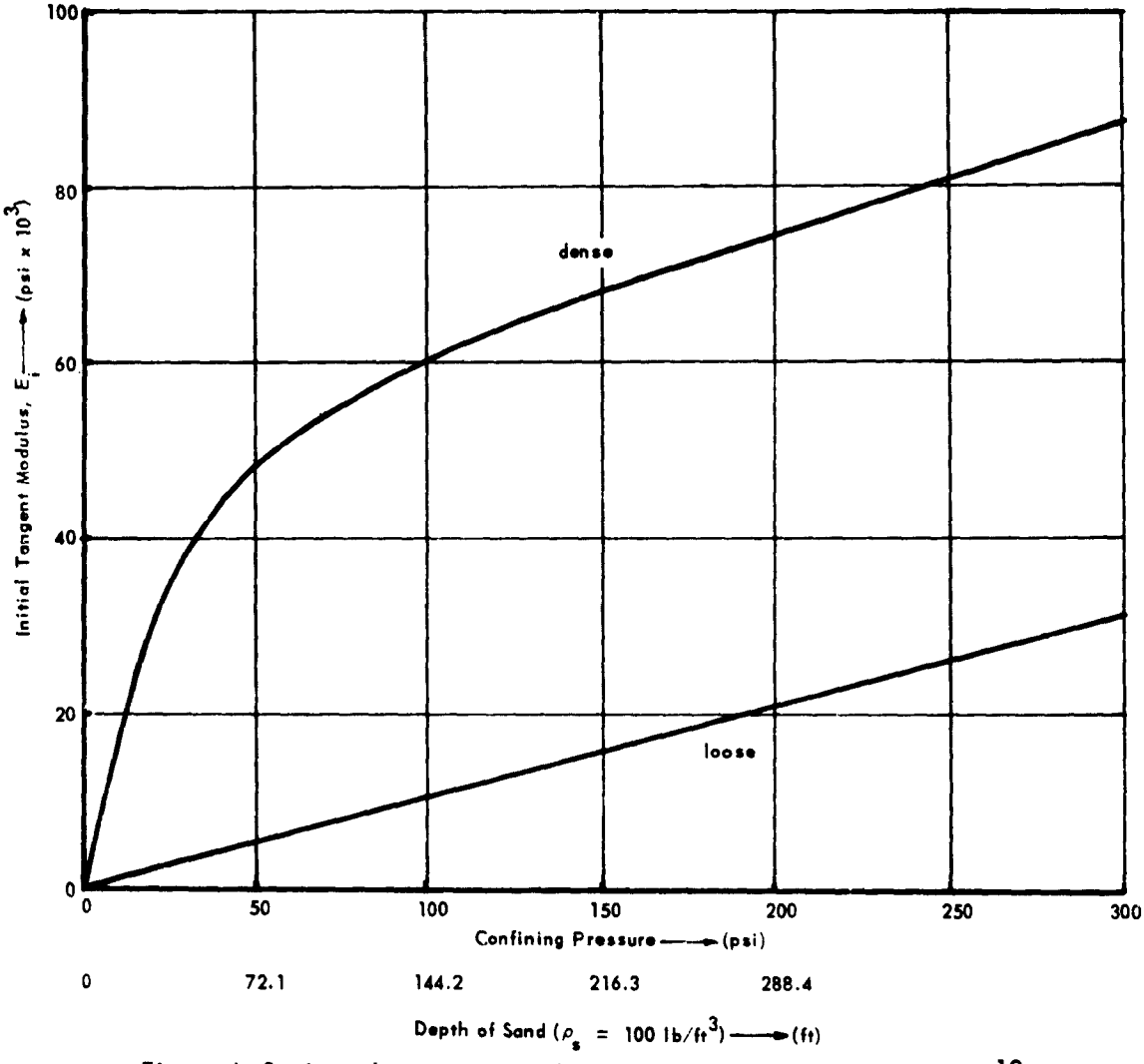

Figure A-3. Initial tangent modulus vs depth and confining pressure.[10]

The above reasoning should apply to the angle of internal friction, φ, since it increases with an increase in density. Therefore, it can be said that since density increases with load and with depth, both the initial tangent modulus and the angle of internal friction increase with load and with depth.

Of course, other factors such as grain size distribution and particle shape also influence the angle of internal friction. However, the preceding discussion has been limited to those factors which were variable during the experiments reported. Since the same sand was used for all experiments, the grain size and particle shape were not variables.

When the surface of a mass of sand is loaded, a certain amount of deformation takes place. Upon removal of the load, part of this deformation is regained, but there is usually a considerable amount of permanent set. This is a result of an expenditure of energy in reducing the void ratio of the sand. It is not a completely reversible elastic deformation. Each time the sand is reloaded there is an increase in total deformation, but the magnitude of the increase becomes successively smaller. This decreased increment is a result of the increased density, stiffness and strength of the sand caused by the previous load. An illustration demonstrating the hysteresis is shown in Figure A-4.

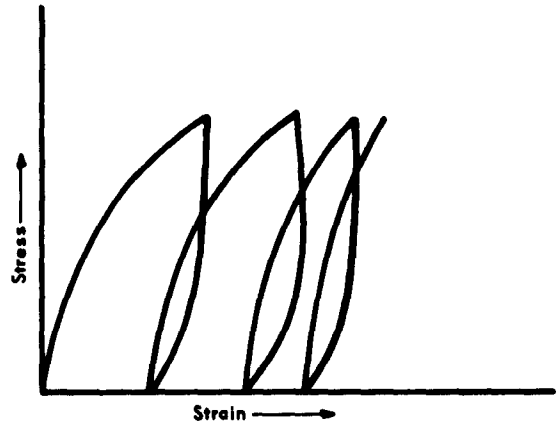

Figure A-4. Stress-strain relationship for sand subjected to repeated loading.

At a certain critical strain, the stress-strain characteristics of completely confined sand approach those of a solid. This occurs when the load has increased the density of the sand to a point where the void ratio no longer decreases with an increase in load. With such a load on a semi-infinite mass of sand loaded vertically on a free horizontal plane, there can be no horizontal deformation and the sand behaves like an elastic solid. A granular material which exhibits this phenomenon is called, by some experimentors, a "locking" medium. A typical example of this is shown in Figure A-5. A similar condition exists in the field when a spread footing is placed on a layer of dense sand overlaying stiff clay or rock. For such a condition to develop, the footing must be sufficiently wide that movement of the sand at the sides of the footing does not affect the lateral restraint of the sand beneath the center. Before the "locked" condition is fully developed, it is likely that crushing of particles commences. This condition continues with increasing pressure.

At least three different pressure conditions can exist in a soil-structure system depending upon the history of the system. These are (1) the at-rest pressure, (2) pressure in the active sense, and (3) pressure in the passive sense. The ratio between the horizontal and vertical pressure in a soil mass, p_h/p_v, is spoken of as the coefficient of lateral earth pressure, K. In the at-rest condition, no movement of the soil mass or of the structure has occurred since placement, and the coefficient of earth pressure at rest is K_o.

When a structure is forced against the surrounding soil mass, the pressure exerted on the interface by the soil is increased. This pressure increases with increasing strain until, at incipient failure, it reaches a maximum in the passive sense. The coefficient of passive earth pressure is

$$K_p = \tan^2\left(45^\circ + \frac{\varphi}{2}\right)$$

It can be exemplified by the increase in pressure in a horizontal direction at a region near the base of a buried semicircular arch loaded at the crown. This increased horizontal pressure just above the springline has a beneficial effect in that it adds to the stability of the arch by resisting further lateral movement of that critical region near the base.

At the crown of the arch where the structure, when loaded, moves down from its original position, the interface pressure becomes less than the at-rest pressure. It reaches a minimum called active pressure at incipient failure, and the coefficient of active earth pressure is

$$K_A = \tan^2\left(45^\circ - \frac{\varphi}{2}\right)$$

K_o, the coefficient of earth pressure at rest, is numerically between K_A and K_p.

In the main body of this report, the range of pressures between at-rest and active pressure are spoken of as pressure in the active sense. Similarly, the range of pressures between at-rest and passive pressure are spoken of as pressure in the passive sense. Also in this report, the reduction in vertical load on the structure caused by the active-sense pressure condition, expressed as a percentage of the total vertical load on the surface of the soil immediately above the structure, is called arching. The arching of the soil, as well as the passive resistance of the soil near the springline, has a primary influence on the behavior of the structure and must be considered in the analysis of any soil-structure interaction problem.

The load-settlement relationship of a footing can best be represented by a modulus of subgrade reaction, k. Its magnitude depends not only upon the strength of the soil but also upon the size of the loaded area, the relative magnitude of the load, and the depth of the footing below the surface.[32] The k value of a particular soil is found by means of a plate-bearing test. The value obtained must be adjusted to account for the size and shape of the footing placed upon the soil. Since a plate-bearing test requires much time and expense, research is needed to associate the modulus of subgrade reaction with some of the more easily determined soil properties.

Figure A-6, for a circular footing on the soil surface, shows that settlement of a footing, and therefore its k value, depends to a great extent upon the diameter of the footing. For diameters greater than approximately 12 inches, settlement is governed by compression of the soil mass directly beneath the footing.[31] Therefore, for this type of footing, the modulus of subgrade reaction, k, will very almost inversely with the footing diameter.[10,33] The same variation will hold for strip footings of more than about 12-inch width.

For very narrow footings, such as those in the small-structure tests reported in the main body of this report, bearing capacity is governed by shearing resistance of the soil. Lateral movement of the soil beneath the footing occurs, and the footing punches through the soil. For a given pressure, there is a critical width of footing which determines whether soil shear or soil compression will govern settlement. At less than critical width, shear controls; at greater than critical width, compression controls. In sand, the critical width depends to a great extent upon the shear strength of the sand. Shear strength, in turn, depends upon density and confinement, which

are functions of depth of burial. Hence, critical width will, in general, decrease with increasing depth of burial of the footing. It is difficult to predict the settlement of narrow footings, since bearing capacity is so sensitive to the many variables encountered in the soil environment. Certainly punching should be considered in studies involving extremely narrow footings.

For a wide footing, the relative magnitude of the load has a significant influence upon the modulus of subgrade reaction, k. Since the stress-strain relationship of sand is nonlinear at loads commonly encountered, the k value will decrease with increasing load. For loads less than one-half the ultimate, the load-settlement relationship may be represented by the tangent modulus, but for higher loads, various secant moduli should be used. This is shown in Figure A-7.

There have been several theories advanced concerning the variation of the modulus of subgrade reaction with depth. It is generally accepted that the k value of cohesionless soils increases in some manner with depth because of the increase in density and lateral confinement of the soil with depth. For sand, a straight-line variation seems to be most widely used (Figure A-8). An exponential variation over a pile length, L, of the form $f(y) = K(y/L)^n$ has been suggested.[34] By varying the constants K and n, a variation with depth which agrees with experimental data has been obtained.

A hyperbolic variation of the form $f(y) = Ky/(y + A)$ has been assumed, where K and A are constants.[35] This also is more flexible, and possibly more realistic than a straight-line variation. It also is more expedient mathematically than the preceding method.

A method has been proposed for the prediction of footing settlement.[8] In the derivation it is assumed that the subgrade modulus of sand varies directly with depth of burial. However, the defined "depth of burial" includes the actual depth plus an additional depth equivalent to the unit pressure under the footing divided by the soil density. A Boussinesq distribution of vertical stress is assumed and the incremental soil strains beneath the footing are integrated to obtain the total settlement. By integrating to an infinite depth, a closed mathematical solution is obtained for determining the k value of a particular footing from the k value obtained from a plate-bearing test.

The k value of sand also is influenced by moisture content. The addition of a small amount of moisture to sand increases its bearing capacity through apparent cohesion. A further addition of moisture will destroy this effect and reduce the bearing capacity by decreasing the intergranular pressure. The moisture contents at which these phenomena occur depend upon the density and grain-size distribution of the sand.

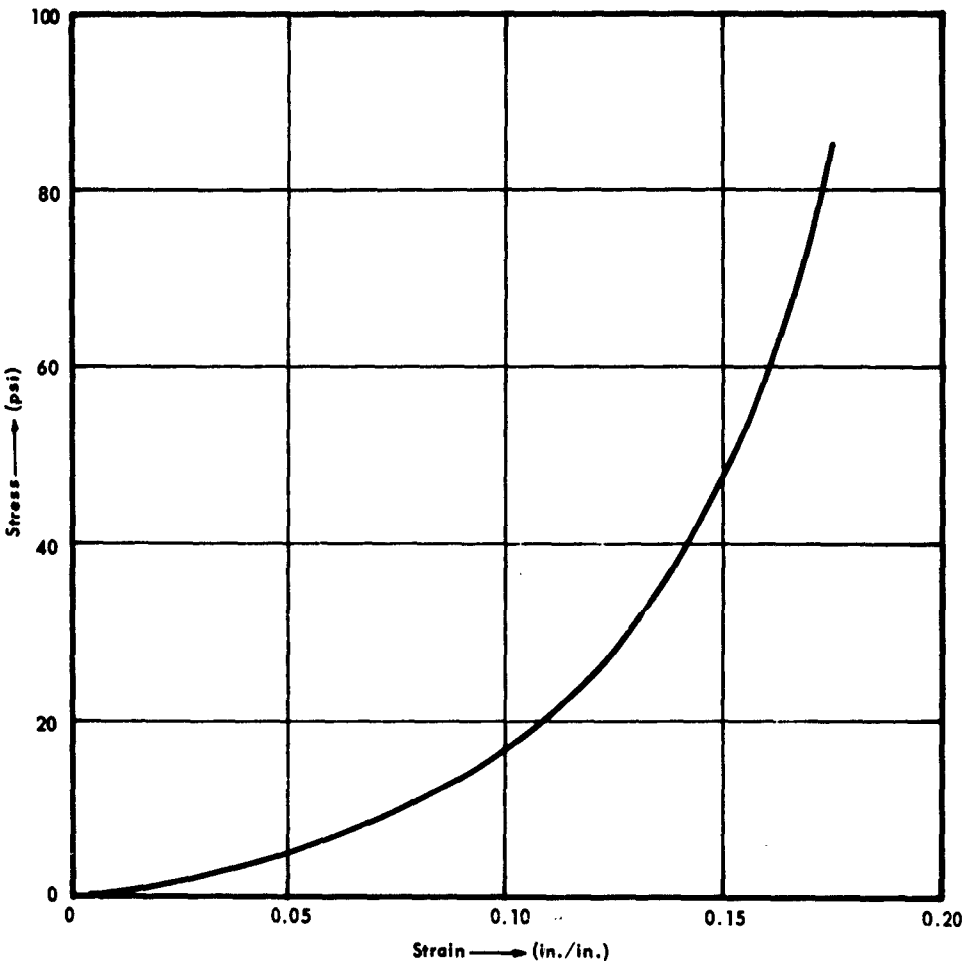

Figure A-5. Stress-strain relationship for laterally confined dense sample consisting of 90 percent sand and 10 percent mica.[10]

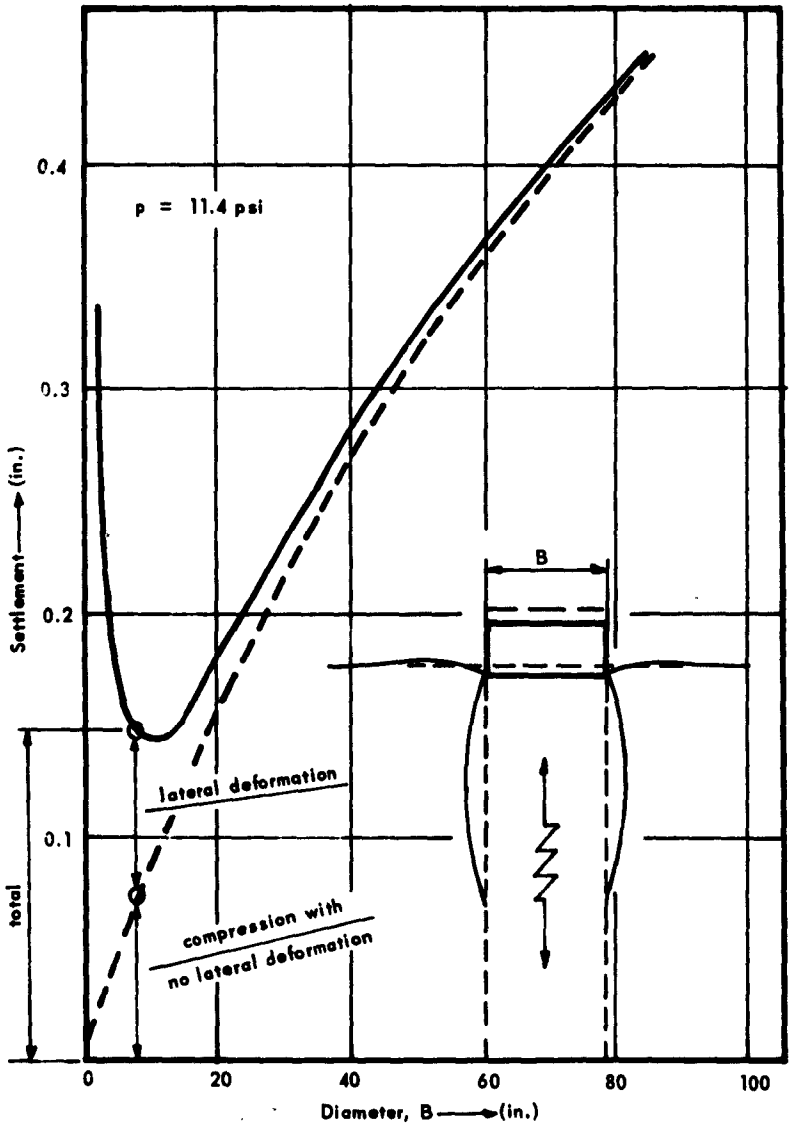

Figure A-6. The influence of lateral deformation on settlement in cohesionless soils.[32]

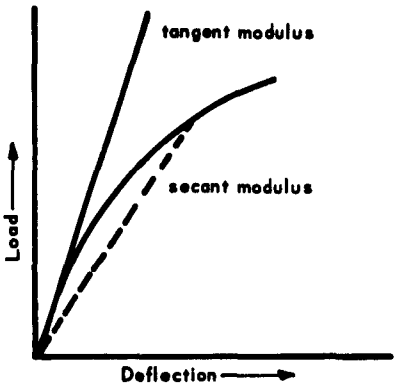

Figure A-7. Typical load-deflection curve for sand.

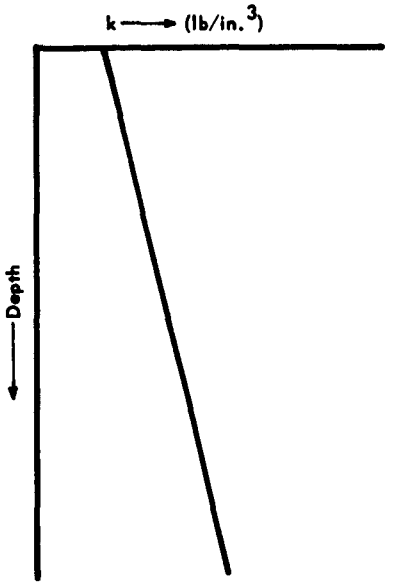

Figure A-8. Assumed variation of modulus of subgrade reaction of sand with depth.

The permeability of the sand is another variable influenced by density. Figure A-9 shows that an increase in density decreases the permeability of small-grained sand by a considerable amount, while it has little effect upon the permeability of large-grained sand.

This discussion has been primarily limited to the static behavior of sand. It has previously been believed that behavior similar qualitatively to static behavior occurs during dynamic loading, with some expected differences quantitatively. Knowledge of the dynamic behavior of footings on sand is very limited, and the analytical approaches which have been suggested have not as yet been proven or disproven by tests.

In 1954, the Massachusetts Institute of Technology conducted static and dynamic tests of small footings resting on moist sand and compacted silt.[25,26] The results of the tests were informative, but they were inconclusive as far as an accurate comparison of static and dynamic footing behavior is concerned.

McKee,[2] at the Illinois Institute of Technology, noted very little resemblance between the static and dynamic resistance of similar small footings. He concluded that it is inappropriate to use the static resistance of a footing, directly or with any simple modification, to predict its dynamic resistance.

At present, the University of Illinois, the U. S. Army Waterways Experiment Station, and others are engaged in dynamic tests on footings. Also, work along these lines is being done at the Naval Civil Engineering Laboratory. Results of static and dynamic plate-bearing tests without surcharge on dry sand in the blast simulator pit at NCEL have indicated that the dynamic load for a given settlement is in the vicinity of 10 to 15 percent higher than the static load for that same settlement. The tests are to be continued with various surcharges in an attempt to disclose the mode of variation of the modulus of subgrade reaction with depth.

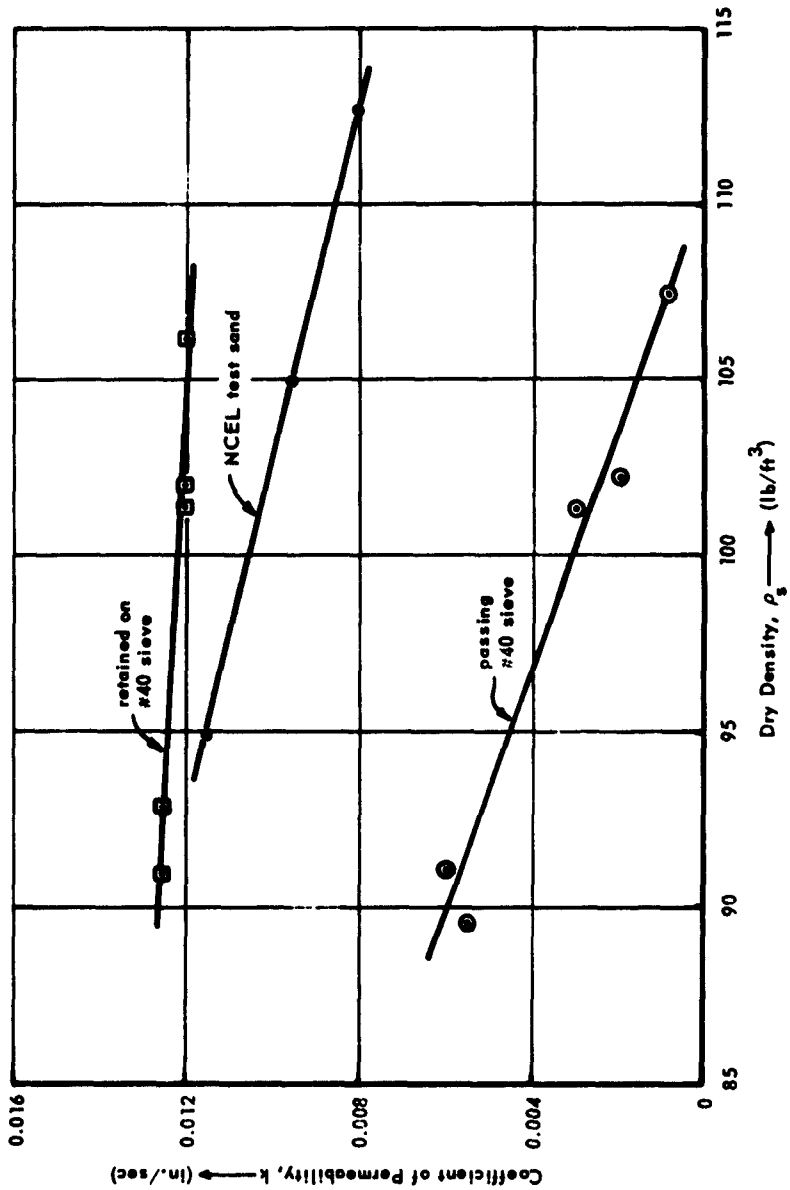

Figure A-9. Permeability of NCEL test sand.

Appendix B

MODEL TO PROTOTYPE CONSIDERATIONS

In the body of the report, the arch tested was considered as a small structure to avoid the problems of modeling. The purpose of this appendix is to review the requirements of similitude for an arch buried in dry sand.

A recent report outlines the meager background information available on the modeling of underground structures and cites the lack of experimental data on structure-medium interaction.[3] The report also identifies pertinent parameters as related to the blast, structure, and soil, and reviews the basic tenents of model analysis. Areas of uncertainty and difficulty also are cited.

One of the major difficulties in achieving true modeling is chargeable to strain-rate effects. Strain-rate effects, however, are not particularly important for dense dry sand. Unpublished test data obtained at the Laboratory and other available experiments[26] have shown that the influence of strain rate upon the properties of dry sand are less than 10 percent. A second difficulty occurs by virtue of the energy absorption and dispersion of a transmitted wave. The seriousness of the latter phenomenon is unknown at present, but the effects are probably small for shallow-buried structures.

The theory of Reference 3 may be applied to the arch-sand system as indicated in Table B-I. In this analysis it is assumed that the same materials are used in the model and in the prototype and that the properties of the sand are as discussed in Appendix A. Further, it is presumed that the stress-strain properties of the sand are analytically definable with the parameters listed.

The procedure followed in developing Table B-I, as in most model analyses, was to:

1. List the pertinent parameters.
2. Determine the number of dimensionless independent parameters.
3. Apply the Buckingham Pi Theorem.
4. Form suitable pi terms.

5. Fix a number of parameters equal to the number of independent dimensions.

6. Determine the design and operating conditions.

The Newtonian constant was introduced to permit nondimensionalizing the mass density.

In Table B-I the variables associated with the load, the structure, the soil, and the inertial effects are listed. Certain of the parameters, of course, are associated with more than one component of the system, in which case the primary association is given. A standard exponentially decaying blast load is presumed in forming the list. Inertial forces associated with the structure, and all gravity forces were assumed to be negligible.

It is significant that the inertial forces associated with the structure can be readily included if desired by including the mass density of the arch material as a pertinent parameter. Inclusion of unit weight to account for gravity forces, however, results in an incompatible condition. It turns out that the length scale, the modulus-of-elasticity scale, and the unit-weight scale cannot be fixed independently because the three are not dimensionally independent.

As indicated in the summary of Table B-I, there are 15 variables and three independent dimensions which permit the formation of 12 pi terms. Force and mass are related through Newton's second law of motion and are not independent. Since there are three independent dimensions, three independent scales may be established from which all others are determinable. In addition to the geometry or length scale, it is expedient to establish scales on the basis of two-dimensionally independent properties of the material. Since these should be the most significant properties of the system, the soil modulus and the mass density of the soil were chosen. With these properties fixed, the primary design and operating conditions are found as indicated in the last column of Table B-I.

The essence of the design and operating conditions is that the unit pressure in the prototype must equal the unit pressure in the model, the time scale must be the same as the length scale, and the stiffness of the arch must scale as the fourth power of the length scale.

Two problem areas, other than the ones previously cited, which deserve mention arise from the variation of the soil modulus with depth (surcharge pressure) and the difference in the action of footings of different sizes. The soil modulus is expected to vary approximately linearly with surcharge pressure. Notably, the soil cannot distinguish between the surcharge pressure caused by depth of cover and that caused

by the surface load. Since the surface load must be the same in the model and the prototype and since the surface load in the cases of prime concern will be so much greater than the pressure due to the soil cover, the variation of the soil modulus between the model and the prototype should be very little. That is, the chosen design condition should be met.

From the previous discussion, then, one would conclude that the analysis of Table B-I is expected to result in the correct modeling. Correlation of the results of the Plumbbob Structure 3.3 tests and the small-structure tests conducted in the simulator has been accomplished in the body of the report where it is shown that reasonable agreement exists in comparing deflections.

Table B-1. Dimensional Analysis

No.	Associated Variable	Symbol	Parameter Description	Dimensions	Pi Terms $\pi_{12} = f(\pi_1, \pi_2 \cdots \pi_{11})$	Model-to-Prototype Relations	Conditions From Setting $\frac{r}{r_m} = \eta$, $\frac{E}{E_m} = 1$ and $\frac{\rho_s}{\rho_{sm}} = 1$
1	Load	p_o	Peak surface overpressure	FL^{-2}	$\pi_1 = \frac{p_o r^4}{k}$	$\frac{p_o}{p_{om}} = \frac{k r_m^4}{k_m r^4}$	$\frac{p_o}{p_{om}} = 1$
2		t	Any time	T	$\pi_2 \quad \frac{t}{\tau}$	$\frac{t}{t_m} = \frac{\tau}{\tau_m}$	
3		t_r	Rise time of pressure	T	$\pi_3 \quad \frac{t_r}{\tau}$	$\frac{t_r}{t_{rm}} = \frac{\tau}{\tau_m}$	
4		τ	Pressure duration	T			
5	Structure	r	Radius of arch	L	$\pi_4 = \frac{\lambda}{r}$	$\frac{\lambda}{\lambda_m} = \frac{r}{r_m}$	
6		λ	Any other pertinent length	L	$\pi_5 \quad \epsilon$	$\frac{\epsilon}{\epsilon_m} \quad 1$	
7		k	Stiffness of arch (EI)	FL^2	$\pi_6 \quad \frac{Er^4}{k}$	$\frac{E}{E_m} = \frac{k r_m^4}{k_m r^4}$	
8	Soil	ϵ	Unit strain	none			
9		E	Soil modulus	FL^{-2}	$\pi_7 \quad a$	$\frac{a}{a_m} = 1$	$\frac{k}{k_m} = \eta^4$
10		a	σ-ϵ shape parameter	none	$\pi_8 = \epsilon_o$	$\frac{\epsilon_o}{\epsilon_{om}} \quad 1$	
11		ϵ_o	σ-ϵ energy dissipation parameter	none	$\pi_9 \quad \frac{\sigma_f r^4}{k}$	$\frac{\sigma_f}{\sigma_{fm}} = \frac{k r_m^4}{k_m r^4}$	
12		σ_f	Failure stress of soil	FL^{-2}			
13		ν	Velocity of soil stress wave	LT^{-1}	$\pi_{10} = \frac{\nu\tau}{r}$	$\frac{\nu}{\nu_m} = \frac{r\tau_m}{r\tau_m}$	
14	Inertia	ρ_s	Mass density of sand	ML^{-3}	$\pi_{11} \quad \frac{\rho_s N_e r^6}{k\tau^2}$*	$\frac{\rho_s}{\rho_{sm}} = \frac{k\tau^2 r_m^6}{k_m \tau_m^2 r^6}$	
15	Dependent variable	δ	Displacement at time t	L	$\pi_{12} \quad \frac{\delta}{r}$	$\frac{\delta}{\delta_m} = \frac{r}{r_m}$	$\frac{\tau}{\tau_m} = \eta$

* Where N_e = Newtonian constant in $F = N_e Ma = 1/32\ FM^{-1}L^{-1}T^2$.

Appendix C

FOAMED-PLASTIC MODEL

A configuration of a buried structure was made from a sheet of foamed plastic and other available materials, as shown in Figure C-1. Though not a true model, the setup will be referred to as a model for convenience. The purpose of the setup was to provide some idea of the character of the deformations to facilitate location of instrumentation in the small-structure tests in the blast simulator.

At the time the plastic model was made, it was not intended to report the deformation patterns obtained; however, they seemed to be worth including since the results, while of no quantitative value, do present an interesting qualitative picture of probable relative deflections in a media-structure system.

As may be seen in Figure C-1, the model consisted of a 3/4-inch-thick foamed-plastic sheet, with a semicylinder cut out for an arch, and blocks cut out to accommodate footings. The sheet was fixed along the bottom edge, but not constrained at the sides. Paper liners and wooden blocks were subsequently inserted in the cutout to represent an arch and its footings. Two weights of paper card were used to represent arches of different stiffnesses, and two sizes of footings were employed. Loads were applied along the top surface of the plastic sheet by means of pumping air into a double strip of rubber medical drain tubing, which was confined by a notched piece of fir two-by-four. The pump, Bourdon pressure gage, and metal tubing which attaches to the end of the medical drain tube are visible in Figure C-1. A grid was ruled on the plastic sheet to permit recording deflection patterns.

Tests were performed as follows: (1) a photograph of a given setup was made prior to the application of any load, (2) a uniform load of 1-1/2 psi was applied to the top surface of the sheet, and (3) a second exposure was made on the same film. This resulted in double-lined pictures which showed the original and final position of the grid lines and, thus, defined the deformation patterns for various conditions as follows:

1. Figure C-2. Thin-card arch, rectangular footings, and semicircular plug in the cutout.

2. Figure C-3. Sheet loaded with nothing in the cutout.

3. Figure C-4. Plastic sheet with thin-card arch and rectangular footings.

4. Figure C-5. Same as 3 except with tied footings.

5. Figure C-6. Plastic sheet with thick-card arch and rectangular footings.

6. Figure C-7. Plastic sheet with thin-card arch and trapezoidal footings.

Several interesting observations were made from these tests, some of which confirmed expected behavior and others which were somewhat serendipitious. Figure C-3 shows that with no arch liner in the cutout, large deformations occurred in the region of the crown but that there was essentially no deformation beneath the footing cutout. Insertion of the thin-card arch and rectangular footings, Figure C-4, reduced the crown deflection appreciably and resulted in deformations under the footing and the floor. (The latter deformation explains the failure which occurred in the floor slab of the Operation Plumbbob 3.3 structures.) There was considerable outward deflection at and near the right footing; consequently, the footings were tied with a piece of wire and the load reapplied, Figure C-5. Tying the footings resulted in a marked decrease in lateral deformations. (The right half of the system of Figure C-4 did not deform properly because of being caught on a sliver in the two-by-four reaction.) Use of a thick-card arch, Figure C-6, produced a similar pattern but resulted in smaller lateral deformations distributed throughout a greater depth. Doubling the size of the footings, Figure C-7, reduced the downward deflection thereof very slightly.

Two observations were made from the tests which are not shown in Figures C-2 through C-7: (1) the footings tended to rotate for the heavy-card arch, and (2) local inward buckling occurred in the thin-card arch near the right footing when the load was increased to about 4 psi. The buckling was a "snap-through" action similar to the "bottom-of-the-oil-can" type buckling and occurred in about the third symmetrical mode. Further study of this buckling phenomenon would appear to be warranted.

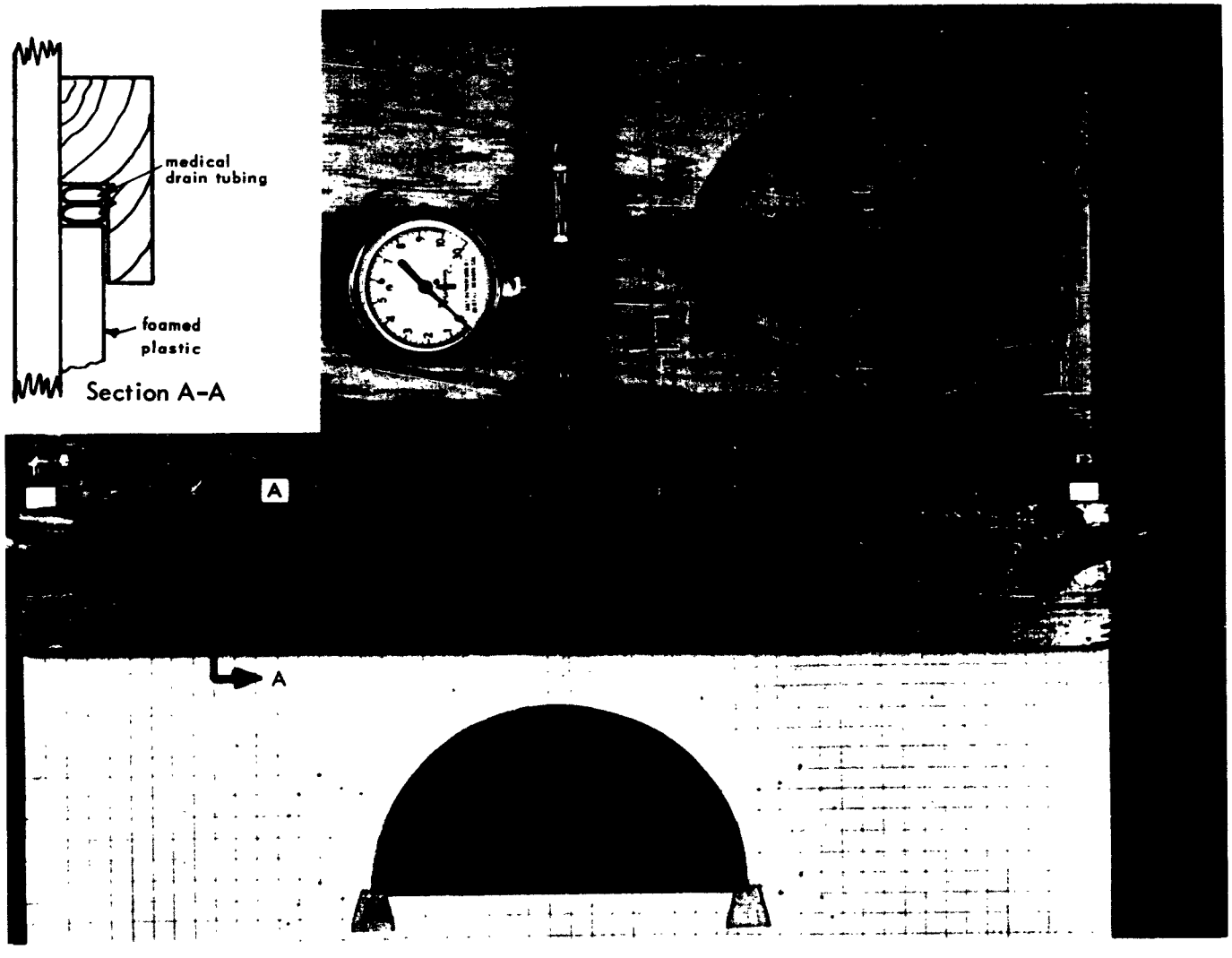

Figure C-1. Test setup for foamed-plastic model.

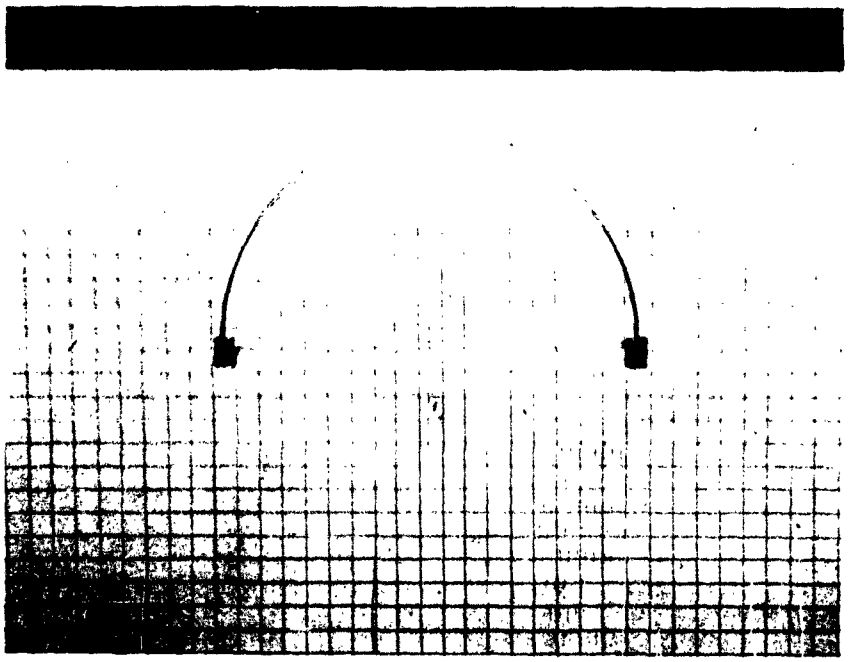

Figure C-2. Plastic sheet with plug in the cutout.

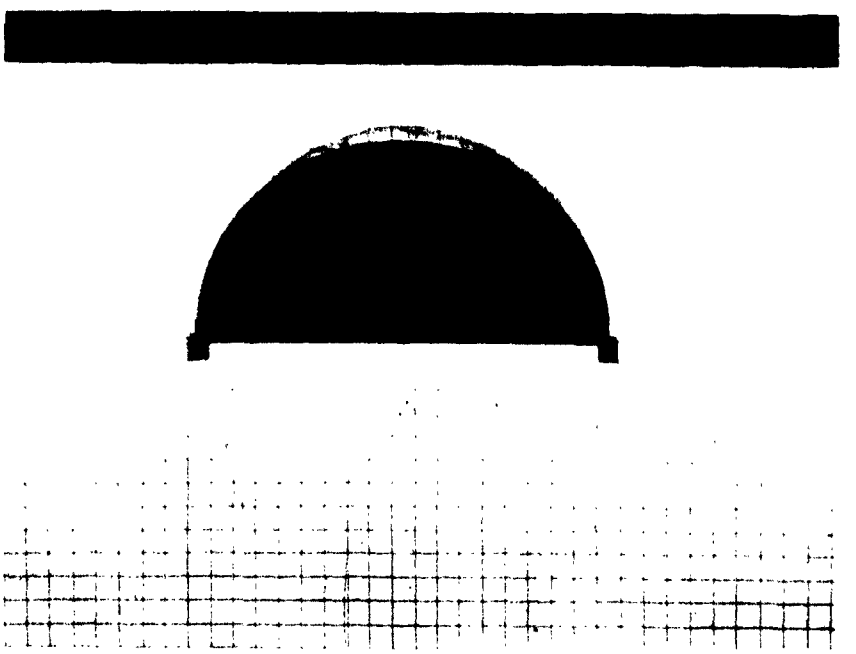

Figure C-3. Plastic sheet with nothing in the cutout.

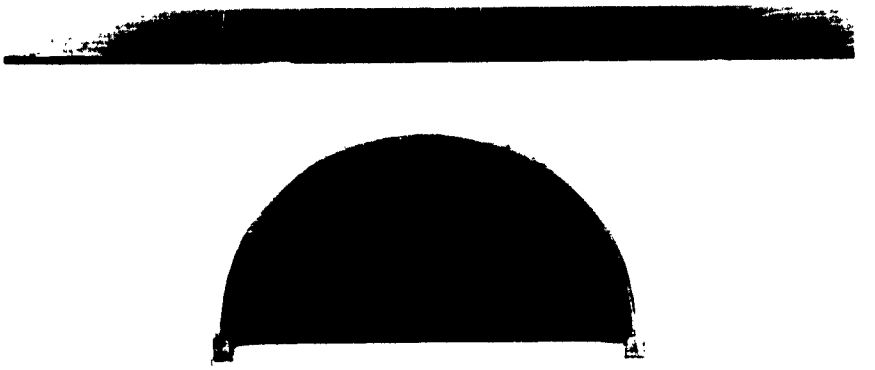

Figure C-4. Thin-card arch and rectangular footings.

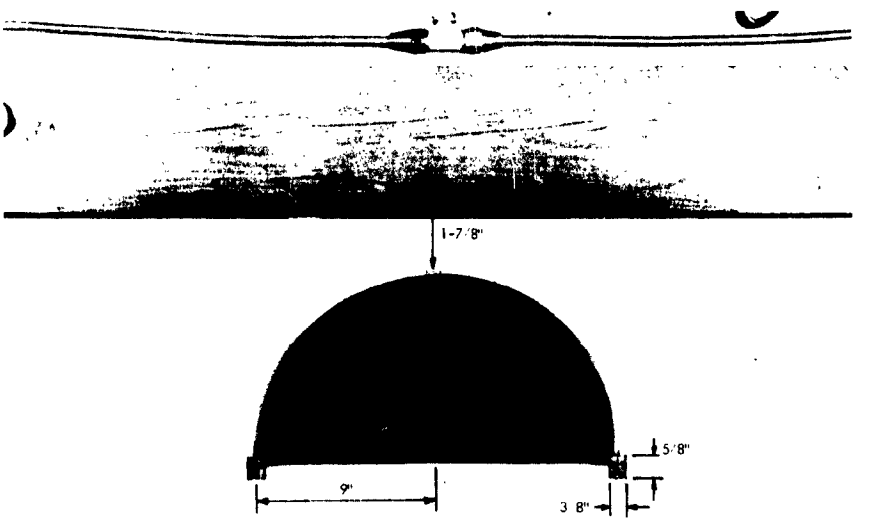

Figure C-5. Thin-card arch and rectangular tied footings.

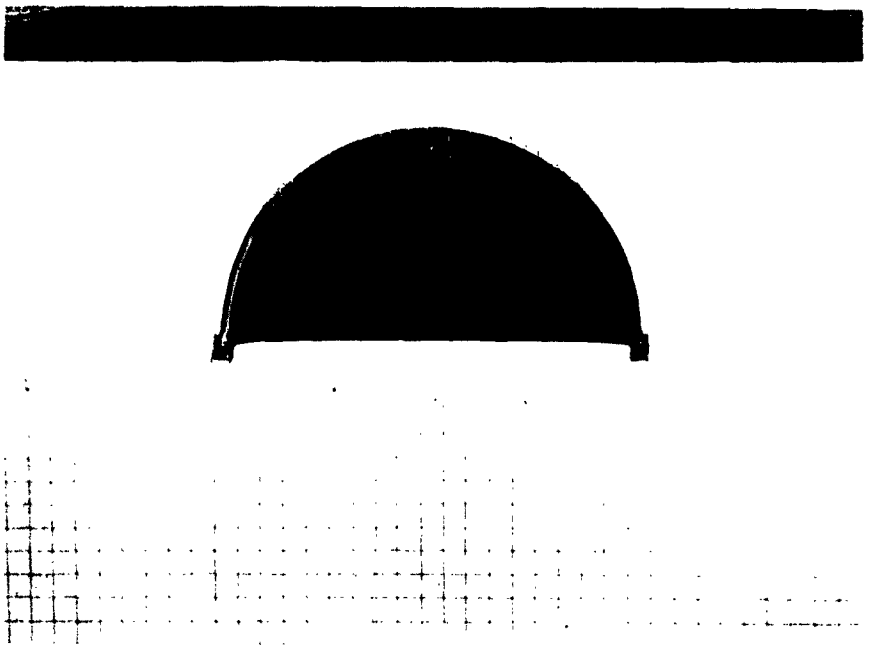

Figure C-6. Thick-card arch and rectangular footings.

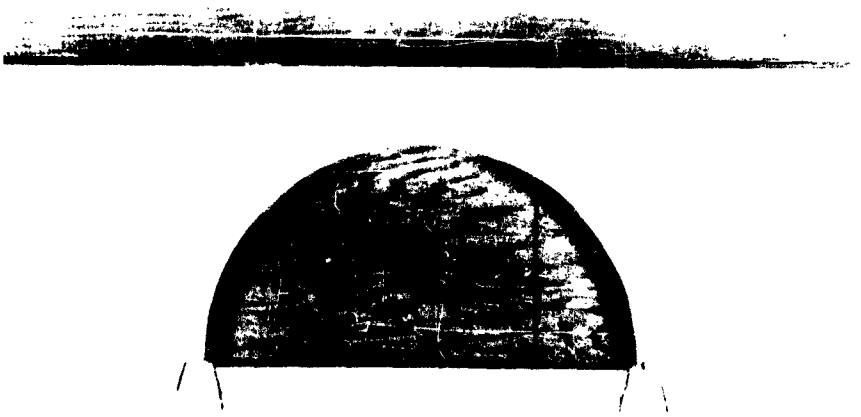

Figure C-7. Thick-card arch and trapezoidal footings.

Appendix D

TWO-DIMENSIONAL TESTS

Two-dimensional soil-structure interaction experiments were conducted in the skirt extensions of the NCEL blast simulator. The chamber formed by the skirt extensions is used to contain various blast experiments. For these experiments, the skirts were assembled in a box configuration with the open top bolted to the bottom of the simulator. The inside dimensions of the skirts when so arranged are 8 inches wide, 6 feet high, and 9 feet long. The two-dimensional model structures used in the experiment were 7-3/4-inch-long sections of 15-inch-diameter semicircular metal arches. The arches were hinge-mounted on wooden footings 1-1/5 inches wide, 1-4/5 inches high, and 7-3/4 inches long. For testing, the arch was oriented with the horizontal axis perpendicular to the horizontal axis of the blast simulator. The arches were, in effect, "slices" from the central portion of an arch structure. Boundaries for the slice and the surrounding soil were the inside surfaces of the skirt extensions.

The arches were fitted with soft neoprene seals faced with thin sheet Teflon at the intersections of the arch and the skirt walls. The ends of the footings were fitted with soft foam pads with thin Teflon facings where they met the skirt walls. A neoprene seal was laid upon the surface of the sand covering the arch to prevent the surface gas pressure from acting directly through the air in the soil voids. Rather, the surface loads acted upon the buried structure through intergranular pressure. The depth of soil over the crown was 6 inches. For all but Static Tests 1 and 2 and Dynamic Test 1, the sealing lips of the neoprene seal were faced with Teflon to reduce friction against the skirt-extension walls. Pertinent dimensions of the two-dimensional test structure are shown in Figure D-1.

Instrumentation consisted of a colored-sand grid pattern monitored by pretest and post-test photography, a linear-motion potentiometer, and pressure gages. In the static tests a supplementary Bourdon-tube pressure gage was employed. A Bourns linear-motion potentiometer, Model 108, was used to measure motion of the crown of the arch relative to a point on the floor of the model directly beneath the crown. Soil pressures against the arch were measured at three locations with Consolidated Electrodynamics Corporation (CEC) pressure pickups, Model 4-312. Locations were 30, 60, and 90 degrees above the footing. All instrumentation signals were fed through CEC System "D" equipment and recorded on a CEC Model 5-119 recording oscillograph. Arrangement of the instrumentation is shown in Figure D-2. Specifications of the instruments used are indicated in Table II in the instrumentation section of this report.

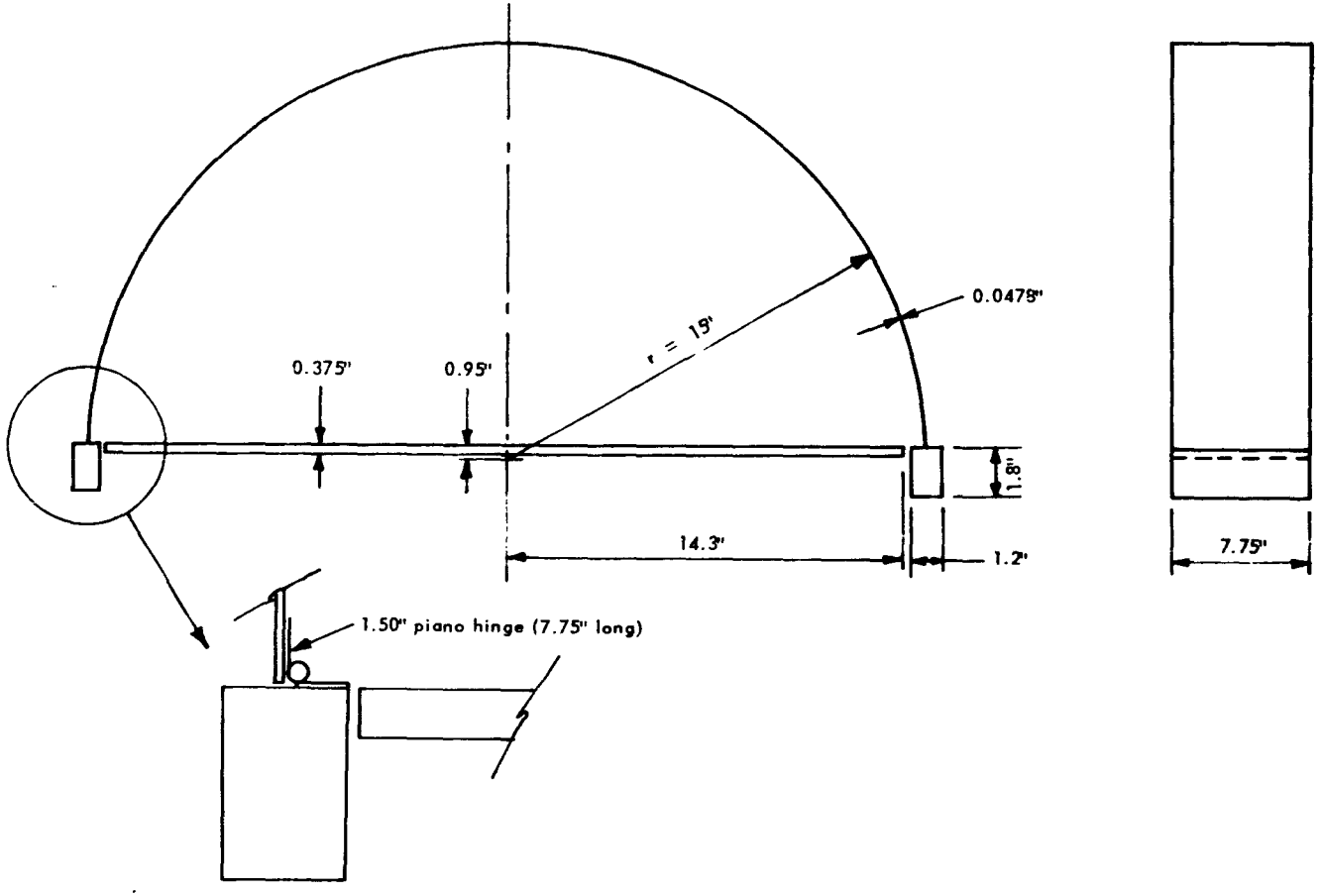

Figure D-1. Pertinent dimensions of the two-dimensional test structure.

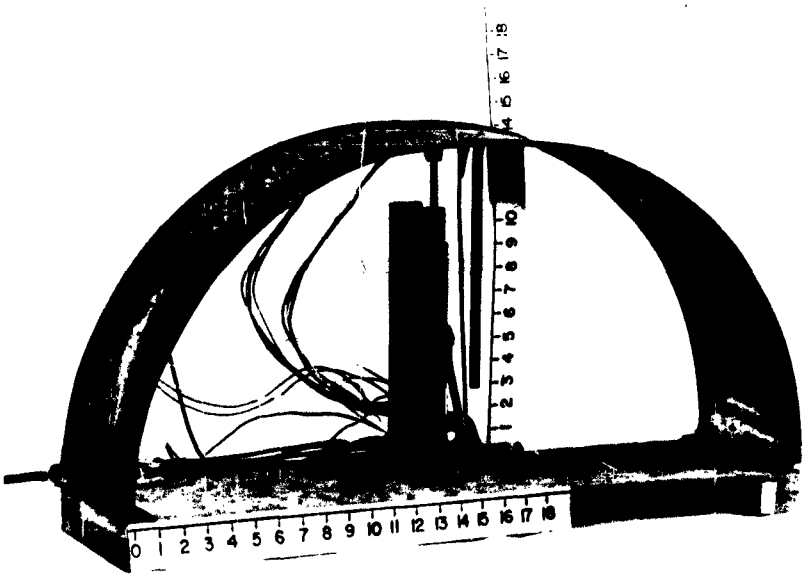

Figure D-2. Instrumentation arrangement for two-dimensional soil-structure interaction experiments.

The soil environment surrounding the test structures was a well-graded dry sand. Gradation is given in Figure A-1, Appendix A. Sand was placed in the skirts in 7-inch layers, and compacted by vibration with a 1-1/8-inch-diameter concrete spud vibrator. The vibrator was slowly inserted and withdrawn in a regular pattern to produce as nearly uniform density as possible. As the configuration of the chamber formed by the skirt extensions precluded measuring in-place sand density by ordinary methods, the average density of the sand was determined by measuring the volume of sand in place and noting the weight of sand used.

A portion of one wall of the skirt-extension chamber is made of strong, thick glass. Approximately 60 percent of the arch was visible through this glass. In order to observe the failure patterns of the sand, a grid of black sand stripes approximately 1/2 inch wide and 1/2 inch deep was placed against the glass observation panel. Special templates were used to place the stripes only against the glass; they did not extend through the sand from wall to wall of the skirt extensions. The sand used for the stripes was the same sand used to fill the remainder of the chamber. It was colored by the addition of 0.1 percent by weight of lampblack.

Of a total of nine two-dimensional soil-structure interaction tests conducted in the skirt extensions of the blast simulator, three were static and six were dynamic.

Static Test 1 was unsuccessful from the standpoint of furthering soil-structure interaction knowledge. Excessive leakage of the compressed air permitted only 1.5 psi to be applied to the surface of the soil. However, the test did serve as a pilot experiment which illustrated the need for improved sealing of the test chamber. Though inadequate for a static test, the installation was considered suitable for dynamic loading, and it was used intact as Dynamic Test 1. As such, it will be commented upon in proper sequence.

Suitable seals were placed in the joint between the skirt-extension chamber and the blast simulator for Static Test 2. In this test the structure failed at a pressure of 1.6 psi on the soil surface. The primary cause of failure was spreading of the footings of the test structure. Deflection of the crown was only 0.08 inch with 1.6 psi on the soil surface just prior to the gross failure illustrated in Figure D-3. In all subsequent experiments in this two-dimensional series, the footings were tied with a steel bracket to prevent spreading and rotation.

For Static Test 3, the last of the two-dimensional static series, a slight modification was made in the neoprene seal used on the top surface of the sand. A thin strip of Teflon was cemented to each lip of the seal to reduce friction between the seal and the skirt-extension walls. This arrangement was used in Dynamic Tests 2 through 6.

The maximum crown deflection in Static Test 3 was 0.17 inch. This occurred at a pressure of 10 psi on the surface of the sand cover. At that pressure, the footing deflection was 5/16 inch down and the floor deflection was 3/16 inch down. Figures D-4 and D-5 show, respectively, the conditions before loading and at 10 psi. Deformation patterns are visible in the stripes of the sand. No damage to the structure was apparent.

The six dynamic two-dimensional experiments were fraught with difficulties. Some of these were instrumentation failure, nonhomogeneous soil conditions, leakage of seals, and initially deformed model arches. The earliest of the dynamic experiments served to improve instrumentation, soil placement, and sealing of the test chamber. Most valuable of the dynamic two-dimensional experiments was No. 5.

Two-dimensional Dynamic Test 5 was at a pressure level of 15.7 psi on the soil surface. The peak crown deflection was 1.96 inches, the footing deflection was 0.75 inch, and the floor deflection was zero. Figures D-6 and D-7 are photographs made before and after load application. Disturbance of the horizontal sand stripes at the crown was caused in part by gas leaking downward past the neoprene seal on the sand surface.

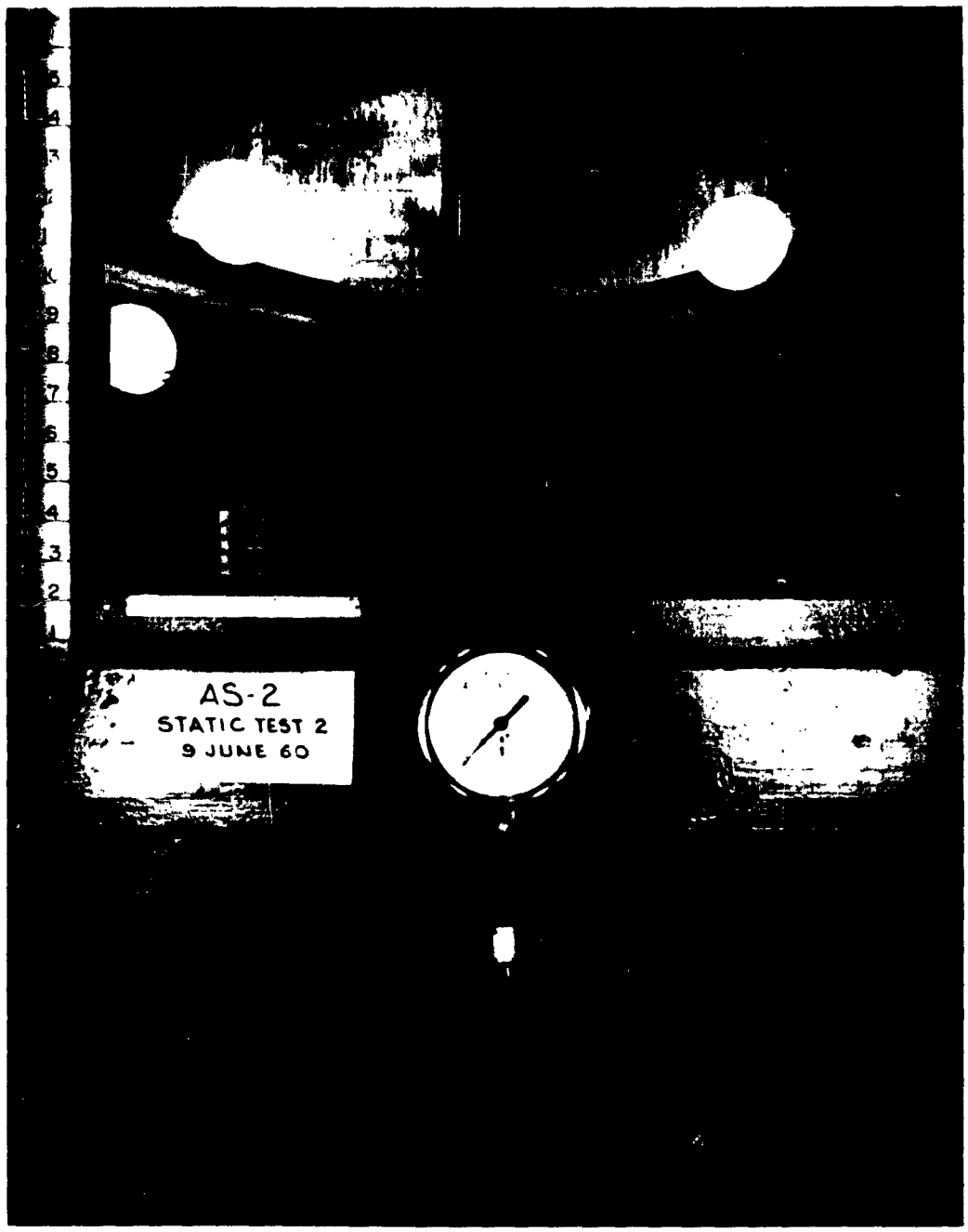

Figure D-3. Two-dimensional Static Test 2 after failure.

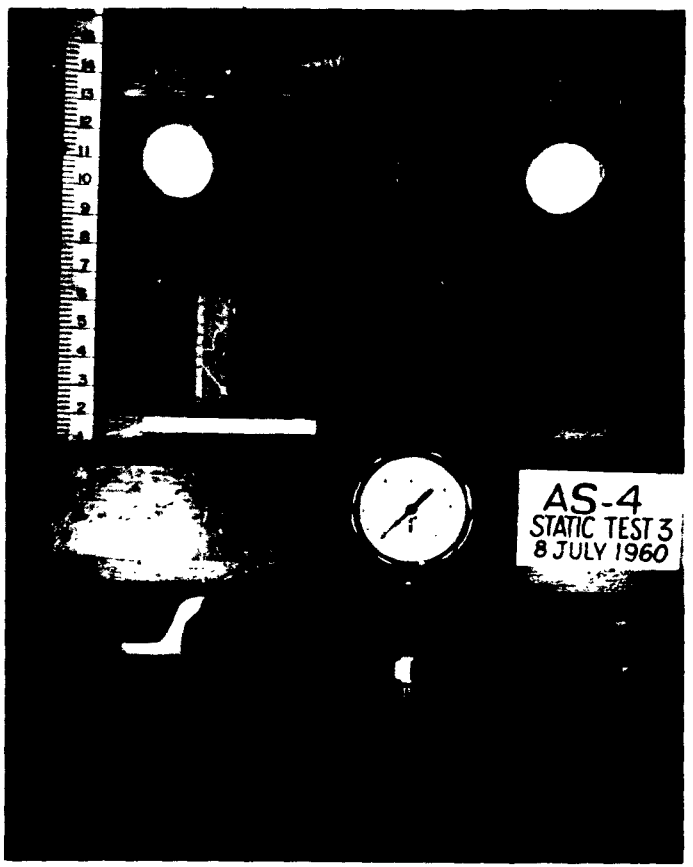

Figure D-4. Two-dimensional Static Test 3 before loading.

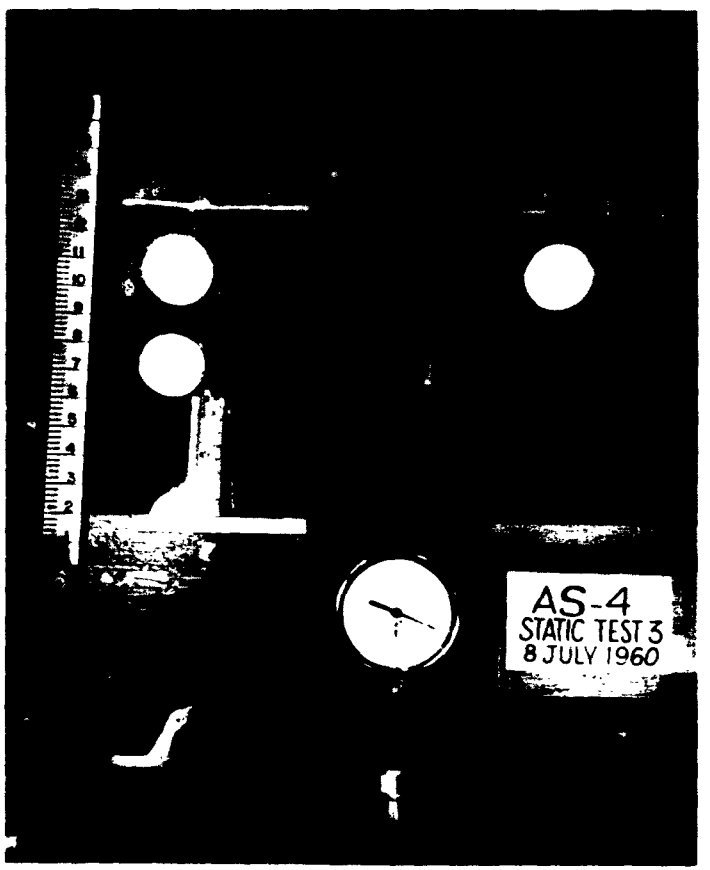

Figure D-5. Two-dimensional Static Test 3 at 10 psi surface pressure.

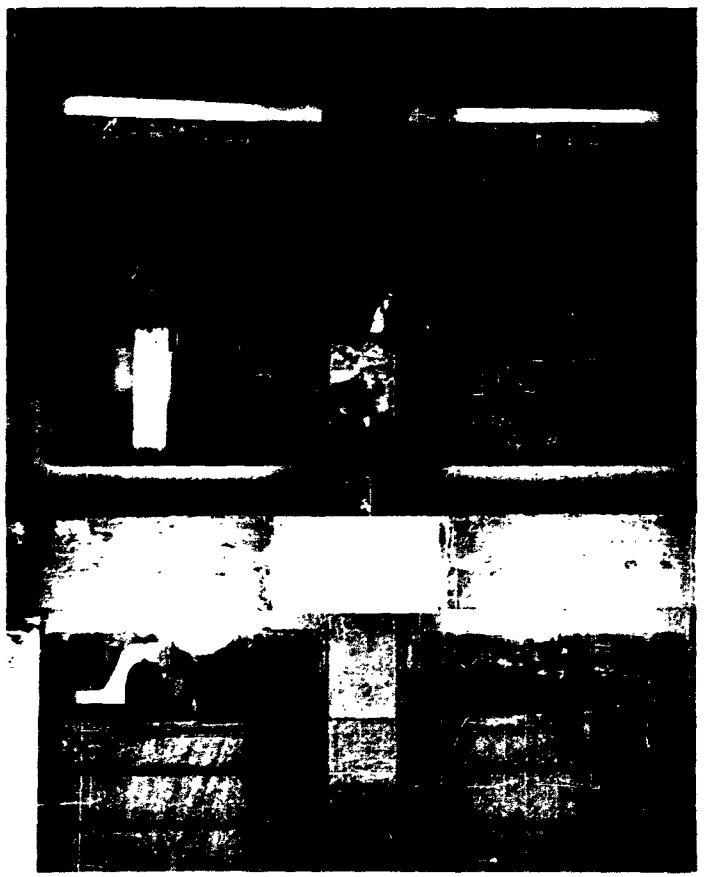

Figure D-6. Two-dimensional Dynamic Test 5 before loading.

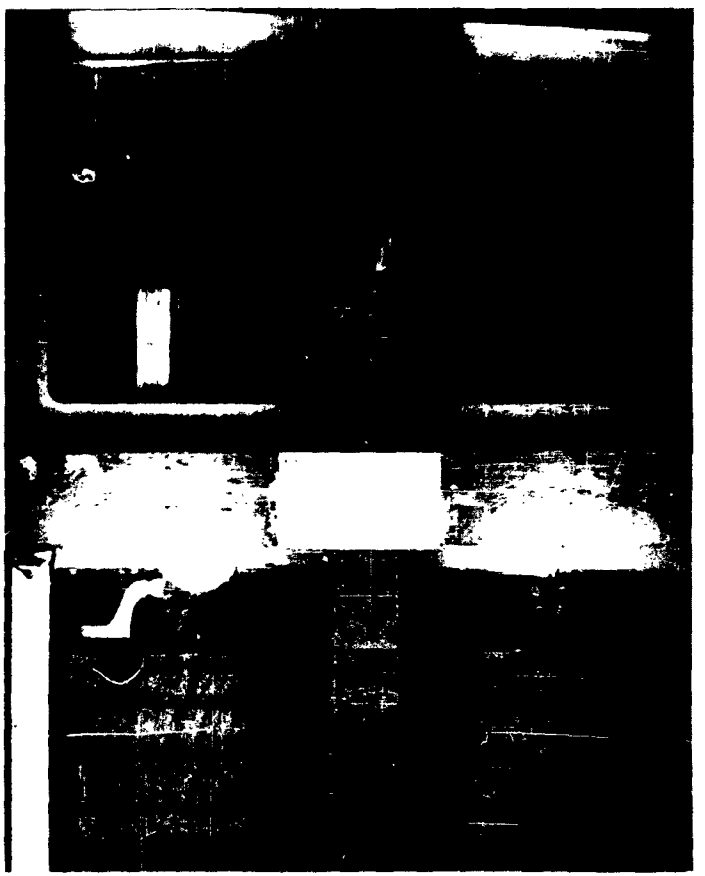

Figure D-7. Two-dimensional Dynamic Test 5 after application of 15.7-psi surface load.

The geometry of the NCEL blast simulator is such that two-dimensional, small-scale experimental studies of soil-structure interaction are less expensive and, in some respects, easier to perform than the more realistic three-dimensional experiments. Therefore, in the early stages of experimentation it became necessary to determine the magnitudes of any adverse boundary effects which might be imposed upon a two-dimensional experiment. One of the primary effects was friction, and this friction was from two sources. The first of these was friction between the ends of the test structure and the boundary formed by the skirt extensions of the blast simulator. The second was between the skirt extensions and the soil used to cover the test structure. While not studied extensively, satisfactory reduction of the friction between the test structure and the skirt extensions was considered to be relatively easy of accomplishment. Effort was concentrated upon the more difficult problem of friction between the skirt extensions and the soil.

The general arrangement of the experiment to evaluate skirt friction is shown in Figure D-8. A steel beam (8WF35) was supported at the one-third points by two Baldwin SR-4 load cells in the bottom of the box formed by the skirt extensions of the blast simulator. A neoprene seal with upturned edges was placed on the beam; sand, at a controlled uniform density, was placed to a preselected depth on the neoprene seal; and a second steel beam (8WF35) was seated on the upper surface of the sand. Vertical static loads were imposed upon the horizontal upper surface of the sand by jacking downward on the topmost steel beam. Three similar hydraulic jacks were used for loading. These three jacks were connected to a common manifold, to which a pressure gage also was connected. With this arrangement, it was possible to apply a known load to the top beam and to measure that portion of the load which was transmitted through the sand to the bottom beam. The difference in the top and bottom loads was attributed to friction between the sand and the skirt-extension walls, and between the neoprene seal and the skirt-extension walls.

Two initial tests were performed. The first was as described above, with a 46-1/2-inch depth of sand. The second test was similar to the first, except that the sand was contained in a plastic bag of the shape and size of the inside of the skirt-extension chamber. Silicon grease was used to lubricate the surfaces between the plastic bag and the steel walls of the skirt extensions. The depth of sand in this second experiment was 47 inches.

As a result of these first two experiments for evaluating skirt friction, it was apparent that most of the load applied to the top surface of the sand was lost to friction on the skirt-extension walls. Actual magnitudes will be discussed later.

Before proceeding further, it was deemed advisable to make some smaller scale friction experiments. These were made in a modified soil shear box, the bottom half of which was replaced by a steel plate. In the first of these shear-box

experiments, the coefficient of friction between sand and steel was determined. In the second, a sheet of Teflon 5 mils in thickness was placed between the sand and the steel. In the third experiment, the sand and steel were separated by a piece of the plastic bag used in the skirt-friction test. As in the skirt-friction test, silicon grease was used between the steel plate and the plastic. In the fourth experiment, two pieces of Teflon, each 5 mils thick, were placed between the sand and the steel. The lowest coefficient of friction was exhibited in the experiment in which two thicknesses of Teflon were used. Figure D-9 illustrates the relative merits of the various friction-reducing methods tested in the shear box.

Following these friction determinations in the modified soil shear box, two additional experiments were conducted in the skirt extensions. For both of these latter experiments, a double sheet of Teflon, each 5 mils thick, was placed between the sand and the skirt walls. The two experiments differed in the depth of sand used. In the first a 13-inch depth was placed on the bottom beam, and in the second a 25-inch depth was placed.

A final experiment to determine the amount of friction contributed by the neoprene seal was made by placing a 1-inch depth of sand on the seal.

Figure D-10 illustrates the magnitude of surface load lost to friction under various conditions in the skirt extensions. The soil-structure interaction experiments, for which these friction tests were auxiliaries, utilized a small buried structure which required approximately 21 inches of soil cover above the footings. This depth is slightly less than the 25-inch depth of skirt-friction test No. 5. It may be seen in Figure D-10 that the load lost to friction with this depth of sand is a very large percentage of the applied surface load. This loss occurred even though double sheets of Teflon were used to reduce friction between the sand and the steel walls of the skirt extensions. The friction loss was large enough to obscure inertia effects which might be present in dynamic experiments. Consequently, the decision was made to abandon the plan of two-dimensional testing in the skirt extensions, and to resort to three-dimensional testing in the blast simulator test pit.

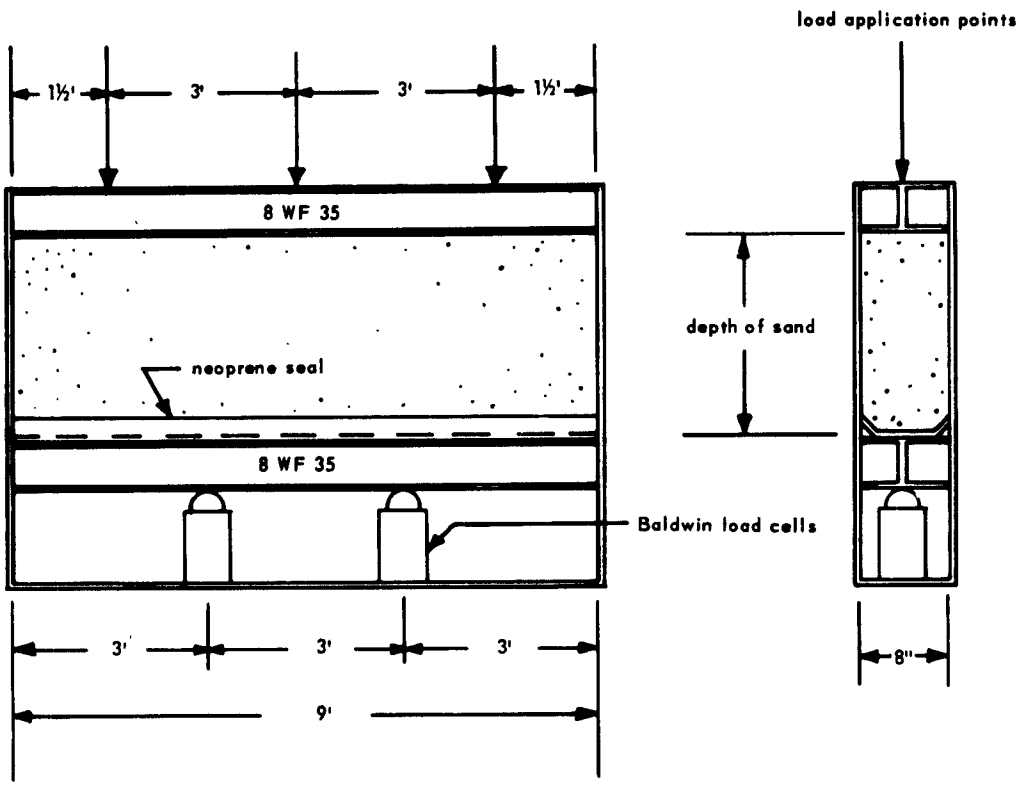

Figure D-8. Arrangement of wall friction experiment in blast simulator skirt extensions.

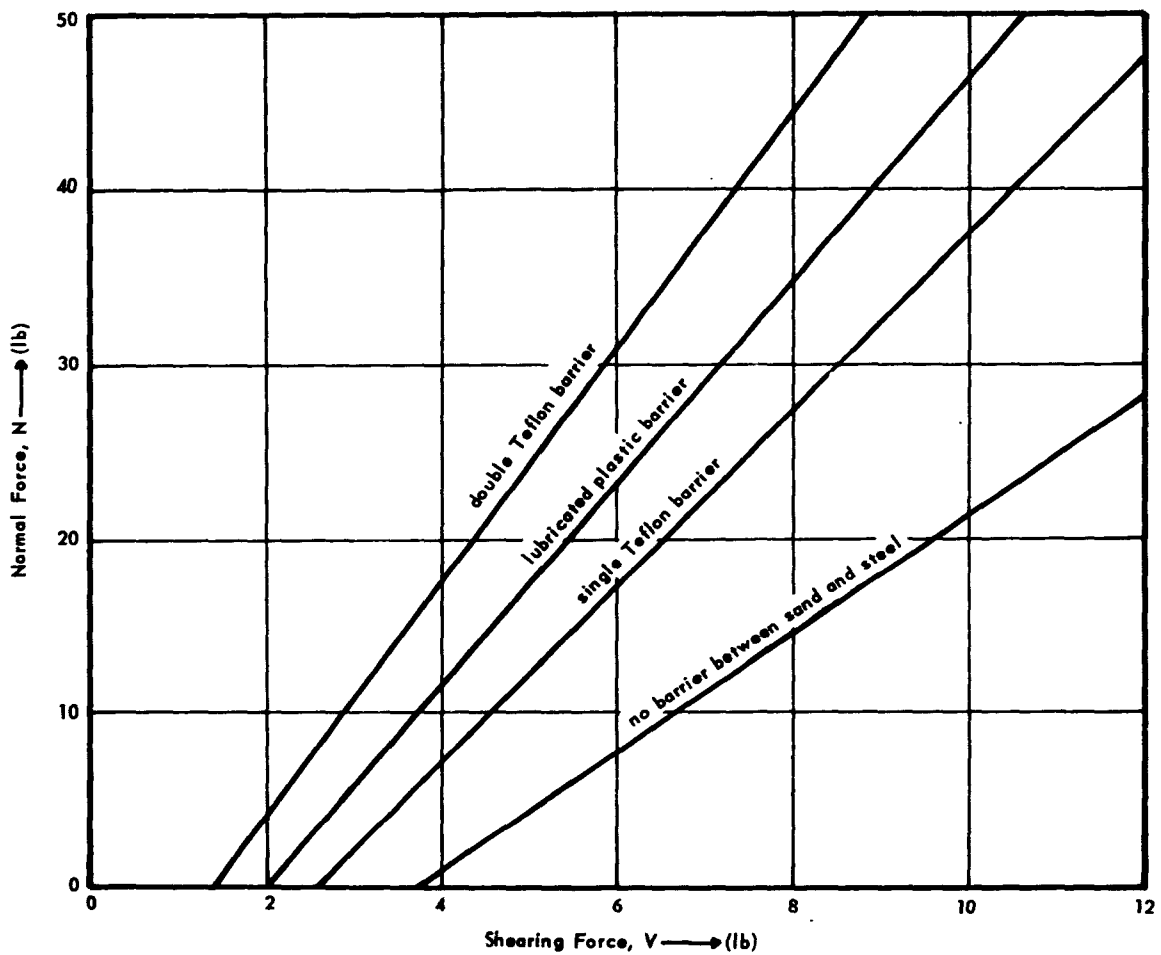

Figure D-9. Relative merits of friction-reducing methods tested in the modified shear box.

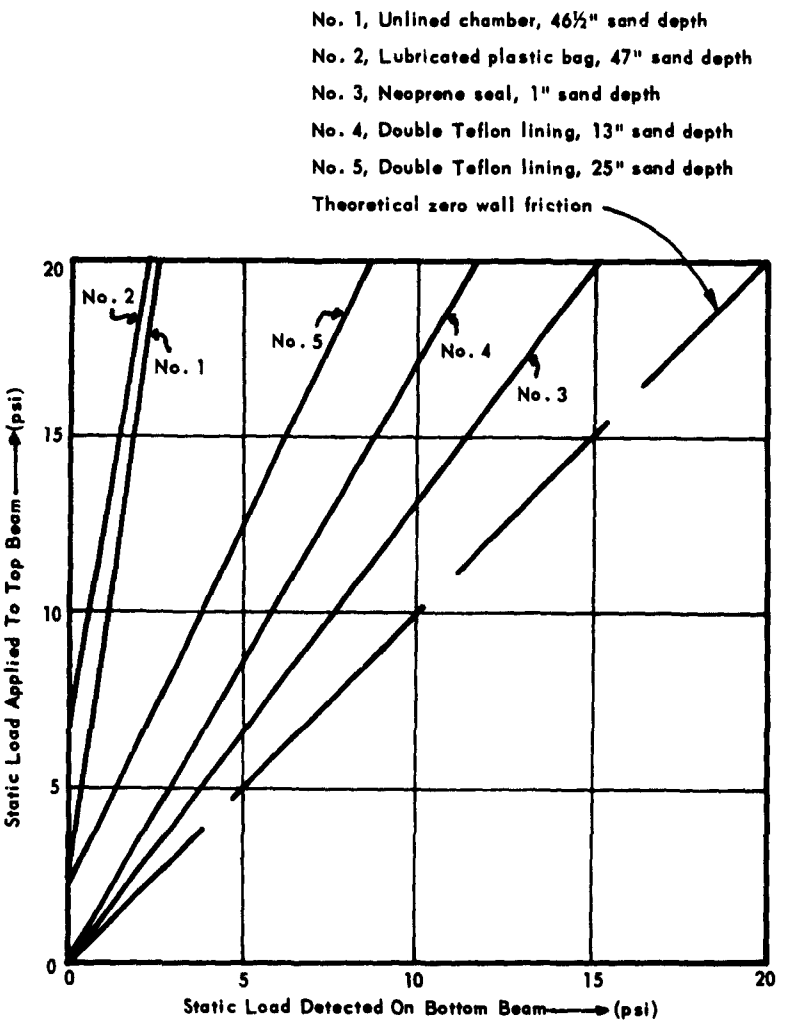

Figure D-10. Magnitude of surface load lost to friction under various conditions in the skirt extensions.

Appendix E

OSCILLOGRAMS

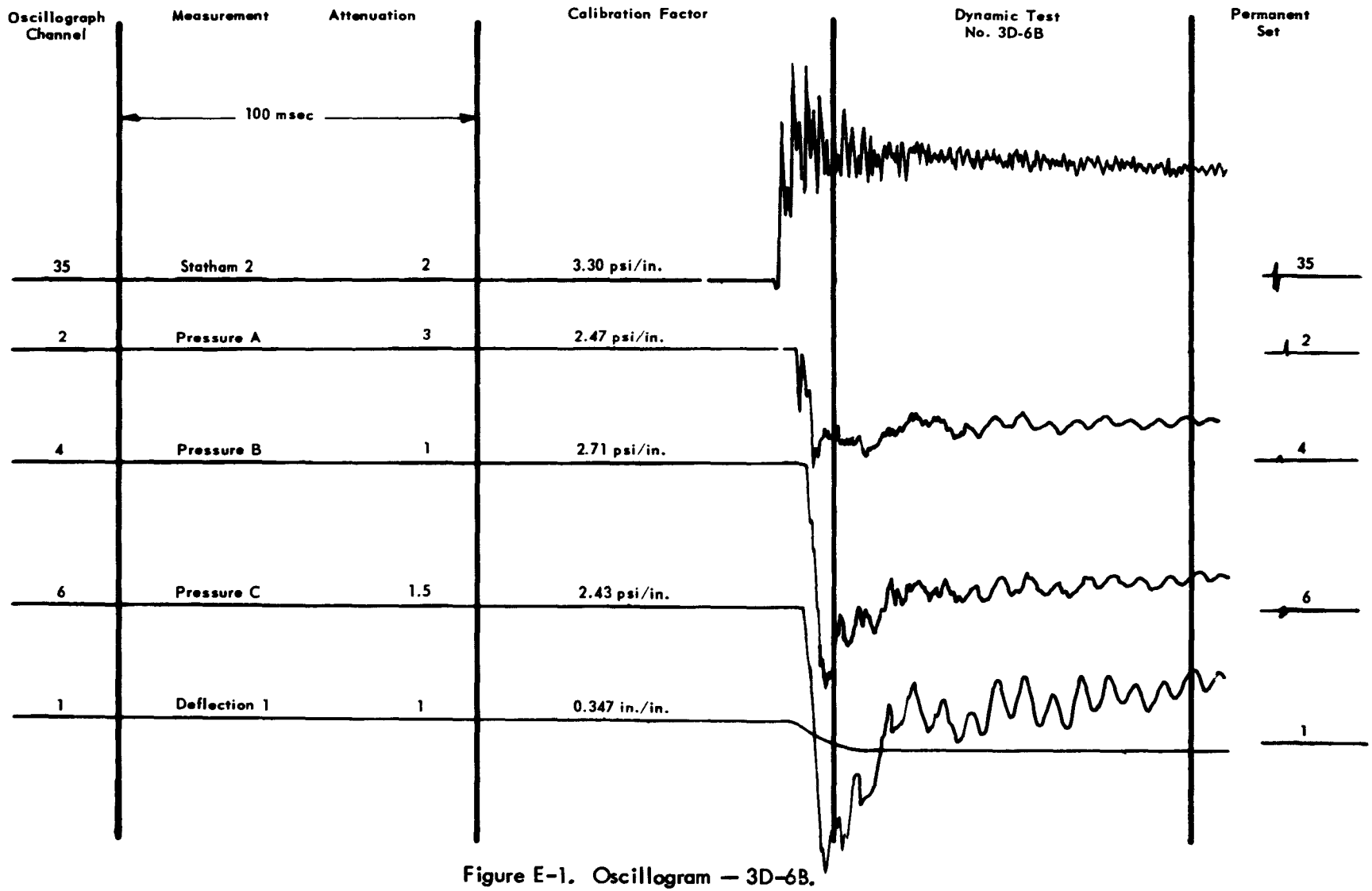

Figure E-1. Oscillogram — 3D-6B.

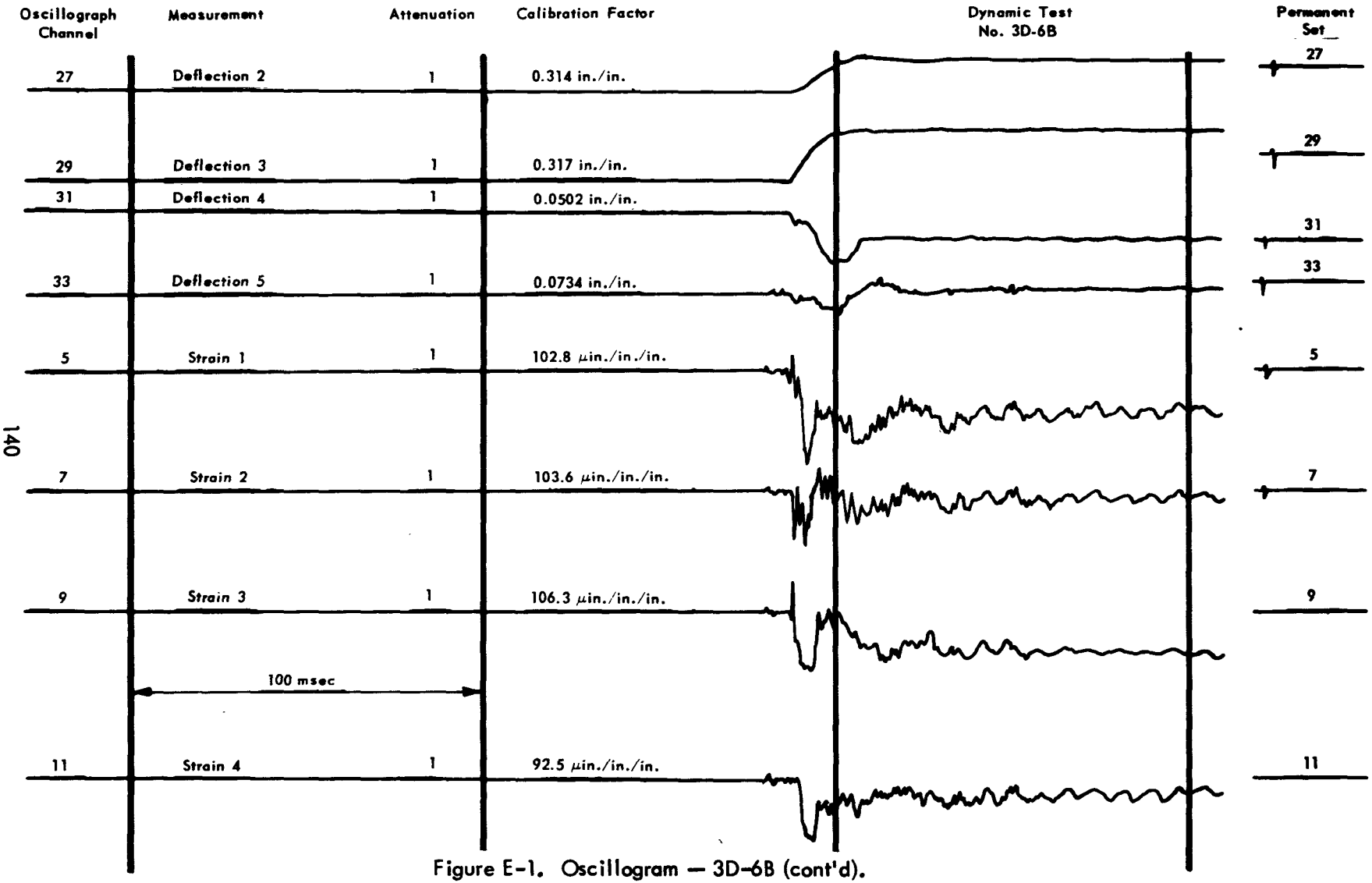

Figure E-1. Oscillogram — 3D-6B (cont'd).

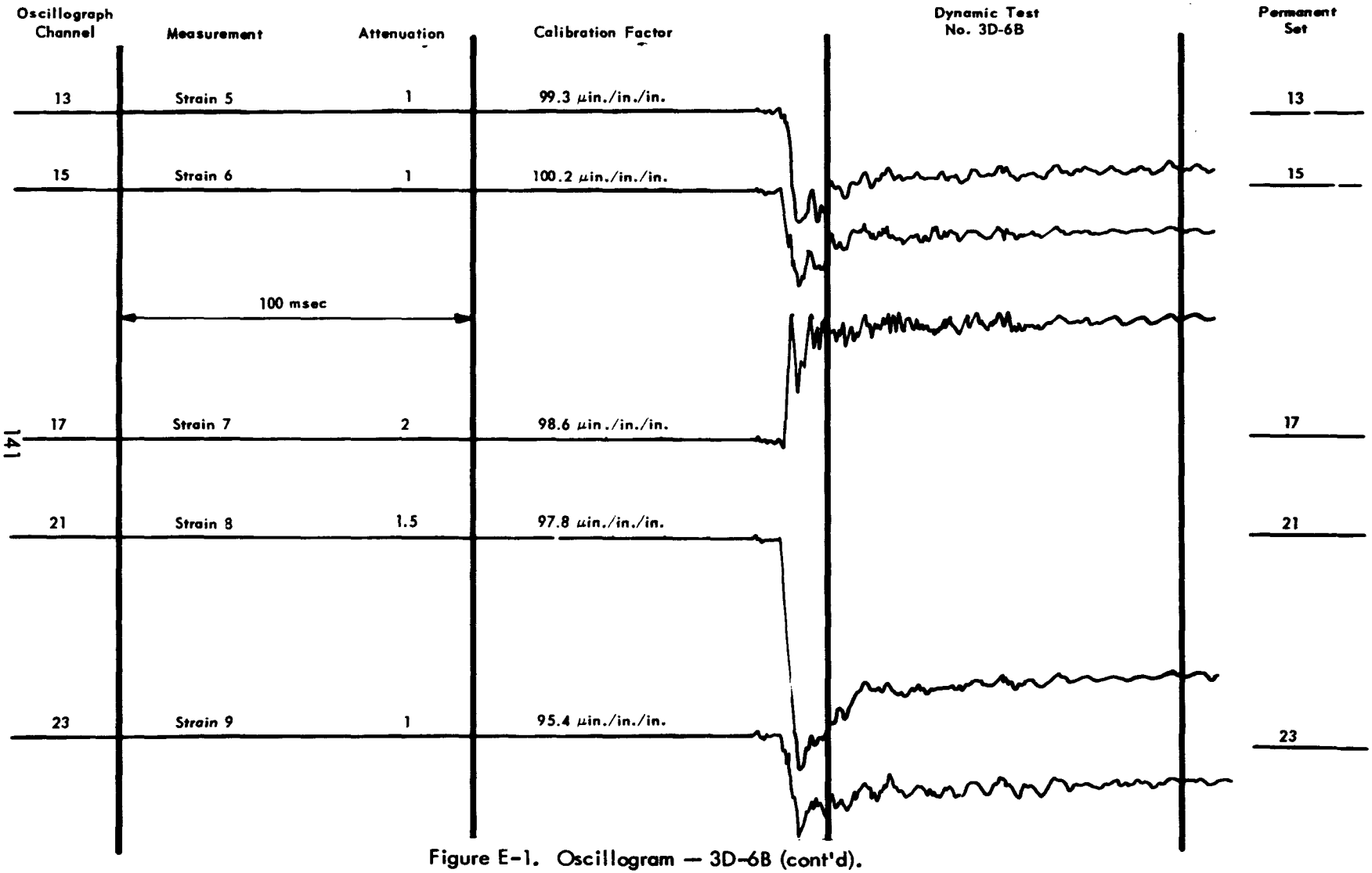

Figure E-1. Oscillogram — 3D-6B (cont'd).

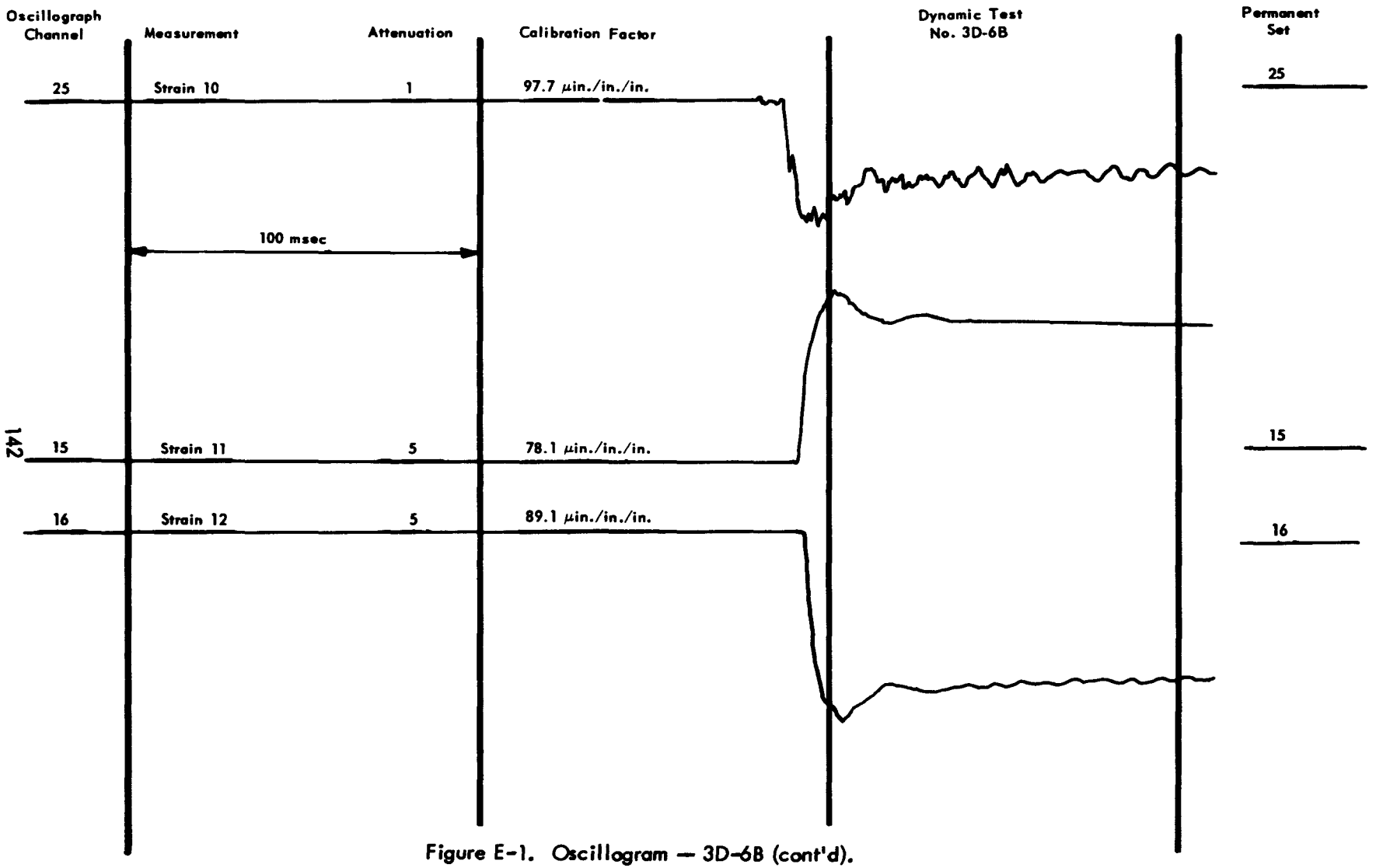

Figure E-1. Oscillogram — 3D-6B (cont'd).

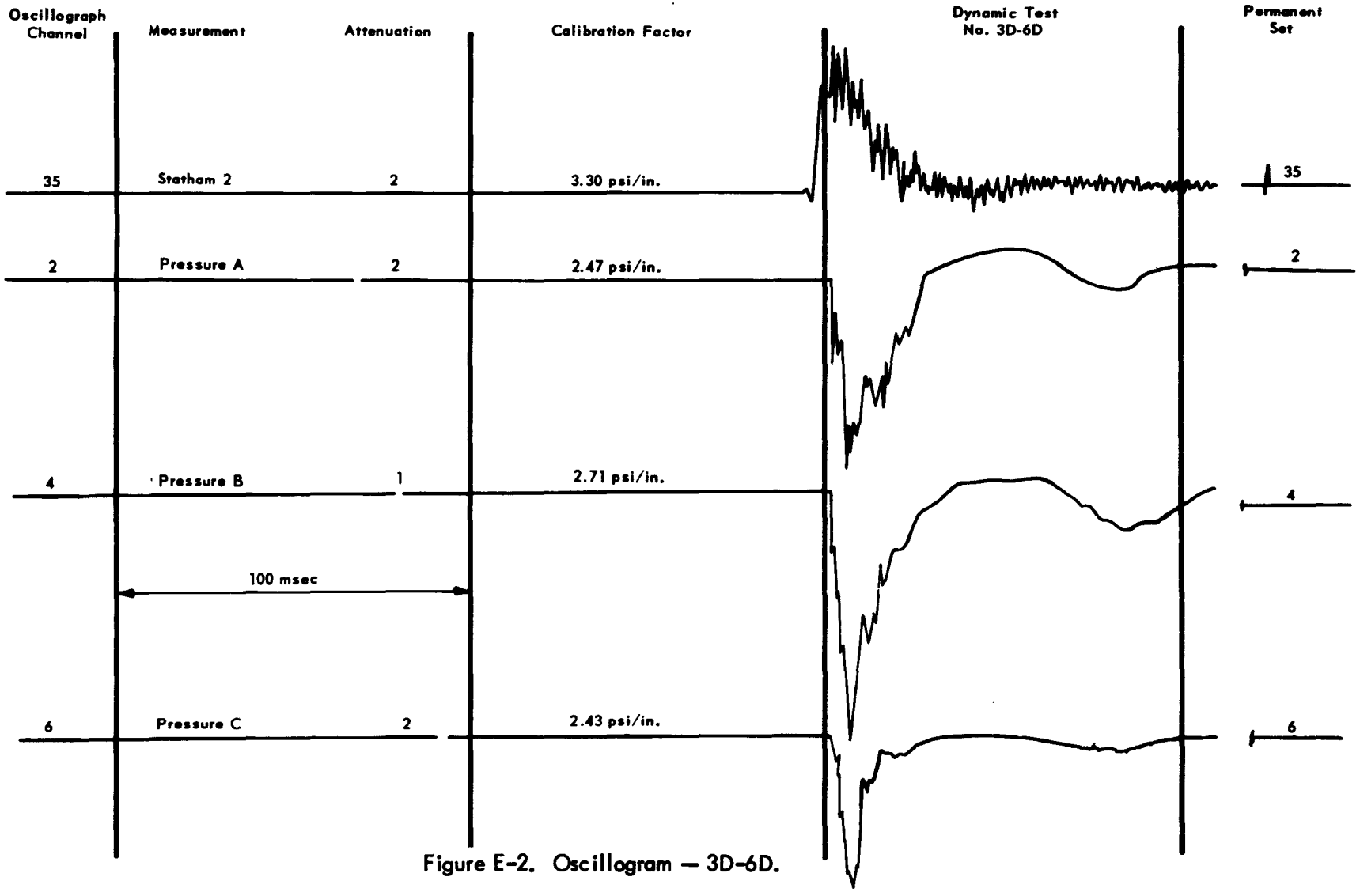

Figure E-2. Oscillogram — 3D-6D.

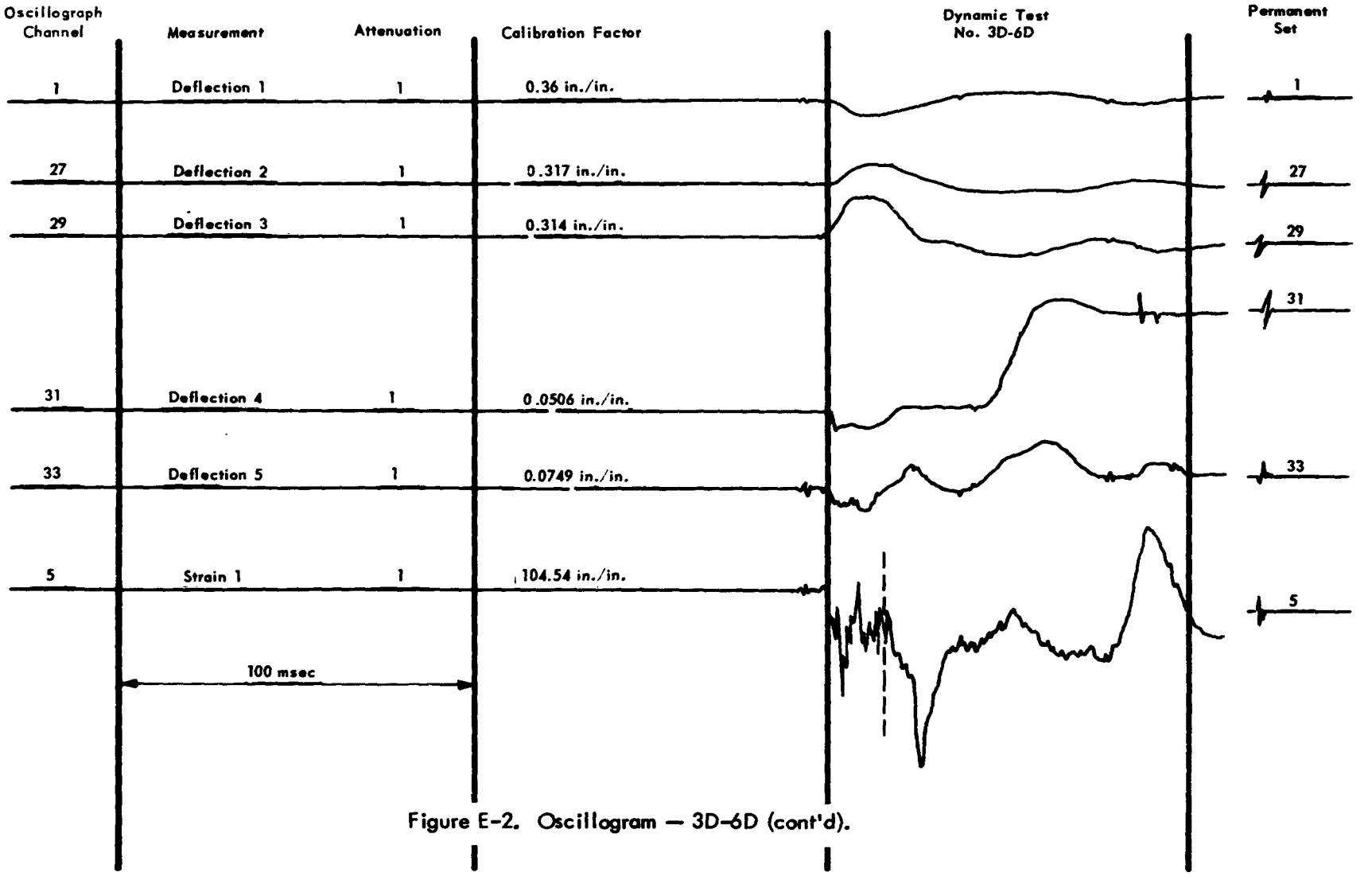

Figure E-2. Oscillogram — 3D-6D (cont'd).

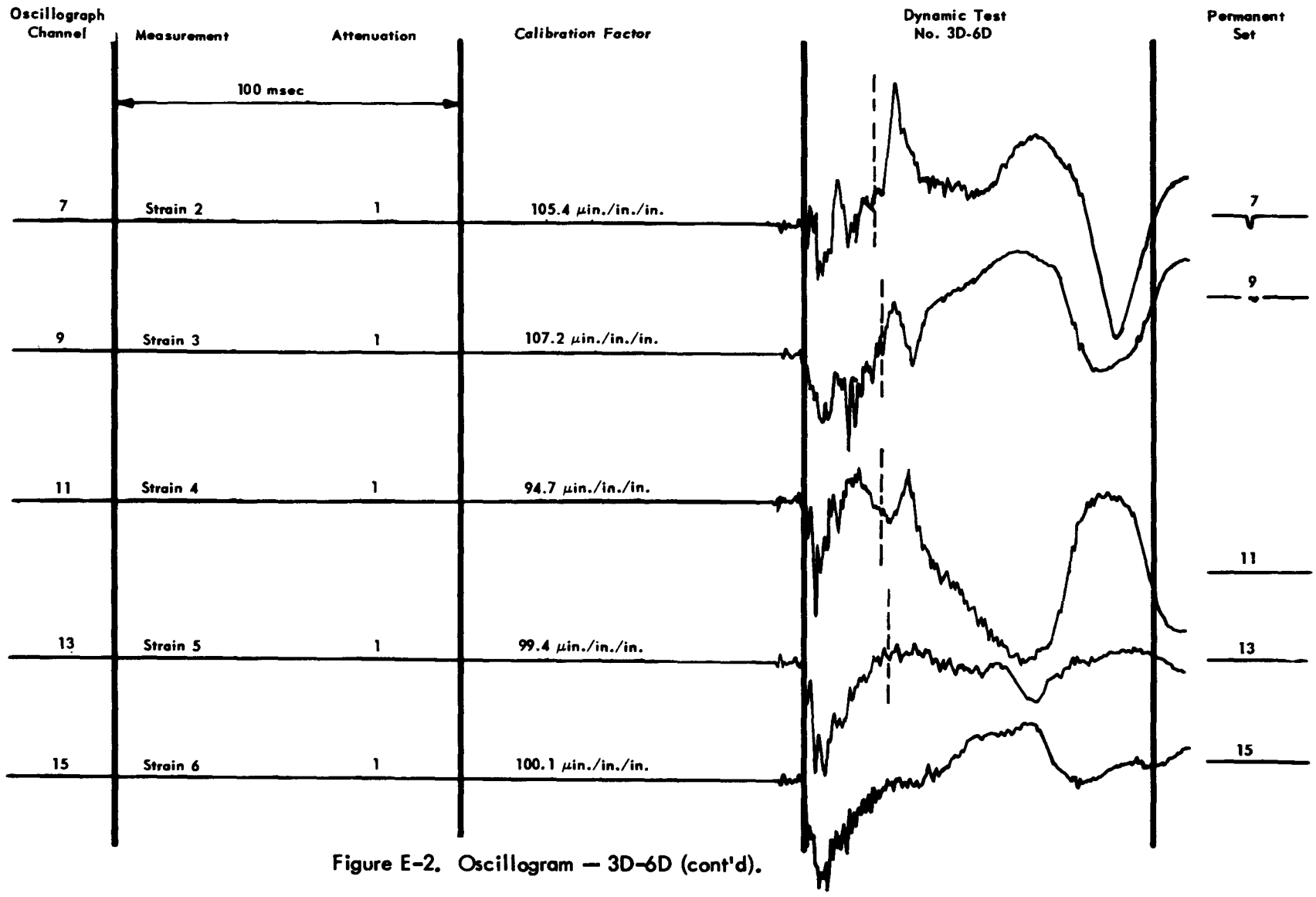

Figure E-2. Oscillogram — 3D-6D (cont'd).

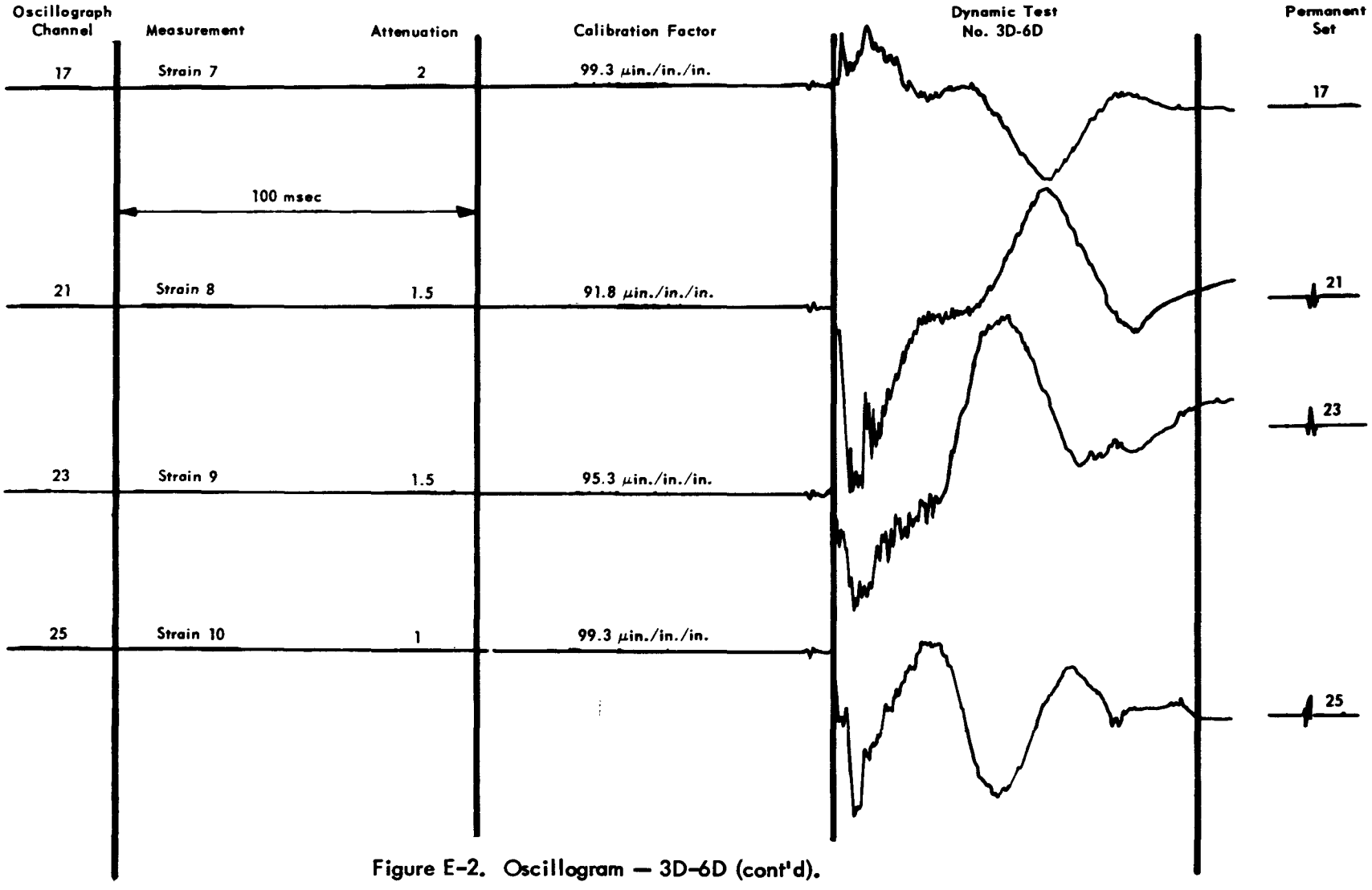

Figure E-2. Oscillogram — 3D-6D (cont'd).

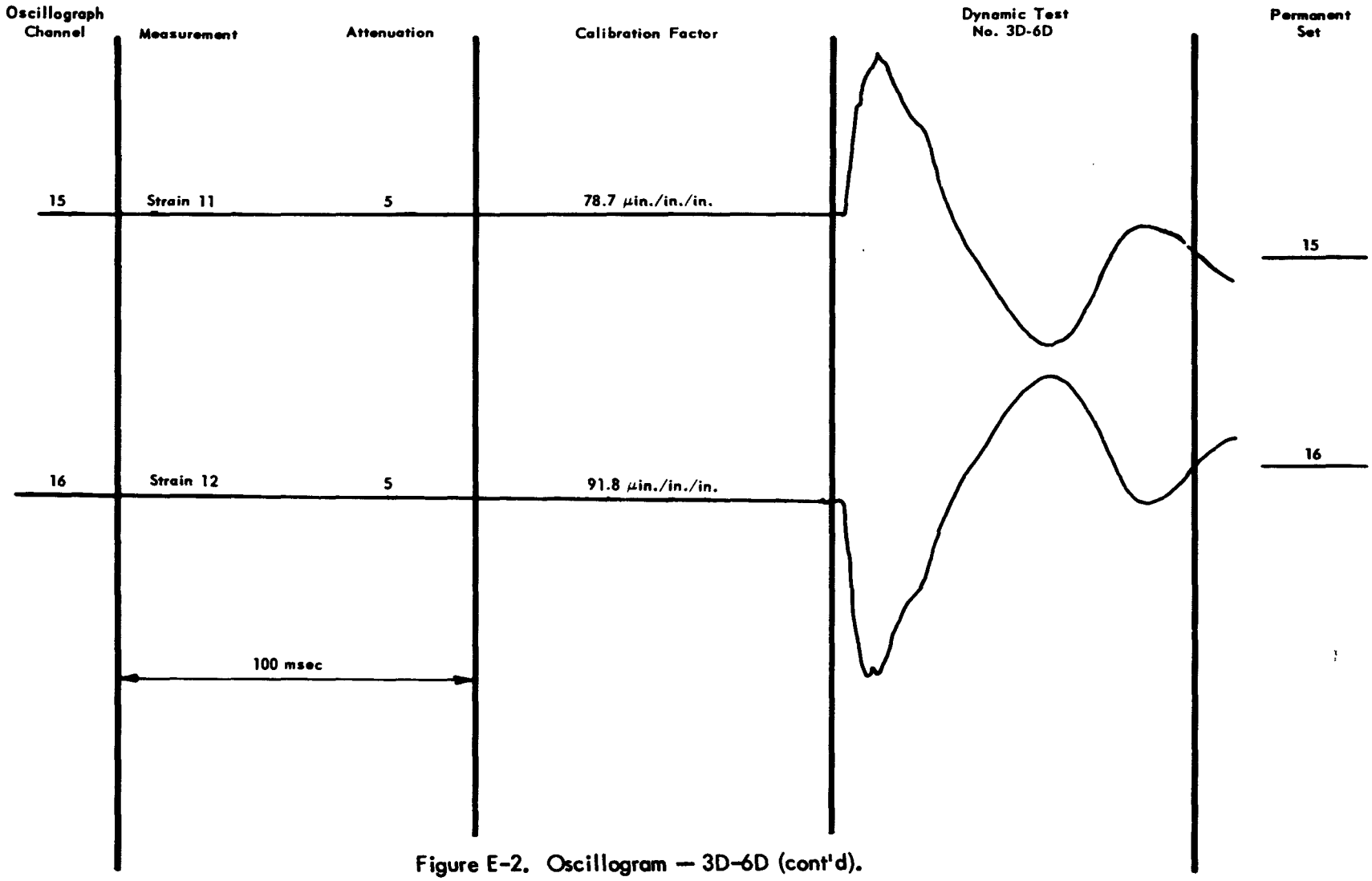

Figure E-2. Oscillogram — 3D-6D (cont'd).

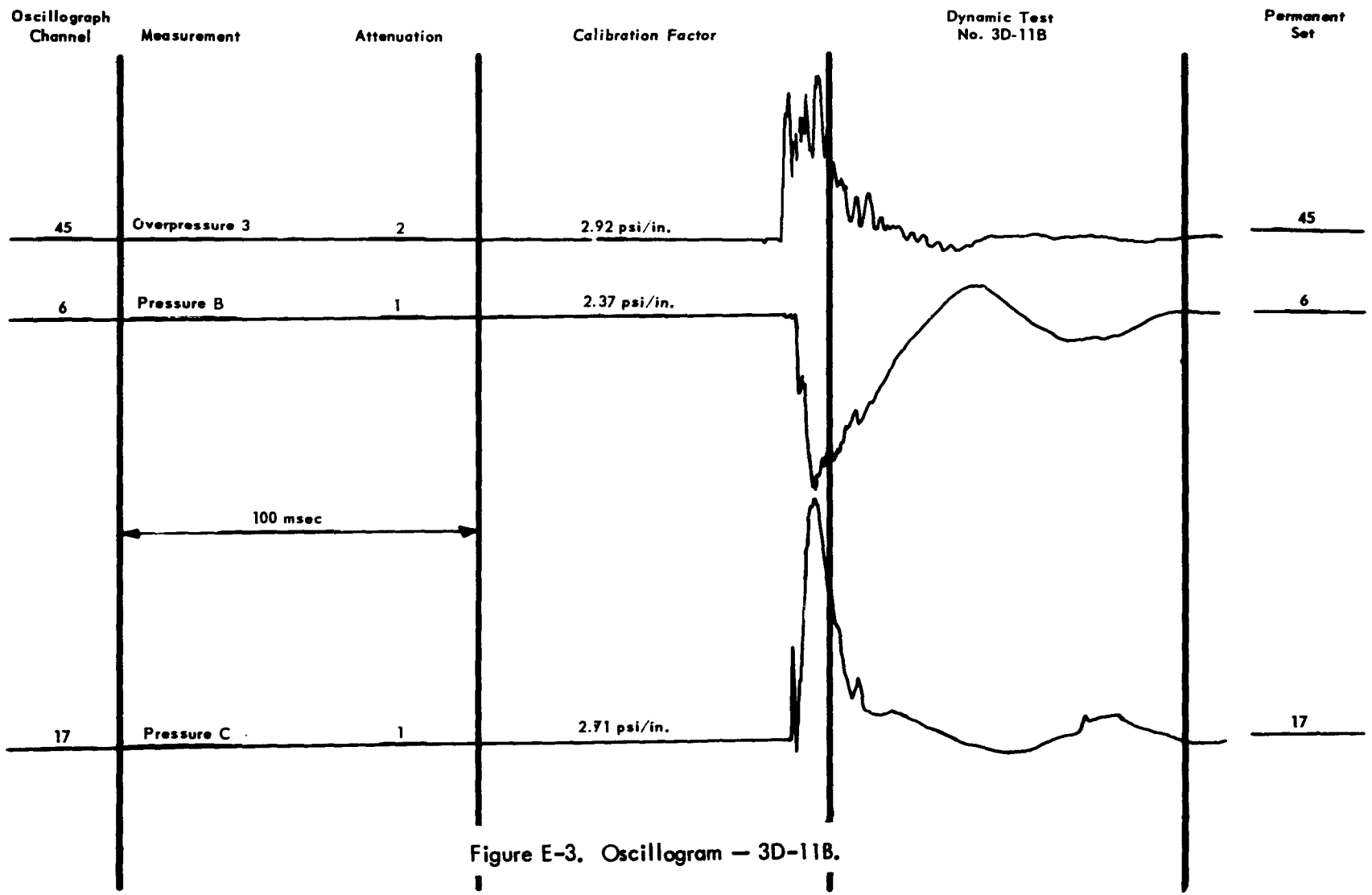

Figure E-3. Oscillogram — 3D-11B.

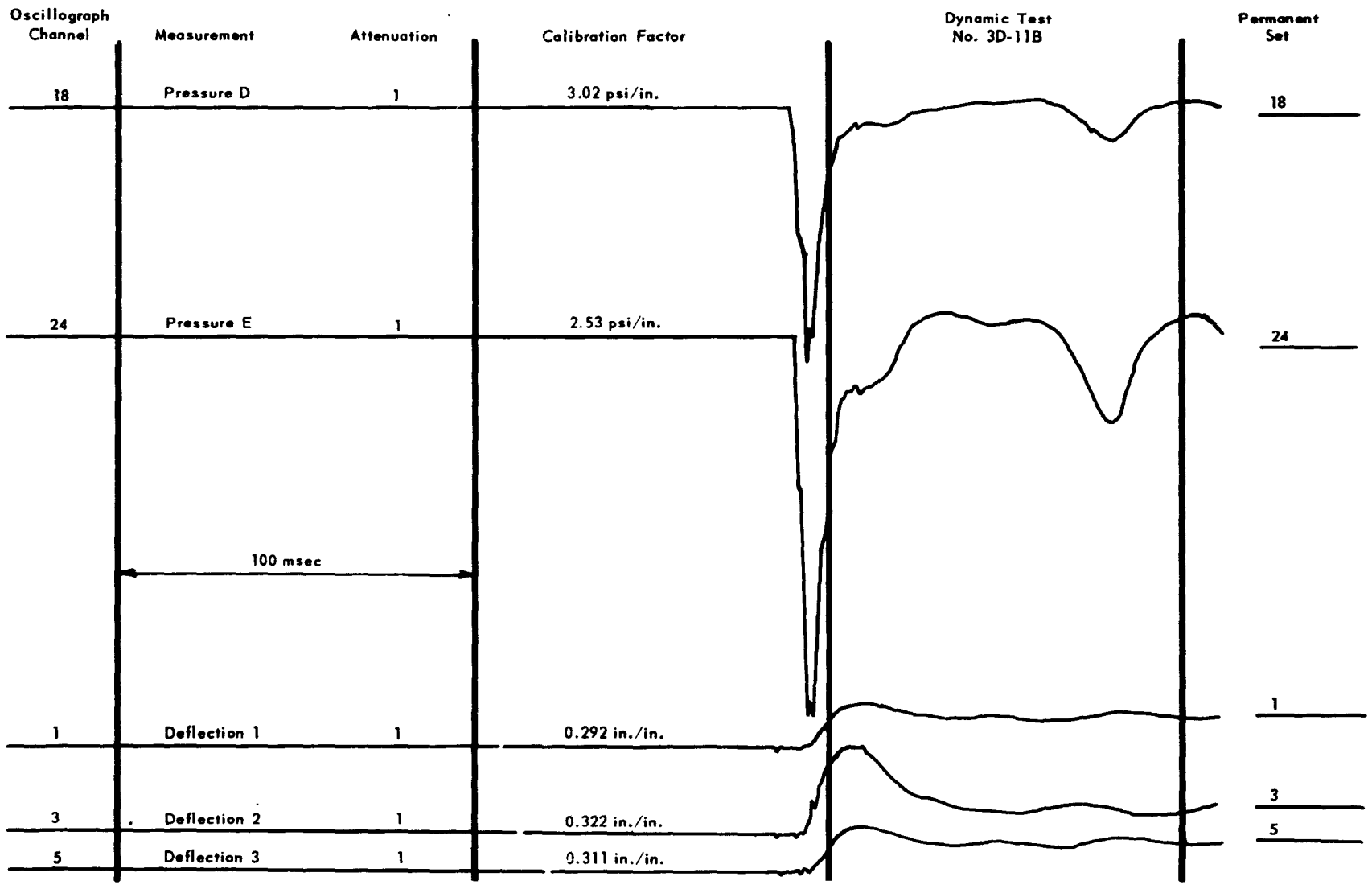

Figure E-3. Oscillogram — 3D-11B (cont'd).

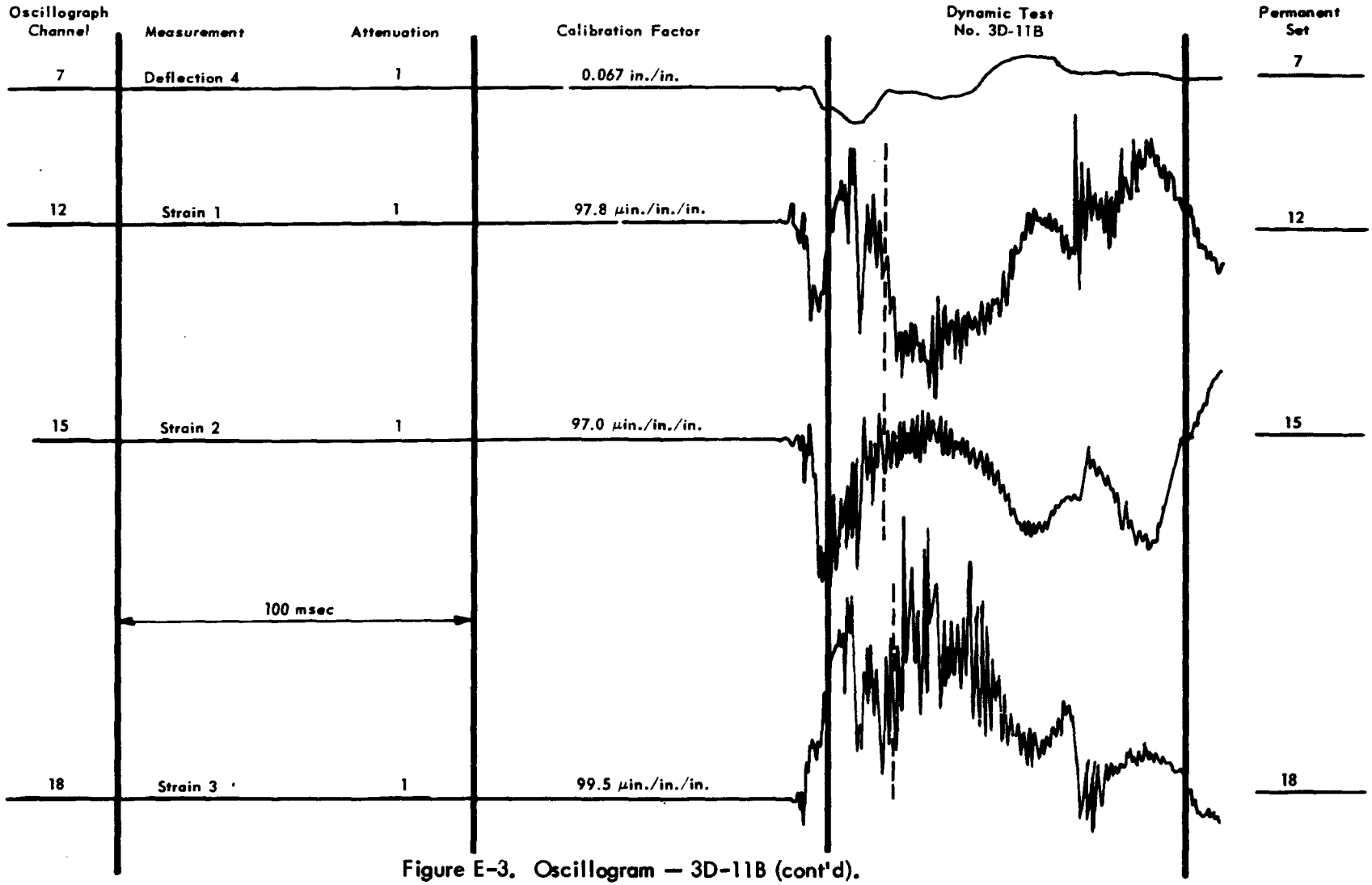

Figure E-3. Oscillogram — 3D-11B (cont'd).

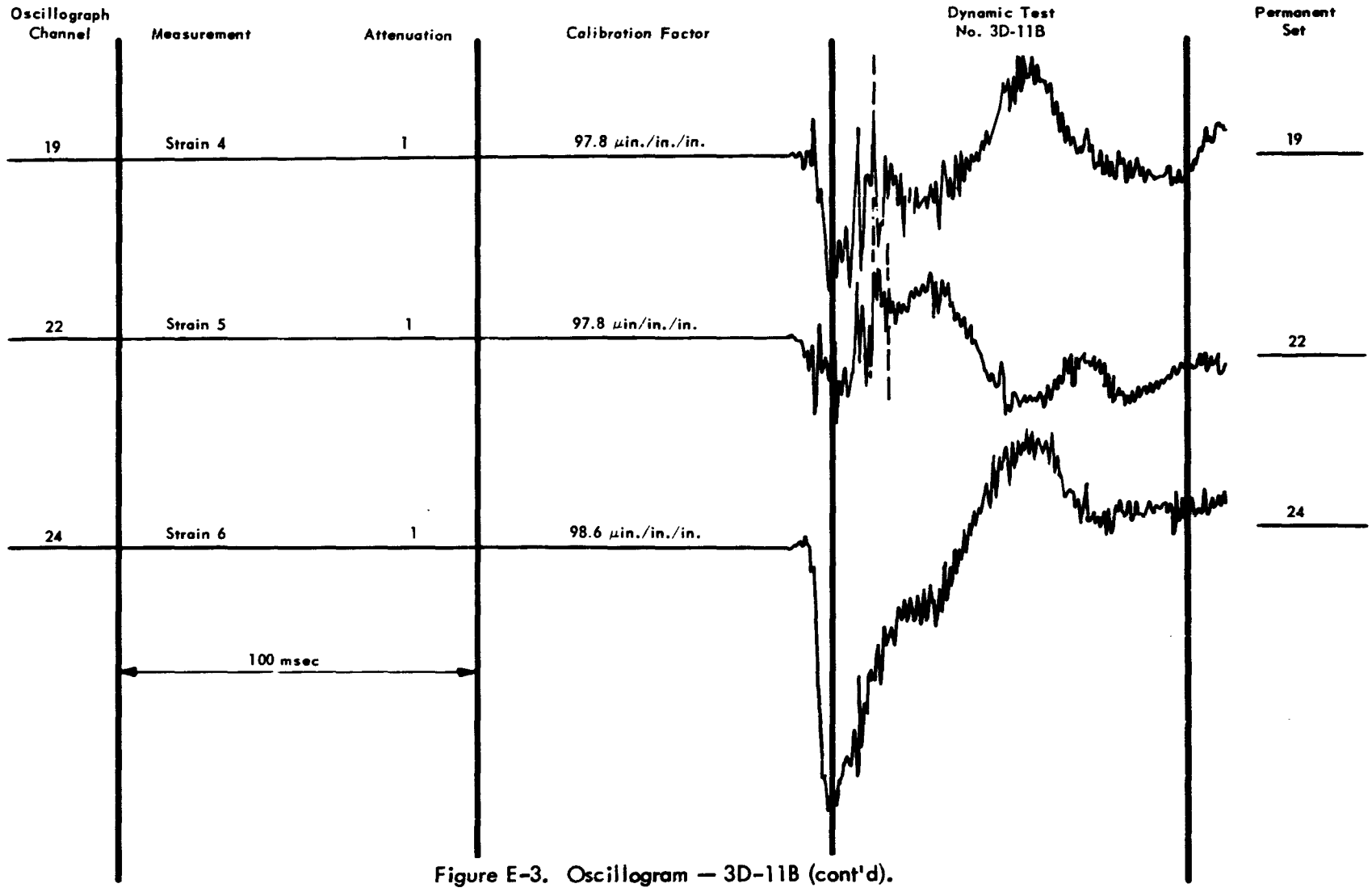

Figure E-3. Oscillogram — 3D-11B (cont'd).

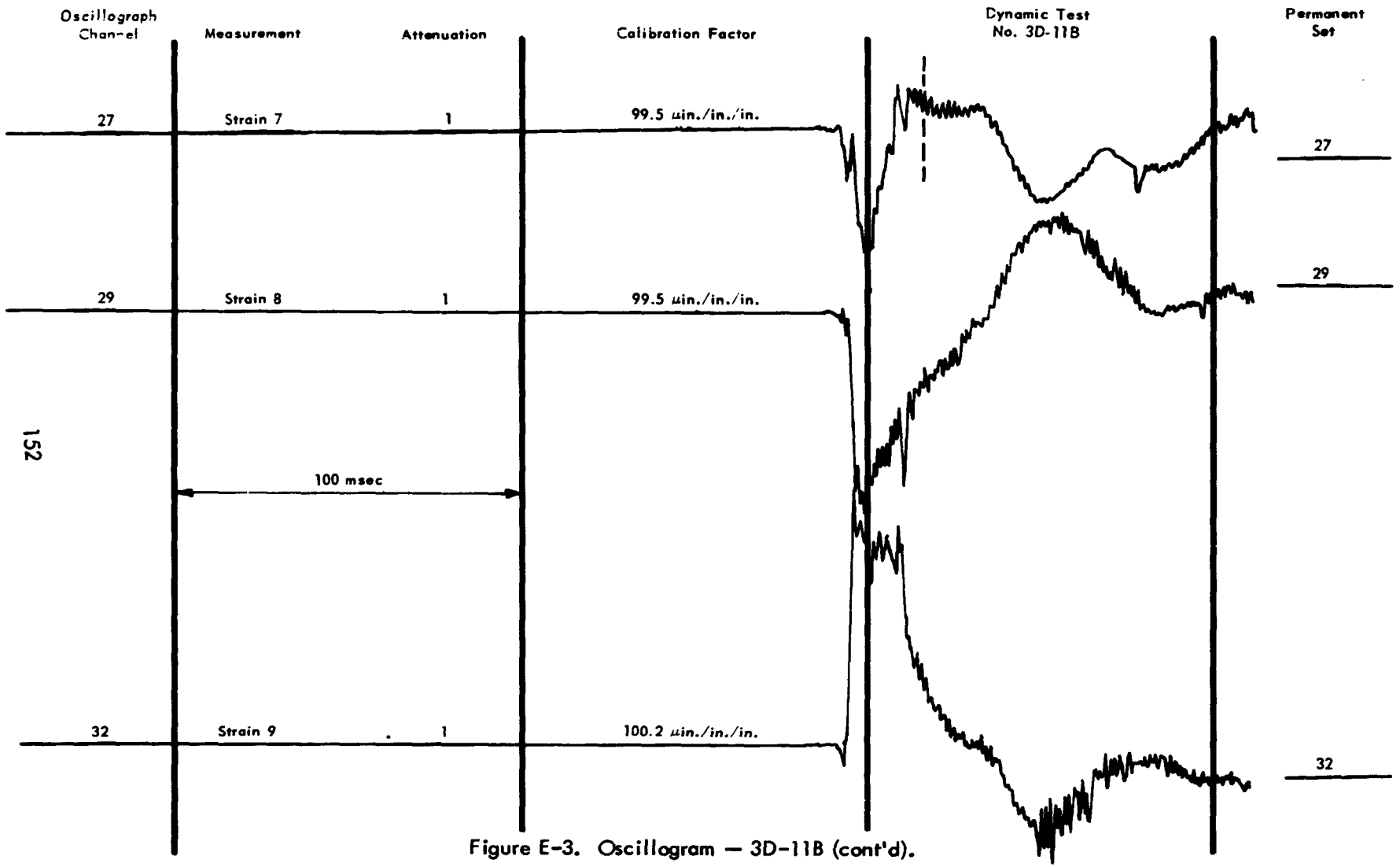

Figure E-3. Oscillogram — 3D-11B (cont'd).

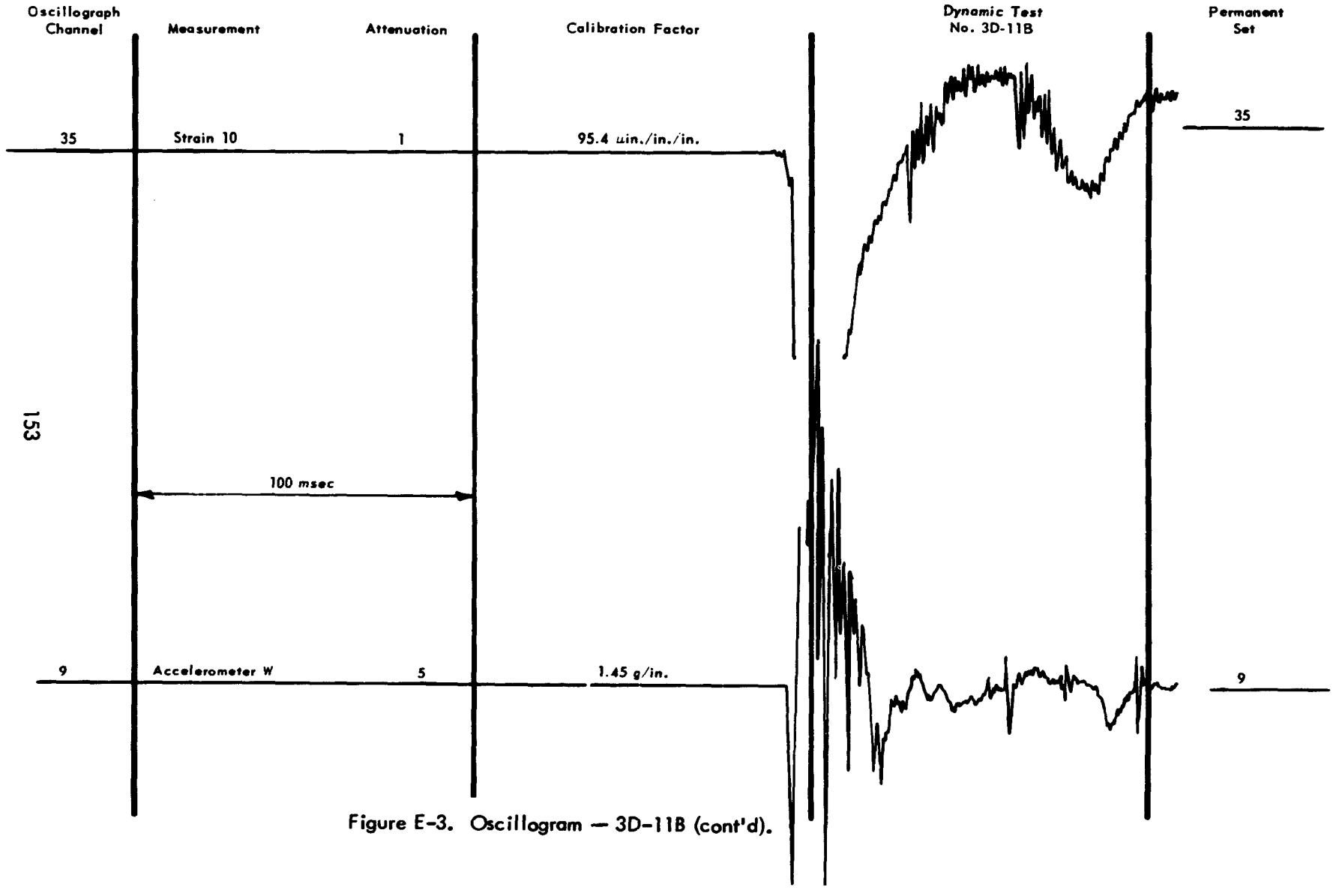

Figure E-3. Oscillogram — 3D-11B (cont'd).

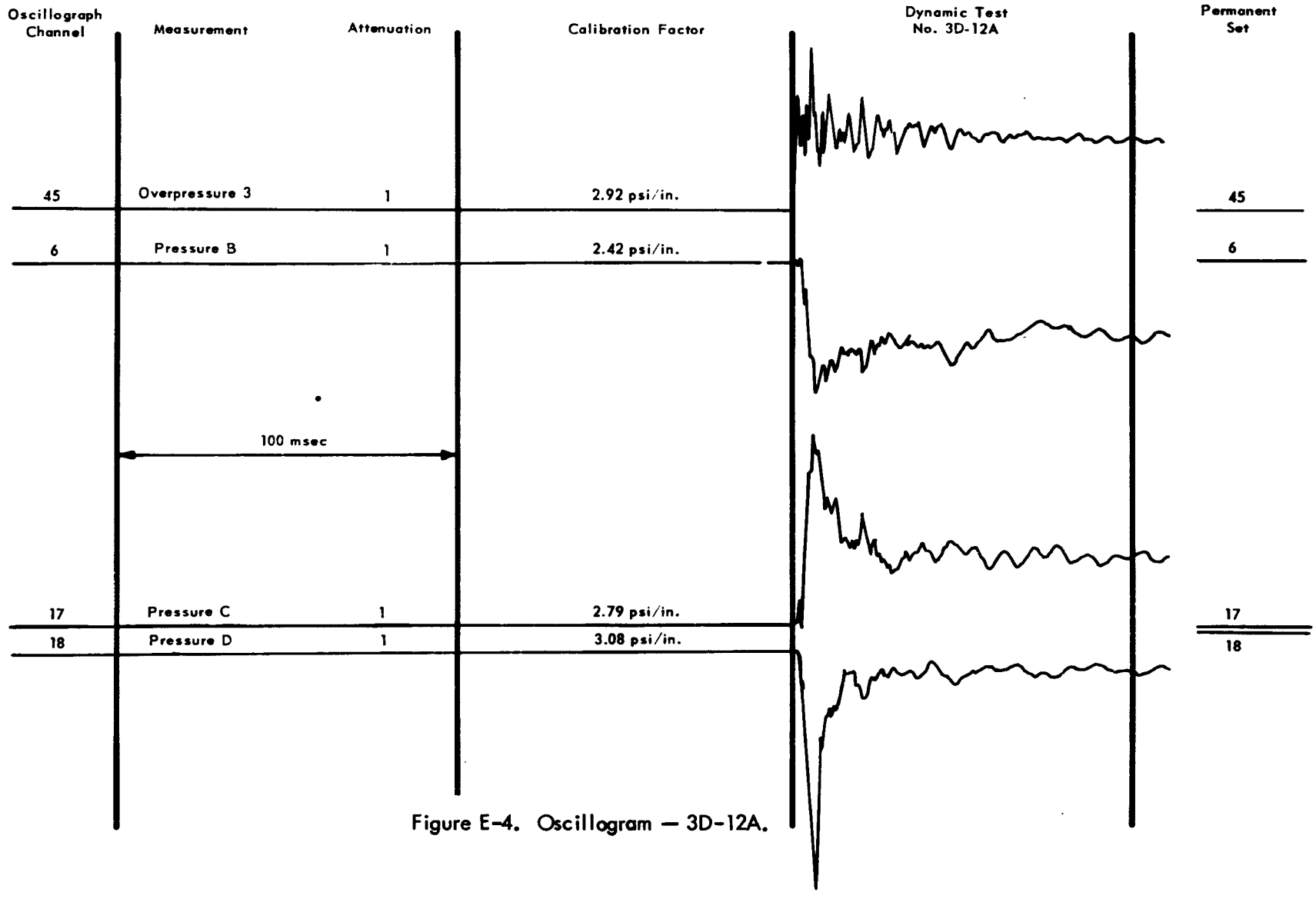

Figure E-4. Oscillogram — 3D-12A.

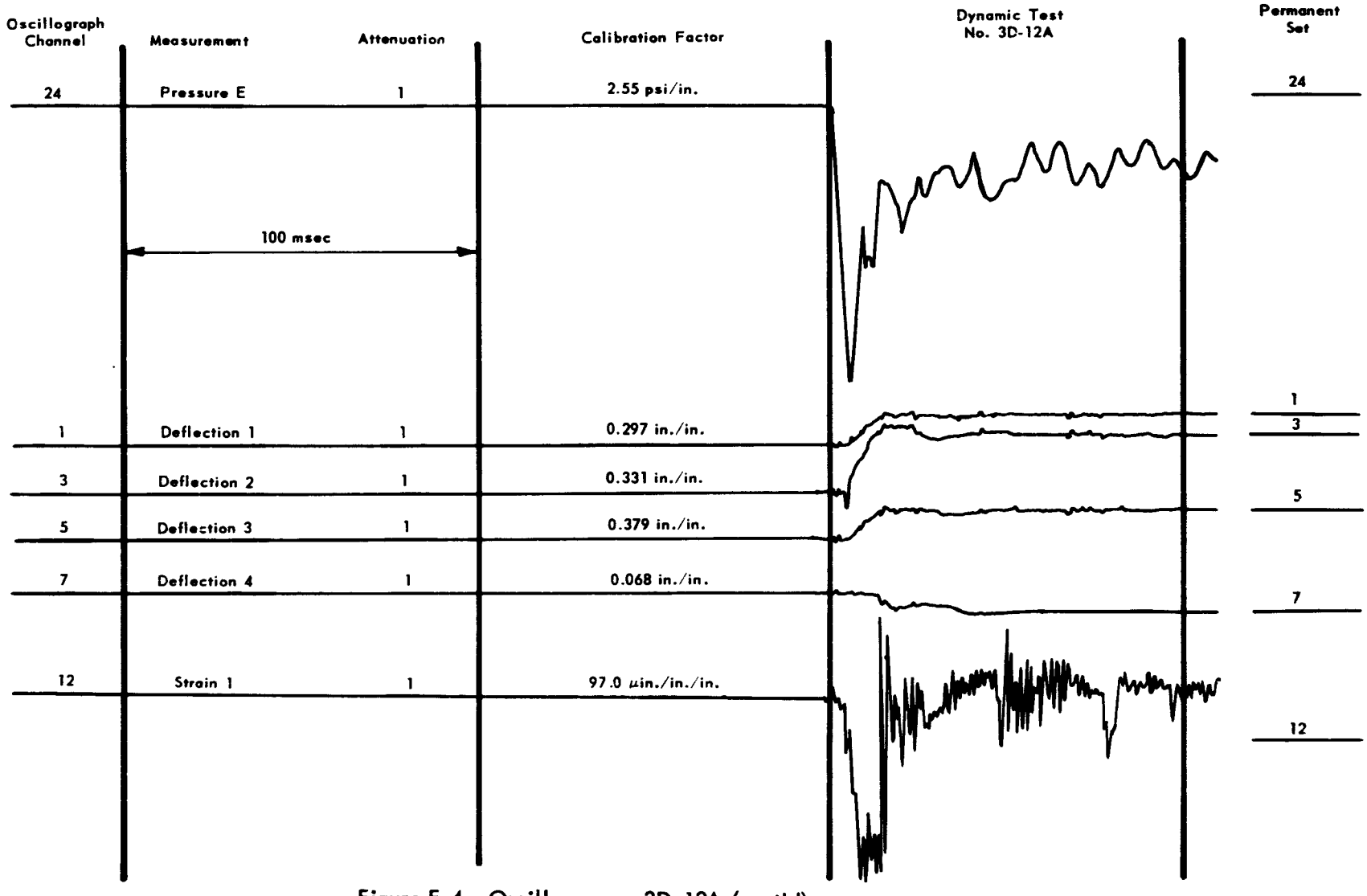

Figure E-4. Oscillogram — 3D-12A (cont'd).

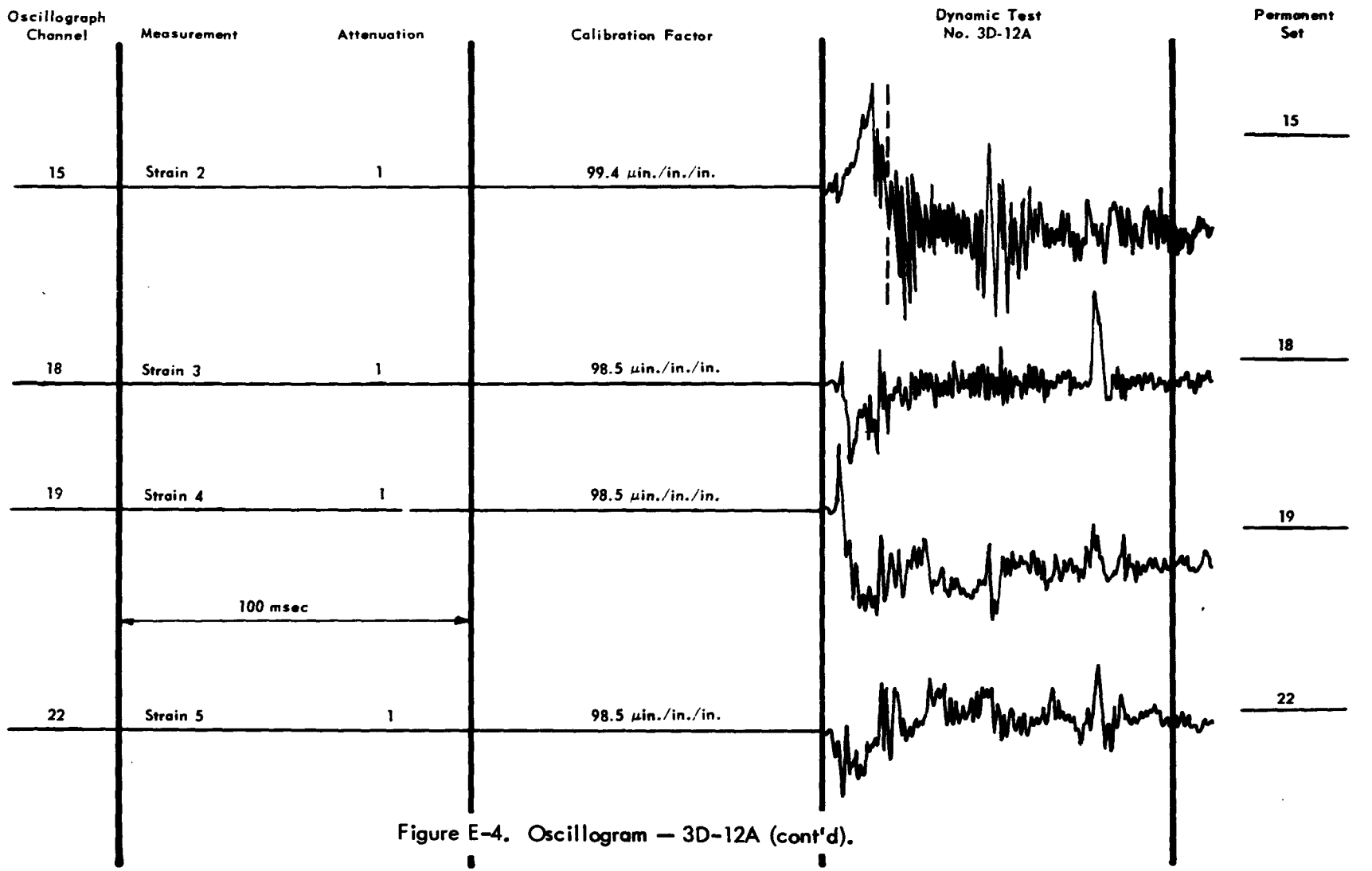

Figure E-4. Oscillogram — 3D-12A (cont'd).

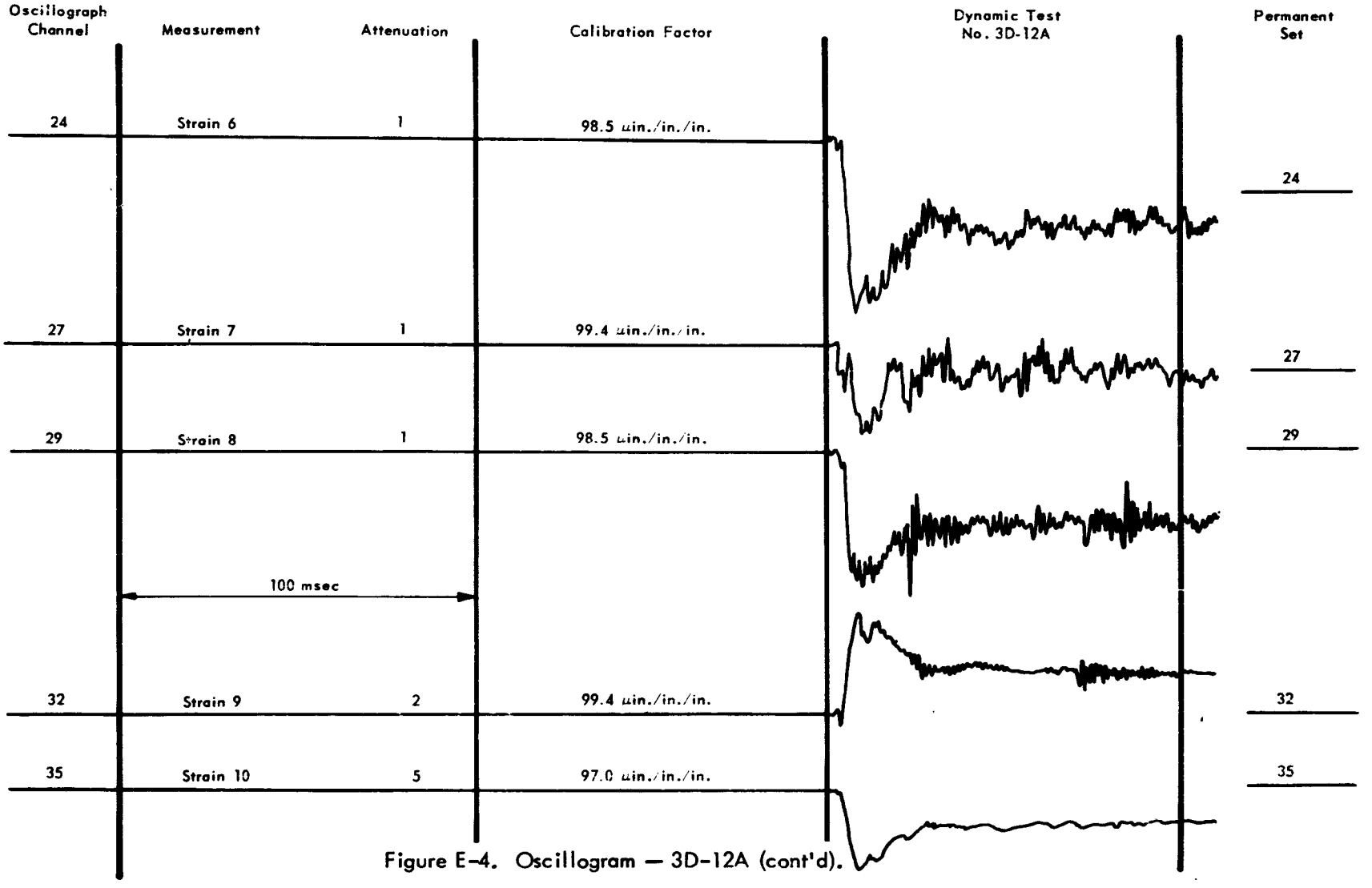

Figure E-4. Oscillogram — 3D-12A (cont'd).

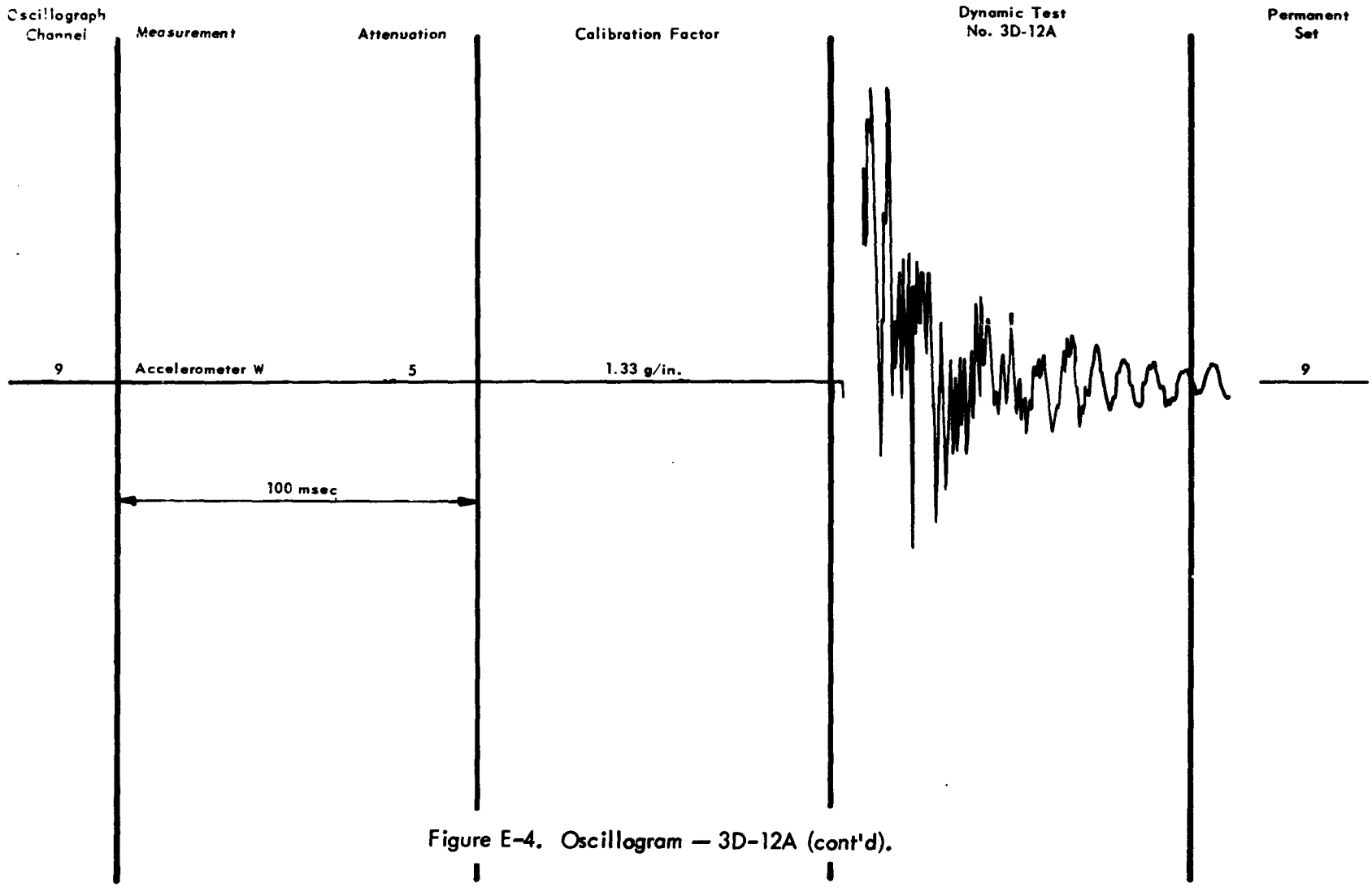

Figure E-4. Oscillogram — 3D-12A (cont'd).

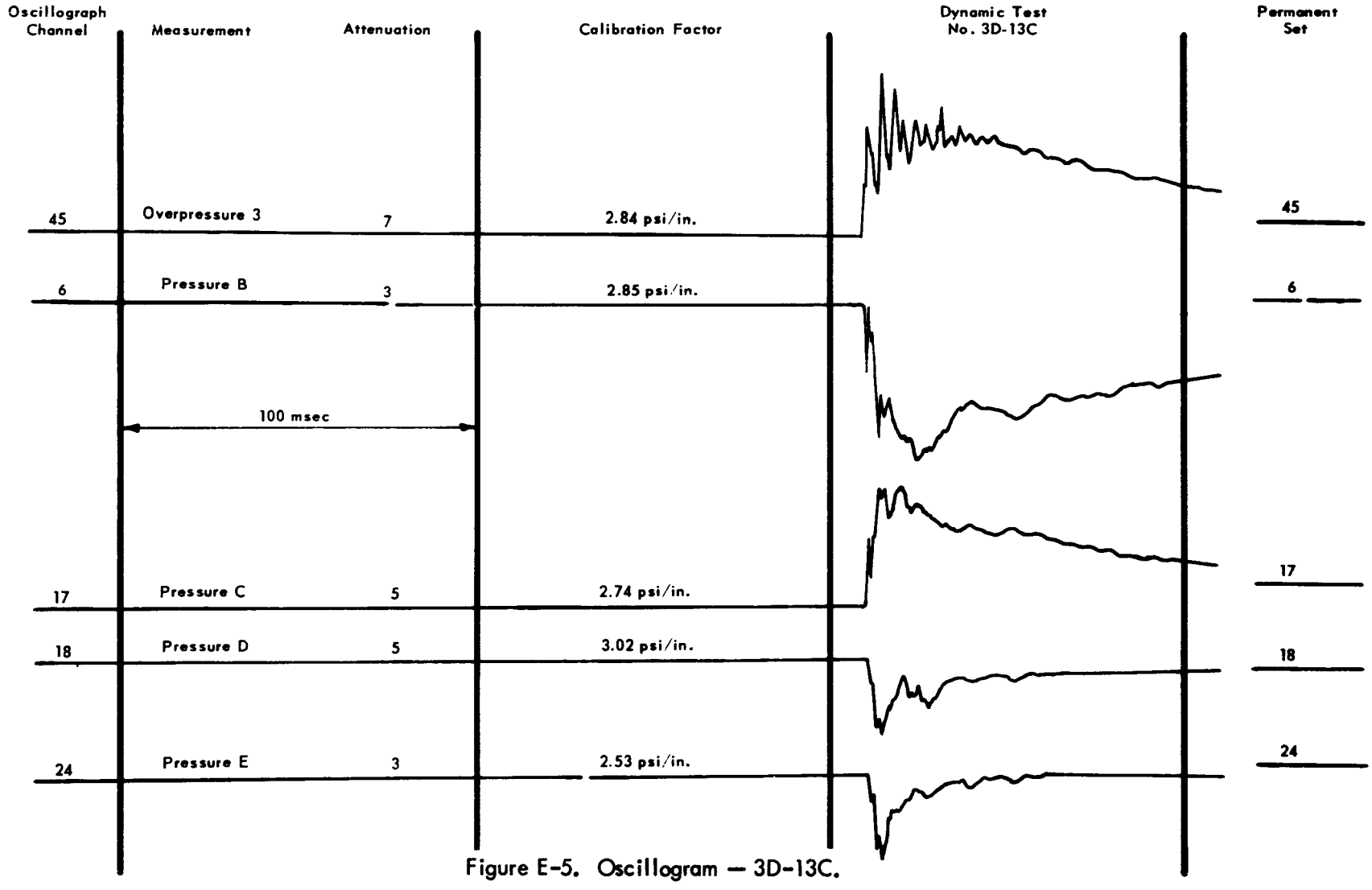

Figure E-5. Oscillogram — 3D-13C.

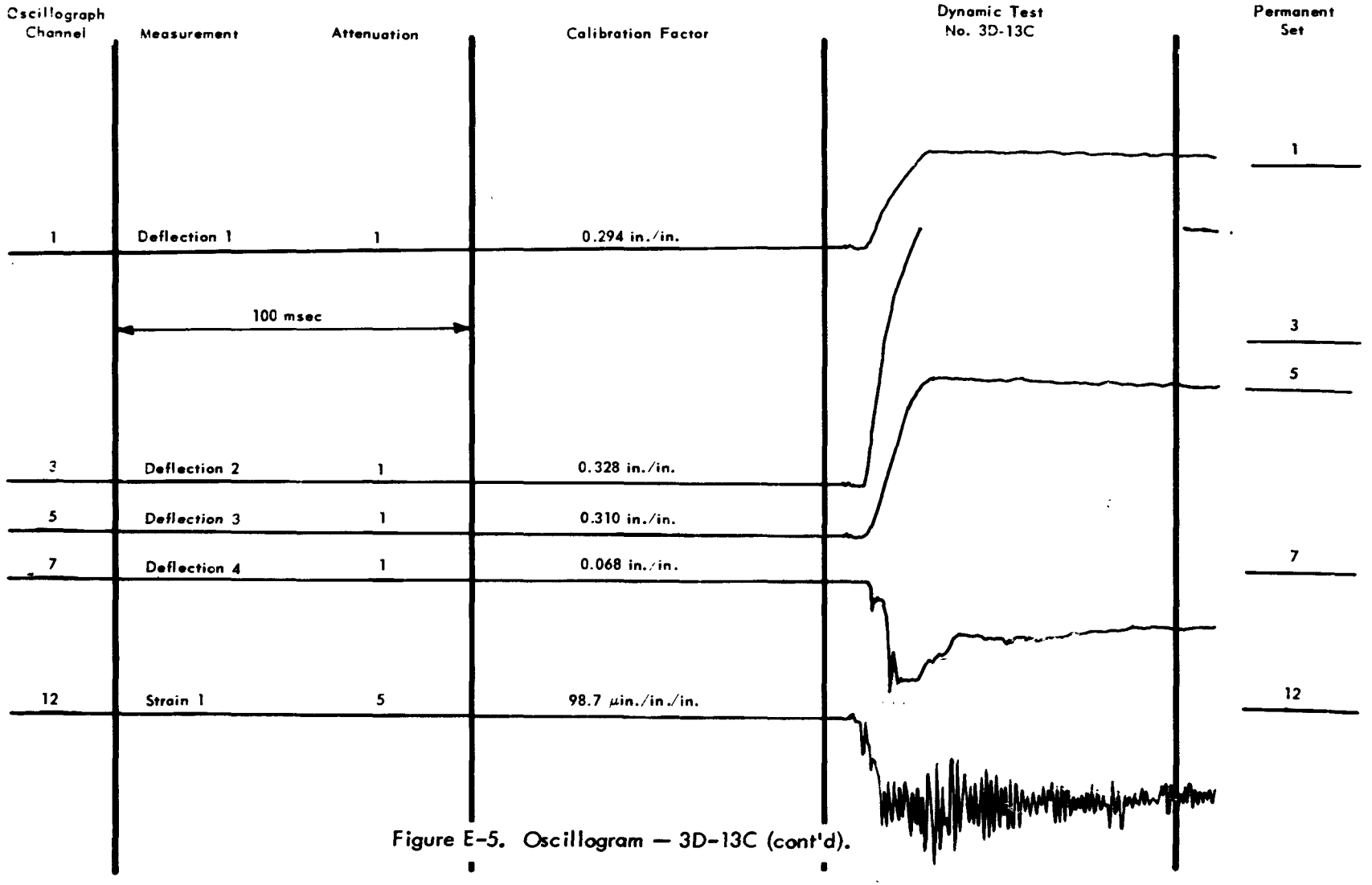

Figure E-5. Oscillogram — 3D-13C (cont'd).

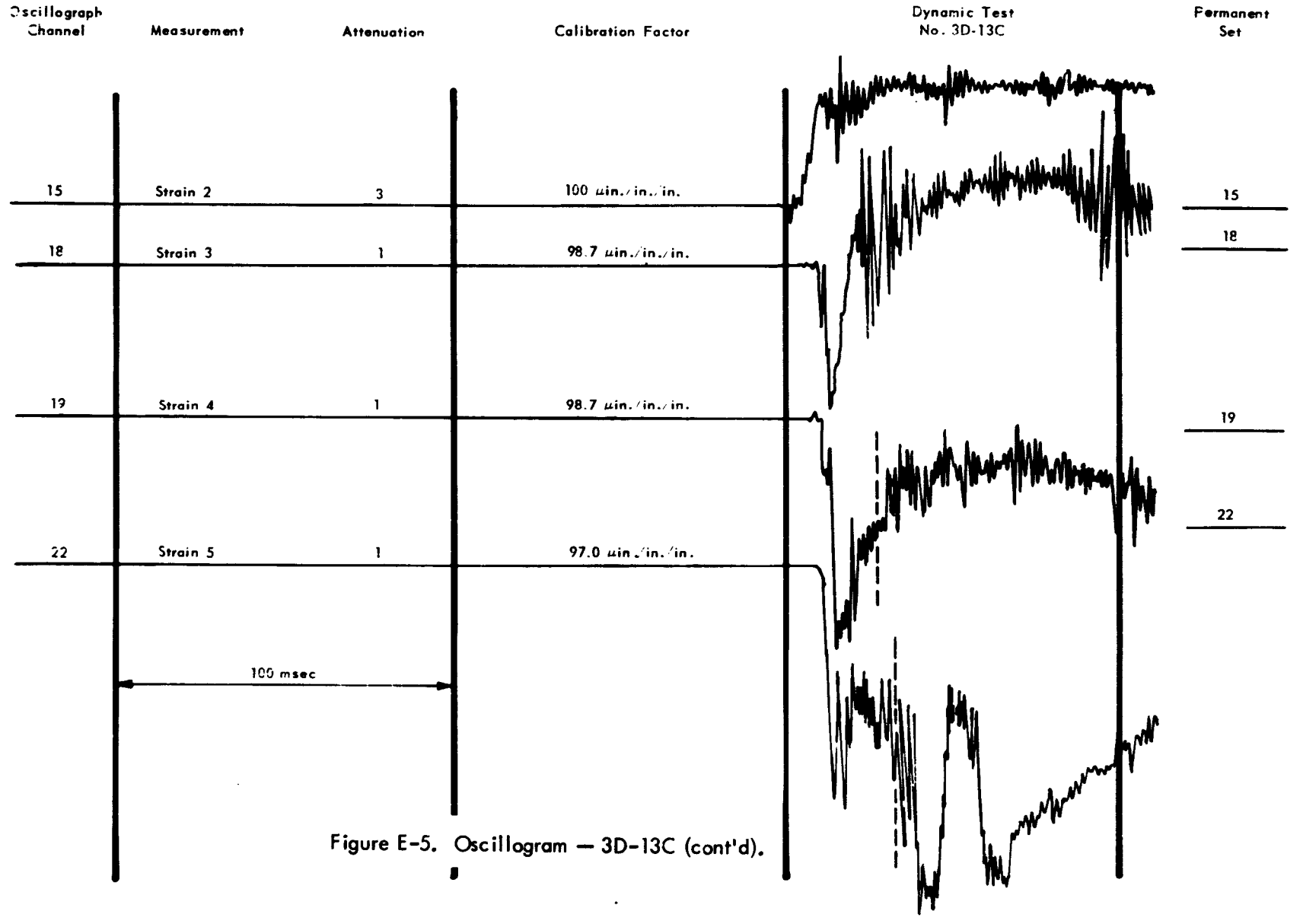

Figure E-5. Oscillogram — 3D-13C (cont'd).

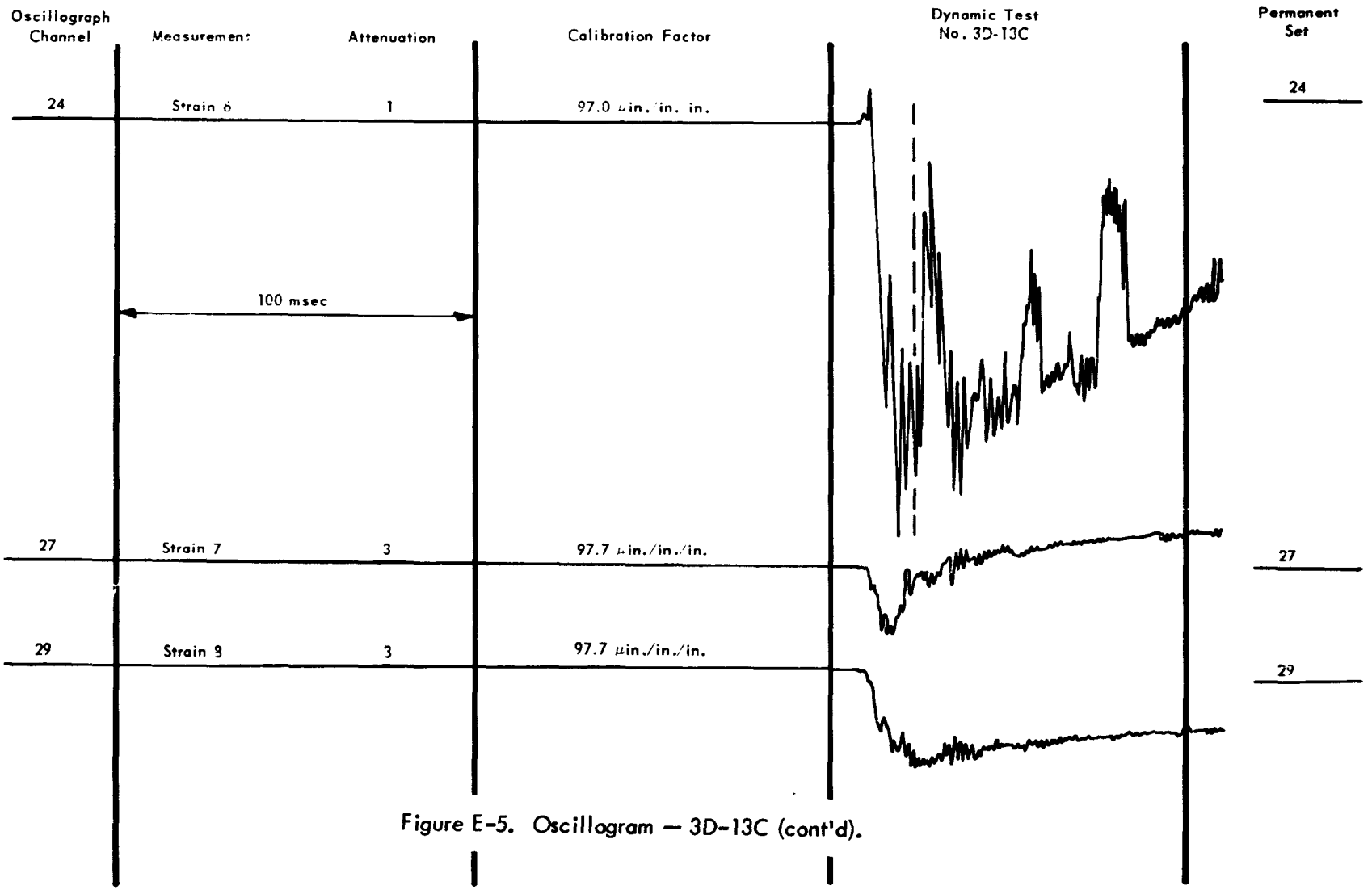

Figure E-5. Oscillogram — 3D-13C (cont'd).

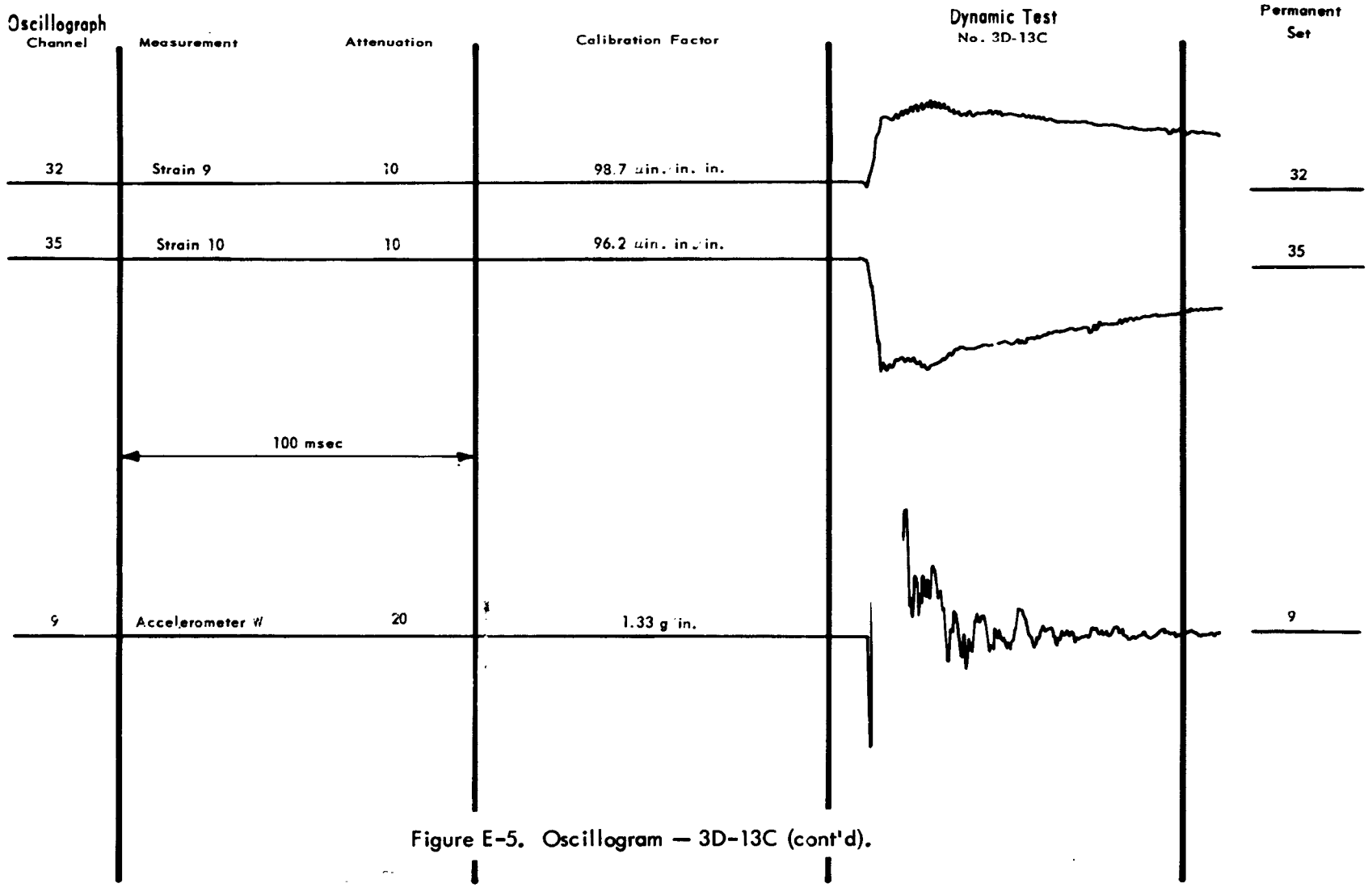

Figure E-5. Oscillogram — 3D-13C (cont'd).

DISTRIBUTION LIST

No. of copies	SNDL Code	
25		Chief, Defense Atomic Support Agency, Department of Defense, Washington, D. C.
10		Chief, Bureau of Yards and Docks (Code 70)
1	23A	Naval Forces Commanders (Taiwan Only)
4	39B	Construction Battalions
10	39D	Mobile Construction Battalions
3	39E	Amphibious Construction Battalions
2	39F	Construction Battalion Base Units
1	A2A	Chief of Naval Research - Only
2	A3	Chief of Naval Operation (OP-07, OP-04)
5	A5	Bureaus
2	B3	Colleges
2	E4	Laboratory ONR (Washington, D. C. only)
1	E5	Research Office ONR (Pasadena only)
1	E16	Training Device Center
7	F9	Station - CNO (Boston; Key West; San Juan; Long Beach; San Diego; Treasure Island; and Rodman, C. Z. only)
6	F17	Communication Station (San Juan; San Francisco; Pearl Harbor; Adak, Alaska; and Guam only)
1	F41	Security Station
1	F42	Radio Station (Oso and Cheltanham only)
1	F48	Security Group Activities (Winter Harbor only)
8	H3	Hospital (Chelsea; St. Albans, Portsmouth, Va; Beaufort; Great Lakes; San Diego; Oakland; and Camp Pendleton only)
1	H6	Medical Center
2	J1	Administration Command and Unit - BuPers (Great Lakes and San Diego only)
1	J3	U. S. Fleet Anti-Air Warfare Training Center (Virginia Beach only)
2	J4	Amphibious Bases
1	J19	Receiving Station (Brooklyn only)
1	J34	Station - BuPers (Washington, D. C. only)
1	J37	Training Center (Bainbridge only)
1	J46	Personnel Center
1	J48	Construction Training Unit
1	J60	School Academy
1	J65	School CEC Officers
1	J84	School Postgraduate
1	J90	School Supply Corps

Distribution List (Cont'd)

No. of copies	SNDL Code	
1	J95	School War College
1	J99	Communication Training Center
11	L1	Shipyards
4	L7	Laboratory - BuShips (New London; Panama City; Carderock; and Annapolis only)
5	L26	Naval Facilities - BuShips (Antigua; Turks Island; Barbados; San Salvador; and Eleuthera only)
1	L30	Submarine Base (Groton, Conn. only)
2	L32	Naval Support Activities (London & Naples only)
2	L42	Fleet Activities - BuShips
4	M27	Supply Center
6	M28	Supply Depot (Except Guantanamo Bay; Subic Bay; and Yokosuka)
2	M61	Aviation Supply Office
18	N1	BuDocks Director, Overseas Division
25	N2	Public Works Offices
7	N5	Construction Battalion Center
5	N6	Construction Officer-in-Charge
1	N7	Construction Resident-Officer-in-Charge
12	N9	Public Works Center
1	N14	Housing Activity
2	R9	Recruit Depots
2	R10	Supply Installations (Albany and Barstow only)
1	R20	Marine Corps Schools, Quantico
3	R64	Marine Corps Base
1	R66	Marine Corps Camp Detachment (Tengan only)
6	W1A1	Air Station
35	W1A2	Air Station
8	W1B	Air Station Auxiliary
4	W1C	Air Facility (Phoenix; Monterey; Oppama; Naha; and Naples only)
6	W1E	Marine Corps Air Station (Except Quantico)
9	W1H	Station - BuWeps (Except Rota)
1		Deputy Chief of Staff, Research and Development, Headquarters, U. S. Marine Corps, Washington, D. C.
1		President, Marine Corps Equipment Board, Marine Corps School, Quantico, Va.
2		Library of Congress, Washington, D. C.

Distribution List (Cont'd)

No. of copies	
1	Chief of Staff, U. S. Army, Chief of Research and Development, Department of the Army, Washington, D. C.
1	Office of the Chief of Engineers, Assistant Chief of Engineering for Civil Works, Department of the Army, Washington, D. C.
1	Chief of Engineers, Department of the Army, Washington, D. C., Attn: Engineering R & D Division
1	Chief of Engineers, Department of the Army, Washington, D. C., Attn: ENGCW-OE
1	Director, U. S. Army Engineer Research and Development Laboratories, Fort Belvoir, Va., Attn: Information Resources Branch
1	Headquarters, Wright Air Development Division, (WWAD-Library), Wright-Patterson Air Force Base, Ohio
3	Headquarters, U. S. Air Force, Directorate of Civil Engineering, Washington, D. C., Attn: AFOCE-ES
1	Commanding Officer, U. S. Naval Construction Battalion Center, Port Hueneme, Calif., Attn: Materiel Dept., Code 140
1	Deputy Chief of Staff, Development, Director of Research and Development, Department of the Air Force, Washington, D. C.
1	Director, National Bureau of Standards, Department of Commerce, Connecticut Ave., Washington, D. C.
2	Office of the Director, U. S. Coast and Geodetic Survey, Washington, D. C.
20	Armed Services Technical Information Agency, Arlington Hall Station, Arlington, Va.
2	Director of Defense Research and Engineering, Department of Defense, Washington, D. C.
2	Director, Division of Plans and Policies, Headquarters, U. S. Marine Corps, Washington, D. C.
2	Director, Bureau of Reclamation, Washington, D. C.
1	Commanding Officer, U. S. Navy Yards and Docks Supply Office, U. S. Naval Construction Battalion Center, Port Hueneme, Calif.
1	Facilities Officer (Code 108), Office of Naval Research, Washington, D. C.
1	Federal Aviation Agency, Office of Management Services, Administrative Services Division, Washington, D. C., Attn: Library Branch
1	Director, U. S. Naval Ordnance Laboratory, White Oak, Silver Springs, Md.
1	Office of Naval Research, Branch Office, Navy No. 100, Box 39, FPO, New York
1	U. S. Naval Radiological Defense Laboratory, San Francisco
1	Officer in Charge, CECOS, Port Hueneme, Calif., Attn: ADCE Course
1	U. S. Air Force, Asst. Chief of Staff, Intelligence, Bldg. B., AHS, Washington, D. C., Attn: Mr. Sargent White
1	Commander, Air Force Ballistic Missile Division, Air Research and Development Command, P.O. Box 262, Inglewood, Calif.
1	Directorate of Research, Air Force Special Weapons Center, Kirtland Air Force Base, N. Mex.
1	Director, U. S. Army Engineer Waterways Experiment Station, P.O. Box 631, Vicksburg, Miss., Attn: Mr. G. L. Arbuthnot, Jr.
1	U. S. Army Chemical Center, Nuclear Defense Laboratory, Edgewood, Md.
1	U. S. Army Engineer School, Department of Engineering, Fort Belvoir, Va., Attn: Mr. C. D. Kepple
1	Formulation and Analysis Branch, Mathematics and Computation Laboratory, National Resource Evaluation Center, Office of Emergency Planning, Washington, D. C.

Distribution List (Cont'd)

No. of copies	
1	Director. Ballistic Research Laboratories, Aberdeen, Md.
1	U. S. Atomic Energy Commission, Technical Information Service, P.O. Box 62, Oak Ridge, Tenn.
1	Director, Civil Effects Test Group, Atomic Energy Commission, Washington, D. C.
1	Headquarters, Field Command, Defense Atomic Support Agency, Sandia Base, Albuquerque, N. Mex.
1	Office of the Chief of Engineers, Department of the Army, T-7, Gravelly Point, Washington, D. C., Attn: ENGNB
1	Office of the Chief of Engineers, Department of the Army, T-7, Gravelly Point, Washington, D. C., Attn: ENG MC-EB
1	Commanding Officer, Engineer Research and Development Laboratories, Fort Belvoir, Va.
1	Sandia Corporation, Box 5800, Albuquerque, N. Mex.
1	Library, Engineering Department, University of California, 405 Hilgard Ave., Los Angeles
1	Mr. William J. Taylor, Terminal Ballistics Laboratory, Aberdeen Proving Ground, Aberdeen Proving Ground, Md.
1	CAPT W. M. McLellon, CEC, USN, Office of Civil Defense Support, Bldg. T-7, Washington, D. C.
1	LT Edward S. Perry, U. S. Naval School, CEC Officers, Port Hueneme, Calif.
1	CAPT L. N. Saunders, CEC, USN, Commander, U. S. Naval Support Forces, Antarctica, 6th and Independence Ave., N.W., Tempo D, Washington, D. C.
1	CDR E. M. Saunders, CEC, USN, Bureau of Yards and Docks, Code 74, Washington, D. C.
1	CDR H. W. Stephens, CEC, USN, Division of Military Applications, Atomic Energy Commission, Washington, D. C.
1	LCDR Charles W. Gulick, Jr., CEC, USN, U. S. Naval School, CEC Officers, Port Hueneme, Calif.
1	LCDR W. A. Walls, CEC, USN, Defense Atomic Support Agency, Washington, D. C.
1	LCDR C. R. Whipple, CEC, USN, U. S. Naval Ordnance Laboratory, White Oak, Md. ton, D. C.
1	Major F. A. Verser, Jr., USA, Defense Atomic Support Agency, Washington, D. C.
1	Mr. L. Neal FitzSimons, Office of Civil Defense, Department of Defense, Pentagon - 3B265, Washington, D. C.
1	Mr. Ben Taylor, Office of Civil Defense, Department of Defense, Washington, D. C.
1	Mr. Charles M. Eisenhauer, Radiation Physics Laboratory, National Bureau of Standards, Washington, D. C.
1	Mr. O. H. Hill, Bldg. 12, Rm. 505, Radiation Physics Division, National Bureau of Standards, Washington, D. C.
1	Dr. Lewis V. Spencer, Ottawa University, Physics Department, Ottawa, Kan.
1	Mr. E. E. Shalowitz, Protective Construction, GSA Bldg. 19th and F St., N. W., Washington, D. C.
1	Mr. G. H. Albright, Pennsylvania State University, College of Engineering and Architecture, University Park, Pa.
1	Mr. A. F. Dill, Civil Engineering Hall, University of Illinois, Urbana, Ill.
1	Dr. N. M. Newmark, Civil Engineering Hall, University of Illinois, Urbana, Ill.
1	Professor J. Neils Thompson, Civil Engineering Department, University of Texas, Austin, Tex.
1	Mr. Fred Sauer, Physics Department, Stanford Research Institute, Menlo Park, Calif.
1	Mr. W. E. Fisher, Air Force Special Weapons Center, Kirtland Air Force Base, Albuquerque, N. M.
1	Dr. John Balloch, Director, Operations Analysis, 26th Air Division, (SAGE), Hancock Field, Syracuse, N. Y.

Distribution List (Cont'd)

No. of copies	
1	Dr. T. H. Schiffman, Armour Research Foundation of Illinois Institute of Technology, Technology Center, Chicago, Ill.
1	Dr. Robert V. Whitman, Massachusetts Institute of Technology, Cambridge, Mass.
1	Mr. Werner Weber, Nuclear Engineering Consultant, N. Y. State Civil Defense Commission, P.O. Box 7007, State Office Bldg., Albany, N. Y.
1	LCDR J. D. Andrews, CEC, USN, SHAPE Headquarters, Paris, France, A.P.O. 55, New York
1	CDR W. J. Christensen, CEC, USN, U. S. Naval Civil Engineering Laboratory, Port Hueneme, Calif.
1	LCDR N. W. Clements, CEC, USN, Navy Nuclear Power Unit, Fort Belvoir, Va.
1	LTJG L. K. Donovan, CEC, USN, Navy Nuclear Power Unit, Fort Belvoir, Va.
1	LTJG Clinton W. Kelly, III, CEC, USN, Bureau of Yards and Docks, Program Officer, U. S. Naval Radiological Defense Laboratory, San Francisco
1	CDR W. J. Francy, CEC, USN, Bureau of Yards and Docks, Director, Southeast Division, U. S. Naval Base, Charleston, S. C.
1	CDR C. F. Krickenberger, CEC, USN, Bureau of Yards and Docks, Code 51, Washington, D. C.
1	Dr. Harold Brode, The Rand Corporation, 1700 Main St., Santa Monica, Calif.
1	Dr. William Kreger, Naval Radiological Defense Laboratory, San Francisco
1	Dr. Hans Tiller, Nuclear Defense Laboratory, Army Chemical Center, Md.
1	Mr. Irving Gaskill, National Resource Evaluation Center, Executive Office Bldg., Washington, D. C.
1	Major Robert S. Marcum, Defense Atomic Support Agency, Department of Defense, Washington, D. C.
1	Dr. Carl F. Miller, Office of Civil Defense, Department of Defense, Washington, D. C.
1	Mr. James C. Pettee, National Resource Evaluation Center, Executive Office Bldg., Washington, D. C.
1	Dr. A. B. Chilton, Civil Engineering Hall, University of Illinois, Urbana, Ill.
1	Mrs. Shea Valley, CRTZS, A. F. Cambridge Research Center, Bedford, Mass.
1	Dr. Ronald W. Shephard, University of California, Engineering Field Station, 1301 South 46th St., Richmond, Calif.
1	LTCOL Russell J. Hutchinson, 052921, Office of the Engineer, Camp Wolters, Mineral Wells, Tex.
1	LT R. B. Reeves, CEC, USN, Field Command, Defense Atomic Support Agency, Sandia Base, Albuquerque, N. Mex.
1	Professor J. T. Hanley, Department of Civil Engineering, University of Illinois, Urbana, Ill.
1	Asst. Professor J. Silverman, Department of Chemical Engineering, University of Maryland, College Park, Md.
1	Mr. R. D. Cavenaugh, Barry Controls, Inc., 700 Pleasant St., Watertown, Mass.
1	Mr. Kenneth Kaplan, Broadview Research Corporation, 1811 Trousdale Dr., Burlingame, Calif.
1	Mr. Thomas Morrison, American Machine and Foundry Co., 7501 North Natchez Ave., Niles, Ill.
1	Mr. W. R. Perret - 5112, Sandia Corporation, Sandia Base, Albuquerque, N. Mex.
1	Mr. Lyndon Welch, Eberle M. Smith Associates, Inc., 153 East Elizabeth St., Detroit, Mich.
1	Dr. Lauriston S. Taylor, Chief, Radiation Physics Division, National Bureau of Standards, Washington, D. C.
1	Professor Herbert M. Bosch, Public Health Engineering, School of Public Health, University of Minnesota, Minneapolis, Minn.
1	Mr. J. F. Tamanini, A & E Development Division, Office of Civil Defense, Department of Defense, Washington, D.C.

U. S. Naval Civil Engineering Laboratory
Technical Report R-216
BLAST LOADING OF SMALL BURIED ARCHES, by
J. R. Allgood, C. R. White, R. F. Swalley, H. L. Gill
169 p. illus 3 Apr 63 UNCLASSIFIED

To gain information which will serve as a guide in developing design methods for underground structures, tests were conducted on small buried arches to determine the response to blast loads, including the deflection, thrust, and moment patterns. One static test also was performed, and curves are given showing the form of arching under static and blast loading.

1. Structural tests — Buried arches
I. Allgood, J. R.
II. White, C. R.
III. Swalley, R. F.
IV. Gill, H. L.
V. Y-F008-10-108
VI. Y-F008-10-402

U. S. Naval Civil Engineering Laboratory
Technical Report R-216
BLAST LOADING OF SMALL BURIED ARCHES, by
J. R. Allgood, C. R. White, R. F. Swalley, H. L. Gill
169 p. illus 3 Apr 63 UNCLASSIFIED

To gain information which will serve as a guide in developing design methods for underground structures, tests were conducted on small buried arches to determine the response to blast loads, including the deflection, thrust, and moment patterns. One static test also was performed, and curves are given showing the form of arching under static and blast loading.

1. Structural tests — Buried arches
I. Allgood, J. R.
II. White, C. R.
III. Swalley, R. F.
IV. Gill, H. L.
V. Y-F008-10-108
VI. Y-F008-10-402

U. S. Naval Civil Engineering Laboratory
Technical Report R-216
BLAST LOADING OF SMALL BURIED ARCHES, by
J. R. Allgood, C. R. White, R. F. Swalley, H. L. Gill
169 p. illus 3 Apr 63 UNCLASSIFIED

To gain information which will serve as a guide in developing design methods for underground structures, tests were conducted on small buried arches to determine the response to blast loads, including the deflection, thrust, and moment patterns. One static test also was performed, and curves are given showing the form of arching under static and blast loading.

1. Structural tests — Buried arches
I. Allgood, J. R.
II. White, C. R.
III. Swalley, R. F.
IV. Gill, H. L.
V. Y-F008-10-108
VI. Y-F008-10-402

U. S. Naval Civil Engineering Laboratory
Technical Report R-216
BLAST LOADING OF SMALL BURIED ARCHES, by
J. R. Allgood, C. R. White, R. F. Swalley, H. L. Gill
169 p. illus 3 Apr 63 UNCLASSIFIED

To gain information which will serve as a guide in developing design methods for underground structures, tests were conducted on small buried arches to determine the response to blast loads, including the deflection, thrust, and moment patterns. One static test also was performed, and curves are given showing the form of arching under static and blast loading.

1. Structural tests — Buried arches
I. Allgood, J. R.
II. White, C. R.
III. Swalley, R. F.
IV. Gill, H. L.
V. Y-F008-10-108
VI. Y-F008-10-402

Distribution List (Cont'd)

No. of copies	
1	Dr. Merit P. White, Civil Engineering Department, School of Engineering, University of Massachusetts, Amherst, Mass.
1	Dr. Robert J. Hansen, Department of Civil and Sanitary Engineering, Massachusetts Institute of Technology, Cambridge, Mass.
1	Mr. Harold Horowitz, Building Research Institute, National Academy of Sciences, 2101 Constitution Ave., N.W., Washington, D. C
1	Mr. Luke Vortman - 5112, Applied Experiments Division, Sandia Corporation, Albuquerque, N. Mex.
1	Mr. Richard Park, National Academy of Sciences, 2101 Constitution Ave., N.W., Washington, D. C.
1	Dr. Harold A. Knapp, Fallout Studies Branch, Division of Biology and Medicine, U. S. Atomic Energy Commission, Washington, D. C.
1	Dr. Karl Z. Morgan, Director, Health Physics Division, Oak Ridge National Laboratory, Oak Ridge, Tenn.
1	Mr. Frederick A. Pawley, AIA Research Secretary, American Institute of Architects, 1735 New York Ave., N.W., Washington, D. C.
1	Dr. David Kleinecke, Engineering Field Station, University of California, 1301 South 46th St., Richmond, Calif.
1	Dr. E. E. Massey, Defense Research Board, Department of National Defense, Ottawa, Canada
1	Dr. Joseph D. Coker, National Resource Evaluation Center, Executive Office Bldg. Washington, D. C.
1	Dr. Charles F. Ksanda, Military Evaluations Division, U. S. Naval Radiological Defense Laboratory, San Francisco
1	Mr. F. T. Mavis, Dean, College of Engineering, University of Maryland, College Park, Md.
1	Dr. George E. Pugh, Institute of Defense Analyses, Weapons Systems Evaluation Division, Washington, D. C.
1	Dr. Robert Rapp, The Rand Corporation, 1700 Main St., Santa Monica, Calif.
1	Dr. Stephen B. Withey, Program Director, Survey Research Center, University of Michigan, Ann Arbor, Mich.
1	Mr. John Auxier, Oak Ridge National Laboratory, Oak Ridge, Tenn.
1	Dr. Eric T. Clarke, Technical Operations, Inc., Burlington, Mass.
1	LT Walter J. Eager, Jr., CEC, USN, Naval Postgraduate School, Monterey, Calif.
1	LCDR C. Curione, CEC, USN, U. S. Naval Civil Engineering Laboratory, Port Hueneme, Calif.
1	LTCOL James R. Bohanan, USAF, Headquarters, U. S. Air Force, Directorate of Civil Engineering Washington, D. C.
1	Mr. Walter Gunther, The Mitre Corporation, P.O. Box 208, Lexington, Mass
1	LCDR R. C. Vance, Mobile Construction Battalion 11, FPO San Francisco
1	LCDR J. C. LeDoux, Office of Civil Defense, Department of Defense, Washington, D. C.
1	LT R. D. Crowley, CEC, USN, U. S. Naval School, CEC Officers, Port Hueneme, Calif.
1	LT S. F. Matties, CEC, USN U. S. Naval Construction Battalion Center, Port Hueneme, Calif.
1	Dr. James C. Buchanan, Technical Operations, Inc., South Ave., Burlington, Mass.
1	Mr. Jack C. Greene, Office of Civil Defense, Department of Defense Washington, D. C.
1	Mr. John Lewis, Defense Atomic Support Agency, Department of Defense, Washington, D. C.
1	CAPT Robert Crawford, USAF, Air Force Special Weapons Center, Kirtland Air Force Base Alburquerque, N. M.